REPORT DOCUMENTATION PAGE

Public reporting burden for this collection of information is estimated to average 1 hour per response, including the time for reviewing instructions, sear the collection of information. Send comments regarding this burden estimate or any other aspect of this collection of information, including sugg Operations and Reports, 1215 Jefferson Davis Highway, Suite 1204, Arlington, VA 22202-4302, and to the Office of Management and Budget, Paper

AFRL-SR-BL-TR-00-

0702

eviewing ormation

1. AGENCY USE ONLY *(Leave blank)*	2. REPORT DATE	3. REPOF
	December, 1996	

4. TITLE AND SUBTITLE
1996 Summer Research Program (SRP), Summer Research Extension Program (SREP), Final Report, Volume 1, Armstrong Laboratory and Program Management

5. FUNDING NUMBERS
F49620-93-C-0063

6. AUTHOR(S)
Gary Moore

7. PERFORMING ORGANIZATION NAME(S) AND ADDRESS(ES)
Research & Development Laboratories (RDL)
5800 Uplander Way
Culver City, CA 90230-6608

8. PERFORMING ORGANIZATION REPORT NUMBER

9. SPONSORING/MONITORING AGENCY NAME(S) AND ADDRESS(ES)
Air Force Office of Scientific Research (AFOSR)
801 N. Randolph St.
Arlington, VA 22203-1977

10. SPONSORING/MONITORING AGENCY REPORT NUMBER

11. SUPPLEMENTARY NOTES

12a. DISTRIBUTION AVAILABILITY STATEMENT
Approved for Public Release

12b. DISTRIBUTION CODE

13. ABSTRACT *(Maximum 200 words)*

The United States Air Force Summer Research Program (SRP) is designed to introduce university, college, and technical institute faculty members to Air Force research. This is accomplished by the faculty members, graduate students, and high school students being selected on a nationally advertised competitive basis during the summer intersession period to perform research at Air Force Research Laboratory (AFRL) Technical Directorates and Air Force Air Logistics Centers (ALC). AFOSR also offers its research associates (faculty only) an opportunity, under the Summer Research Extension Program (SREP), to continue their AFOSR-sponsored research at their home institutions through the award of research grants. This volume consists of the SREP program background, management information, statistics, a listing of the participants, and the technical report for each participant of the SREP working at the AF Armstrong Laboratory.

14. SUBJECT TERMS
Air Force Research, Air Force, Engineering, Laboratories, Reports, Summer, Universities, Faculty, Graduate Student, High School Student

15. NUMBER OF PAGES

16. PRICE CODE

17. SECURITY CLASSIFICATION OF REPORT	18. SECURITY CLASSIFICATION OF THIS PAGE	19. SECURITY CLASSIFICATION OF ABSTRACT	20. LIMITATION OF ABSTRACT
Unclassified	Unclassified	Unclassified	UL

Standard Form 298 (Rev. 2-89) (EG)
Prescribed by ANSI Std. 239.18
Designed using Perform Pro, WHS/DIOR, Oct 94

UNITED STATES AIR FORCE

SUMMER RESEARCH PROGRAM -- 1996

SUMMER RESEARCH EXTENSION PROGRAM FINAL REPORTS

VOLUME 1

ARMSTRONG LABORATORY

PROGRAM MANAGEMENT REPORT

RESEARCH & DEVELOPMENT LABORATORIES

5800 Uplander Way

Culver City, CA 90130-6608

Program Director, RDL
Gary Moore

Program Manager, AFOSR
Major Linda Steel-Goodwin

Program Manager, RDL
Scott Licoscos

Program Administrator, RDL
Johnetta Thompson

Program Administrator
Rebecca Kelly-Clemmons

Submitted to:

AIR FORCE OFFICE OF SCIENTIFIC RESEARCH

Bolling Air Force Base

Washington, D.C.

December 1996

20010319 062

AQM01-06-0915

PREFACE

This volume is part of a five-volume set that summarizes the research of participants in the 1996 AFOSR Summer Research Extension Program (SREP.) The current volume, Volume 1 of 5, presents the final reports of SREP participants at Armstrong Laboratory. Volume 1 also includes the Management Report.

Reports presented in this volume are arranged alphabetically by author and are numbered consecutively – e.g., 1-1, 1-2, 1-3; 2-1, 2-2, 2-3, with each series of reports preceded by a 35 page management summary. Reports in the five-volume set are organized as follows:

VOLUME	TITLE
1	Armstrong Laboratory
2	Phillips Laboratory
3	Rome Laboratory
4A	Wright Laboratory
4B	Wright Laboratory
5	Arnold Engineering Development Center Air Logistics Centers

1996 SREP FINAL REPORTS

Armstrong Laboratory

VOLUME 1

Report #	Report Title Author's University	Report Author
1	Chlorinated Ethene Transformation, Sorption & Product Distr in Metallic Iron/Water Systems: Effect of Iron Properties Washington State University, Pullman, WA	Dr. Richelle M Allen-King Dept. of Geology AL/EQ
2	Dynamically Adaptive Interfaces: A Preliminary Investigation Wright State University, Dayton, OH	Dr. Kevin B Bennett Dept. of Psychology AL/CF
3	Geographically Distributed Collaborative Work Environment California State University, Hayward, CA	Dr. Alexander B Bordetsky Dept. Decesion Sciences AL/HR
4	Development of Fluorescence Post Labeling Assay for DNA Adducts: Chloroacetaldeh New York Univ Dental/Medical School, New York, NY	Dr. Joseph B Guttenplan Dept. of Chemistry AL/OE
5	The Checkmark Pattern & Regression to the Mean in Dioxin Half Life Studies University of South Alabama, Mobile, AL	Dr. Pandurang M Kulkarni Dept. of Statistics AL/AO
6	Determination of the Enzymatic Constraints Limiting the Growth of Pseudomonas University of Dayton, Dayton, OH	Dr. Michael P Labare Dept. of Marine Sciences AL/HR
7	Tuned Selectivity Solid Phase Microextraction Clarkson University, Potsdam, NY	Dr. Barry K Lavine Dept. of Chemistry AL/EQ
8	A Cognitive Engineering Approach to Distributed Team Decision Making During University of Georgia, Athens, GA	Dr. Robert P Mahan Dept. of Psychology AL/CF
9	Repetative Sequence Based PCR: An Epidemiological Study of a Streptococcus Stonehill College, North Easton, MA	Dr. Sandra McAlister Dept. of Biology AL/CF
10	An Investigation into the Efficacy of Headphone Listening for Localization of Middle Tennessee State University, Murfreesbord, TN	Dr. Alan D. Musicant Dept. of Psychology AL/CF
11	The Neck Models to Predict Human Tolerance in a G-Y CUNY-City College, New York, NY	Dr. Ali M. Sadegh Dept. of Mech Engineering AL/CF

1996 SREP FINAL REPORTS

Armstrong Laboratory

VOLUME 1 (cont.)

Report #	Report Title Author's University	Report Author
12	Tracer Methodology Development for Enhanced Passive Ventilation for Soil University of Florida, Gainesville, FL	Dr. William R. Wise Dept. of Civil Engineering AL/EQ
13	Application of a Distribution-Based Assessment of Mission Readiness System for the Evaluation of Personnel Training Texas A&M University, College Station, TX	Dr. David J. Woehr Dept. of Psychology AL/HR
14	Electrophysiological, Behaviorial, and Subjective Indexes of Workload when Performing Multiple Tasks Washington State University, Pullman, WA	Ms. Lisa Fournier Dept. of Psychology AL/CF
15	Methods for Establishing Design Limits to Ensure Accomodation for Ergonomic Design Miami University, Oxford, OH	Ms. Kristie Nemeth Dept. of Psychology AL/HR

1996 SREP FINAL REPORTS

Phillips Laboratory

VOLUME 2

Report #	Report Title Author's University	Report Author
1	Experimental Study of the Tilt Angular Anisopalantaic Correlation & the Effect Georgia Tech Research Institute, Atlanta, GA	Dr. Mikhail Belen'kii Dept. of Electro Optics PL/LI
2	Performance Evaluations & Computer Simulations of Synchronous & Asynchronous California State University, Fresno, CA	Dr. Daniel C. Bukofzer Dept. of Elec Engineering PL/VT
3	MM4 Model Experiments on the Effects of Cloud Shading Texas Tech University, Lubbock, TX	Dr. Chia-Bo Chang Dept. of Geosciences PL/GP
4	Miniature Laser Gyro consisting in a Pair of Unidirectional Ring Lasers University of New Mexico, Albuquerque, NM	Dr. Jean-Claude M. Diels Dept. of Physics PL/LI
5	Simulations & Theoretical Studies of Ultrafast Silicon Avalanche Old Dominion University, Norfolk, VA	Dr. Ravindra P. Joshi Dept. of Elec Engineering PL/WS
6	Theory of Wave Propagation in a Time-Varying Magnetoplasma Medium & Applications to Geophysical Phenomena University of Massachusetts Lowell, Lowell, MA	Dr. Dikshitulu K. Kalluri Dept. of Elec Engineering PL/GP
7	Thermal Analysis for the Applications of High Power Lasers in Large-Area Materials Processing University of Central Florida, Orlando, FL	Dr. Arvinda Kar Dept. of Engineering PL/LI
8	Analytical Noise Modeling and Optimization of a Phasor-Based Phase Texas Tech University, Lubbock, TX	Dr. Thomas F. Krile Dept. of Elec Engineering PL/LI
9	Mathematical Modeling of Thermionic-AMTEC Cascade System for Space Power Texas Tech University, Lubbock, TX	Dr. M. Arfin K. Lodhi Dept. of Physics PL/VT
10	Preparation & characterization of Polymer Blends Ohio State University, Columbus, OH	Dr. Charles J. Noel Dept. of Chemistry PL/RK
11	Evaluation of Particle & Energy Transport to Anode, Cathode University of Texas-Denton, Denton, TX	Dr. Carlos A. Ordonez Dept. of Physics PL/WS
12	Analysis of the Structure & Motion of Equatorial Emission Depletion Bands Using Optical All-Sky Images University of Massachusetts Lowell, Lowell, MA	Dr. Ronald M. Pickett Dept. of Psychology PL/GP

1996 SREP FINAL REPORTS

Phillips Laboratory

VOLUME 2 (cont.)

Report #	Author's University	Report Author
13.	**On the Fluid Dynamics of High Pressure Atomization in Rocket Propulsion** **University of Illinois-Chicago, Chicago, IL**	**Dr. Dimos Poulikakos** **Dept. of Mech Engineering** **PL/RK**
14	**Gigahertz Modulation & Ultrafast Gain Build-up in Iodine Lasers** **University of New Mexico, Albuquerque, NM**	**Dr. W. Rudolph** **Dept. of Physics** **PL/LI**
15	**Inversion of Hyperspectral Atmospheric Radiance Images for the Measurement of Temperature, Turbulence, and Velocity** **University of New Mexico, Albuquerque, NM**	**Dr. David Watt** **Dept. of Mech Engineering** **PL/GP**

1996 SREP FINAL REPORTS

Rome Laboratory

VOLUME 3

Report #	Author's University	Report Author
1	Performance Analysis of an ATM-Satellite System Florida Atlantic University, Boca Raton, FL	Dr. Valentine Aalo Dept. of Elec Engineering RL/C3
2	Reformulatiang Domain Theories to Improve their Computational Usefulness Oklahoma State University, Stillwater, OK	Dr. David P. Benjamin Dept. of Comp Engineering RL/C3
3	An Analysis of the Adaptive Displaced Phase Centered Antenna Lehigh University, Bethlehem, PA	Dr. Rick S. Blum Dept. Elec Engineering RL/OC
4	Effect of Concatenated Codes on the Transport of ATM-Based Traffic California Polytechnic State, San Luis Obispo, CA	Dr. Mostafa Chinichian Dept. of Engineering RL/C3
5	Development of Efficient Algorithms & Software Codes for Lossless and Near-Lossless Compression of Digitized Images Oakland University, Rochester, MI	Dr. Manohar K. Das Dept. Elec Engineering RL/IR
6	Mode-Locked Fiber Lasers Rensselaer Polytechnic Institution, Troy, NY	Dr. Joseph W. Haus Dept. of Physics RL/OC
7	Magnitude & Phase Measurements of Electromagnetic Fields Using Infrared University of Colorado, Colorado Springs, CO	Dr. John D. Norgard Dept. Elec Engineering RL/ER
8	Image Multiresolution Decomposition & Progressive Transmision Using Wavelets New Jersey Institute of Technology, Newark, NJ	Dr. Frank Y. Shih Dept. of Comp Science RL/IR
9	Investigation of Si-Based Quantum Well Intersubband Lasers University of Massachusetts-Boston, Boston, MA	Dr. Gang Sun Dept. of Physics RL/ER
10	Numerical Study of Bistatic Scattering from Land Surfaces at Grazing Incidence Oklahoma State University, Stillwater, OK	Dr. James C. West Dept. of Elec Engineering RL/ER

1996 SREP FINAL REPORTS

Wright Laboratory

VOLUME 4A

Report #	Author's University	Report Author
1	Barrel-Launched Adaptive Munition Experimental Round Research Auburn University, Auburn, AL	Dr. Ronald M. Barrett Dept. of Aerospace Eng WL/MN
2	Modeling & Design of New Cold Cathode Emitters & Photocathodes University of Cincinnati, Cincinnati, OH	Dr. Marc M. Cahay Dept. of Elec Engineering WL/EL
3	Unsteady Aerodynamics University of California-Berkeley, Berkeley, CA	Dr. Gary Chapman Dept. of Aerospace Eng WL/MN
4	Characteristics of the Texture Formed During the Annealing of Copper Plate University of Nebraska-Lincoln, Lincoln, NE	Dr. Robert J. DeAngelis Dept. of Mech Engineering WL/MN
5	Development of Perturbed Photoreflectance, Implementation of Nonlinear Optical Parametric Devices Bowling Green State University	Dr. Yujie J. Ding Dept. of Physics WL/EL
6	Computations of Drag Reduction & Boundary Layer Structure on a Turbine Blade with an Oscillating Bleed Flow University of Dayton, Dayton, OH	Dr. Elizabeth A. Ervin Dept. of Mech Engineering WL/PO
7	Low Signal to Noise Signal Processor for Laser Doppler Velocimetry North Carolina State University, Raleigh, NC	Dr. Richarad D. Gould Dept. of Mech Engineering WL/PO
8	Modeling & Control for Rotating Stall in Aeroengines Louisiana State University, Baton Rouge, LA	Dr. Guoxiang Gu Dept. of Elec Engineering WL/FI
9	Scaleable Parallel Processing for Real-time Rule-Based Decision Aids University of Missouri-Columbia, Columbia, MO	Dr. Chun-Shin Lin Dept. of Elec Engineering WL/FI
10	Quantitative Image Location & Processing in Ballistic Holograms University of West Florida, Pensacola, FL	Dr. James S. Marsh Dept. of Physics WL/MN
11	Experimental & Computational Investigation of Flame Suppression University of North Texas, Denton, TX	Dr. Paul Marshall Dept. of Chemistry WL/ML
12	Investigations of Shear Localization in Energetic Materials Systems University of Notre Dame, Notre Dame, IN	Dr. James J. Mason Dept. of Aerospace Eng WL/MN

Report #	Author's University	Report Author
13	A Time Slotted Approach to Real-Time Message Scheduling on SCI University of Nebraska-Lincoln, Lincoln, NE	Dr. Sarit Mukherjee Dept. of Comp Engineering WL/AA
14	Dielectric Resonator Measurements on High Temperature Superconductor (HTS) Wright State University, Dayton, OH	Dr. Krishna Naishadham Dept. Elec Engineering WL/ML
15	Modeling of Initiation & Propagation of Detonation Energetic Solids University of Notre Dame, Notre Dame, IN	Dr. Joseph M. Powers Dept. of Aerospace WL/MN
16	Robust control Design for Nonlinear Uncertain Systems by Merging University of Central Florida, Orlando, FL	Dr. Zhihua Qu Dept. of Elec Engineering WL/MN

1996 SREP FINAL REPORTS

Wright Laboratory

VOLUME 4B

Report #	Author's University	Report Author
17	HELPR: A Hybrid Evolutionary Learning System Wright State University, Dayton, OH	Dr. Mateen M. Rizki Dept. of Comp Engineering WL/AA
18	Virtual Materials Processing: automated Fixture Design for Materials Southern Illinois University-Carbondale, IL	Dr. Yiming K. Rong Dept. of Technology WL/ML
19	A Flexible Architecture for Communication Systems (FACS): Software AM Radio Wright State University, Dayton, OH	Dr. John L. Schmalzel Dept. of Engineering WL/AA
20	A Design Strategy for Preventing High Cycle Fatigue by Minimizing Sensitivity of Bladed Disks to Mistuning Wright State University, Dayton, OH	Dr. Joseph C. Slater Dept. of Mech Engineering WL/FI
21	Growth of Silicon Carbide Thin Films by Molecular Beam Epitaxy University of Cincinnati, Cincinnati, OH	Dr. Andrew J. Steckl Dept. of Elec Engineering WL/FI
22	Performance of Iterative & Noniterative Schemes for Image Restoration University of Arizona, Tucson, AZ	Dr. Malur K. Sundareshan Dept. of Elec Engineering WL/MN
23	Improving the Tribological Properties of Hard TiC Coatings University of New Orleans, New Orleans, IA	Dr. Jinke Tang Dept. of Physics WL/ML
24	Development of Massively Parallel Epic Hydrocode in Cray T3D Using PVM Florida Atlantic University, Boca Raton, FL	Dr. Chi-Tay Tsai Dept. of Mech Engineering WL/MN
25	Supramolecular Multilayer Assemblies w/Periodicities in a Submicron Range Western Michigan University, Kalamazoo, MI	Dr. Vladimir V. Tsukruk Dept. of Physics WL/ML
26	Distributed Control of Nonlinear Flexible Beams & Plates w/Mechanical & Temperature Excitations University of Kentucky, Lexington, KY	Dr. Horn-Sen Tzou Dept. of Mech Engineering WL/FI
27	A Progressive Refinement Approach to Planning & Scheduling University of Colorado-Denver, Denver, CO	Dr. William J. Wolfe Dept. of Comp Engineering WL/MT
28	Development of a New Numerical Boundary condition for Perfect Conductors University of Idaho, Moscow, OH	Dr. Jeffrey L. Young Dept. of Elec Engineering WL/FI

Report #	Author's University	Report Author
29	Eigenstructure Assignment in Missile Autopilot Design Using a Unified Spectral Louisiana State University, Baton Rouge, LA	Dr. Jianchao Zhu Dept. of Elec Engineering WL/FI
30	Design & Implementation of a GNSS Software Radio Receiver Ohio University, Athens, OH	Dr. Dennis M. Akos Dept. of Elec Engineering
31	Experimental & Numerical Study of Localized Shear as an Initiation Mechanism University of Notre Dame, Notre Dame, IN	Mr. Richard J. Caspar Dept. of Aero Engineering WL/MN
32	A Molecular-Level view of Solvation in Supercritical Fluid Systems State University of New York – Buffalo, Buffalo, NY	Ms. Emily D. Niemeyer Dept. of Chemistry WL/PO
33	Initiation of Explosives by High Shear Strain Rate Impact University of Notre Dame, Notre Dame, IN	Mr. Keith M. Roessig Dept. of Aero Engineering WL/MN

1996 SREP FINAL REPORTS

VOLUME 5

Report #	Author's University	Report Author
	Arnold Engineering Development Center	
1	**Facility Health Monitoring & Diagnosis** **Vanderbilt University, Nashville, TN**	**Dr. Theodore Bapty** **Dept. of Elec Engineering** **AEDC**
	Air Logistic Centers	
2	**Fatigue Crack Growth Rates in Naturally-Coroded Aircraft Aluminum** **University of Oklahome, Norman, OK**	**Dr. James D. Baldwin** **Dept. of Mech Engineering** **OCALC**
3	**A Novel Artificial Neural Network Classifier for Multi-Modal** **University of Toledo, Toledo, OH**	**Dr. Gursel Serpen** **Dept. of Elec Engineering** **OOALC**
4	**Development of a Cost-Effective Organizational Information System** **West Virginia University, Morgantown, WV**	**Dr. Michael D. Wolfe** **Dept. Mgmt Science** **SAALC**
5	**Implementation of a Scheduling Software w/Shop Floor Parts Tracking Sys** **University of Wisconsin-Stout, Menomonie, WI**	**Dr. Norman D. Zhou** **Dept. of Technology** **SMALC**
6	**Development of a High Performance Electric Vehicle Actuator System** **Clarkson University, Potsdam, NY**	**Dr. James J. Carroll** **Dept. Elec Engineering** **WRALC**

1996 SUMMER RESEARCH EXTENSION PROGRAM (SREP) MANAGEMENT REPORT

1.0 BACKGROUND

Under the provisions of Air Force Office of Scientific Research (AFOSR) contract F49620-90-C-0076, September 1990, Research & Development Laboratories (RDL), an 8(a) contractor in Culver City, CA, manages AFOSR's Summer Research Program. This report is issued in partial fulfillment of that contract (CLIN 0003AC).

The Summer Research Extension Program (SREP) is one of four programs AFOSR manages under the Summer Research Program. The Summer Faculty Research Program (SFRP) and the Graduate Student Research Program (GSRP) place college-level research associates in Air Force research laboratories around the United States for 8 to 12 weeks of research with Air Force scientists. The High School Apprenticeship Program (HSAP) is the fourth element of the Summer Research Program, allowing promising mathematics and science students to spend two months of their summer vacations working at Air Force laboratories within commuting distance from their homes.

SFRP associates and exceptional GSRP associates are encouraged, at the end of their summer tours, to write proposals to extend their summer research during the following calendar year at their home institutions. AFOSR provides funds adequate to pay for 75 SREP subcontracts. In addition, AFOSR has traditionally provided further funding, when available, to pay for additional SREP proposals, including those submitted by associates from Historically Black Colleges and Universities (HBCUs) and Minority Institutions (MIs). Finally, laboratories may transfer internal funds to AFOSR to fund additional SREPs. Ultimately the laboratories inform RDL of their SREP choices, RDL gets AFOSR approval, and RDL forwards a subcontract to the institution where the SREP associate is employed. The subcontract (see Appendix 1 for a sample) cites the SREP associate as the principal investigator and requires submission of a report at the end of the subcontract period.

Institutions are encouraged to share costs of the SREP research, and many do so. The most common cost-sharing arrangement is reduction in the overhead, fringes, or administrative charges institutions would normally add on to the principal investigator's or research associate's labor. Some institutions also provide other support (e.g., computer run time, administrative assistance, facilities and equipment or research assistants) at reduced or no cost.

When RDL receives the signed subcontract, we fund the effort initially by providing 90% of the subcontract amount to the institution (normally $18,000 for a $20,000 SREP). When we receive the end-of-research report, we evaluate it administratively and send a copy to the laboratory for a technical evaluation. When the laboratory notifies us the SREP report is acceptable, we release the remaining funds to the institution.

2.0 THE 1996 SREP PROGRAM

SELECTION DATA: A total of 516 faculty members (SFRP Associates) and 250 graduate students (GSRP associates) applied to participate in the 1994 Summer Research Program. From these applicants 190 SFRPs and 115 GSRPs were selected. The education level of those selected was as follows:

1995 SRP Associates, by Degree			
SFRP		GSRP	
PHD	MS	MS	BS
186	4	55	53

Of the participants in the 1995 Summer Research Program 75 percent of SFRPs and 16 percent of GSRPs submitted proposals for the SREP. Seventy-three proposals from SFRPs and five from GSRPs were selected for funding, which equates to a selection rate of 51% of the SFRP proposals and of 28% for GSRP proposals.

1996 SREP: Proposals Submitted vs. Proposals Selected			
	Summer 1995 Participants	Submitted SREP Proposals	SREPs Funded
SFRP	190	143	73
GSRP	115	18	5
TOTAL	305	161	78

The funding was provided as follows:

Contractual slots funded by AFOSR	58
Laboratory funded	20
Total	78

Proposals Submitted and Selected, by Laboratory		
	Applied	Selected
Armstrong Laboratory	38	15
Air Logistic Centers	7	4
Arnold Engineering Development Center	1	1
Frank J. Seiler Research Laboratory	2	0
Phillips Laboratory	31	15
Rome Laboratory	18	10
Wilford Hall Medical Center	1	0
Wright Laboratory	63	33
TOTAL	161	78

Note: Phillips Laboratory funded 4 SREPs; and Wright Laboratory funded 16

The 305 1995 Summer Research Program participants represented 135 institutions.

Institutions Represented on the 1995 SRP and 1996 SREP		
Number of schools represented in the Summer 95 Program	Number of schools represented in submitted proposals	Number of schools represented in Funded Proposals
135	106	66

Twenty schools had more than one participant submitting proposals.

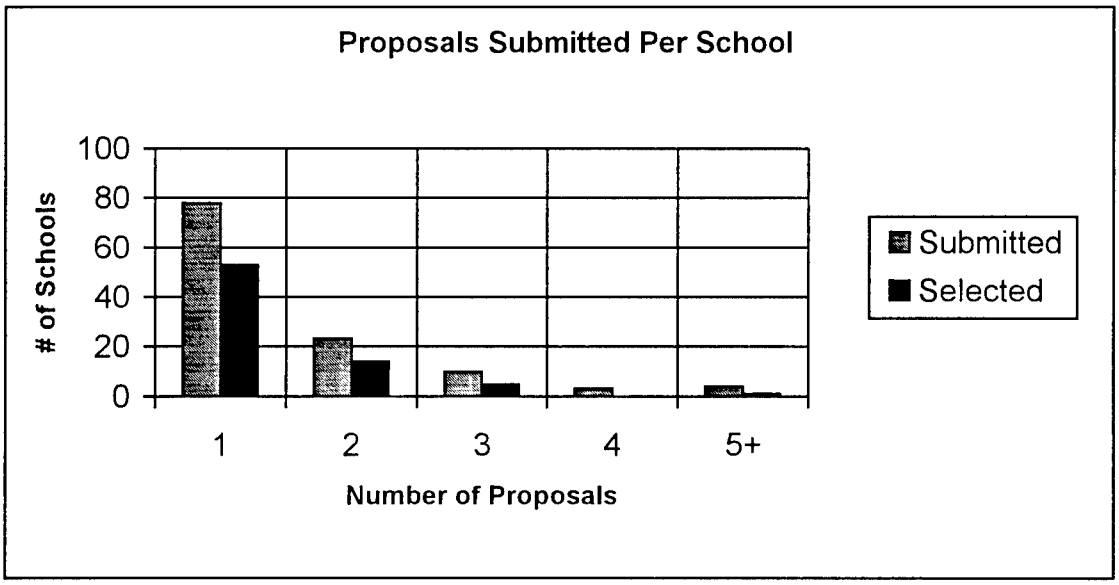

The selection rate for the 78 schools submitting 1 proposal (68%) was better than those submitting 2 proposals (61%), 3 proposals (50%), 4 proposals (0%) or 5+ proposals (25%). The 4 schools that submitted 5+ proposals accounted for 30 (15%) of the 161 proposals submitted.

Of the 161 proposals submitted, 57 offered institution cost sharing. Of the funded proposals which offered cost sharing, the minimum cost share was $3000.00, the maximum was $51,000.00 with an average cost share of $13,266.56.

Proposals and Institution Cost Sharing		
	Proposals Submitted	Proposals Funded
With cost sharing	161	57
Without cost sharing	104	21
Total	265	78

The SREP participants were residents of 30 different states. Number of states represented at each laboratory were:

States Represented, by Proposals Submitted/Selected per Laboratory		
	Proposals Submitted	Proposals Funded
Armstrong Laboratory	27	15
Arnold Engineering Development Center	8	1
Air Logistics Centers	11	4
Phillips Laboratory	33	15
Rome Laboratory	22	10
US Air Force Academy	0	0
Wilford Hall Medical Center	0	0
Wright Laboratory	61	33

Eleven of the 1996 SREP Principal Investigators also participated in the 1995 SREP.

ADMINISTRATIVE EVALUATION: The administrative quality of the SREP associates' final reports was satisfactory. Most complied with the formatting and other instructions provided to them by RDL. Seventy-eight final reports have been received and are included in this report. The subcontracts were funded by $499,972.00 of Air Force money. Institution cost sharing totaled $138,340.00.

TECHNICAL EVALUATION: The form used for the technical evaluation is provided as Appendix 2. ninety-two evaluation reports were received. Participants by laboratory versus evaluations submitted is shown below:

	Participants	Evaluations	Percent
Armstrong Laboratory	15	15	100
Air Logistics Centers	4	4	100
Arnold Engineering Development Center	1	1	100
Phillips Laboratory	15	15	100
Rome Laboratory	10	10	100
Wright Laboratory	33	33	100
Total	78	78	100

The number of evaluations submitted for the 1996 SREP (100%) shows a marked improvement over the 1995 SREP submittals (65%).

PROGRAM EVALUATION: Each laboratory focal point evaluated ten areas (see Appendix 2) with a rating from one (lowest) to five (highest). The distribution of ratings was as follows:

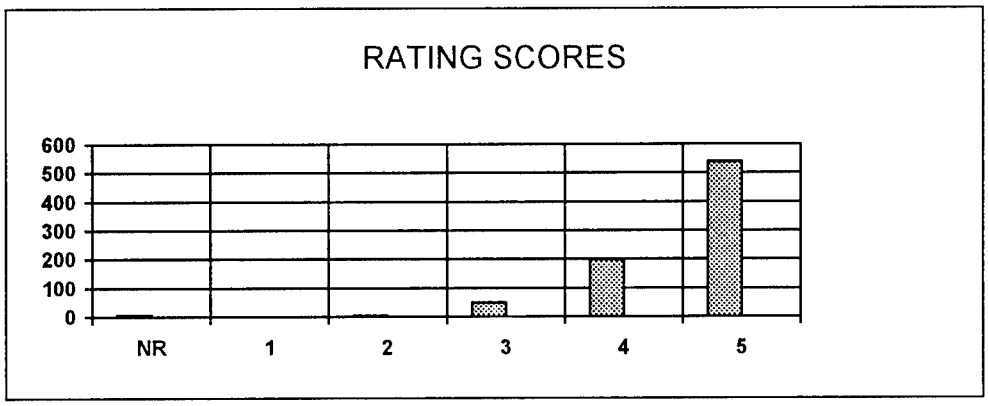

Rating	Not Rated	1	2	3	4	5
# Responses	7	1	7	62 (6%)	226 (25%)	617 (67%)

The 8 low ratings (one 1 and seven 2's) were for question 5 (one 2) "The USAF should continue to pursue the research in this SREP report" and question 10 (one 1 and six 2's) "The one-year period for complete SREP research is about right", in addition over 30% of the threes (20 of 62) were for question ten. The average rating by question was:

Question	1	2	3	4	5	6	7	8	9	10
Average	4.6	4.6	4.7	4.7	4.6	4.7	4.8	4.5	4.6	4.0

The distribution of the averages was:

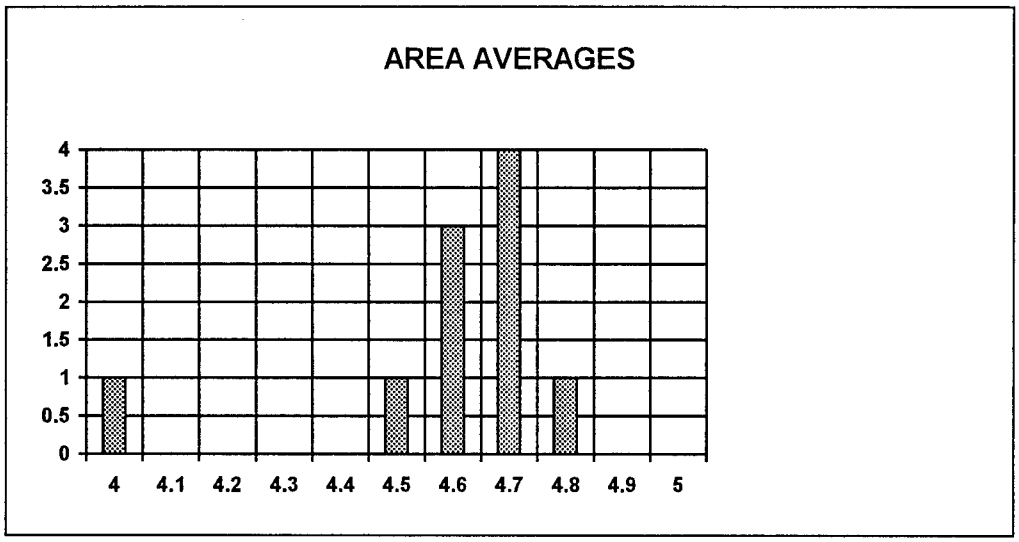

Area 10 "the one-year period for complete SREP research is about right" had the lowest average rating (4.1). The overall average across all factors was 4.6 with a small sample standard deviation of 0.2. The average rating for area 10 (4.1) is approximately three sigma lower than the overall average (4.6) indicating that a significant number of the evaluators feel that a period of other than one year should be available for complete SREP research.

The average ratings ranged from 3.4 to 5.0. The overall average for those reports that were evaluated was 4.6. Since the distribution of the ratings is not a normal distribution the average of 4.6 is misleading. In fact over half of the reports received an average rating of 4.8 or higher. The distribution of the average report ratings is as shown:

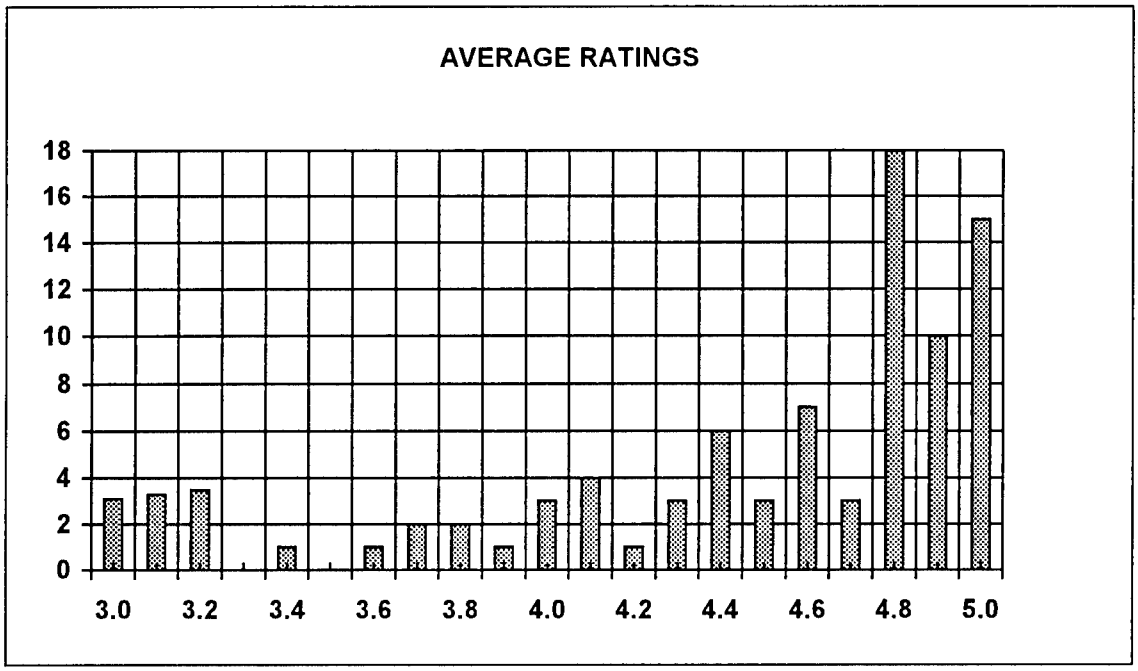

It is clear from the high ratings that the laboratories place a high value on AFOSR's Summer Research Extension Programs.

3.0 SUBCONTRACTS SUMMARY

Table 1 provides a summary of the SREP subcontracts. The individual reports are published in volumes as shown:

Laboratory	Volume
Armstrong Laboratory	1
Arnold Engineering Development Center	5
Air Logistics Centers	5
Phillips Laboratory	2
Rome Laboratory	3
Wright Laboratory	4A, 4B

SREP SUB-CONTRACT DATA

Report Author Author's University	Author's Degree	Sponsoring Lab	Performance Period		Contract Amount	Univ. Cost Share
Allen-King , Richelle **Earth Sciences** **Washington State University, Pullman, WA**	**PhD** 96-0810	**AL/EQ** Chlorinated Ethene Transformation,Sorption & Product Distr in Metallic Iron/Wate	**01/01/96**	**12/31/96**	**$25000.00**	**$4779.00**
Bennett , Kevin **Applied Experimental Psychology** **Wright State University, Dayton, OH**	**PhD** 96-0816	**AL/CF** A Dynamically Adaptive Interface for Precision, Low-Level Navigation Tasks	**01/01/96**	**12/31/96**	**$25000.00**	**$5768.00**
Bordetsky , Alexander **Decision Sciences** **California State University, Hayward, CA**	**PhD** 96-0807	**AL/HR** Geographically Distributed Collaborative Work Environment Requirements Analysis	**01/01/96**	**12/31/96**	**$24967.00**	**$3000.00**
Guttenplan , Joseph **Chemistry** **New York Univ Dental/Medical School, New**	**PhD** 96-0814	**AL/OE** Development of Fluorescence Post Labelling Assay for DNA Adducts:Chloroacetaldeh	**01/01/96**	**12/31/96**	**$25000.00**	**$23017.00**
Kulkarni , Pandurang **Statistics** **University of South Alabama, Mobile, AL**	**PhD** 96-0809	**AL/AO** The Checkmark Pattern & Regression to the Mean in Dioxin Half Life Studies	**06/15/96**	**12/15/96**	**$24614.00**	**$4212.00**
Labare , Michael **Marine Estuarine Sciences** **Mount Saint Mary College, Newburgh, NY**	**PhD** 96-0811	**AL/EQ** Determination of the Enzymatic Constraints Limiting the Growth of Pseudomonas	**01/01/96**	**12/31/96**	**$19415.00**	**$0.00**
Lavine , Barry **Chemistry** **Clarkson University, Potsdam, NY**	**PhD** 96-0812	**AL/EQ** Tuned Selectivity Solid Phase Microextraction	**01/01/96**	**12/31/96**	**$25000.00**	**$11180.00**
Mahan , Robert **Applied Cognitive Psychology** **University of Georgia, Athens, GA**	**PhD** 96-0815	**AL/CF** A Cognitive Engineering Approach to Distributed Team Decision Making During Sust	**01/01/96**	**12/31/96**	**$24334.00**	**$14256.00**
McAlister , Sandra **Biology** **Stonehill College, North Easton, MA**	**PhD** 96-0808	**AL/AO** Repetative Sequence Based PCR:An Epidemiological Study of A Streptococcus	**01/15/96**	**05/15/96**	**$25000.00**	**$8200.00**
Musicant , Alan **Behavioral Science** **Middle Tennessee State Univ, Murfreesbord, TN**	**PhD** 96-0817	**AL/CF** An Investigation into the Efficacy of Headphone Listening for Localization of So	**01/01/96**	**12/31/96**	**$24721.00**	**$4452.00**
Sadegh , Ali **Mechanics** **CUNY-City College, New York, NY**	**PhD** 96-0818	**AL/CF** The Neck Models to Predict Human Tolerance in a G-Y Acceleration	**01/01/96**	**12/31/96**	**$25000.00**	**$13191.00**
Wise , William **Dept. of Civil Engineering** **University of Florida, Gainesville, FL**	**PhD** 96-0813	**AL/EQ** Tracer Methodology Development for Enhanced Passive Ventilation for Soil Venting	**01/01/96**	**12/31/96**	**$25000.00**	**$11193.00**
Woehr , David **Department of Psychology** **Texas A & M Univ-College Station, College**	**PhD** 96-0806	**AL/HR** Application of a Distribution-Based Assessment of Mission Readiness Sys	**01/01/96**	**12/31/96**	**$24989.00**	**$16783.00**
Fournier , Lisa **Experimental Psychology** **Washington State University, Pullman, WA**	**PhD** 96-0819	**AL/CF** Electrophysiological,Behavioral,&Subjective Indexes of Workload When Performing	**01/01/96**	**12/31/96**	**$25000.00**	**$6589.00**
Nemeth , Kristie **Psychology** **Miami University, Oxford, OH**	**MA** 96-0805	**AL/HR** Methods for Establishing Design Limits to Ensure Accomodation	**01/01/96**	**12/31/96**	**$24992.00**	**$3703.00**

SREP SUB-CONTRACT DATA

Report Author Author's University	Author's Degree	Sponsoring Lab	Performance Period	Contract Amount	Univ. Cost Share
Bapty , Theodore **Electrical Engineering** **Vanderbilt University, Nashville, TN**	**PhD** 96-0801	**AEDC/E** Facility Health Monitoring & Diagnosis	**01/01/96 12/31/96**	**$24960.00**	**$0.00**
Baldwin , James **Mechanical Engineering** **University of Oklahoma, Norman, OK**	**PhD** 96-0802	**ALC/OC** Fatigue Crack Growth Rates in Naturally-Corroded Aircraft Aluminum	**01/01/96 12/31/96**	**$24986.00**	**$16184.00**
Serpen , Gursel **Dept of Elect Eng & Comp Science** **The University of Toledo, Toledo, OH**	**PhD** 96-0804	**ALC/O** A Novel Artificial Neural Network Classifier for Multi-Modal Distributed Classes	**01/01/96 12/31/96**	**$25000.00**	**$22425.00**
Belen'kii , Mikhail **Philosophy** **Georgia Tech Res Corp, Atlanta, GA**	**PhD** 96-0833	**PL/LI** Experimental Study of the Tilt Angular Anisopalantaic Correlation & the Effect o	**01/01/96 12/31/96**	**$25000.00**	**$0.00**
Bukofzer , Daniel **Electrical & Computer Engineering** **Cal State Univ, Fresno, Fresno, CA**	**PhD** 96-0822	**PL/VT** Performance EValuations & Computer Simulations of Synchronous & Asynchronous	**01/01/96 12/31/96**	**$25000.00**	**$4405.00**
Chang , Chia-Bo **Geosciences/Atomospheric Science** **Texas Tech University, Lubbock, TX**	**PhD** 96-0823	**PL/GP** MM4 Model Experiments on the Effects of Cloud Shading	**01/01/96 12/31/96**	**$24984.00**	**$13495.00**
Diels , Jean-Claude **Physics** **University of New Mexico, Albuquerque, NM**	**PhD** 96-0824	**PL/LI** Miniature Laser Gyro Consisting in a Pair of Unidirectional Ring Lasers	**01/01/96 12/31/96**	**$25000.00**	**$0.00**
Joshi , Ravindra **Electrical & Computer Engineering** **Old Dominion University, Norfolk, VA**	**PhD** 96-0825	**PL/WS** Simulations & Theoretical Studies of Ultrafast Silicon Avalanche	**01/01/96 12/31/96**	**$25000.00**	**$11552.00**
Kalluri , Dikshitulu **Electrical Engineering** **University of Lowell, Lowell, MA**	**PhD** 96-0883	**PL/GP** Theory of Wave Propagation in a Time-Varying Magnetoplasma Medium & Applications	**01/01/96 12/31/96**	**$25000.00**	**$10645.00**
Kar , Aravinda **Engineering** **University of Central Florida, Orlando, FL**	**PhD** 96-0834	**PL/LI** Thermal Analysis for the Applications of High Power Lasers in Large-Area Materia	**01/01/96 12/31/96**	**$25000.00**	**$5027.00**
Krile , Thomas **Electrical Engineering** **Texas Tech University, Lubbock, TX**	**PhD** 96-0826	**PL/LI** Analytical Noise Modeling & Optimization of A Phasor-Based Phase Reconstruction	**01/01/96 12/31/96**	**$25000.00**	**$19572.00**
Lodhi , M. Arfin **Nuclear Physics** **Texas Tech University, Lubbock, TX**	**PhD** 96-0827	**PL/VT** Mathematical Modeling of Thermionic-AMTEC Cascade Sys for Space Power	**01/01/96 12/31/96**	**$25000.00**	**$20182.00**
Noel , Charles **Chemistry** **Ohio State University, Columbus, OH**	**PhD** 96-0828	**PL/RK** Preparation & Characterization of Polymer Blends	**01/01/96 12/31/96**	**$24950.00**	**$25455.00**
Ordonez , Carlos **Physics** **Univ of Texas at Denton, Denton, TX**	**PhD** 96-0829	**PL/WS** Evaluation of Particle & Energy Transport to Anode,Cathode,& Electrically-Floati	**01/01/96 12/31/96**	**$25000.00**	**$11401.00**
Pickett , Ronald **Experimental Psychology** **University of Lowell, Lowell, MA**	**PhD** 96-0830	**PL/GP** Analyses of the Structure & Motion of Equatorial Emission Depletion Bands	**01/01/96 12/31/96**	**$25000.00**	**$0.00**

SREP SUB-CONTRACT DATA

Report Author Author's University	Author's Degree	Sponsoring Lab	Performance Period	Contract Amount	Univ. Cost Share
Poulikakos , Dimos **Mechanical Engineering** **Univ of Illinois at Chicago, Chicago, IL**	**PhD** 96-0831	**PL/RK** On the Fluid Dynamics of High Pressure Atomization in Rocket Propulsion	**01/01/96 12/31/96**	**$24995.00**	**$3200.00**
Rudolph , Wolfgang **Physics** **University of New Mexico, Albuquerque, NM**	**PhD** 96-0835	**PL/LI** Gigahertz Modulation & Ultrafast Gain Build-up in Iodine Lasers	**01/01/96 12/31/96**	**$24982.00**	**$0.00**
Watt , David **Mechanical Engineering** **University of New Hampshire, Durham, NH**	**PhD** 96-0832	**PL/GP** Inversion of Hyperspectral Atmospheric Radiance Images for the Measurement of Te	**01/01/96 12/31/96**	**$25000.00**	**$6918.00**
Aalo , Valentine **Dept of Electrical Engr** **Florida Atlantic University, Boca Raton, FL**	**PhD** 96-0859	**RL/C3** Performance Analysis of an ATM-Satellite System	**01/01/96 12/31/96**	**$25000.00**	**$13485.00**
Benjamin , David **Computer Science** **Syracuse University, Syracuse, NY**	**PhD** 96-0860	**RL/C3** Reformulating Domain Theories to Improve Their Computational Usefulness	**01/01/96 12/31/96**	**$24807.00**	**$0.00**
Blum , Ricky **Electrical Engineering** **Lehigh University, Bethlehem, PA**	**PhD** 96-0868	**RL/OC** An Analysis of the Adaptive Displaced Phase Centered Antenna Space-Time Processi	**01/01/96 12/31/96**	**$25000.00**	**$0.00**
Chinichian , Mostafa **California Polytechnic State University, San Luis**	**PhD** 96-0861	**RL/C3** Effect of Concatenated Codes on the Transport of ATM-Based Traffic by Satellite	**01/01/96 12/31/96**	**$25000.00**	**$4694.00**
Das , Manohar **Electrical Engineering** **Oakland University, Rochester, MI**	**PhD** 96-0865	**RL/IR** Development of Efficient Algorithms & Software Codes for Lossless & Near-Lossles	**01/01/96 12/31/96**	**$25000.00**	**$9296.00**
Haus , Joseph **Physics** **Rensselaer Polytechnic Institution, Troy, NY**	**PhD** 96-0867	**RL/OC** Modelocked Fiber Lasers	**01/01/96 12/31/96**	**$25000.00**	**$0.00**
Norgard , John **Electrical Engineering** **Univ of Colorado at Colorado Springs, Colorado**	**PhD** 96-0862	**RL/ER** Magnitude & Phase Measurements of Electromagnetic Fields Using Infrared Thermogr	**01/01/96 12/31/96**	**$25000.00**	**$2500.00**
Shih , Frank **Computer/Information Science** **New Jersey Inst of Technology, Newark, NJ**	**PhD** 96-0866	**RL/IR** Image Multiresoluton Decomposition & Progressive Transmission Using Wavelets	**01/01/96 12/31/96**	**$25000.00**	**$51575.00**
Sun , Gang **Physics** **Univ of Massachusetts - Boston, Boston, MA**	**PhD** 96-0863	**RL/ER** Investigation of Si Based Quantum Well Intersubband Lasers	**01/01/96 12/31/96**	**$24999.00**	**$10854.00**
West , James **Electrical Engineering** **Oklahoma State University, Stillwater, OK**	**PhD** 96-0864	**RL/ER** Numerical Study of Bistatic Scattering From Land Surfaces at Grazing Incidence	**01/01/96 12/31/96**	**$25000.00**	**$11250.00**
Wolfe , Michael **Management Science** **West Virginia University, Morgantown, WV**	**PhD** 96-0803	**ALC/SA** Development of a Cost-Effective Organizational Information System in Support of	**01/01/96 12/31/96**	**$25000.00**	**$0.00**
Zhou , Norman **Technology Department** **University of Wisconsin-Stout, Menomonie, WI**	**PhD** 96-0821	**ALC/SM** Implementation of a Scheduling Software w/Shop Floor Parts Tracking Sys @ Mfg &	**01/01/96 12/31/96**	**$25000.00**	**$9708.00**

SREP SUB-CONTRACT DATA

Report Author Author's University	Author's Degree	Sponsoring Lab	Performance Period	Contract Amount	Univ. Cost Share
Barrett , Ronald **Aerospace Engineering** **Auburn University, Auburn, AL**	**PhD** 96-0869	**WL/MN**	**01/01/96 12/31/96** Barrel-Launched Adaptive Munition Experimental Round Research	**$25000.00**	**$0.00**
Cahay , Marc **Electrical Engineering** **University of Cincinnati, Cincinnati, OH**	**PhD** 96-0878	**WL/EL**	**01/01/96 09/30/96** Modeling & Design of New Cold Cathode Emitters & Photocathodes	**$24998.00**	**$20760.00**
Carroll , James **Electrical Engineering** **Clarkson University, Potsdam, NY**	**PhD** 96-0874	**ALC/WR**	**01/01/96 12/31/96** Development of a High Performance Electric Vehicle Actuator System	**$25000.00**	**$11180.00**
Chapman , Gary **Aerospace Engineering/Astronomy** **Univ of Calif, Berkeley, Berkeley, CA**	**PhD** 96-0879	**WL/MN**	**01/01/96 12/31/96** Unsteady Aerodynamics	**$25000.00**	**$0.00**
DeAngelis , Robert **Materials Science** **Univ of Nebraska - Lincoln, Lincoln, NE**	**PhD** 96-0846	**WL/MN**	**01/01/96 12/31/96** Characteristics of the Texture Formed During the Annealing of Copper Plate	**$25000.00**	**$35833.00**
Ding , Yujie **Nonlinear Optics, Optoelectronics,** **Bowling Green State University, Bowling Green,**	**PhD** 96-0848	**WL/EL**	**01/01/96 12/31/96** Development of Perturbed Photoreflectance, Implementation of Nonlinear Optical	**$25000.00**	**$17659.00**
Ervin , Elizabeth **Mechanical Engineering** **University of Dayton, Dayton, OH**	**PhD** 96-0853	**WL/PO**	**01/01/96 12/31/96** Computations of Drag Reduction & Boundary Layer Structure on a Turbine Blade	**$24977.00**	**$22007.00**
Gould , Richard **Mechanical Engineering** **North Carolina State U-Raleigh, Raleigh, NC**	**PhD** 96-0855	**WL/PO**	**01/01/96 12/31/96** Low Signal to Noise Signal Processor for Laser Doppler Velocimetry	**$25000.00**	**$14679.00**
Gu , Guoxiang **Electrical Engineering** **Louisiana State University, Baton Rouge, LA**	**PhD** 96-0840	**WL/FI**	**01/01/96 12/31/96** Modeling & Control for Rotating Stall in Aeroengines	**$25000.00**	**$18323.00**
Lin , Chun-Shin **Electrical Engineering** **Univ of Missouri-Columbi, Columbia, MO**	**PhD** 96-0876	**WL/FI**	**01/01/96 12/31/96** Scaleable Parallel Processing for Real-Time Rule-Based Decision Aids	**$25000.00**	**$2568.00**
Marsh , James **Physics** **University of West Florida, Pensacola, FL**	**PhD** 96-0858	**WL/MN**	**01/01/96 05/06/96** Quantitative Image Location & Processing in Ballistic Holograms	**$24998.00**	**$3840.00**
Marshall , Paul **Chemistry** **University of North Texas, Denton, TX**	**PhD** 96-0849	**WL/ML**	**01/01/96 12/31/96** Experimental & Computational Investigations of Flame Suppression	**$25000.00**	**$19095.00**
Mason , James **Applied Mechanics** **University of Notre Dame, Notre Dame, IN**	**PhD** 96-0847	**WL/MN**	**01/01/96 12/31/96** Investigations of Shear Localization in Energetic Matls Systems	**$25000.00**	**$0.00**
Mukherjee , Sarit **Computer Science & Engineering** **University of Nebraska/Lincoln, Lincoln, NE**	**PhD** 96-0842	**WL/AA**	**01/01/96 12/31/96** A Time-Slotted Approach to Real-Time Message Scheduling on SCI	**$25000.00**	**$19996.00**
Naishadham , Krishna **Electrical Engineering** **Wright State University, Dayton, OH**	**PhD** 96-0820	**WL/ML**	**01/01/96 12/31/96** Dielectric Resonator Measurements on High Temperture Superconductors	**$25000.00**	**$6146.00**

SREP SUB-CONTRACT DATA

Report Author Author's University	Author's Degree	Sponsoring Lab	Performance Period	Contract Amount	Univ. Cost Share
Powers , Joseph **Mechanical Engineering** **University of Notre Dame, Notre Dame, IN**	**PhD** 96-0870	**WL/MN**	**01/01/96 12/31/96** Modeling of Initiatin & Propagation of Detonation in Ener	**$25000.00**	**$0.00**
Qu , Zhihua **Systems & Controls** **University of Central Florida, Orlando, FL**	**PhD** 96-0845	**WL/MN**	**01/01/96 12/31/96** Robust Control Design for Nonlinear Uncertain Systems by Merging Lyapunov-Based	**$25000.00**	**$2998.00**
Rizki , Mateen **Computer Science** **Wright State University, Dayton, OH**	**PhD** 96-0881	**WL/AA**	**01/01/96 12/31/96** HELPR: A Hybrid Evolutionary Learning Sys for Pattern Recognition	**$25000.00**	**$14672.00**
Rong , Yiming **Mechanical Engineering** **Southern Illinois U-Carbondale, Carbondale, IL**	**PhD** 96-0851	**WL/ML**	**01/01/96 12/31/96** Virtual Matl's Processing: Automated Fixture Design for Matl's & Process Design	**$25000.00**	**$41734.00**
Schmalzel , John **Engineering** **Rowan College of New Jersey, Glassboro, NJ**	**PhD** 96-0877	**WL/AA**	**01/01/96 12/31/96** A Flexible Architecture for Communication Systems (FACS):Software AM Radio	**$25000.00**	**$25000.00**
Slater , Joseph **Dynamics & Control** **Wright State University, Dayton, OH**	**PhD** 96-0839	**WL/FI**	**01/01/96 12/31/96** A Design Strategy for Preventing High Cycle Fatigue by Minimizing Sensitivity of	**$25000.00**	**$5575.00**
Steckl , Andrew **Electrical and Computer** **University of Cincinnati, Cincinnati, OH**	**PhD** 96-0850	**WL/ML**	**01/01/96 12/31/96** Growth of Silicon Carbide Thin Films by Molecular Beam Epitaxy	**$25000.00**	**$29719.00**
Sundareshan , Malur **Electrical and Computer** **University of Arizona, Tucson, AZ**	**PhD** 96-0844	**WL/MN**	**01/01/96 12/31/96** Performance of Iterative & Noniterative Schemes for Image Restoration	**$25000.00**	**$18893.00**
Tang , Jinke **Physics** **University of New Orleans, New Orleans, LA**	**PhD** 96-0838	**WL/ML**	**01/01/96 12/31/96** Improving the Tribological Properties of Hard TiC Coatings	**$25000.00**	**$10250.00**
Tsai , Chi-Tay **Engineering Mechanics** **Florida Atlantic University, Boca Raton, FL**	**PhD** 96-0857	**WL/MN**	**01/01/96 12/31/96** Development of Massively Parallel Epic Hydrocode in Cray T3D Using PVM	**$25000.00**	**$0.00**
Tsukruk , Vladimir **Physics** **Western Michigan University, Kalamazoo, MI**	**PhD** 96-0836	**WL/ML**	**01/01/96 12/31/96** Supramolecular Multilayer Assemblies w/Periodicities in a Submicron Range	**$25000.00**	**$4100.00**
Tzou , Horn-Sen **Mechanical Engineering** **University of Kentucky, Lexington, KY**	**PhD** 96-0882	**WL/FI**	**01/01/96 12/31/96** Distributed Control of Nonlinear Flexible Beams & Plates w/Mechanical & Temp	**$25000.00**	**$25931.00**
Wolfe , William **Mathematics** **Univ of Colorado at Denver, Denver, CO**	**PhD** 96-0852	**WL/MT**	**01/01/96 12/31/96** A Progressive Refinement Approach to Planning & Scheduling	**$24996.00**	**$0.00**
Young , Jeffrey **Electrical Engineering** **University of Idaho, Moscow, ID**	**PhD** 96-0841	**WL/FI**	**01/01/96 12/31/96** Development of a New Numerical Boundary Condition for Perfect Conductors	**$24326.00**	**$11564.00**
Zhu , Jianchao (Jim) **Electrical Engineering** **LSU Agri/Mech College, Baton Rouge, LA**	**PhD** 96-0856	**WL/MN**	**01/01/96 12/31/96** Eigenstructure Assignment in Missile autopilot Design Using A Unified Spectral	**$24994.00**	**$9401.00**

SREP SUB-CONTRACT DATA

Report Author Author's University	Author's Degree	Sponsoring Lab	Performance Period		Contract Amount	Univ. Cost Share
Akos , Dennis **Electrical & Computer Engineering** **Ohio University, Athens, OH**	**MS** 96-0843	**WL/AA** Design&Implementation of a GNSS Software Radio Receiver	**01/01/96**	**12/31/96**	**$25000.00**	**$0.00**
Caspar , Richard **Mechanical Engineering** **University of Notre Dame, Notre Dame, IN**	**BS** 96-0871	**WL/MN** Experimental & Numerical Study of Localized Shear As An Initiation Mechanism	**01/01/96**	**07/31/96**	**$25000.00**	**$0.00**
Niemeyer , Emily **Chemistry** **SUNY Buffalo, Buffalo, NY**	**BS** 96-0854	**WL/PO** A Molecular-Level View of Solvation in Supercritical Fluid Systems	**01/01/96**	**12/31/96**	**$25000.00**	**$8553.00**
Roessig , Keith **Aeronautical Engineering** **University of Notre Dame, Notre Dame, IN**	**BS** 96-0872	**WL/MN** Initiation of Explosives by High Shear Strain Rate Impact	**01/01/96**	**12/31/96**	**$25000.00**	**$0.00**

APPENDIX 1:

SAMPLE SREP SUBCONTRACT

AIR FORCE OFFICE OF SCIENTIFIC RESEARCH
1996 SUMMER RESEARCH EXTENSION PROGRAM
SUBCONTRACT 96-0881

BETWEEN

Research & Development Laboratories
5800 Uplander Way
Culver City, CA 90230-6608

AND

Wright State University
Research and Sponsored Programs
Dayton, OH 45435

REFERENCE: Summer Research Extension Program Proposal 95-0117
Start Date: 01/01/96 End Date: 12/31/96
Proposal Amount: $25,000
Proposal Title: "HELPR: A Hybrid Evolutionary Learning System For Pattern Recognition

(1) PRINCIPAL INVESTIGATOR:

Dr. Mateen M. Rizki
Dept. of Computer Science & Engineering
Wright State University
Dayton, OH 45435

(2) UNITED STATES AFOSR CONTRACT NUMBER: F49620-93-C-0063

(3) CATALOG OF FEDERAL DOMESTIC ASSISTANCE NUMBER (CFDA): 12.800
PROJECT TITLE: AIR FORCE DEFENSE RESEARCH SOURCES PROGRAM

(4) ATTACHMENTS
1 **REPORT OF INVENTIONS AND SUBCONTRACT**
2 **CONTRACT CLAUSES**
3 **FINAL REPORT INSTRUCTIONS**

*****SIGN SREP SUBCONTRACT AND RETURN TO RDL*****

1. BACKGROUND: Research & Development Laboratories (RDL) is under contract (F49620-93-C-0063) to the United States Air Force to administer the Summer Research Program (SRP), sponsored by the Air Force Office of Scientific Research (AFOSR), Bolling Air Force Base, D.C. Under the SRP, a selected number of college faculty members and graduate students spend part of the summer conducting research in Air Force laboratories. After completion of the summer tour participants may submit, through their home institutions, proposals for follow-on research. The follow-on research is known as the Summer Research Extension Program (SREP). Approximately 61 SREP proposals annually will be selected by the Air Force for funding of up to $25,000; shared funding by the academic institution is encouraged. SREP efforts selected for funding are administered by RDL through subcontracts with the institutions. This subcontract represents an agreement between RDL and the institution herein designated in Section 5 below.

2. RDL PAYMENTS: RDL will provide the following payments to SREP institutions:
    - 80 percent of the negotiated SREP dollar amount at the start of the SREP research period.
    - The remainder of the funds within 30 days after receipt at RDL of the acceptable written final report for the SREP research.

3. INSTITUTION'S RESPONSIBILITIES: As a subcontractor to RDL, the institution designated on the title page will:

a. Assure that the research performed and the resources utilized adhere to those defined in the SREP proposal.

b. Provide the level and amounts of institutional support specified in the SREP proposal..

c. Notify RDL as soon as possible, but not later than 30 days, of any changes in 3a or 3b above, or any change to the assignment or amount of participation of the Principal Investigator designated on the title page.

d. Assure that the research is completed and the final report is delivered to RDL not later than twelve months from the effective date of this subcontract, but no later than December 31, 1999. The effective date of the subcontract is one week after the date that the institution's contracting representative signs this subcontract, but no later than January 15, 1999.

e. Assure that the final report is submitted in accordance with Attachment 3.

f. Agree that any release of information relating to this subcontract (news releases, articles, manuscripts, brochures, advertisements, still and motion pictures, speeches, trade associations meetings, symposia, etc.) will include a statement that the project or effort depicted was or is sponsored by: Air Force Office of Scientific Research, Bolling AFB, D.C.

g. Notify RDL of inventions or patents claimed as the result of this research as specified in Attachment 1.

h. RDL is required by the prime contract to flow down patent rights and technical data requirements to this subcontract. Attachment 2 to this

subcontract contains a list of contract clauses incorporated by reference in the prime contract.

4. All notices to RDL shall be addressed to:

RDL AFOSR Program Office
5800 Uplander Way
Culver City, CA 90230-6609

5. By their signatures below, the parties agree to provisions of this subcontract.

Abe Sopher RDL Contracts Manager	Signature of Institution Contracting Official
	Typed/Printed Name
Date	Title
	Institution
	Date/Phone

ATTACHMENT 2
CONTRACT CLAUSES

This contract incorporates by reference the following clauses of the Federal Acquisition Regulations (FAR), with the same force and effect as if they were given in full text. Upon request, the Contracting Officer or RDL will make their full text available (FAR 52.252-2).

FAR CLAUSES	TITLE AND DATE
52.202-1	DEFINITIONS
52.203-3	GRATUITIES
52.203-5	COVENANT AGAINST CONTINGENT FEES
52.203-6	RESTRICTIONS ON SUBCONTRACTOR SALES TO THE GOVERNMENT
52.203-7	ANTI-KICKBACK PROCEDURES
52.203-8	CANCELLATION, RECISSION, AND RECOVERY OF FUNDS FOR ILLEGAL OR IMPROPER ACTIVITY
52.203-10	PRICE OR FEE ADJUSTMENT FOR ILLEGAL OR IMPROPER ACTIVITY
52.203-12	LIMITATION ON PAYMENTS TO INFLUENCE CERTAIN FEDERAL TRANSACTIONS
52.204-2	SECURITY REQUIREMENTS
52.209-6	PROTECTING THE GOVERNMENT'S INTEREST WHEN SUBCONTRACTING WITH CONTRACTORS DEBARRED, SUSPENDED, OR PROPOSED FOR DEBARMENT
52.215-2	AUDIT AND RECORDS - NEGOTIATION
52.215-10	PRICE REDUCTION FOR DEFECTIVE COST OR PRICING DATA

52.215-12	SUBCONTRACTOR COST OR PRICING DATA
52.215-14	INTEGRITY OF UNIT PRICES
52.215-8	ORDER OF PRECEDENCE
52.215-18	REVERSION OR ADJUSTMENT OF PLANS FOR POSTRETIREMENT BENEFITS OTHER THAN PENSIONS
52.222-3	CONVICT LABOR
52.222-26	EQUAL OPPORTUNITY
52.222-35	AFFIRMATIVE ACTION FOR SPECIAL DISABLED AND VIETNAM ERA VETERANS
52.222-36	AFFIRMATIVE ACTION FOR HANDICAPPED WORKERS
52.222-37	EMPLOYMENT REPORTS ON SPECIAL DISABLED VETERAN AND VETERANS OF THE VIETNAM ERA
52.223-2	CLEAN AIR AND WATER
52.223-6	DRUG-FREE WORKPLACE
52.224-1	PRIVACY ACT NOTIFICATION
52.224-2	PRIVACY ACT
52.227-1	ALT. I - AUTHORIZATION AND CONSENT
52.227-2	NOTICE AND ASSISTANCE REGARDING PATIENT AND COPYRIGHT INFRINGEMENT
52.227-10	FILING OF PATENT APPLICATIONS - CLASSIFIED SUBJECT MATTER
52.227-11	PATENT RIGHTS - RETENTION BY THE CONTRACTOR (SHORT FORM)
52.228-7	INSURANCE - LIABILITY TO THIRD PERSONS

52.230-5	COST ACCOUNTING STANDARDS - EDUCATIONAL INSTRUCTIONS
52.232-23	ALT. I - ASSIGNMENT OF CLAIMS
52.233-1	DISPUTES
52.233-3	ALT. I - PROTEST AFTER AWARD
52.237-3	CONTINUITY OF SERVICES
52.246-25	LIMITATION OF LIABILITY - SERVICES
52.247-63	PREFERENCE FOR U.S. - FLAG AIR CARRIERS
52.249-5	TERMINATION FOR CONVENIENCE OF THE GOVERNMENT (EDUCATIONAL AND OTHER NONPROFIT INSTITUTIONS)
52.249-14	EXCUSABLE DELAYS
52.251-1	GOVERNMENT SUPPLY SOURCES

DOD FAR CLAUSES	DESCRIPTION
252.203-7001	SPECIAL PROHIBITION ON EMPLOYMENT
252.215-7000	PRICING ADJUSTMENTS
252.223-7004	DRUG FREE WORKFORCE (APPLIES TO SUBCONTRACTS WHERE THERE IS ACCESS TO CLASSIFIED INFORMATION)
252.225-7001	BUY AMERICAN ACT AND BALANCE OF PAYMENTS PROGRAM
252.225-7002	QUALIFYING COUNTRY SOURCES AS SUBCONTRACTS
252.227-7013	RIGHTS IN TECHNICAL DATA - NONCOMMERCIAL ITEMS
252.227-7030	TECHNICAL DATA - WITHOLDING PAYMENT
252.227-7037	VALIDATION OF RESTRICTIVE MARKINGS ON TECHNICAL DATA
252.231-7000	SUPPLEMENTAL COST PRINCIPLES
252.232-7006	REDUCTIONS OR SUSPENSION OF CONTRACT PAYMENTS UPON FINDING OF FRAUD

APPENDIX 2:

SAMPLE TECHNICAL EVALUATION FORM

SUMMER RESEARCH EXTENSION PROGRAM
TECHNICAL EVALUATION

SREP No: 96-0869
Principal Investigator: DR Ronald Barrett
Auburn University

Circle the rating level number, 1 (low) through 5 (high), you feel best evaluate each statement and return the completed form to RDL by fax of mail to:

RDL
Attn: SREP Tech Evals
5800 Uplander Way
Culver City, CA 90230-6608
(310)216-5940 or (800)677-1363

1.	This SREP report has a high level of technical merit.	1 2 3 4 5
2.	The SREP program is important to accomplishing the lab's mission.	1 2 3 4 5
3.	This SREP report accomplished what the associate's proposal promised.	1 2 3 4 5
4.	This SREP report addresses area(s) important to the USAF.	1 2 3 4 5
5.	The USAF should continue to pursue the research in this SREP report.	1 2 3 4 5
6.	The USAF should maintain research relationships with this SREP associate.	1 2 3 4 5
7.	The money spent on this SREP effort was well worth it.	1 2 3 4 5
8.	This SREP report is well organized and well written.	1 2 3 4 5
9.	I'll be eager to be a focal point for summer and SREP associates in the future.	1 2 3 4 5
10.	The one-year period for complete SREP research is about right.	1 2 3 4 5

---

11. If you could change any one thing about the SREP program, what would you change:

_____

_____

_____

12. What do you definitely NOT change about the SREP program?

_____

_____

_____

PLEASE USE THE BACK FOR ANY OTHER COMMENTS

Laboratory: Wright Laboratory
Lab Focal Point: Mr Fred Davis
Office Symbol: WL/MNAV Phone: (904)882-8876

CHLORINATED ETHENE TRANSFORMATION, SORPTION AND PRODUCT DISTRIBUTION IN METALLIC IRON/WATER SYSTEMS: EFFECT OF IRON PROPERTIES

Richelle M. Allen-King , Assistant Professor and
Kevin M. Danley, Graduate Student

Department of Geology
Washington State University
Pullman, WA 99164-2812

Final Report for:
Summer Research Extension Program
Armstrong Laboratory

Sponsored by:
Air Force Office of Scientific Research
Bolling Air Force Base, DC

and

Armstrong Laboratory

February 1997

CHLORINATED ETHENE TRANSFORMATION, SORPTION AND PRODUCT DISTRIBUTION IN METALLIC IRON/WATER SYSTEMS: EFFECT OF IRON PROPERTIES

Richelle M. Allen-King , Assistant Professor and Kevin M. Danley, Graduate Student
Department of Geology
Washington State University
Pullman, WA 99164-2812

ABSTRACT

Chlorinated solvents, such as perchloroethene (PCE) and trichloroethene (TCE), are among the most frequently detected groundwater contaminants. One potentially cost-effective alternative remediation/containment method is the metallic iron *in situ* passive barrier, within which dissolved chlorinated compounds are treated.

The goals of this research were to determine the effects of iron properties (differing iron composition and surface coatings) on chloroethene rates of transformation, amount of sorption, and product distribution. We selected PCE as a model chloroethene compound for the majority of our the experiments because it is the chloroethene compound for which sorption to nonreactive surfaces has the greatest effect. The behavior of TCE was determined for comparison to PCE in selected iron samples. Iron samples representative of materials currently being employed in detailed laboratory studies, as well as samples of iron that may be selected for application at field sites, were be tested.

Time series experiments were conducted to determine PCE transformation rate coefficient, reaction order and sorption in metallic iron/water systems with iron from four different suppliers. The same parameters were determined for TCE in similar batch systems for two of the iron samples. The aqueous concentration-based transformation process was determined to be essentially first order for both compounds with the iron samples (within 95% confidence intervals), with the exception that a first order coefficient was not within the 95% confidence interval determined for PCE and one of the iron samples. Once sorption to nonreactive sites was accounted for, the reaction rates were not significantly different for the different iron samples tested. Thus, iron properties were not found to significantly affect reaction rate coefficients.

Sorption of both PCE and TCE were nonlinear in all irons tested. The sorption behavior was characterized with isotherms of the Freundlich form over the concentration range tested. The magnitude of sorption between the two chemicals for any particular iron appears to be scalable and proportional to relative hydrophobicity of the compounds.

Products resulting from PCE transformation in batch systems were determined for each of the four iron samples late in the time series experiments. Total masses determined by headspace analysis (reported as nmol C_2 compound) were in the following proportions for all of the iron samples tested: ethene>> ethane > acetylene > methane, C_3, C_4, C_5, C_6, *cis*-DCE and TCE. Vinyl chloride was not detected in any of the iron/water systems. Chloride adsorption to the iron, if it occurs, was determined to account for a minor proportion of product. The similarities in product distributions indicate that differences in iron properties do not result in environmentally important (e.g. proportion of products which are regulated compounds) differences in the production of products.

CHLORINATED ETHENE TRANSFORMATION, SORPTION AND PRODUCT DISTRIBUTION IN METALLIC IRON/WATER SYSTEMS: EFFECT OF IRON PROPERTIES

Richelle M. Allen-King , Assistant Professor and Kevin M. Danley, Graduate Student

INTRODUCTION

Background

Chlorinated solvents in groundwater are of public concern because they can have negative impacts on human health and the environment. Drinking water standards are typically in the low part-per-billion range. For example, the drinking water standards (maximum contaminant level or MCL) for trichloroethene (TCE) and perchloroethene (PCE) are 5 μg/L [US EPA, 1987; US EPA, 1991]. Chlorinated solvents, such as TCE and PCE, are the most frequently identified organic contaminants in groundwater for several reasons: 1) these highly chlorinated compounds tend to be persistent in aerobic groundwater; 2) during the past 40-50 years, these compounds have been commonly used industrial solvents and they have been discharged to the environment by disposal, leakage and spillage, often as a dense non-aqueous phase liquid (DNAPL); 3) DNAPLs in the subsurface, distributed as both residual and pools, can provide exceptionally long-term sources of groundwater contamination that are challenging to delineate and remediate [Mackay and Cherry, 1989; Westrick, 1990; NRC, 1993; NRC, 1994; MacDonald and Kavanaugh, 1994; Vogel et al., 1987; Pankow et al., 1996].

The US Air Force (USAF) has identified at least 1100 sites contaminated with chlorinated solvents [Burris, pers. comm.]. These compounds are often present in the subsurface as dense non-aqueous phase liquids (metallic DNAPLs) that can provide a source of dissolved groundwater contamination for very long time frames. DNAPLs are not effectively remediated by the conventional "pump and treat" method. Therefore, treatment methods for chlorinated-solvent sites are of particular interest to the USAF. The conventional approach to groundwater remediation has been to pump contaminated groundwater to the surface for treatment [US EPA, 1990]. Because of the ineffectiveness of "pump-and-treat" as a remediation method, focus has shifted to alternative *in situ* remediation methods [NRC, 1993; NRC, 1994].

The use of iron in permeable *in situ* treatment barriers has been proposed and is being tested as an alternative remediation and containment method for chlorinated solvents in groundwater [Gillham, 1995; Wilson, 1995; among others]. Within this concept, contaminated groundwater flows naturally through a portion of the aquifer modified to containing iron, and the contaminants are remediated by reaction with the iron. Because transformation rates are rapid relative to typical groundwater flow velocities [Gillham and O'Hannesin, 1994; Sivavec and Horney, 1995], the *in situ* method has potential to treat groundwater with a passive system that may prove cost-effective relative to the conventional method [Wilson, 1995]. In order to accurately design effective *in situ* remediation systems, a complete understanding of the reaction rates, reaction orders, and products produced are needed.

Research has shown that sorption to nonreactive sites on metallic iron surfaces causes some of the contaminant mass in the system to be unavailable for reaction. Of chloroethenes, sorption is most significant for perchloroethene (PCE).

Additionally, the production of vinyl chloride, a stringently regulated intermediate transformation product, has been observed in some metallic iron/water systems.

Research Goals and Tasks

The goals of this research were to determine the effects of iron properties (differing iron composition and surface coatings) on chloroethene rates of transformation, amount of sorption, and product distribution. We selected PCE as a model chloroethene compound for the majority of our the experiments because it is the chloroethene compound for which sorption to nonreactive surfaces has the greatest effect. The behavior of TCE was determined for comparison to PCE in selected iron samples. Iron samples representative of materials currently being employed in detailed laboratory studies, as well as samples of iron that may be selected for application at field sites, were tested. Chloride adsorption in the iron/water systems was also determined because an understanding of chloride interactions with solids is necessary for accurate chlorine balances.

The following tasks were conducted to achieve these goals:

Task 1. determine the rates of PCE transformation and sorption for four different iron samples (effect of varying iron properties);

Task 2. determine chloride adsorption in the metallic iron/water system for two iron samples;

Task 3. assess the scalability of TCE transformation by determining transformation rate coefficients and sorption coefficients for two iron samples.

MATERIALS AND METHODS

Iron and Chemicals

A standard iron from a lab-supply company, Fisher 40-mesh (F), and three commercial iron samples, Master Builders GX27 (M), Connelly-GPM (C), and Peerless Iron (P), were used in this study. Total carbon analysis was conducted for the different irons as described in the *Analytical* section. The measured carbon values and compositional information reported by the manufacturers are summarized in Table 1. A 400 g batch of each iron was washed in 0.5 L of 1 N HCl for one-half hour and then rinsed with 8 L of nitrogen-sparged nanopure water. The iron was dried under nitrogen atmosphere at 100 °C and stored in argon sparged containers to inhibit oxidation. Pyrite obtained from Wards Natural Science Establishment was used to pH buffer the batch system. Pretreatment of the pyrite consisted of powdering with mortar and pestle and storing in an argon sparged glass jar to inhibit oxidation.

Table 1: Compositional information for the different iron types.

Material	Iron type			
	C	P	F	M
Carbon content,				
treated iron §	3.17 %	3.11 %	2.91 %	2.77 %
(RPD) †	(2.7)	(0.7)	(7.0)	(3.0)
untreated iron §	3.13 %			2.96 %
Carbon	2.85 %	3.2 - 3.9 %		
Iron	89.82 %	85-95 %		
Manganese	0.60 %	1 % max.		
Sulphur	0.107 %	0.15 % max.		
Phosphorous	0.132 %	0.65 % max.		
Silicon	1.85 %	2-3 %		
Nickel	0.05-0.21 %			
Chromium	0.03-0.17 %	0.5 % max.		
Vanadium	Nil			
Molybdenum	0.15 %			
Titanium	0.004 %			
Copper	0.15-0.20 %	1 % max.		
Aluminum	Trace			
Cobalt	0.003 %			
Tin		0.1-0.2 %		
Chromium		0.5 % max.		
Magnesium		0.55 % max.		

§ Carbon content of acid-treated iron samples.
† Relative percent difference for duplicate measurements.
*Values determined at Washington State University using total carbon analysis as described in the *Analytical* section. All other values are included as reported from the iron supplier.
Blank indicates that composition was not reported or determined.

PCE was obtained from Baker Chemical and TCE was obtained from Chem Service with purities of 100% and 99%, respectively. Dichlorobenzene was obtained from Aldrich Chemical with a purity of 99+%. Methanol was Fisher HPLC grade and acetonitrile was Fisher Optima grade. Standard compounds for analysis of volatile PCE transformation products were obtained in the following purities (for liquids) or concentrations (for gasses): 1,2-*cis*-dichloroethene (*cis*-DCE)-97% (Aldrich), vinyl chloride (VC) - 1000 ppmv in N_2 (Alltech), acetylene 1.03% by volume in N_2 (Alltech), ethane, ethene and methane - all 1.00% by volume in N_2 (Alltech), propane - 1.01% by volume in N_2 (Aldrich), and butane - 10.0% by volume in N_2 (Aldrich). All analytes were used as received. All water used in the experiments was treated with an ultrapurification system.

Batch system

Time-series experiments were conducted with PCE and TCE. All four irons were used in the PCE time-series experiment; only iron samples C and P were used in the TCE experiment. The batch systems were prepared according to the method outlined by Burris et al. (1995). Nitrogen sparged nanopure water was added to the vials which were immediately sealed with Teflon-lined rubber septa (Supelco). The iron was allowed to pre-equilibrate with the water for four to five days prior to spiking with the analyte of interest to create an iron surface more typical of a long-term field system (Allen-King, 1997). Iron- and pyrite-free controls were prepared to check for system losses attributable to mechanisms other than reaction. Glass beads (3 mm diameter), approximately equaling the Fe volume added to sample vials, were added to the control vials to aid in mixing. Vials were shaken at 5 rpm at ambient laboratory temperature (20 °C to 22 ° C) until sampled. Two controls vials and two Fe containing vials for each iron sample being tested were sacrificed at each sampling time for measurement of PCE or TCE solution concentrations and total PCE or TCE mass. Water samples were collected (30 µl) from the control and iron batch vials at each sampling time.

Batch systems for chloride adsorption determination were prepared by adding 5.00 g iron (or a comparable volume of glass beads for control vials) to 10 ml (nominal) Wheaton serum vials and filling the vials with nitrogen sparged chloride solutions of ~10, 20 or 30 mg/l Cl^-. Two iron types were tested: irons G and P. Following equilibration for 36 hr, solution samples were analyzed for chloride as described in the *Analytical* section below. Previous research (Allen-King et al., in press) has shown that Fe releases chloride (likely from the acid wash) to solution in batch systems and that the concentration released remains constant following less than 24 h contact time. Batch systems containing each of the iron types and nanopure (chloride-free) water were prepared to account for background chloride for the purposes of both the product and chloride sorption experiments.

Products resulting from PCE transformation in batch systems were determined for each of the four irons. These batch systems were sampled late in the time series experiments. Batch systems (five replicates of each iron type) were prepared for PCE transformation product analysis with the same amounts of iron, pyrite and PCE used in the reaction time-series experiments. Fe-free control vials were also prepared. Hydrocarbons (methane, ethene, acetylene, ethane, C3, C4, and C5 compounds) and chlorinated ethene products (VC, *cis*-DCE, and TCE) were determined by headspace analysis for duplicate samples after 335 hr contact time. Chloride concentrations were determined at this time on another replicate vial. Final PCE solution concentrations and total masses were determined by the standard time series analytical method for duplicate vials on the following day (after changing the GC method back to the PCE solution and extract determination method), a total of 366 hr after PCE was introduced to the vials. All analytical methods are described in the *Analytical* section.

Analytical

PCE and TCE mass in solution and total mass were analyzed according to the method outlined by Burris et al.

(1995) with slight modification. Autosampler vials contained a volume of 1.5 ml of acetonitrile instead of 1 ml. Sample aliquots for solution mass determination were increased (30 µl) proportionally. Sample aliquots for total mass determination were 60 µl and the internal standard concentration for the extraction methodology was increased to 3 mg/L to account for the smaller volume. All samples were analyzed on a Hewlett-Packard model 5890 gas chromatograph equipped with an ECD, model 7673 autosampler, and a 30 m, 0.32 mm DB-624 (J&W Scientific) capillary column. The GC operating parameters were: injector at 120 °C, detector at 250 °C, initial temperature at 50 °C for 2 minutes, ramp at 30 °C/min for five minutes to 200 °C, and column flow set at 2 ml/min. The PCE and TCE concentrations were determined by a multilevel calibration curve obtained by analyzing standards with known concentrations.

Total carbon content was determined for all four irons in their pretreated condition and two untreated iron samples (M and C) for comparison of uncleaned and cleaned iron characteristics. High temperature combustion (950 °C) under pure oxygen was used to evolve CO_2; CO_2 was quantified using a coulometric system (CM5120, UIC). Sample weights analyzed ranged from 0.06 to 0.2 grams. The carbon content in uncleaned iron was not substantially different than the acid-washed iron (Table 1).

Hydrocarbon (methane, ethene, acetylene, ethane, C3, C4, and C5 compounds) and chlorinated ethene products (VC, *cis*-DCE, and TCE) were determined by headspace analysis using methods similar to Allen-King et al. (in press) and Roberts et al. (1996). A 4.00 ml headspace was created in each vial by displacing water with nitrogen under positive pressure. Pentane was added as an internal standard and vials were shaken at 400 rpm for 5 minutes prior to analysis. A 100 µl sample of the headspace was analyzed by GC equipped with a GS-Q PLOT column (J&W Scientific) and flame-ionization detector. Duplicate standards were prepared for headspace analysis with potential volatile transformation products (methane, ethane, acetylene, ethene, propane, butane, VC, *cis*-DCE, and TCE) at three concentration levels in systems containing the same volume of water as the samples (9.9 ml), 4.0 ml headspace, and a volume of glass beads equivalent to the volume of iron in the samples.

Chloride concentrations were determined for filtered solution samples from Fe-containing vials (0.45 μm disposable syringe filters, Acrodisc) using a chloride ion-selective electrode (ISE, Orion) and ISE compatible meter (Orion). A 5.00 ml pre-filtered solution sample was mixed with an equal volume of complex ionic strength adjustor solution (CISA, Orion) and stirred for approximately 5 minutes before measuring. Chloride concentrations were determined following 5 minute electrode equilibration using a standard curve generated based on standards prepared at the following concentrations: 5, 10, 20, 40, and 100 mg/l Cl^-. Particularly in the PCE transformation experiment vials, the chloride electrode results were found to drift with time; the drift was equivalent to approximately 2 to 3 mg/l per 5 minutes of equilibration for the product samples. Apparently, oxidation of iron in the solution sample caused interference with the measurement, even in the presence of the CISA buffer. As a consequence, the analytical uncertainty of these results is relatively large.

RESULTS AND DISCUSSION

PCE transformation rate coefficients and reaction orders for iron samples

The PCE solution concentration and total mass were reduced over time in time course experiments with each of the iron types (Figure 1). The difference between the total and solution masses represents the mass sorbed in the system. The PCE mass remaining at the end of the time course experiments was greater for iron samples F and M than for iron samples C and P.

Transformation rate coefficients (λ) and reaction orders (N) were determined using the method of Burris et al. (1995) for the following equations:

$$\frac{dM_T}{dt} = -\lambda_T M_T^{N_T} \quad (1)$$

and

$$\frac{dM_T}{dt} = -\lambda_a C_a^{N_a} \quad (2)$$

where M_T is the total PCE mass in the vial, C_a is the PCE concentration, and the superscripts T and a refer to coefficients determined based on total system mass and aqueous concentration, respectively. The equations were linearized by ln-transformation and the coefficients were determined by linear regression (Figures 2 and 3, Table 2). The results of replicate samples for each time were averaged.

The coefficients for PCE transformation for the different irons are summarized in Table 2. For comparison, standard pseudo-first order rate coefficients (λ_1) were also determined (Table 2) (Schwarzenbach et al., 1993). All of the iron samples exhibit non-first order behavior on a total mass basis. First order behavior in solution concentration is within the 95% confidence intervals determined for N_a for all irons in this study, with the exception of the M iron. The solution-based rate constants, ln λ_a, range between -4.58 and -5.25, and are not significantly different from each other when the 95% confidence intervals are considered. The total mass based rate constants are much lower than the solution concentration based rate constants. The pseudo-first order rate constants are similar to the solution-concentration based, fit-order rates constants.

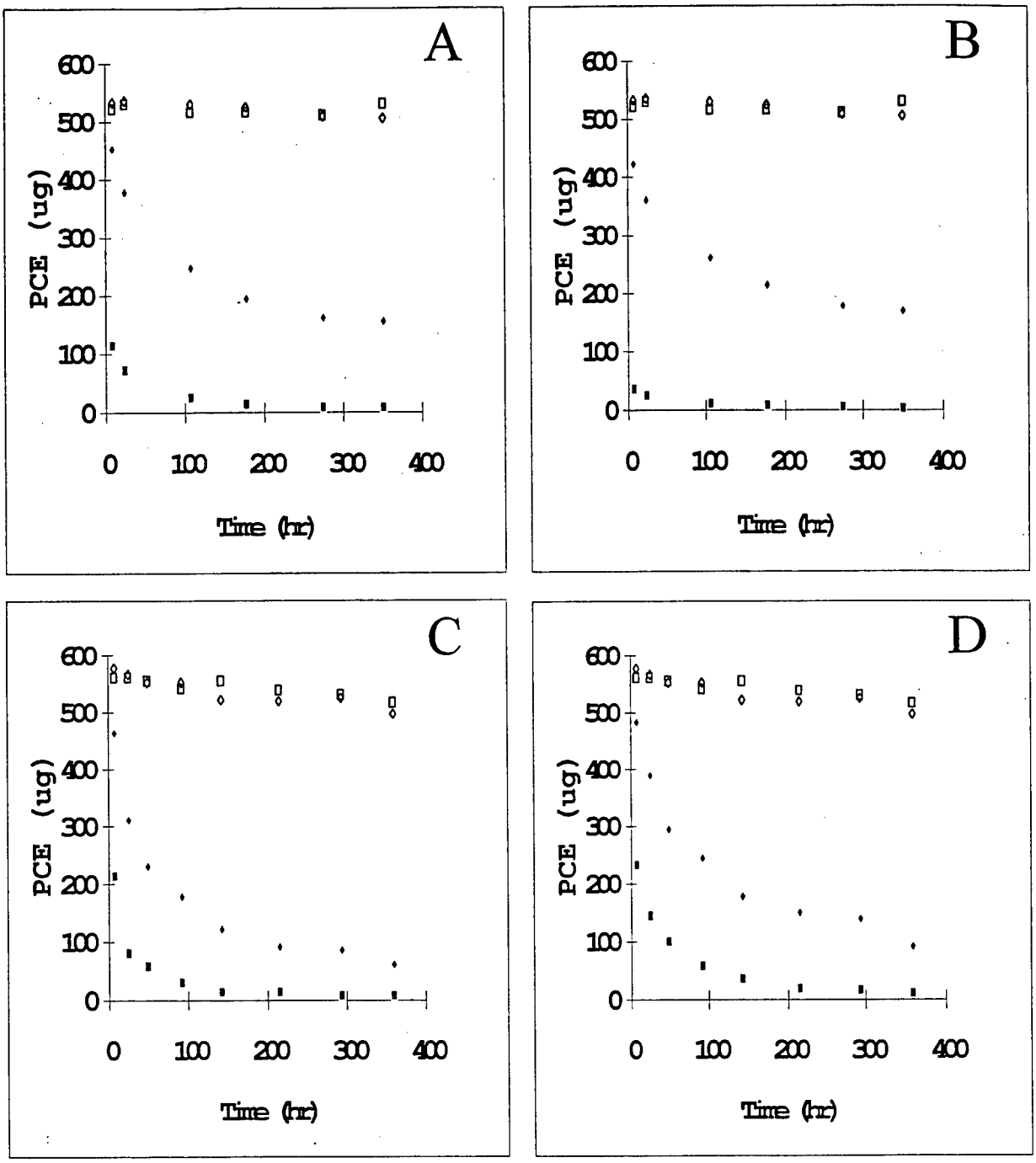

Figure 1. Total and dissolved PCE masses over the experiment time course for (A) iron F, (B) iron M, (C) iron C, and (D) iron P. Open square represents control solution mass. Open diamond represents control total mass. Closed diamond represents sample total mass. Closed square represents sample solution mass.

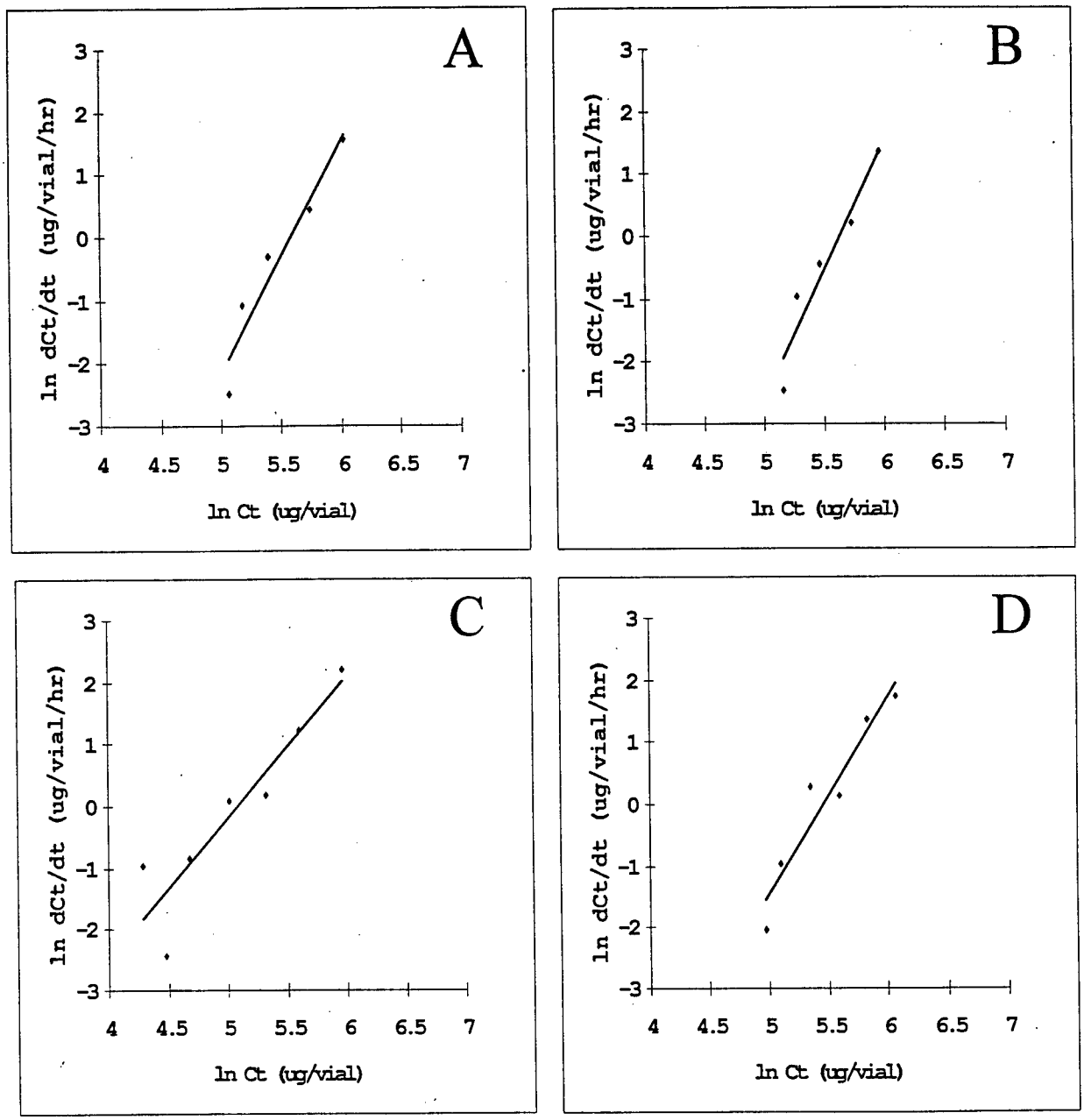

Figure 2. Transformation rate-law determination on a total mass (M_T) basis for PCE and (A) iron F, (B) iron M, (C) iron C, and (D) iron P.

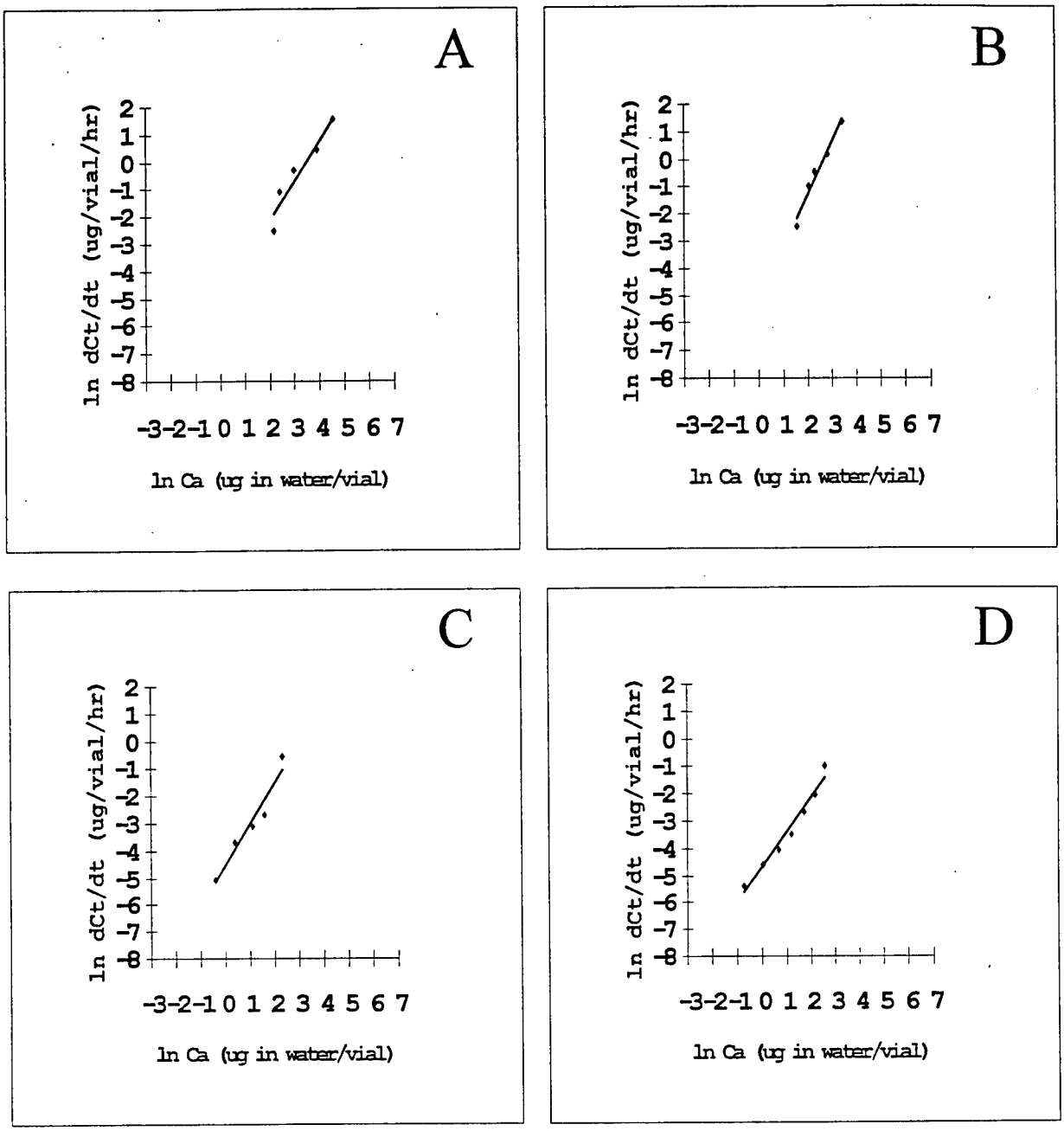

Figure 3. Transformation rate-law determination on a solution concentration (C_a) basis for PCE and (A) iron F, (B) iron M, (C) iron C, and (D) iron P.

Table 2: Transformation rate coefficients (λ) and reaction orders (N) (95% C.I.) for PCE experiments with the different irons.

Iron	$\ln \lambda_1$	N_T	$\ln \lambda_T$	N_a	$\ln \lambda_a$
F	-4.9 (+/- 0.1)	3.7 (+/- 1.9)	-21 (+/- 10)	1.5 (+/- 0.80)	-5.1 (+/- 2.7)
M	-5.1 (+/- 0.3)	4.1 (+/- 2.2)	-23 (+/- 12)	2.0 (+/- 0.64)	-5.3 (+/- 1.6)
C	-4.1 (+/- 0.2)	2.3 (+/- 1.1)	-12 (+/- 5.6)	1.5 (+/- 0.66)	-4.6 (+/- 0.92)
P	-4.6 (+/- 0.1)	3.2 (+/- 1.3)	-17 (+/- 7.3)	1.3 (+/- 0.27)	-4.7 (+/- 0.41)

The first-order rate coefficient (λ_1)is determined as ln C_T(ug/vial) vs. Time. Dimensions are hr^{-1} for λ_1, [nmol/hr]/[(nmol)^{NT}]for_λ_T, and [nmol/hr]/[(nmol/ml)^{Na}] for _λ_a.

Transformation rate coefficients and reaction orders for TCE compared to PCE

Time series batch experiments were conducted with TCE and iron samples C and P (Figure 4). Coefficients for TCE transformation were determined using equations (1) and (2) (Figures 5 and 6), and are summarized in Table 3. The total mass based and aqueous concentration based TCE reaction order are unity (within 95% confidence intervals) for both irons. The total mass based rate coefficient for TCE transformation is lower than the rate coefficient obtained for PCE transformation for both irons, presumably due to sorption effects. However, the aqueous concentration-based TCE transformation rate coefficients are the same as the coefficients determined for PCE (within 95% confidence intervals). The pseudo first- order rate coefficient for TCE transformation with iron P is higher for TCE than PCE. The pseudo first-order rate coefficients for iron C appear the same for both PCE and TCE.

PCE Sorption

Sorbed concentrations were determined for each sample from the difference between the total PCE mass and mass in solution at each sampling time. A generalized Langmuir isotherm, of the form:

$$C_s = \frac{kb C_{aq}^M}{1 + kC_{aq}^M} \tag{3}$$

where C_s is the sorbed concentration, k and b represent the magnitude of sorption, and M indicates the degree of isotherm nonlinearity was fit to the iron F sorption data using a nonlinear method (SYSTAT). The coefficients determined (Table 4) are similar to those observed by Burris et al. (1995) (k=0.156, b=692, and M=0.673), for iron from the same supplier, although the M coefficient was approximately 20 percent lower in the current study. Only the iron F sorption data were successfully fit with the generalized Langmuir isotherm in the concentration range studied.

Freundlich sorption isotherms of the form:

$$C_s = K_F C_a^m \tag{4}$$

where K_F and m represent the magnitude and degree of sorption nonlinearity, respectively, were fit to the results for all iron samples (Figure 7, Table 4) using a nonlinear method (SYSTAT). Based on the graphical presentation of the results, the magnitude of sorption for the iron samples (descending order) is: M > F > C and P. The relative differences in the magnitude of sorption cannot be accounted for by differences in carbon content between iron samples (Table 1). The different irons have similar total carbon percentages with apparently variable sorption behavior.

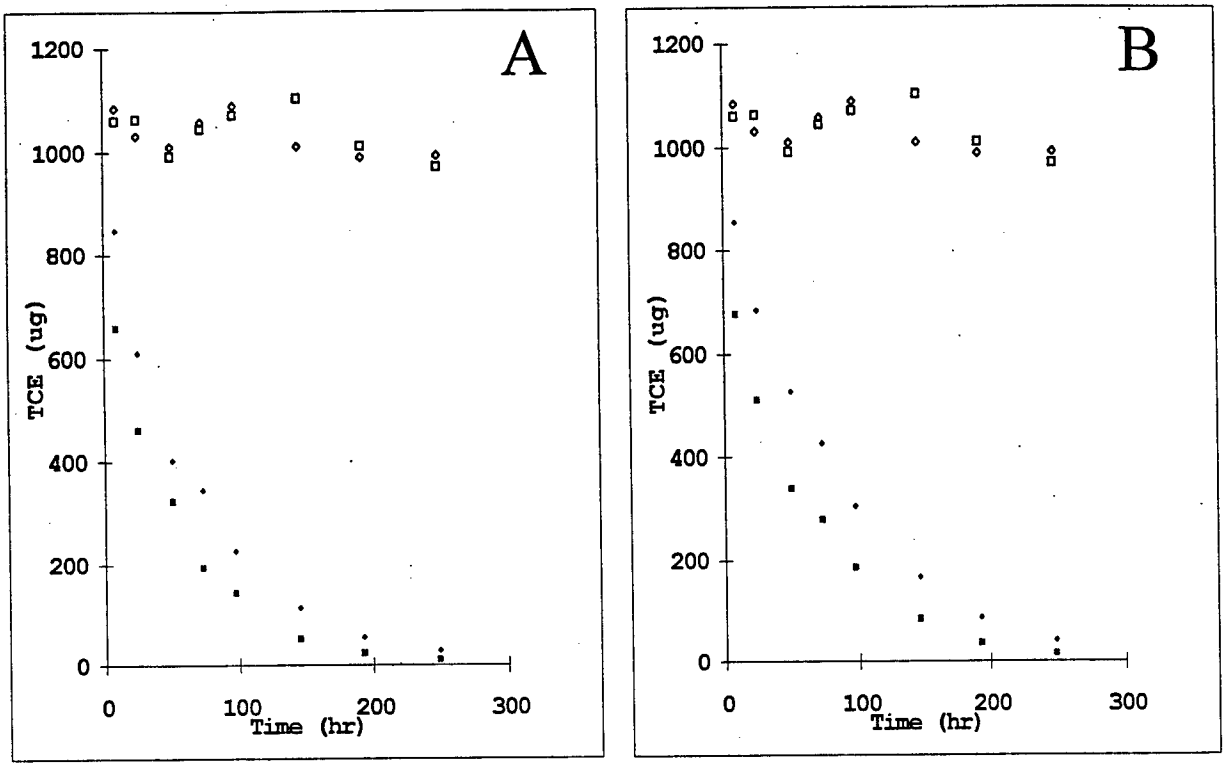

Figure 4. Total and dissolved TCE masses over the experiment time course for (A) iron C, (B) iron P. Open square represents control solution mass. Open diamond represents control total mass. Closed diamond represents sample total mass. Closed square represents sample solution mass.

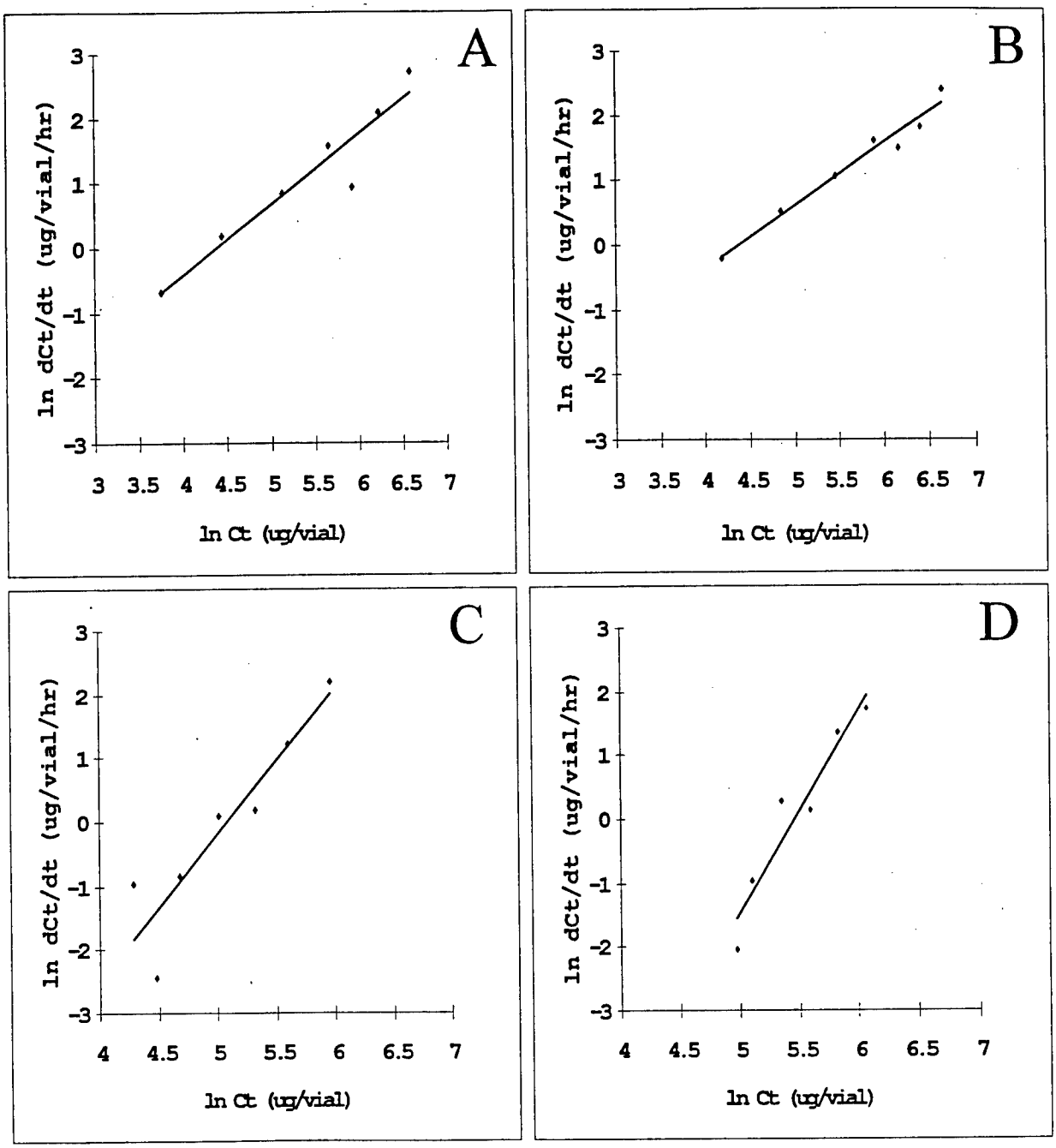

Figure 5. Transformation rate-law determination on a total mass (M_T) basis for TCE and (A) iron C and (B) iron P. Transformation rate-law determination for PCE on a total mass (M_T) basis for PCE and (C) iron C and (D) iron P.

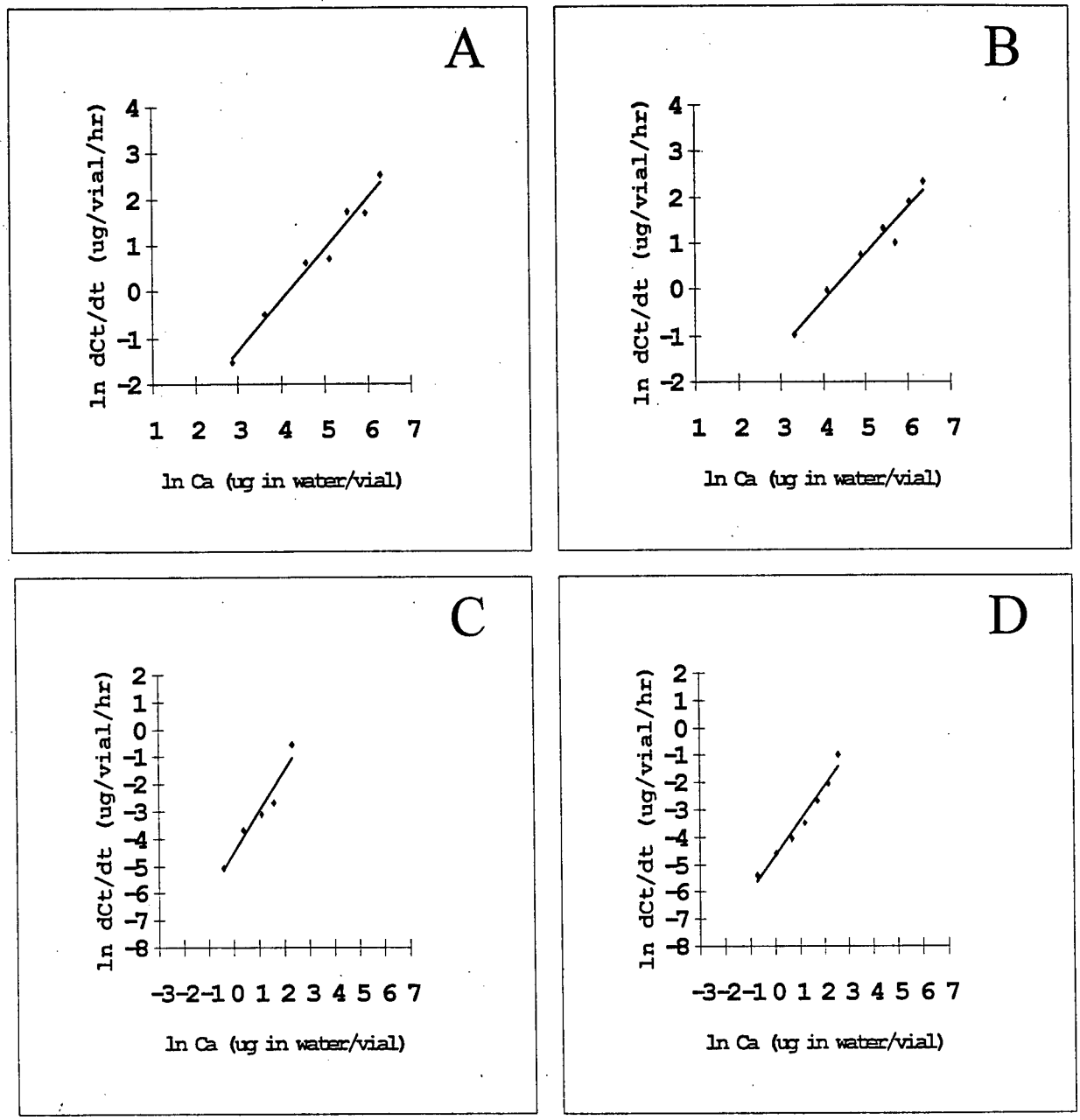

Figure 6. Transformation rate-law determination on a solution concentration (C_a) basis for TCE and (A) iron C and (B)iron P. Transformation rate-law determination on a solution concentration (C_a) basis for PCE and (C) iron C and (D) iron P.

Table 3: Transformation rate coefficients (λ) and reaction orders (N) (95% C.I.) for TCE experiments with irons C and P.

Iron	ln λ_1	N_T	ln λ_T	N_a	ln λ_a
C	-4.07 (+/- 0.07)	1.1 (+/- 0.38)	-4.8 (+/- 2.1)	1.1 (+/- 0.21)	-4.6 (+/- 1.0)
P	-4.20 (+/- 0.03)	0.96 (+/- 0.20)	-4.2 (+/- 1.1)	1.1 (+/- 0.31)	-4.3 (+/- 1.3)

The first-order rate coefficient (λ_1)is determined as ln C_T(ug/vial) vs. Time. Dimensions are hr^{-1} for λ_1, [nmol/hr]/[(nmol)^{NT}] for_λ_T, and [nmol/hr]/[(nmol/ml)^{Na}] for _λ_a.

Table 4: Generalized Sorption Isotherms Coefficients for PCE and the different iron types.

	Freundlich	Coefficients		Langmuir	Coefficients		
Iron	K_F	m	r^2	k	b	M	r^2
F	120	0.33	0.997	0.167	724	0.527	0.997
M	155	0.41	0.891				
C	69	0.38	0.944				
P	107	0.22	0.812				

Dimensions of K_F are [nmol/g]/[(nmol/ml)^m]

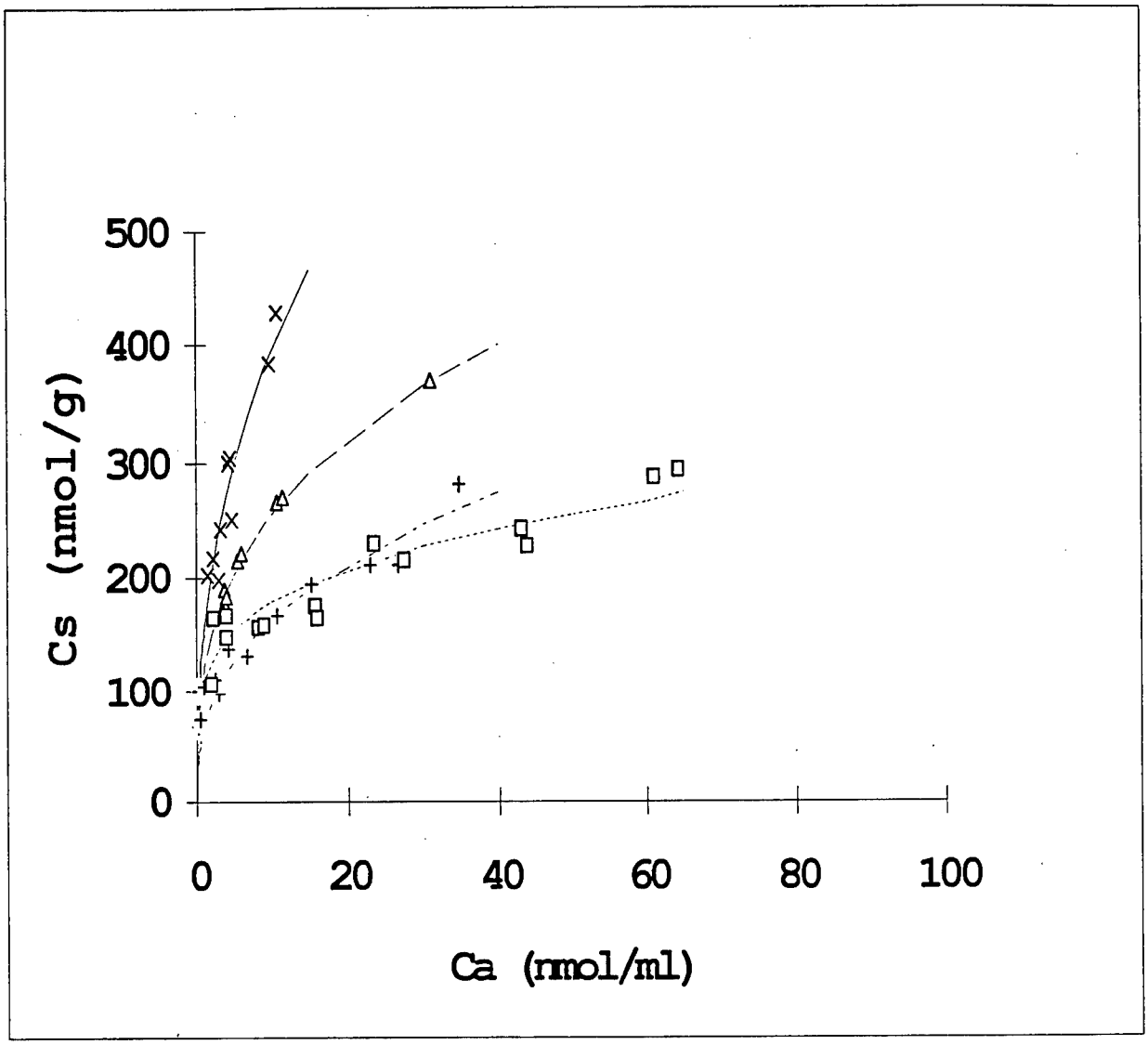

Figure 7. PCE sorption isotherms for irons F, M, C, and P. The symbols represent observations for the different irons: open triangle represents iron F, X represents iron M, + represents iron C, and open square represents iron P. Lines are Freundlich isotherm fits of the results.

TCE sorption compared to PCE sorption

Freundlich isotherm sorption coefficients were determined for TCE and two of the iron samples: C and P (Figure 8, Table 5). The TCE K_F coefficients for irons C and P (18.7 (nmol/g)/(nmol/ml)^m and 27.2 (nmol/g)/(nmol/ml)^m , respectively) were much lower than their corresponding PCE K_F coefficients (69 (nmol/g)/(nmol/ml)^m and 107 (nmol/g)/(nmol/ml)^m, respectively). The ratio of the PCE:TCE K_F values for the two iron types are 3.69 and 3.86 for irons C and P, respectively. The ratio of the octanol-water partitioning coefficients (PCE K_{ow}: TCE K_{ow}) for these chemicals, which indicates the relative hydrophobicity of the two compounds, is approximately 3.7- 15 (Allen-King et al., 1996). Thus, the magnitude of sorption between the two chemicals for any particular iron appears to be scalable and proportional to relative hydrophobicity of the compounds.

Chloride adsorption

Expected versus observed chloride concentrations for the chloride adsorption experiment are shown in Figure 9 for the two iron samples tested. Expected concentrations assume no chloride sorption and are equal to the sum of the background concentration for the particular iron sample and the observed concentration in the Fe-free control. Uncertainties in the expected concentrations estimates, determined by standard error propagation techniques, are approximately ±10%. These results show that chloride adsorption, if it occurs, is not large. For all concentrations, except the observations at approximately 25 mg/L, the difference between the observed and expected concentrations is less than or equal to the analytical uncertainty.

Reaction products and chloride analysis

Products resulting from PCE transformation in batch systems were determined for each of the four iron samples tested. The batch systems were sampled late in the time series experiments. Total masses determined by the headspace analysis (reported as nmol C_2 compound) were in the following proportions for all of the iron samples tested: ethene>> ethane > acetylene > methane, C_3, C_4, C_5, C_6, *cis*-DCE and TCE. Sorption of TCE is not accounted for in the analysis. However, the TCE sorption tests suggest that the sorption will not account for a large TCE mass. Significantly, no VC was detected in any of the iron/water systems. The *cis*-DCE comprised approximately 1% of the PCE transformed in all the iron systems. Chloride concentrations were increased above the background level; concentrations at the time of sampling were 13 to 32 mg/l, or 5.4 to 16 mg/l Cl^- above the background concentrations. Because of the drift reported for the ISE method when used for these samples, these measurements are estimated to underestimate the true concentrations by as much as approximately 5 mg/l. The expected chloride concentrations produced by PCE transformation fall within the range of the measurements, given the large uncertainties.

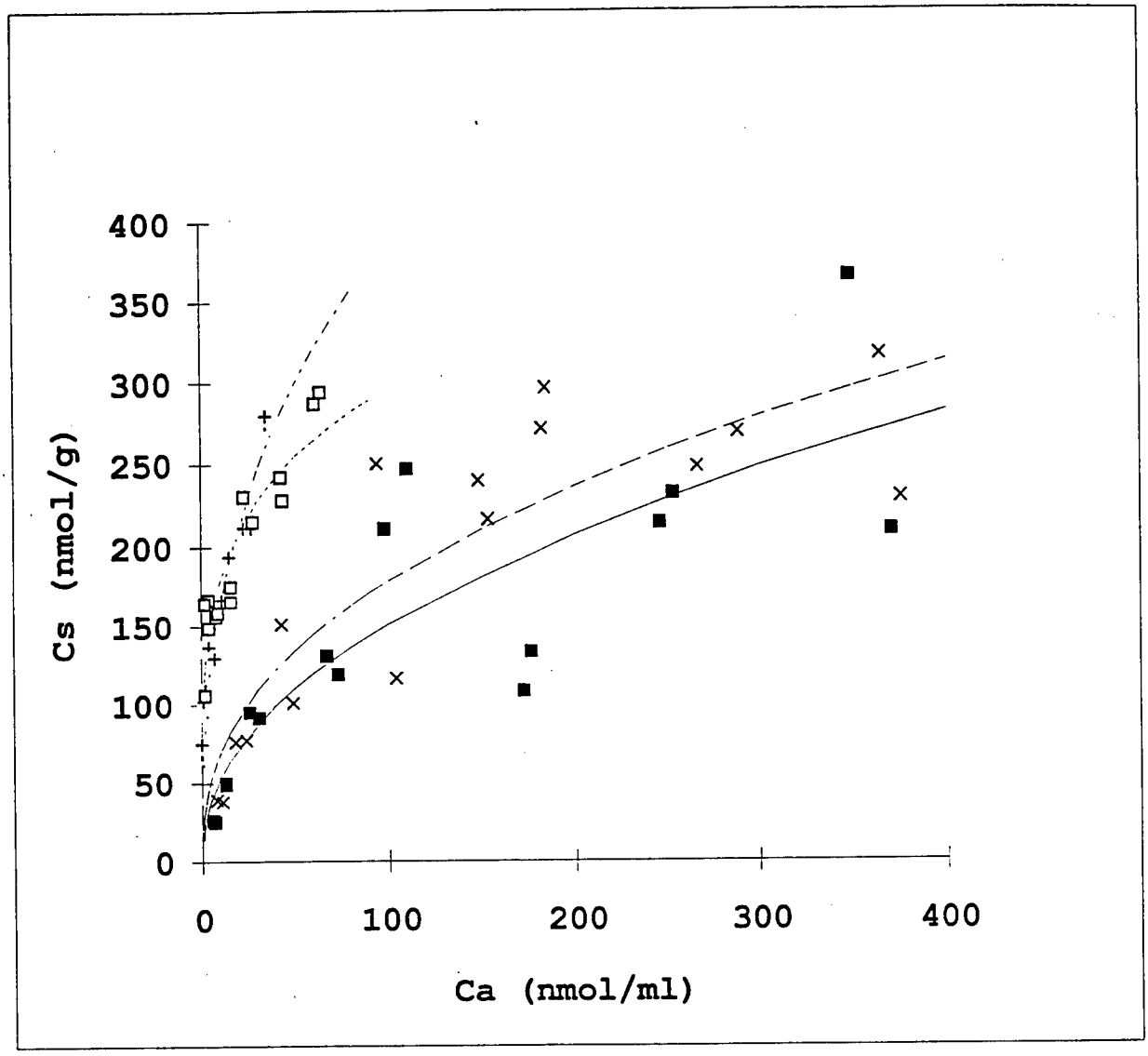

Figure 8. TCE and PCE sorption isotherms for irons C and P. The symbols represent observations for the different irons: closed square represents iron C (TCE), X represents iron P (TCE), + represents iron C (PCE), and open square represents iron P (PCE). Lines are Freundlich isotherm fits of the results.

Table 5: Freundlich Sorption Isotherm Coefficients for TCE and irons C and P.

	Freundlich	Coefficients	
Iron	K_F	m	r^2
C	18.7	0.45	0.716
P	27.2	0.41	0.797

Dimensions of K_F are [nmol/g]/[(nmol/ml)^m]

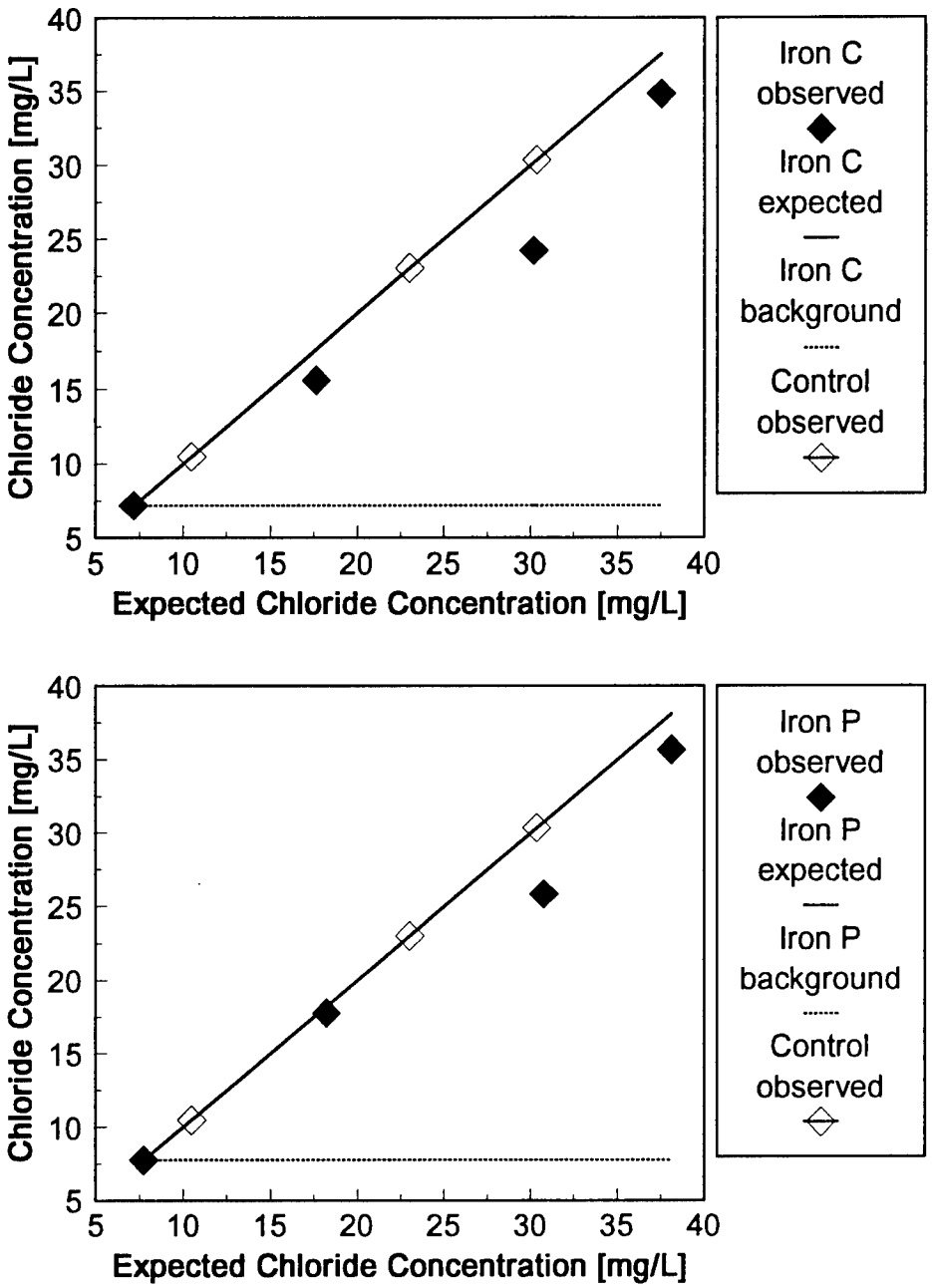

Figure 9. Observed versus expected chloride concentrations in chloride adsorption experiment. Expected concentrations assume no chloride sorption and are equal to the sum of the background concentration for the particular iron sample and the observed concentration in the Fe-free control.

SUMMARY

Time series experiments were conducted to determine PCE transformation rate coefficient, reaction order and sorption in metallic iron/water systems with iron from four different suppliers. The same parameters were determined for TCE in similar batch systems for two of the iron samples. The aqueous concentration-based transformation process was determined to be essentially first order for both compounds (within 95% confidence intervals), with the exception that a first order coefficient was not within the 95% confidence interval determined for PCE and one of the iron samples. Once sorption to nonreactive sites was accounted for, the reaction rates were not different for the different irons. Thus, iron properties were not found to significantly affect reaction rate coefficients.

Sorption of both PCE and TCE were nonlinear in all irons tested. The sorption behavior was characterized with isotherms of the Freundlich form over the concentration range tested. The magnitude of sorption between the two chemicals for any particular iron appears to be scalable and proportional to relative hydrophobicity of the compounds.

Products resulting from PCE transformation in batch systems were determined for each of the four iron samples late in the time series experiments. Total masses determined by a headspace analysis (reported as nmol C_2 compound) were in the following proportions for all of the iron samples tested: ethene>> ethane > acetylene > methane, C_3, C_4, C_5, C_6, *cis*-DCE and TCE. Vinyl chloride was not detected in any of the iron/water systems. The *cis*-DCE comprised approximately 1% of the PCE transformed in all the iron/water systems. Chloride concentrations were increased above the background level, further indicating transformation. Chloride adsorption to the iron, if it occurs, was determined to account for a minor proportion of product. The similarities in product distributions indicate that differences in iron properties do not result in environmentally important (e.g. proportion of products which are regulated compounds) differences in the production of products.

REFERENCES

Allen-King, R. M.,R. M. Halket, and D. R. Burris. In press. Reductive transformation and sorption of cis- and trans-1,2-dichloroethene in a metallic iron/water system. *Environ. Toxicol. Chem.*

Allen-King, R. M., H. Groenevelt, C. J. Warren, and D. M. Mackay. 1996. Nonlinear chlorinated-solvent sorption in four aquitards. *J. Contamin. Hydrol.*

Allen-King, R. M. 1997. Reduction kinetics in a batch metallic iron/water system: effect of iron/water exposure. Report prepared for US Air Force.

Burris, D. R., T. J. Campbell, and V. S. Manoranjan. 1995. Sorption of Trichloroethylene and Tetrachloroethylene in a Batch Reactive Metallic Iron-Water System. *Environ. Sci. Technol.* 29:2850-55.

Gillham, R. W. 1995. Resurgence in research concerning organic transformations enhanced by zero-valent metals and potential application in remediation of contaminated groundwater. *209th ACS National Meeting, Anaheim, CA* 35, 1 (April 2-7):691-94.

Gillham, R. W., and S. F. O'Hannesin. 1994. Enhanced degradation of halogenated aliphatics by zero-valent iron. *Ground Water* 32:958-67.

MacDonald, J. A., and M. C. Kavanaugh. 1994. Restoring contaminated groundwater: An achievable goal? *Environ. Sci. Technol.* 28:362-68.

Mackay, D. M., and J. A. Cherry. 1989. Groundwater contamination: Pump-and-treat remediation. *Environ. Sci. Technol.* 23, 6:630-36.

NRC (National Research Council). 1993. *In Situ Bioremediation: When Does it Work?* Washington, D.C.: National Academy Press.

NRC (National Research Council). 1994. *Alternatives for Groundwater Cleanup.* Washington, D.C.: National Academy Press.

Pankow, J. F., S. Feenstra, J. A. Cherry, and M. C. Ryan. 1996. Dense chlorinated solvents in groundwater: Background and history of the problem. **In** *Dense Chlorinated Solvents and Other DNAPLs in Groundwater.* J. Pankow, and J.

A. Cherry (eds.), 1-52. Portland, OR: Waterloo Press.

Roberts, A. L., L. A. Totten, W. A. Arnold, D. R. Burris, and T. J. Campbell. 1996. Reductive elimination of chlorinated ethylenes by zero-valent metals. *Environ. Sci. Technol.* 30:2654-2659.

Schwarzenbach, R. P., P. M. Gschwend, and D. M. Imboden. 1993. *Environmental Organic Chemistry*, 342-348. New York, NY: John Wiley & Sons, Inc.

US EPA (Environmental Protection Agency). 1987. *Federal Register,* July 8, 1987. Washington, D.C.: U. S. Government Printing Office.

US EPA (Environmental Protection Agency). 1990. A Guide to Pump and Treat Groundwater Remediation Technology. EPA/540/2-90/018.

US EPA (Environmental Protection Agency). 1991. *Federal Register,* January 30, 1990. Washington, D.C.: U. S. Government Printing Office.

Vogel, T. M., C. S. Criddle, and P. L. McCarty. 1987. Transformations of halogenated aliphatic compounds. *Environ. Sci. Technol.* 21:722-36.

Westrick, J. J. 1990. National surveys of volatile organic compounds in ground and surface waters. **In** *Significance and Treatment of Volatile Organic Compounds in Water Supplies* N. M. Ram (ed.), 103-25. Chelsea, MI: Lewis.

Wilson, E. K. 1995. Zero-valent metals provide possible solution to groundwater problems. *Chemical & Engineering News,* July 3, 19-22.

DYNAMICALLY ADAPTIVE INTERFACES: A PRELIMINARY INVESTIGATION

Kevin B. Bennett, Ph. D.
Associate Professor
Psychology Department

Wright State University
Dayton, OH 45435

Final Report for:
Summer Research Extension Program
Armstrong Laboratory

Sponsored by the
Air Force Office Of Scientific Research
Bolling Air Force Base, DC

and

Armstrong Laboratory

March 1997

DYNAMICALLY ADAPTIVE INTERFACES: A PRELIMINARY INVESTIGATION

Kevin B. Bennett, Ph. D.
Associate Professor
Psychology Department
Wright State University

Abstract

A "dynamically adaptive interface" (DAI) is a computer interface that changes the display or control characteristics of the system (perhaps both) in real time. The goal of dynamically adaptive interfaces is to anticipate informational needs or desires and to provide that information without the requirement for an explicit control input by the user. DAI's have the potential to improve overall human machine system performance if properly designed; they also have the very real potential to degrade performance if they are not properly designed. The fundamental challenge in designing effective DAI's is to provide dynamic changes in displays or controls that provide the right information at the right time. A collaborative research program to explore both theoretical and practical issues in dynamically adaptive interfaces has been initiated. A DAI concept demonstrator has been developed to assist in precision low level navigation tasks. Advanced controls (a force reflecting stick) and displays (a flight director display) have been incorporated into the dynamically adaptive interface concept demonstrator. The force reflecting stick uses the haptic perceptual channel to provide feedback with regard to the optimal flight path (thus, it is not only a control, but also a display). The visual display is a redesign of the Flight Director (FD) that provides a single configural format with all information relevant to the navigation task. A pilot study to evaluate the DAI was conducted. Three experimental conditions were evaluated: a baseline interface (conventional controls and displays), an advanced interface (advanced controls and displays), and an adaptive interface (dynamically alternating between baseline and advanced). The results indicate that there were significant performance advantages associated with both the advanced and adaptive interfaces relative to the baseline interface for tracking the optimal flight path. The baseline interface produced significantly better performance than the advanced interface for timing-related aspects of the navigation task. There were no significant differences between the advanced and the adaptive interfaces.

DYNAMICALLY ADAPTIVE INTERFACES: A PRELIMINARY INVESTIGATION

Kevin B. Bennett

Introduction

The overall goal for the design of complex sociotechnical systems is to maximize total human-machine system performance. Several characteristics of these systems (e.g., complexity, dynamics, consequences of accidents or sub-par performance) provide numerous challenges to achieving this goal. On the other hand, advances in computer science, engineering, human factors and related disciplines provide numerous resources that can be leveraged for effective design. A research program has been initiated to investigate an advanced interface design concept, the "dynamically adaptive interface" (DAI), in the domain of aviation. A DAI is an interface that changes the display or control characteristics of the system (perhaps both) in real time. Although the DAI concept may appear at first glance to be a radically new idea, we believe that it is simply an extension of useful and commonplace interface designs. Although the DAI concept may also appear to be a radical departure from traditional design wisdom ("consistency is the key to effective interface design"), we believe that DAI's will improve system performance if designed properly. The remainder of the introduction section will outline the DAI concept and related topics.

Sociotechnical systems are comprised of both human and machine components, and the allocation of tasks between these two components has been a traditional, long-standing concern for human factors. Initial guidelines for allocation consisted of lists of preferred activities that matched the perceived capabilities and limitations of each component; allocation was viewed as a discrete design decision with tasks being allocated in an all-or-none fashion. The term "automation" has historically been used to describe the most common form of allocation, where tasks performed by the human were reallocated to the computer. However, the meaning of the term automation has evolved through the years. In a recent discussion of automation Wickens (1992, p. 531) states that "Automation varies from that which totally replaces the human operator by computer or machine to computer-driven aids that help an overloaded operator." When viewed from this perspective it is readily apparent that other areas of research are very closely related to automation. For example, a primary focus in decision aiding is the provision of computerized decision support. To illustrate the overlap between automation and decision aiding consider the following quote by Rouse (1988, pp. 438-

439): "There are three general methods for aiding a user: (1) an aid can make a task easier, (2) an aid can perform part of a task, and (3) an aid can completely perform a task."

The relationship between automation and decision aiding can be made clearer by considering two alternative approaches to decision aiding. "Representation aiding" and "computational aiding" fall essentially at the endpoints of the continuum represented by Rouse's general methods. The representation aiding approach to decision support emphasizes the first two general methods (Bennett, 1992; Bennett & Flach, 1992; Bennett, Nagy, & Flach, In Press; Bennett, Toms, & Woods, 1993; Woods, 1991; Zachary, 1986). The task is made easier (Method 1) by presenting relevant system information in graphical formats, which allows an individual to use his/her powerful pattern-recognition capabilities. Although it is much more subtle, representation aids also perform part of the task for the user (Method 2). Properly designed configural displays will collect and integrate the subset of system data that is relevant to a particular issue and present that subset in the context of system goals. This is clearly a form of automation. To summarize, representation aiding seeks to capitalize upon, rather than to replace, natural human intelligence in the design of decision aids. The connection to automation is quite direct for computational aiding, where mathematical or artificial intelligence techniques (e.g., expert systems, neural networks, signal processing, queuing theory, nonlinear control) are used to provide a direct solution to a task or problem, thereby replacing the user (Method 3). For example, in summarizing their approach to decision support Berkan, Upadhyaya, Tsoukalas, Kisner, and Bywater (Berkan, Upadhyaya, Tsoukalas, Kisner, & Bywater, 1991, p. 8) state that "Operator tasks are emulated by building computer-based algorithms which validate sensor signals, strategies, commands, performance tracking, and which generate reliable decisions, and control actions."

The conceptual development and research literatures on automation and aiding have shown an historical parallel. Traditionally, decisions about both the allocation of tasks between human and machine (automation) and the type of support that was provided to assist the human in the completion of the allocated tasks (aiding) were made during the design phase and remained consistent during the operational phase. However, a great deal of recent interest has been shown in research efforts to develop "adaptive" automation and aiding, where the task allocation or decision support is changed in real time. For example, Hilburn, Parasuraman, & Mouloua (1995b, p. 347) have defined adaptive automation as the "...real-time allocation of functions between human operator and automated system..." Similarly,

Rouse (1988, p. 431) defines adaptive aiding as the "...human-machine design concept that involves using aiding/ automation only at those points in time when human performance in a system needs support to meet operational requirements -- in the absence of such needs, human performance remains unaided/manual, and thereby humans remain very much 'in the loop.'"

The present research investigates the concept of a dynamically adaptive interface, which cross-cuts the concepts of automation, aiding, and adaptation. The concept of an adaptive interface is not a novel concept. For example, many current software packages allow an individual to "personalize" their interfaces by choosing among options in a "preference" menu or window. The same general capability has been implemented in other applications, including advanced aircraft. Although these interfaces are adaptive in a certain sense, the adaptation does not occur in real time. Similarly, the concept of a dynamically adaptive interface is also not a novel concept. A simple example is found in many software packages today. Most applications incorporate pull-down menus that adapt dynamically as a function of a particular interactive sequence (e.g., menus that are updated dynamically to reflect the most recently accessed files or functions).

DAI's have the potential to improve overall performance of the human-machine system dramatically through an increased capability to provide the right information, in the right format, at the right time. The dominant theoretical perspective on human computer interface design describes effective interfaces as those which achieve "transparency" (Hutchins, Hollan, & Norman, 1986). That is, the interface effectively disappears, thus enabling the user to interact directly with the objects of interest in the domain, and to achieve effective interaction with a minimum of cognitive effort. Dynamically adaptive interfaces have the potential to take transparency one step farther. In traditional interfaces appropriate control inputs must be provided by the user when additional information is needed or desired; in dynamically adaptive interfaces this need or desire will be anticipated and the relevant information will be provided without the requirement for control input by the user. The potential benefits for complex dynamic domains are obvious. Operators must consider a great deal of information when completing domain tasks; at the same time, the amount of display "real estate" is often limited. The latter constraint is particularly evident in the domain of aviation (e.g., jet fighters) although the problem exists in other domains as well (e.g., process control). Because all information cannot be presented simultaneously, the operator must select the relevant subset. This requirement serves to increase

already high levels of workload and may occur at peak levels of workload (when the operator needs additional or different information to respond to domain challenges).

DAI's have the potential to improve overall human machine system performance by anticipating informational needs and providing that information in a timely fashion. However, the same characteristics of DAI's that enable these benefits also enable potential costs. Greenburg & Witten (1985, p. 31) summarize the concerns: "Although obvious advantages accrue... there are also obvious disadvantages to presenting users with a changing, adapting and perhaps apparently inconsistent interface." If designed improperly, DAI's have the potential to degrade system performance by preventing the development of automatic processes in the operator, by presenting irrelevant information, or in the worst case, by eliminating information that is currently needed. There is some empirical evidence supporting the benefits of dynamically adaptive interfaces. Greenburg & Witten (1985) developed a dynamically adaptive menu system for a telephone database system. They compared performance with this menu system to performance with a static menu system and found that "The results... support the use of adaptive user modeling. In the (admittedly highly constrained) example system, a computer interface can indeed adapt successfully to every user." It remains an open empirical question as to whether adaptive interfaces can be effective in domains that are not highly constrained. Critical issues include decisions about the choice of dynamic behaviors, about the information and knowledge that should be used to trigger these adaptive behaviors, and about the orchestration of these behaviors and information sources to facilitate performance.

Theoretical perspectives on dynamically adaptive interfaces

As the introduction suggests, a central component of dynamically adaptive displays is that they anticipate informational needs and adapt without explicit control inputs from the operator. Viewing DAI's from the perspective of automation allows us to benefit from the lessons that have been learned about automation through the years. Automation is often viewed (incorrectly) as a panacea for human error: by removing the human from the loop designers believe that the performance of the overall human machine system will be improved. Woods & Cook (1991, p. 1279) summarize what often happens instead: automation increases "... human workload at critical times, a condition called clumsy automation by Earl Wiener. Overall, technology centered automation appears to produce increments in workload and subtle decrements in practitioners' understanding of their environment. Significantly,

these deficits can create opportunities for human error that would not exist in less automated systems, producing a new class of failures."

From this perspective, the fundamental challenge in designing effective DAI's is to ensure that the dynamic changes are consistent with knowledge of the user (including current goals, workload, and levels of performance), knowledge of the task at hand, and knowledge of the current context (current system state and the inherent constraints associated with the domain). Another way of stating this is that dynamically adaptive interfaces should not be clumsy. As a form of automation they have the potential to create new types of errors and to degrade overall human machine system performance. For example, clumsy adaptation might not provide information that is relevant, or might take away information that is currently needed.

A theoretical approach referred to as "cognitive systems engineering" (CSE, Rasmussen, 1986; Rasmussen, Pejtersen, & Goodstein, 1994) can be applied to the practical problem of developing DAI's. The "cognitive system triad" (Woods & Roth, 1988) represents an assumption that the quality of performance in complex, dynamic domains is the result of three interactive and mutually constraining components (see Fig. 1): the cognitive demands produced by the domain of interest, the cognitive resources of the agent(s) that meet those demands, and the representation of the domain through which the agent experiences and interacts with the domain (the interface). From this perspective an adaptive interface must be able to recognize that a cognitive demand / cognitive resource mismatch has occurred (i.e., that the cognitive demands produced by the domain have exceeded the cognitive resources that the agent has available to meet them). After recognizing a demand/resource mismatch an adaptive interface must be able to determine the appropriate change in the amount or type of information that is required to alleviate the mismatch, and to adapt accordingly. The CSE approach, and the implications for the design of DAI's, will be considered further.

Cognitive Demands (Knowledge of domain)

Developing effective interfaces (especially dynamically adaptive interfaces) requires a deep understanding and explicit description of the "semantics" of a work domain. This requirement is even more important for developing dynamically adaptive interfaces. Rasmussen's abstraction hierarchy (Rasmussen, 1986; Rasmussen et al., 1994) is a theoretical framework for describing domain semantics in terms of a nested hierarchy of functional constraints (including goals, physical laws, regulations, organizational/structural constraints, equipment constraints, and

Conceptual Framework for Dynamically Adaptive Interfaces

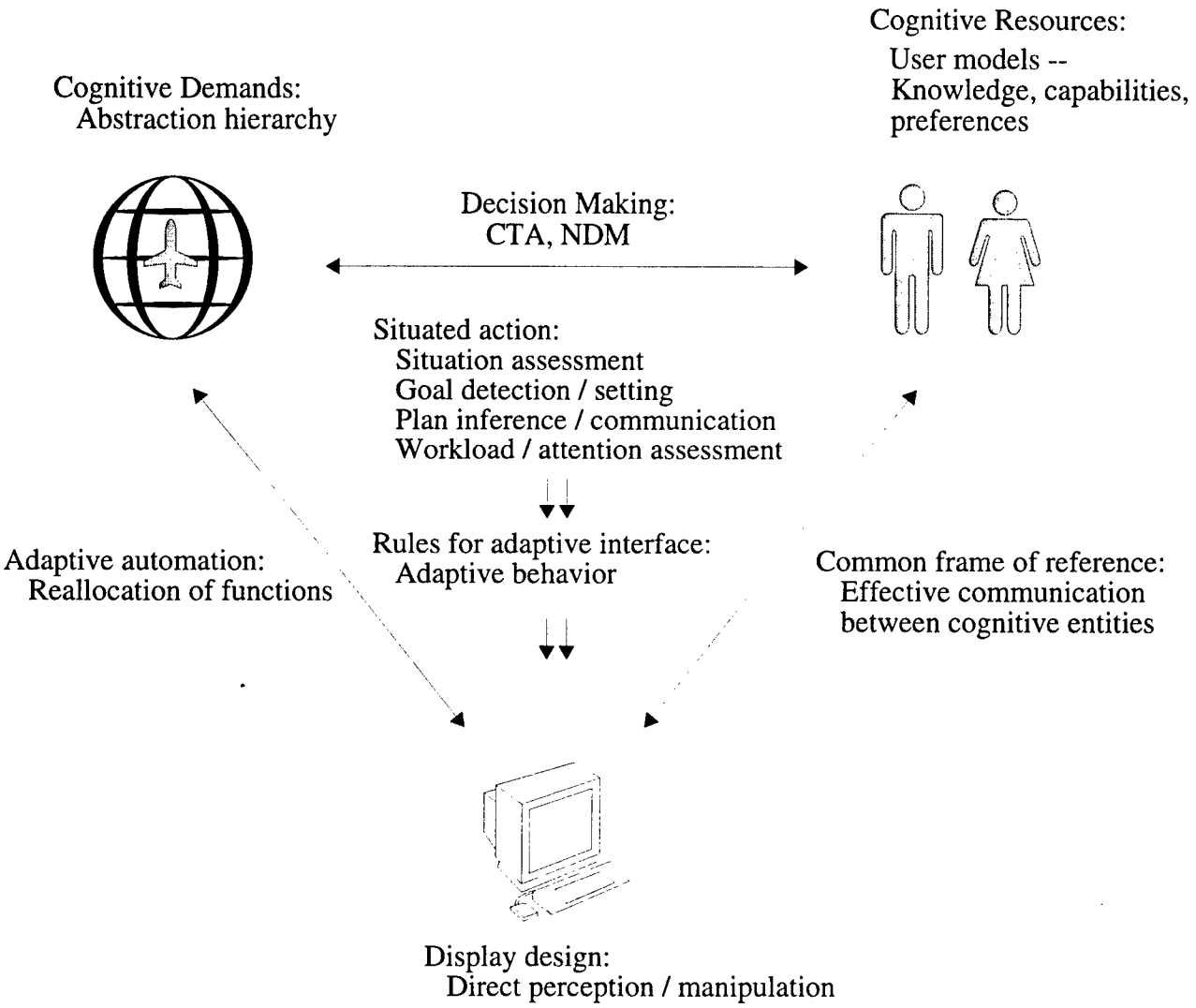

Figure 1.

temporal/spatial constraints). One way to think about the abstraction hierarchy is that it provides structured categories of information (i.e., the alternative conceptual perspectives) that an individual must consider in the course of accomplishing system goals. Thus, in complex domains, situation awareness requires the operator to understand the process at different levels of abstraction. Further, the operator must be able to understand constraints at one level of abstraction in terms of constraints at other levels.

Cognitive Resources (Knowledge of user)

Knowledge of decision making in domain. An abstraction hierarchy analysis provides a description of the domain constraints, independent of decision making in the domain. The design of effective adaptive interfaces will also require a complementary analysis of decision making within the constraints imposed by domain, including procedures, strategies, steps, subgoals, required information, and interrelations between procedures. Historically, decision research has focused on developing models that describe the generation of multiple alternatives (potentially all alternatives), the evaluation (ranking) of these alternatives, and the selection of the most appropriate alternative. By and large, perception was ignored. In contrast, recent developments in decision research, stimulated by research on naturalistic decision making (e.g., Klein, Orasanu, & Zsambok, 1993) has begun to give more consideration to the generation of alternatives in the context of dynamic demands for action. Experts are viewed as generating and evaluating a few "good" alternatives. The emphasis is on recognition (e.g., how is this problem similar, or dissimilar, to problems that I have encountered before?). As a result, perception plays a dominant role. This change in emphasis has increased awareness of perceptual processes and dynamic action constraints in decision making. These trends have, either directly or indirectly, led researchers in interface design to focus on the representation problem. Thus, the challenge for display design from this perspective is to provide appropriate representations that support humans in their problem solving endeavors.

Support for cognitive demand / cognitive resource mismatch: Interface design

Recently, a number of researchers have developed approaches to interface design that include an explicit consideration of the cognitive demands imposed by a work domain (i.e., explicitly recognize and support the human's role as a problem solver). Different terms have been used to describe these approaches, including direct perception (Moray, Lee, Vicente, Jones, & Rasumssen, 1994), ecological interface design (Rasmussen & Vicente, 1989), representational

design (Woods, 1991), or semantic mapping (Bennett & Flach, 1992; Bennett et al., In Press; Bennett et al., 1993). However, all these approaches share the same basic philosophical principles; collectively, they complement the principles of direct manipulation articulated by Hutchins, Hollan, and Norman (1986). There are two critical components of effective display design: correspondence and coherence.

Correspondence refers to the issue of content --- what information should be present in the interface in order to meet the cognitive demands of the work domain? Correspondence is defined neither by the domain itself, nor the interface itself: it is a property that arises from the interaction of the two. Thus, in Fig. 1 correspondence is represented by the labelled arrow that connects the domain and the interface. One convenient way to conceptualize correspondence is as the quality of the mapping between the interface and the work space, where these mappings can vary in terms of the degree of specificity (consistency, invariance, or correspondence).

Coherence refers to the mapping between the representation and the human perceiver. Here the focus is on the visual properties of the representation. What distinctions within the representation are discriminable to the human operator? How do the graphical elements fit together or coalesce within the representation? Is each element distinct or separable? Are the elements absorbed within an integral whole, thus losing their individual distinctness? Or do the elements combine to produce configural or global properties? Are some elements or properties of the representation more or less salient than other elements or properties? In general, coherence addresses the question of how the various elements within a representation compete for attentional and cognitive resources. Just as work domains can be characterized in terms of a nested hierarchy of constraints, so too, can complex visual representations be perceived as a hierarchy of nested structures, with local elements combining to produce more global patterns or symmetries.

Whether a display will be effective or not is be determined by both correspondence and coherence. More specifically, the effectiveness of a display is determined by the quality of the mapping between the constraints that exist in the domain and the geometrical constraints that exist in the display. The display constraints are defined by the spatio-temporal structure (the visual appearance of the display over time) that results from the particular representation chosen. In configural representations the geometrical display constraints will generally take the form of symmetries --- equality (e.g., length, angle, area), parallel lines, colinearity, or reflection. The core problem in implementing effective displays is to provide visual representations that are perceived as accurate reflections of the abstract domain

constraints: Are the critical domain constraints appropriately reflected in the geometrical constraints in the display? Are breaks in the domain constraints (e.g., abnormal or emergency conditions) reflected by breaks in the geometrical constraints (e.g., emergent features such as non-equality, non-parallelism, non-closure, bad form)? Only when this occurs will the cognitive agent be able to obtain meaning about the underlying domain in an effective fashion.

Situated action. The quality of the interface is especially important in coordinating intelligent machine and human activities. Researchers have investigated this facet of the interface problem in the context of systems that have a machine expert system (e.g., Roth, Bennett, & Woods, 1987; Suchman, 1987). Two central principles have emerged: "situated action" and "mutual intelligibility" (which depends upon a "common frame of reference"). Suchman (1987) has proposed that human-human communication provides a particularly relevant analogy to frame questions of human computer interaction. She contrasts the traditional view of intelligent action (the development and implementation of plans) to situated action, stating that "... purposeful actions are inevitably *situated actions*. By situated actions I mean simply actions taken in the context of particular, concrete circumstances" (p. viii). Suchman (1987) applies this view of intelligent action to the design of human computer systems, and observes that "Interaction between people and machines implies mutual intelligibility, or shared understanding" (p. 6). Roth, Bennett, and Woods (1987) reached similar conclusions in their evaluation of an expert system designed to assist technicians in the repair of an electro-mechanical device. The design of the system interface was "opaque" and therefore inhibited the development of a mutual understanding between the human and machine experts. As a result the two cognitive entities worked independently and in parallel (rather than orchestrating their activities), and overall system performance was degraded significantly.

Dynamic adaptations

All of these considerations come together when considering dynamic adaptive behaviors on the part of the interface. One basis for adaptive changes has been referred to as "human performance models" (Rouse, 1988). The goal of these models is to predict when degradations in performance are likely to occur, which serves as a basis for changing the level of aiding. Models could be devised to represent many aspects of human performance, capabilities and limitations, including 1) knowledge of the system (e.g., capabilities, limitations, tendencies that are specific to the interface and its adaptive behaviors), 2) knowledge of the task domain (e.g., declarative or procedural knowledge), or

3) other information (e.g., processing capabilities, interaction style, preferences, strategies). Rouse (1988, p. 434) summarizes the role that human performance models may play: "Thus models are needed whereby on-line predictions of performance can be obtained based on the current state of task demands and the availability of human sensori-motor and information-processing resources. These models represent one of the ways in which expertise about human behavior and performance can be embedded in an intelligent support system."

Human performance models of mental workload would be particularly useful in this context. It is a fairly well established fact that the relationship between workload and performance is not necessarily a linear one. More specifically, equal increases or decreases in workload are not reflected by equal increments or decrements in performance. As workload increases from a low to a high level individuals are often able to mobilize resources to meet the increased demand, and performance may not suffer. However, as an individual approaches the maximum level of workload small increases may have precipitous (and negative) effects on performance (e.g., the "straw that broke the camel's back"). From the perspective of dynamically adaptive interfaces, on-line psychophysiological measurements of workload might be useful through the provision of information that could be used to improve the timing of adaptive interface changes, and therefore overall performance.

Rouse (1988, p. 435) refers to "on-line assessment" as a second category of techniques that could be used to trigger changes in the interface: "Beyond predicting human performance and anticipating degradations, adaptive aiding requires on-line assessments of what the human is doing and, if possible, what the human intends to do..." An obvious example of on-line assessment is the levels of performance that are being maintained. If performance is showing trends of degradation then adaptive measures could be considered. A version of on-line assessment that Rouse believes to have particular promise is a category that he refers to as "leading indicators." Leading indicators are secondary performance measures which exhibit performance decrements in advance of primary performance indicators (and therefore would be quite useful in triggering adaptive changes). On-line assessment can also refer to the assessment of user intent: "It was recognized quite early... that knowledge of humans' intentions was necessary if adaptive aiding was to succeed fully." (Rouse, 1988, p. 435). The attempts to develop intelligent tutoring systems (e.g., Polson & Richardson, 1988) have demonstrated unequivocally that to do so represents a formidable challenge.

Summary

The preceding theoretical perspective, and the analyses that it suggests, forms the basis for the development of dynamically adaptive interfaces. The abstraction hierarchy analysis reveals the critical domain constraints (the cognitive demands that must be met, and the domain resources that are available to meet them). The cognitive task analysis defines the decisions that need to be made to meet domain goals, and the information that is relevant to those decisions. This information is used, in conjunction with the semantic mapping principles of display design, to develop displays that appropriately reflect domain constraints and thereby assist in decision making and problem solving. These analyses also provide knowledge about situated action, and constitute the basis for dynamically adaptive behaviors on the part of the interface. Applying these analyses will result in a definition of what adaptations are appropriate in the interface, and the development of rules / models that describe when those adaptations should occur. These rules / models include knowledge of the operator's performance, the operator's workload, general aspects of the task/domain, and specific aspects of current system state (i.e., an assessment and continuous monitoring of the domain for changes that have implications for goals and required actions -- the context or situation). The end result will be a common frame of reference, or mutual intelligibility, between the human and the adaptive interface. Dynamic alterations in the interface will be consistent with current goals and context; the intelligent action on the part of the interface will improve overall human-machine system performance.

Concept demonstrator

A concept demonstrator was developed to investigate issues in the design of dynamically adaptive interfaces for a class of aviation tasks -- precision low level navigation. A characteristic of these tasks is the requirement to fly an aircraft along a predetermined path (or, at a minimum, to intersect predetermined waypoints) and to be at a specific point in the flight path at a specific time. One example of a low level navigation task is to deliver ordnance in enemy territory. To accomplish this task a pilot may be required to fly along a particular path (to avoid ground based threats), and to arrive at waypoints or the target site at a particular point in time (to benefit from air cover that has been provided to mask arrival, or to coordinate with other offensive activities). An advanced control (a force reflecting stick) and an advanced display (a flight director display) were developed to support pilots in these tasks. The force reflecting stick provides changes in resistance to a pilot's control input (or the amount of force that is required to implement the control input) that varies as a function of the airplane's deviation from the optimal flight path. The flight director display

integrates several pieces of navigation-related information (e.g., altitude, line-up information, airspeed) in a single "configural" display that provides a commanded steering input to the pilot. The advanced controls and displays will be described in greater detail.

Advanced display: Configural flight director HUD

The configural flight director (CFD) HUD display combines aspects of both representational and computational aiding. The computational aiding component of this display should be considered as a subtle form of automation. Consider the following quote by Rouse (1981, p. 75): "... consider an aircraft flight director, where the computer integrates a variety of sources of information, referenced to a desired flight path and profile, and displays a 'command' telling the pilot what to do (i.e., keep the aircraft symbol lined up with the cross hairs). One can easily argue that the computer is controlling through the pilot in the sense that it is directing the pilot's actions (hence the term flight director). Certainly the pilot is not 'closing the loop' in the usual sense that an automobile driver does." The algorithms that underlie this form of calculational aiding are described in Appendix A.

The representation aiding component of consists of two rectangular boxes (see Fig. 2a) and a visual reference point (the watermark symbol). The visual reference point remains in a fixed position in the HUD and both rectangles move dynamically to signify deviations from the recommended flight path. Both rectangles have a dashed and a solid component. The solid component serves as a reference to ground, while the dashed component serves as a reference to the sky. This aspect of the display serves as a cue for the aircraft-ground relationship: when the plane is right side up the solid portion will appear on the bottom, when the plane is upside down the solid portion will appear on the top.

Deviations of the aircraft from the flight path resulted in movements of the configural display from a fixed reference at the center (waterline). Changes in the location and orientation of these two rectangles (relative to the fixed visual reference point) provide "emergent features" that signify commanded roll and pitch inputs to the pilot. If the values of all variables are consistent with the optimal flight path then the rectangles will enclose the watermark symbol and will be centered and aligned with it (see Fig. 2a). A deviation in altitude (pitch) is represented by a vertical displacement of the rectangles. When the rectangles are above the watermark the airplane is below the recommended flight path (see Fig. 2c); when the rectangles are below the watermark the plane is above the recommended flight path (see Fig. 2d). A deviation in heading is represented by rotation of the rectangles. When the airplane's course is to the

Figure 2

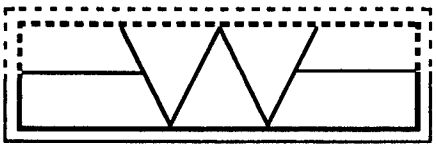

A.

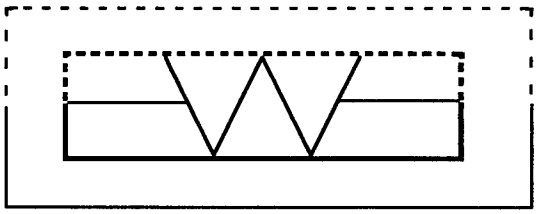

B.

C.

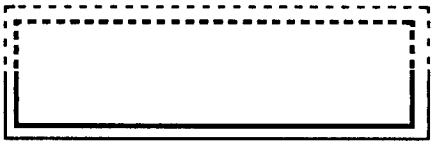

D.

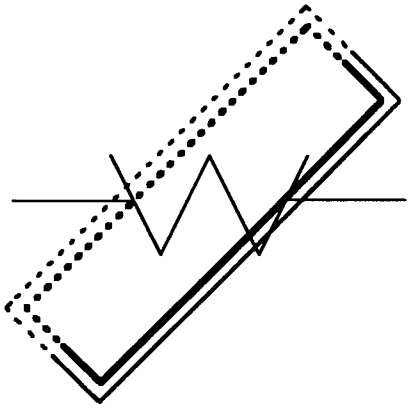

E.

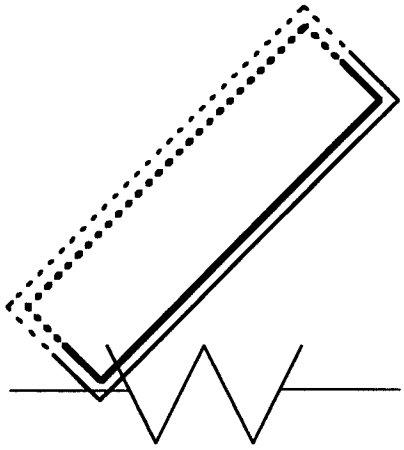

F.

left of the recommended flight path the rectangles will rotated clockwise, relative to the watermark (see Fig. 2e), and vice-versa. A lateral and vertical deviation from the flight path is in Fig. 2f. This figure represents a commanded input to turn the plane to the left and to simultaneously increase altitude. Thus, the display was designed to be a "fly-to" type of display in which the pilot attempts to match the roll and pitch suggested by the rectangles, thereby keeping the waterline within the rectangles and the aircraft on the desired flight path.

Airspeed. The two rectangles represent actual and commanded airspeed. The bold rectangle provides a visual representation of the airspeed goal; the non-bold rectangle provides a visual representation of current airspeed with respect to this goal. When current airspeed is greater than the goal airspeed the non-bold rectangle will be smaller than the bold rectangle (see Fig. 2b); when current airspeed is less than the goal airspeed the non-bold rectangle will be larger than the bold rectangle. When considered together, the two rectangles provide an "emergent visual feature" that specifies both the goal for airspeed and the degree of deviation from this goal directly.

It is important to note that the bold rectangle represents the goal airspeed (which can change, even though the size of the rectangle does not) and that the bold rectangle represents the deviation between actual and commanded airspeed, not current airspeed. For illustrative purposes, imagine that a pilot is maintaining a constant airspeed while navigating towards a waypoint. Further imagine that this constant airspeed is less than the airspeed required to place the aircraft at the waypoint at the appropriate time. In this scenario the distance between the plane and the waypoint is decreasing at a constant rate, but the time error is constant.

Advanced control. Brickman, Hettinger, Roe, Lu, Repperger, and Haas (In Press) developed a force-reflecting, haptically-augmented aircraft control stick and evaluated it in the context of an instrument landing task. When the ground surface is obstructed (e.g., when flying through low clouds), a pilot relies upon instruments that provide information with respect to an optimal approach path to the runway (in particular, glideslope and line-up information). The force reflection stick represents an augmentation of existing instrumentation. In contrast to a conventional stick, the augmented stick serves as both a control and a display. For example, if the plane deviated to the right of the optimal approach path the pilot would experience an increase in resistance when attempting control inputs to the right, and a decrease in resistance when attempting control inputs to the left. Thus, the force reflecting stick is not only a control, but also a display which uses the haptic channel to provide feedback with regard to the optimal approach path.

Dynamically adaptive interface: Preliminary evaluation

The concept demonstrator was used to perform a preliminary investigation of dynamic adaptive interfaces. Three different interface conditions constituted the primary independent variable of the experiment; each will be described in greater detail.

Baseline interface. The baseline interface contained typical controls and displays and was fairly representative of current fighter HUDs in the "declutter mode" (see Fig. 3a). A heading scale was positioned near the bottom of the display, and airspeed (KCAS) and barometric altitude tapes were arranged vertically on the left and right sides of the HUD, respectively. A horizon bar and flight path marker (FPM) were also provided, however, no pitch and dive scale was depicted. Digital readouts of instantaneous load factor (G) and angle of attack (degrees) were presented on the left side above the airspeed scale. Waypoint information was presented in the format "__ D__" (read as __nautical miles from waypoint number __) on the lower right of the HUD, next to the heading scale. Two sets of carets were presented on each of the three tapes. One set of carets depicted the current values for heading, altitude, and airspeed. The second set of carets depicted the desired or "commanded" values for each of these variables. For heading and altitude these commanded values are the corresponding information with regard to the next way point; for airspeed it is an estimated time of arrival (see method section for additional details).

Advanced interface. The advanced interface contained the CFD HUD and the force-reflective stick described previously. The calculational aiding component consists of the algorithms lying behind the flight director and force-reflective stick. As opposed to the baseline interface (which presents current values for task-relevant variables), the advanced interface calculates commanded control input(s) to the pilot that minimize spatial and temporal errors relative to the optimal flight path. The representational aiding component of the advanced interface consists of multi-modal, configural representations of this information. The combined haptic-visual displays suggest the appropriate control input through coherent representations that integrate all of the relevant variables (consistent with the principle of "correspondence") in a centralized and easily interpretable format (consistent with the principle of "coherence").

Adaptive interface. The adaptive interface consisted of both the advanced and the baseline interfaces. The primary source of information that was used as a basis for the dynamic adaptation of the interface was the on-line assessment of performance. The aircraft's spatial position relative to the pre-planned flight path and its temporal position relative

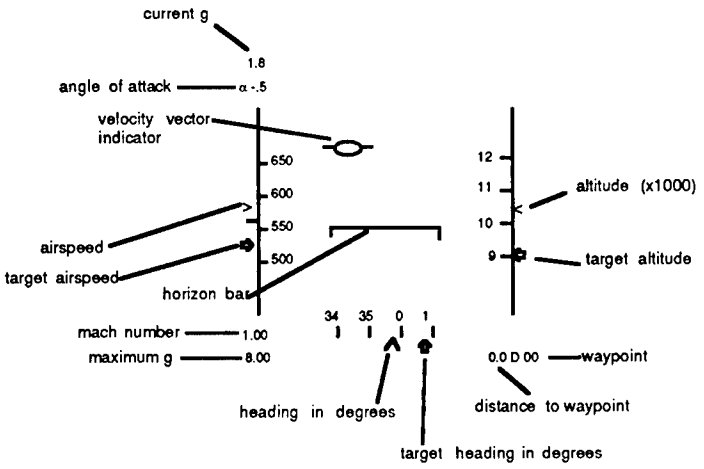

Figure 3a. Baseline HUD

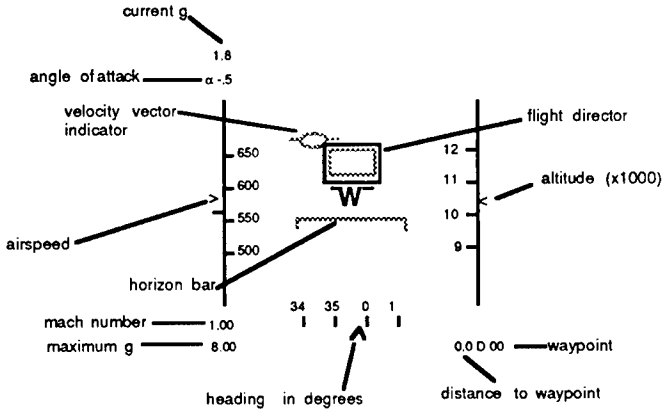

Figure 3b. CFD HUD

to the timing goals were monitored constantly, and the degree of deviation served as the basis for dynamic adaptation (switching between the two interfaces). When performance was within spatial and temporal performance boundaries the baseline interface was present; when these boundaries were violated the advanced interface became present (the visual aspects of the baseline interface were still present in the HUD, but dimmed). Spatial and temporal "dead-bands" were implemented to ensure that interface "hysteresis" (rapid alternation between the two interfaces) did not occur.

Two air force pilots completed a precision, low-level navigation task. Pilots completed this mission under six experimental conditions: three different interfaces (baseline, advanced, adaptive) in combination with two levels of turbulence (present / not present). Performance was evaluated on several dependent measures, including spatial deviation from the optimal flight path (horizontal and vertical), temporal deviation from timing goals, and subjective measures of workload.

Method

Subjects. Two experienced US Air Force pilots served as subjects. Subject A was 31 years of age and had in excess of 2300 hours of flight experience. Subject B was 55 years of age and had over 3200 hours of flight experience. Both subjects had normal or corrected-to-normal vision.

Apparatus. The experiment was conducted in the SIRE facility's Fusion Interfaces for Tactical Environments (FITE) laboratory. The simulated F-16 cockpit (fiberglass body) contained six Liquid Crystal Display (LCD) head-down displays (only one LCD was used, and only to provide feedback), an F-16C throttle and sidestick controller (connected to a McFadden hydraulic control loader). The cockpit was located in the center of a cubic (8' x 8' x 8') projection room; visual scenes were produced by four Apollo color projectors, driven by two Intergraph TDZ-310 graphics workstations running Windows NT. The workstations had Realism Z-13 graphics accelerator boards, using graphics generated with the OpenGVS Application Programming Interface (API). The output to each projector was 32-bit color on a 1024x768 pixel display.

Stimuli. An out-the-window (OTW) display of simulated terrain was presented on the inside of the projection room. Each HUD was incorporated into the OTW display, at a fixed location directly in front of the cockpit, occupying approximately a 20-degree field of view. There were three interface conditions: baseline, advanced, and adaptive.

The baseline interface is illustrated in Figure 3a. The commanded heading was the straight-line heading to next waypoint. The commanded altitude was 300 feet throughout the majority of the flight, but changed to 1000 feet at the end of a trial. The commanded airspeed consisted of an estimated time of arrival (ETA) at the upcoming waypoint, assuming a direct path and a constant speed. The equation was ETA = t + d / v, where "t" is the current time in seconds, "d" is the distance in feet to the upcoming waypoint, and "v" is the current aircraft ground speed (horizontal velocity component) in feet-per-second. At each update, the ETA was computed and compared to the waypoint's target arrival time (determined in advance). If the ETA was sooner than the target time, the commanded airspeed directed the pilot to slow down; if the target time was sooner than the ETA, the pilot was directed to speed up. The maximum directed change was 100 knots, which occurred if the subject was 45 seconds or more off schedule, and timing errors were mapped linearly to directed airspeed changes.

The advanced interface contained an advanced control (force-reflective, haptic stick) and an advanced display (a configural flight-director HUD -- CFD HUD). The CFD HUD used both computational and representational aiding. The representational aiding was provided by the analog configural display, as discussed previously (see Fig. 2 and the related discussion). The computational aiding component was provided by "flight director" algorithms that provided command inputs: the CFD HUD represented the roll, pitch and throttle inputs that were necessary for maintaining the aircraft's position on the pre-planned flight path, rather than the direct representation of those parameters. The algorithms included "centerline recovery mode", with "turn short mode" for primary waypoint sequencing and the "90-degree test" for backup waypoint sequencing. The navigation calculations resulted in a directed bank and pitch angle for the pilot, which was then displayed graphically in the HUD via the Flight Director, after being filtered using a simple "delta-limit filter" to prevent abrupt changes in the display. The details of these algorithms are provided in Appendix A. The CFD HUD also used the commanded airspeed calculations employed in the baseline interface.

The advanced interface condition also contained a force-reflective haptic stick. The sidestick controller was connected to a McFadden hydraulic control loader, which allowed numerous aspects of stick feel to be modified in real-time. The force-reflective stick was also programmed to provide a command input: a pilot who initiated inappropriate control inputs (those which would move the aircraft away from the optimal flight path) would receive haptic feedback in the form of increased resistance. The amount of resistance depended upon the amount of deviation from the optimal flight

path, both horizontal and vertically (resistance was proportional to the cube of the positional error). For example, if the subject's altitude was below the target flight path, more force was required to push the stick forward (pitch down); if the subject's altitude was too high, more force was required to pull the stick back (pitch up). Similarly, if the subject was left of the flight path, the stick was harder to push left, and if the subject was to the right, the stick was harder to push right. No force was ever required to keep the stick centered.

In the adaptive interface the baseline interface was present when the aircraft was within performance boundaries (spatial deviations from the optimal flight path of less than 500 feet laterally or 50 feet vertically; timing deviations between the ETA and timing goal of less than 10 seconds). The advanced interface was present when the aircraft was outside these performance boundaries (the visual components of the baseline interface remained in the HUD, but were dimmed). To prevent interface "hysteresis" (rapid switching between interfaces) deadbands were implemented. After an interface exchange had occurred, a return to the previous interface could only transpire when the performance boundary was exceeded by an additional 10 feet (e.g., a 40 feet vertical deviation would trigger a return to the baseline interface) or when the performance boundary was exceeded by less than 10 feet but was maintained for more than 10 seconds (e.g., a 45 feet vertical deviation maintained for 10 seconds would trigger a return to the baseline interface).

Simulated wind turbulence could be present in some experimental trials. The turbulence model consisted of a sum of seven sinusoids, attenuated with a high-pass filter to emphasize disturbances in the lower frequencies. The turbulence model used the following sum of sinusoids ("t" is time in seconds): $F(t) = 0.99 \sin(0.2512\,t + 3.0) + 0.95 \sin(2.1352\,t + 11.0) + 0.93 \sin(3.8936\,t + 19.0) + 0.85 \sin(5.4008\,t + 31.0) + 0.75 \sin(6.6568\,t + 37.0) + 0.68 \sin(8.4152\,t + 41.0) + 0.59 \sin(9.9224\,t + 47.0)$. The turbulence was applied separately to the x-, y-, and z-components of the aircraft's velocity, resulting in a seemingly random three-dimensional wind velocity.

Procedure. Each subject participated in one training session and three experimental sessions, with each session lasting about 90 minutes. Training consisted of a briefing on the experimental task and procedures, instructions describing the use of each of HUDs and cockpit controls, a subsequent question and answer period regarding the use of HUDs, and several minutes of unconstrained flight in the simulated environment. During both training and experimental sessions subjects completed 6 blocks of trials. These 6 blocks of trials resulted from the factorial combination of the 3 interface conditions (baseline, advanced, or adaptive) with the 2 turbulence conditions (turbulence or no turbulence).

The presentation order of blocks was randomized. In the training session subjects completed 2 trials within a block; in the experimental sessions subjects completed 3 trials within a block.

Pilots were informed of their display and turbulence condition prior to each block. Each trial began with the simulated aircraft flying at an airspeed of 450 knots with a heading of 5 degrees and an altitude of 300 feet above ground level altitude (AGL). Pilots were instructed to maintain their flight path and approach the first waypoint which was 6 nautical miles away. Pilots were told to proceed past the first waypoint to a second waypoint 6 nautical miles beyond the first. Upon reaching the second waypoint, pilots had to change their heading to 55 degrees and begin an approach to the next waypoint, also 6 nautical miles away. After reaching the third and final waypoint, pilots were instructed to change their heading to 100 degrees and proceed toward a runway. On the approach to the runway, pilots were required to increase their altitude to 1000 feet in preparation for a weapons delivery. The trial was completed when the simulated aircraft passed over the front edge of the runway. Each trial was approximately three and one-half minutes in length. After each trial subjects were provided feedback (RMS error values for lateral and vertical deviations from the prescribed flight path; RMS error for temporal deviations from waypoint timing goals). Upon completing each block of trials, subjects were asked to assess their workload for that particular condition using a multidimensional self-report of workload (NASA TLX -- Hart and Staveland, 1988).

Results

Analyses were performed for four dependent measures (horizontal error, vertical error, timing error, and workload assessments). A 3 (display) x 2 (turbulence) x 3 (day) repeated-measures, within-subjects ANOVA was performed on each dependent measure; post-hoc analyses (the Tukey Honest Significant Difference test) was conducted on significant effects. RMS error provides a single, summarized estimate of performance within a trial and RMS error scores were conducted for horizontal error, vertical error, and timing error. Horizontal and vertical errors were calculated by comparing the optimal flight path to the actual flight path. Ten data samples were taken for each second of flight time. The formula for RMS error is $\sqrt{\Sigma(F-X)^2/(n-1)}$, where X is the value of the horizontal or vertical position of the aircraft during a sample, F is the horizontal or vertical position of the optimal flight path, and n is the number of samples. An average RMS score for a block of trials was computed by averaging the three trials within that block. For horizontal error the interaction effects between display and day, $F(4,4) = 9.13$, $p < 0.03$, and display, day,

and turbulence, F (4,4) = 15.26, $p < 0.02$, were significant. The means for the three-way interaction effect are illustrated in Fig. 4a. The post-hoc analysis for this effect indicated that no comparisons between the advanced interface and the adaptive interface were significant. With no turbulence both the adaptive and advanced interface produced significantly better performance than the baseline interface in the first experimental session; the advanced interface produced significantly better performance than the baseline interface in the second session; there were no significant differences in the third experimental session. With turbulence present both the adaptive and the advanced interfaces produced significantly better performance in all three experimental sessions. For vertical error the interaction effect between display and day, F (4,4) = 10.70, $p < 0.03$ was significant. The means for this effect are illustrated in Fig. 4b. Again, the post-hoc analysis revealed that no comparisons between the advanced interface and the adaptive interface were significant. Both the adaptive and advanced interface produced significantly better performance than the baseline interface in the first experimental session; the advanced interface produced significantly better performance than the baseline interface in the second and third sessions. An RMS timing error score was also calculated (substituting an optimal flight time for the optimal flight path in the RMS formula listed above). The main effect of display was significant, F (2,2) = 19.59, $p < 0.05$. The post hoc analysis revealed that the baseline interface produced significantly better timing performance than the advanced interface. For illustrative purposes the display by day interaction effect means are illustrated in Fig. 4c. An overall estimate of subjective workload for each block of trials was obtained by averaging across the six subscale ratings of the NASA TLX. The ANOVA revealed no significant effects; the means for the three-way interaction are illustrated in Fig. 4d.

General discussion

Due to the low number of subjects, and the limited evaluation performed, the results must be interpreted with caution. The results appear to indicate that the decision support (a combination of representational and calculational aiding) provided by the advanced controls and displays was generally successful in improving performance at the low-level precision navigation task. Both horizontal and vertical tracking measures revealed significant improvements in performance when these controls and displays were present, relative to the baseline interface. The best tracking performance was associated with the advanced interface (controls and displays always present): all statistical comparisons with the baseline interface were significant, with the exception of the horizontal error on Day 3 with no

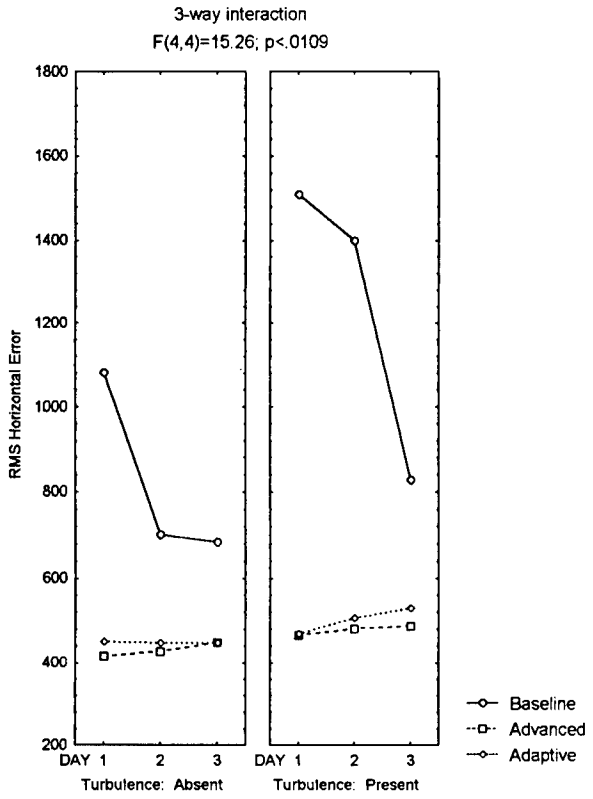

Figure 4a

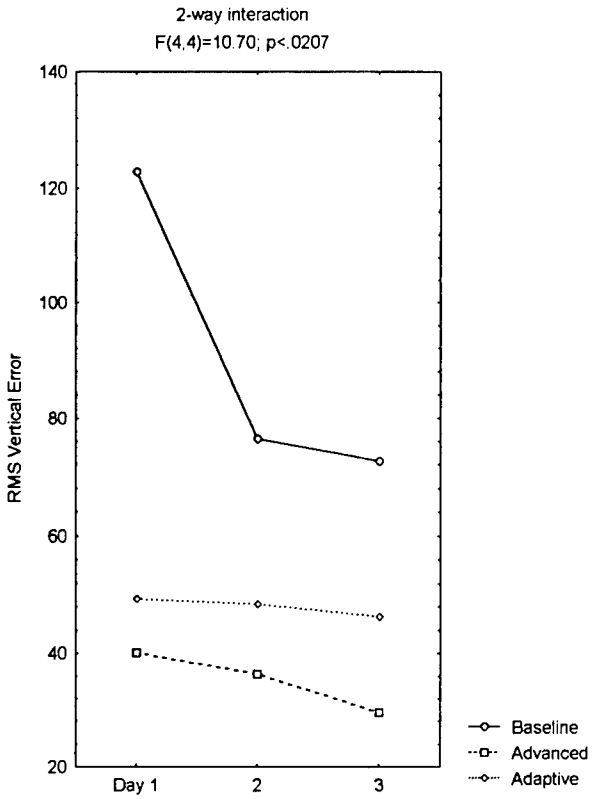

Figure 4b

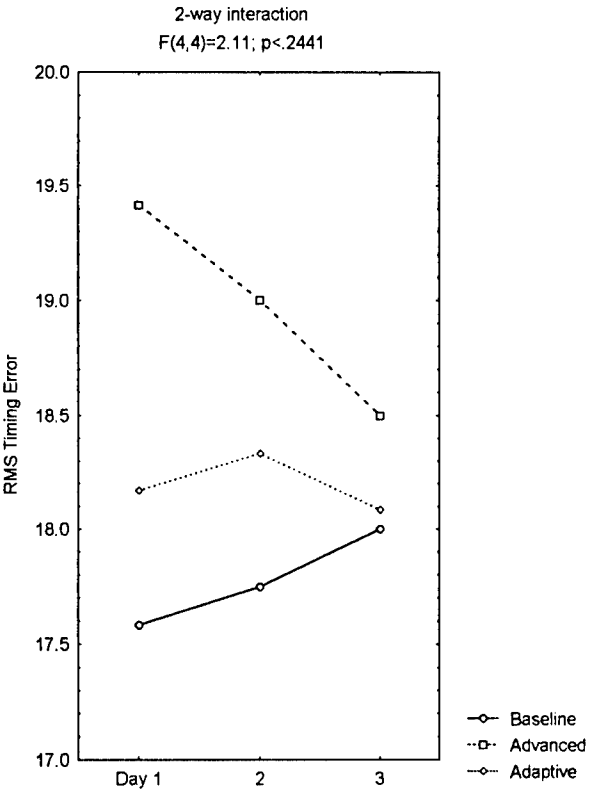

Figure 4c

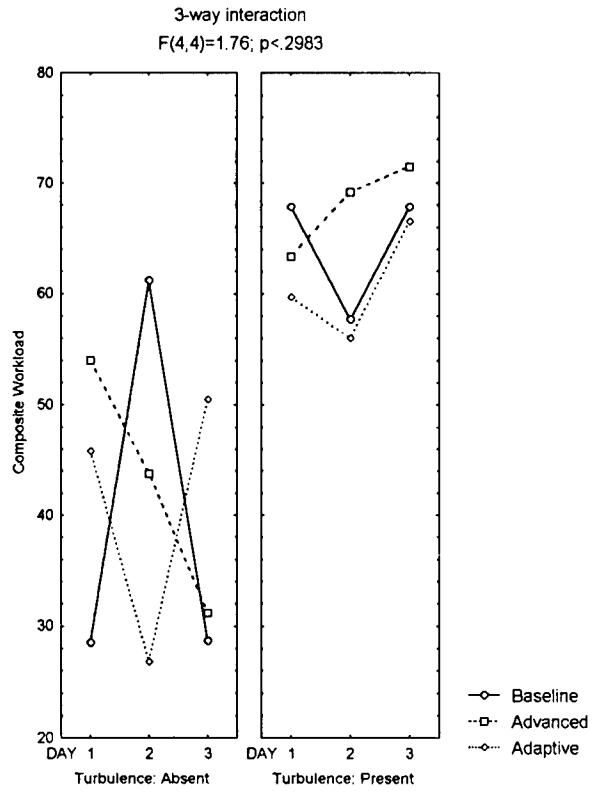

Figure 4d

turbulence present. The adaptive interface (dynamic adaptation between advanced and baseline interface) produced consistently better tracking performance than the baseline interface. For both horizontal (turbulence and no turbulence) and vertical RMS error the adaptive interface produced significantly better performance on Day 1. These performance advantages remained significant across Days 2 and 3 for horizontal error when turbulence was present; for horizontal error without turbulence and for vertical error the significance of the performance advantages disappeared with experience at the task.

Given the limitations of the pilot study, these results provide a strong validation of the utility of the advanced control and display in supporting the pilots in a critical aspect of precision, low-level navigation: following a pre-determined flight path. These results were obtained despite the fact that several factors worked against these controls and displays: only two pilots participated in the experiment, they were much more familiar with the traditional interface, and the six hours of experience with the advanced controls and displays represents a very short learning period.

In contrast to tracking error, the advanced controls and displays did not appear to support the pilots' efforts to meet the timing goals of the low-level navigation task. The advanced interface produced significant decrements in RMS timing error relative to the baseline interface; the adaptive interface produced worse performance than the baseline interface, although the differences were not significant. Consideration of timing performance across display and day yields some interesting insights (see Fig. 4c). Performance was always best for the baseline interface. However, by the third experimental session the difference between the baseline and the adaptive interfaces was negligible. In contrast, performance for the advanced display was extremely poor at the outset of the experiment, but improved steadily with experience at the task.

Because all three interfaces used the exact same algorithm to produce commanded and actual airspeed, the difference must lie in issues of representation. There are at least two potential explanations for this decrement. The first is relatively simple, and is related to perceptual salience: it was difficult to make the two configural rectangles sufficiently discriminable with the lighting and projection hardware configuration that was used. Increasing the difference in perceptual salience between the commanded and actual rectangles may produce better results. An alternative explanation is related to the quality of the basic perceptual judgments that the two representations required the pilots to make. The baseline interface required pilots to make a judgment of the differences in vertical extent

between two symbols (the carets representing actual and commanded airspeed) that shared a common baseline. In contrast, the advanced interface (and the adaptive interface when the advanced HUD was present) required pilots to compare the relationship between two rectangles (either size, area, or the space between sides) that were changing in both location and orientation. These results are consistent with the findings of Cleveland and his colleagues (e.g., Cleveland, 1985) and suggest that the most likely explanation of the significant performance decrements in RMS timing error with the advanced HUD is related to the difficulty of the perceptual judgments that it required (relative to the baseline). A redesign of the representation of timing information should be considered; these modifications would be fairly simple.

In terms of the overall goal of the proposed research program -- to investigate theoretical and practical issues in the development of dynamically adaptive interfaces -- the critical comparisons in performance were between the advanced and the adaptive interfaces. Differences in performance between these two interfaces were negligible for horizontal error. For vertical error the differences were small, but consistent, and favored the advanced interface. However, for both these dependent measures no direct comparisons were significant (or even approached significance). The differences in timing error were more pronounced, and favored the adaptive interface.

These results represent an encouraging pattern of results. One of the primary concerns with the concept of a dynamically adaptive interface is based on the potential for a "changing, adapting and perhaps apparently inconsistent interface." (Greenberg & Witten, 1985, p. 31). Both practical guidelines and theoretical approaches to interface design identify consistency as a fundamental component of effective design. This conclusion is a very reasonable one, as evidenced by both common sense and experimental research. When individuals are presented with consistent information they are typically able to develop extremely effective patterns of behavior over time, behavior that is characterized by the parallel and automatic processing of both external information and overt responses. With some nuances to differentiate between terms, researchers have labelled this type of behavior as "automatic processing" (e.g., Shiffrin & Schneider, 1977), "skill-based behavior" (Rasmussen, 1986), "procedural knowledge" (Anderson, 1982), and "associative skill" (Fitts & Posner, 1967). One fundamental challenge in designing effective DAI's is to provide dynamic changes in display or control information that do not interfere with either the development or the execution of skilled behavior. The results of the present experiment appear to indicate that this is possible.

A more extensive evaluation (with modification of the advanced control and display) will be required to solidify the preceding conclusions. However, the long-range goal of the research program is to demonstrate that dynamically adaptive interfaces can produce increments in performance, relative to a static interfaces that portray the same information. A fundamental step in this direction will require the development of a more rich experimental environment. The factors that drive the need for dynamically adaptive interfaces (a wealth of information, limited display real estate) are not currently present. Therefore, additional task requirements that are typically associated with low-level navigation (e.g., avoiding threats, delivering ordnance) should be incorporated. A complementary step will be the incorporation of more complex mechanisms to trigger adaptive changes on the part of the interface. Performance models will be difficult to implement, however there are several viable alternatives. Real-time assessments of workload are a possibility, and are consistent with on-going projects within the branch. A second possibility is to exploit Rouse's notion of leading indicators. For example, micro-analysis of control inputs should provide a reasonable indicator of workload and therefore a predictor of impending performance declines (and the need for adaptive behavior).

Acknowledgments

I would like to thank those individuals and organizations who have contributed their time, effort, and resources to making the REP appointment successful and mutually beneficial. First, I would like to thank the Air Force Office of Scientific Research, Research & Development Laboratories, the Human Engineering Division of Armstrong Laboratories, and the Human Interface Technologies Branch for making the appointment possible. I would also like to thank the contractors who assisted in both the conceptual and physical development of the concept demonstrator (Bob Shaw, Larry Hettinger, David Snyder). Finally, I would like to extend a special thanks to Michael Haas, Jeff Cress, Dean Stautberg, and Brett Walters, who contributed significantly to the development and evaluation of the concept demonstrator.

References

References that are relevant to dynamically adaptive aiding, but were not cited in text, have been added to the following reference list.

Anderson, J. R. (1982). Acquisition of cognitive skill. Psychological Review, 89, 369-406.

Andes, R. C., Jr. (1987). Adaptive aiding in complex systems: An implementation. In Proceedings of the 1987 IEEE Conference on Systems, Man, and Cybernetics. New York, NY: IEEE.

Bainbridge, L. (1983). Ironies of automation. Automatica, 19, 775-779.

Ballas, J. A., Heitmeyer, C. L., and Perez, M. A. (1992a). Direct manipulation and intermittent automation in advanced cockpits (Final Report. NRL/FR/5534-92-9375). Washington, DC: Naval Research Laboratory.

Ballas, J. B., Heitmeyer, C. L., and Perez, M. A. (1991). Interface sytles for the intelligent cockpit: Factors influencing automation deficit. In Proceedings of AIAA Computing in Aerospace (pp. 657-667). Baltimore, MD: AIAA.

Ballas, J. B., Heitmeyer, C. L., and Perez, M. A. (1992b). Evaluating two aspects of direct manipulation in advanced cockpits. In Proceedings of CHI'92 Human Factors in Computing Systems. New York, NY: Association for Computing Machinery.

Barnes, M. J., and Grossman, J. (1985). The intelligent assistant concept for electronic warfare systems (Final Report No. NWCTP5585). China Lake, CA: Naval Weapons Center.

Bennett, K. B. (1992). Representation aiding: Complementary decision support for a complex, dynamic control task. IEEE Control Systems, 12(4), 19-24.

Bennett, K. B., and Flach, J. M. (1992). Graphical displays: Implications for divided attention, focused attention, and problem solving. Human Factors, 34(5), 513-533.

Bennett, K. B., and Flach, J. M. (1994). When automation fails... In M. Mouloua and R. Parasuraman (Eds.), Human performance in automated systems: Current research and trends (pp. 229-234). Hillsdale, NJ: Lawrence Earlbaum Associates.

Bennett, K. B., Nagy, A. L., and Flach, J. M. (In Press). Visual Displays. In G. Salvendy (Ed.), Handbook of Human Factors and Ergonomics (2nd ed.). New York, NY: John Wiley and Sons.

Bennett, K. B., Toms, M. L., and Woods, D. D. (1993). Emergent features and configural elements: Designing more effective configural displays. Human Factors, 35(1), 71-97.

Berkan, R. C., Upadhyaya, B. R., Tsoukalas, L. H., Kisner, R. A., and Bywater, R. L. (1991). Advanced automation concepts for large-scale systems. IEEE Control Systems Magazine, 11(6), 4-11.

Billings, C. E., and Woods, D. D. (1994). Concerns about adaptive automation in aviation systems. In M. Mouloua and R. Parasuraman (Eds.), Human performance in automated systems: Current research and trends (pp. 264-269). Hillsdale, NJ: Lawrence Erlbaum Associates.

Braune, R. J., and Trollip, S. R. (1982). Towards an internal model in pilot training. Aviation, Space, and Environmental Medicine, 53(10), 996-999.

Brickman, B. J., Hettinger, L. J., Roe, M. M., Lu, L., Repperger, D. W., and Haas, M. W. (In Press). Haptic specification of environmental events: Implications for the design of adaptive, virtual interfaces. In Proceedings of VRAIS 1996. New York, NY:

Buxton, W., Lamb, M. R., Sherman, D., and Smith, K. C. (1983). Towards a comprehensive user interface management system. Computer Graphics, 17(3), 35-42.

Byrne, E. A., and Parasuraman, R. (in press). Psychophysiology and adaptive automation. Biological Psychology.

Chambers, A. B., and Nagel, D. C. (1985). Pilots of the future: Human or computer? Communications of the ACM, 28, 1187-1199.

Chignell, M. H., and Hancock, P. A. (1988). Intelligent interface design. In M. Helander (Ed.), Handbook of human-computer interaction (pp. 969 - 995). Amsterdam: Elsevier Science Publishers B. V. (North-Holland).

Cleveland, W. S. (1985). The elements of graphing data. Belmont, CA: Wadsworth.

Croft, W. B. (1984). The role of context and adaptation in user interfaces. International Journal of Man-Machine Studies, 21, 283-292.

Duley, J. A., Scallen, S. F., and Hancock, P. A. (in press). The response of experienced pilots to interface configuration changes for adaptive allocation. Journal of Military Psychology.

Edmonds, E. A. (1981). Adaptive man-computer interfaces. In M. J. Coombs and J. L. Alty (Eds.), Computing skills and the user interface (pp. 389 - 426). Amsterdam: Elsevier Science Publishers B. V. (North-Holland).

Endsley, M., and Kiris, E. (1994). The out-of-loop performance problem: Impact of level of automation and situation awareness. In M. Mouloua and R. Parasuraman (Eds.), Human performance in automated systems: Current research and trends (pp. 50-56). Hillsdale, NJ: Lawrence Erlbaum Associates.

Fischer, G., Lemke, A., and Schwab, T. (1985). Knowledge-based help systems. In Proceedings of CHI'85 Human Factors in Computing Systems (pp. 161-167). New York, NY: Association for Computing Machinery.

Fitts, P. M., and Posner, M. I. (1967). Human performance. Belmont, CA: Brooks Cole.

Forester, J. A. (1986). An assessment of variable format information presentation. In Proceedings of NATO AGARD Symposium on Information Management and Decision Making in Advanced Airborne Weapon Systems. Paris: NATO AGARD.

Freedy, A., Davis, K. B., Steeb, R., Samet, M. G., and Gardiner, P. C. (1976). Adaptive computer aiding in dynamic decision processes: Methodology, evaluation, and application (Tech. Report PFTR-1016-76-8/30). Washington, DC: ARPA.

Freedy, A., Madni, A., and Samet, M. (1985). Adaptive user models: Methodology and apoplications in man-computer systems. In W. B. Rouse (Ed.), Advances in man-machine systems research (Vol. 2, pp. 249-293). Greenwich, CT: JAI Press.

Garland, D. J., and Wise, J. A. (Eds.). (1993). Human factors and advanced aviation technologies. Daytona Beach, FL: Embry-Riddle Aeronautical University Press.

Geddes, N. D. (1991). Automatic display management using dynamic plans and events. In Proceedings of the 6th

International Symposium on Aviation Psychology (pp. 90-95). Columbus, OH:

Gluckman, J. P., Morrison, J. G., and Deaton, J. E. (1991). Complex task performance as a basis for developing cognitive engineering guidelines in adaptive automation. In Proceedings of the Human Factors Society 35th Annual Meeting (pp. 116-120). Santa Monica, CA: Human Factors and Ergonomics Society.

Greenberg, S., and Witten, I. H. (1985). Adaptive personalized interfaces --- A question of viability. Behavior and Information Technology, 4(1), 31-45.

Hammer, J. M., and Rouse, W. B. (1982). Design of an intelligent computer-aided cockpit. In Proceedings of the 1982 IEEE Conference on Systems, Man, and Cybernetics (pp. 627-630). New York, NY: IEEE.

Hancock, P. A., and Chignell, M. H. (1986). Toward a theory of mental workload: Stress and adaptability in human-machine systems. In Proceedings of the IEEE International Conference on Systems, Man, and Cybernetics (pp. 378-383). New York, NY: IEEE.

Hancock, P. A., and Chignell, M. H. (1987). Adaptive control in human-machine systems. In P. A. Hancock (Ed.), Human Factors Psychology (pp. 305-345). Amsterdam: North-Holland.

Hancock, P. A., and Chignell, M. H. (1988). Mental Workload dynamics in adaptive interface design. IEEE Transactions on Systems, Man, and Cybernetics, SMC-18, 647-658.

Hancock, P. A., and Chignell, M. H. (Eds.). (1989). Intelligent interfaces: Theory, research, and design. Amsterdam: North Holland.

Hancock, P. A., Chignell, M. H., and Loewenthal, A. (1985). An adaptive human-machine system. In Proceedings of the IEEE International Conference on Systems, Man, and Cybernetics (pp. 627-630). New York, NY: IEEE.

Hancock, P. A., Duley, J. A., and Scallen, S. F. (1993a). The response of experienced pilots to interface configuration changes for adaptive allocation (Report HFRL, Nav-4). Warminster, PA: Naval Air Warfare Center.

Hancock, P. A., Duley, J. A., and Scallen, S. F. (1994a). The control of adaptive function allocation (Report HFRL, Nav-6). Warminster, PA: Naval Air Warfare Center.

Hancock, P. A., and Harris, W. C. (1992). Evaluation of the structure and function of intelligent interfaces for adaptive automated task allocation (Report HFRL, Nav-1). Warminster, PA: Naval Air Warfare Center.

Hancock, P. A., and Scallen, S. F. (in press). The performance and workload effects of task display re-location during automation. Displays.

Hancock, P. A., Scallen, S. F., and Duley, J. A. (1993b). Initiation and cessation of automation: location versus configuration change (Report HFRL, Nav-3). Warminster, PA: Naval Air Warfare Center.

Hancock, P. A., Scallen, S. F., and Duley, J. A. (1994b). Partitioning a task for automation: More than the sum of its parts? (Report HFRL, Nav-8, Part II). Warminster, PA: Naval Air Warfare Center.

Hancock, P. A., Scallen, S. F., and Duley, J. A. (1994c). Pilot performance and preference for cycles of automation in adaptive function allocation (Report HFRL, Nav-5). Warminster, PA: Naval Air Warfare Center.

Hancock, P. A., Scallen, S. F., and Duley, J. A. (1994d). Proximal and distal automated displays: relocated but not forgotten (Report HFRL, Nav-7, Part I). Warminster, PA: Naval Air Warfare Center.

Hancock, P. A., and Williams, G. (1993). The effect of task load and task load increment on performance and workload (Report HFRL, Nav-2). Warminster, PA: Naval Air Warfare Center.

Hart, S. G., and Staveland, L. E. (1988). Development of NASA TLX (Task Load Index): Results of empirical and theoretical research. In P. A. Hancock and Meshkati (Eds.), Human mental workload (pp. 139-183). Amsterdam: Elsevier Science Publishers B.V. (North-Holland).

Hawley, J. K. (1996). Automation doesn't automatically solve problems. Quality Progress, 29, 59-63.

Hilburn, B., Jorna, P. G. A. M., and Parasuraman, R. (1995a). The effect of advanced ATC automation on mental workload and monitoring performance: An empirical investigation in dutch airspace. In Proceedings of the 8th International Symposium on Aviation Psychology. Columbus, OH:

Hilburn, B., Molloy, R., Wong, D., and Parasuraman, R. (1993). Operator versus computer control of adaptive automation. In J. Morrison (Ed.), The adaptive function allocation for intelligent cockpits (AFAIC) program: Interim research and guidelines for the application of adaptive automation (Tech. Report NAWCADWAR-93031-60) (pp. 31-36). Warminster, PA: Naval Air Warfare Center.

Hilburn, B., Parasuraman, R., and Mouloua, M. (1995b). Effects of short- and long-cycle adaptive function allocation on performance of flight-related tasks. In N. Johnston, R. Fuller, and N. McDonald (Eds.), Aviation psychology: Training and selection. Hampshire, UK: Ashgate Publishing.

Hilburn, B., Singh, I., Molloy, R., and Parasuraman, R. (1992a). Training and adaptive automation. I: Nonadaptive feedback training (Technical Report No. CSL-N92-1). Washington, DC: The Catholic University of America, Cognitive Science Laboratory.

Hilburn, B., Wong, D., Molloy, R., and Parasuraman, R. (1992b). Training and adaptive automation. II: Amount of nonadaptive training (Technical Report No. CSL-N92-3). Washington, DC: The Catholic University of America, Cognitive Science Laboratory.

Hughes, D. (1995). Avionics automates many cockpit functions. Aviation Week & Space Technology, 143, 49.

Hutchins, E. L., Hollan, J. D., and Norman, D. A. (1986). Direct manipulation interfaces. In D. A. Norman and S. W. Draper (Eds.), User centered system design (pp. 87-124). Hillsdale, NJ: Lawrence Earlbaum Associates.

Jacob, R. J. K. (1993). What you look at is what you get. Computer, 26, 65-66.

Johannsen, G., Pfendler, C., and Stein, W. (1986). Human performance and workload in simulated landing approaches with auto-pilot failures. In T. Sheridan and G. Hohannsen (Eds.), Monitoring behavior and supervisory control. New York, NY: Plenum Press.

Jordan, N. (1963). Allocation of functions between man and machines in automated systems. Journal of Applied Psychology, 47, 161-165.

Kantowitz, B., and Sorkin, R. (1987). Allocation of function. In G. Salvendy (Ed.), Handbook of human factors. New York, NY: Wiley.

Kantowitz, E., and Sudarsky, O. (1989). The adaptable user interface. Communications of the ACM, 32(11), 1352-1358.

Kirlik, A. (1993). Modeling strategic behavior in human-automation interaction: why an "aid" can (and should) go

unused. Human Factors, 35(2), 221-242.

Klein, G. A., Orasanu, J., and Zsambok, C. E. (Eds.). (1993). Decision making in action: Models and methods. Norwood, NJ: Ablex Publishing Corp.

Lee, J. D., and Moray, N. (1992). Trust, control strategies, and allocation of function in human-machine systems. Ergonomics, 35, 1243-1270.

Marshall, E. D. (1983). B-1B Software Implementation Requirements Document (Document No. D400-10104-7): The Boeing Company.

Maskery, H. S. (1984). Adaptive interfaces for naive users --- an experimental study. In Proceedings of Interact '84, IFIP Conference (pp. 343-350).

Mason, M. V. (1986). Adaptive command prompting in an on-line documentation system. International Journal of Man-Machine Studies, 25(1), 33-51.

Mason, M. V., and Thomas, R. C. (1984). Experimental adaptive interface: Research, design, applications. Information Technology, 3(3), 162-167.

McDaniel, J. (1988). Rules for fighter cockpit automation. In Proceedings of the IEEE National Aerospace and Electronics Conference (pp. 831-838). New York, NY: IEEE.

Moray, N., Lee, J., Vicente, K. J., Jones, B. G., and Rasumssen, J. (1994). A direct perception interface for nuclear power plants. In Proceedings of the Human Factors and Ergonomics Society 38th Annual Meeting (pp. 481-485). Santa Monica, CA: Human Factors and Ergonomics Society.

Morris, N. M., and Rouse, W. B. (1986). Adaptive aiding for human-computer control: Experimental studies of dynamic task allocation (Report No. AAMRL-TR-86-005). WPAFB, OH: Armstrong Aerospace Medical Research Laboratory.

Morris, N. M., Rouse, W. B., and Frey, P. R. (1985). Adaptive aiding for symbiotic human-computer control: Conceptual model and experimental approach (Tech. Report AFAMRL-TR-84-072). WPAFB, OH: Air Force Aerospace Medical Research Laboratory.

Morris, N. M., Rouse, W. B., Ward, S. L., and Frey, P. R. (1984). Psychological issues in on-line adaptive task allocation. In Proceedings of the Twentieth Annual Conference on Manual Control (pp. 455-466). Moffett Field, CA: NASA.

Morrison, J. G., Chen, D., and Gluckman, J. P. (1993). Prospective principles and guidelines for the design of adaptively automated crewstations. In J. Morrison (Ed.), The adaptive function allocation for intelligent cockpits (AFAIC) program: Interim research and guidelines for the application of adaptive automation (Tech. Report NAWCADWAR-93031-60) (pp. 1-6). Warminster, PA: Naval Air Warfare Center.

Morrison, J. G., Gluckman, J. P., and Deaton, J. E. (1992). Human performance in complex task environments: A basis for the application of adaptive automation (Final Report No. NAWCADWAR-92032-60). Warminster, PA: Naval Air Warfare Center.

Mouloua, M., and Parasuraman, R. (Eds.). (1994). Human performance in automated systems: Current research and trends. Hillsdale, NJ: Lawrence Erlbaum Associates.

Muir, B. M. (1987). Trust between humans and machines, and the design of decision aids. International Journal of Man-Machine Studies, 27, 527-540.

Noah, W., and Halpin, S. M. (1986). Adaptive user interfaces for planning and decision aids in C^3I systems. IEEE Transactions on Systems, Man, and Cybernetics, SMC-16, 909-918.

Norcio, A. F., and Stanley, J. (1989). Adaptive human-computer interfaces: A literature survey and perspective. IEEE Transactions on Systems, Man, and Cybernetics, 19(2), 399-408.

Norman, D. A. (1983). Design rules based upon analyses of human error. Communications of the ACM, 26, 254-258.

Parasuraman, R. (1987). Human-computer monitoring. Human Factors, 29, 695-706.

Parasuraman, R. (1990). Event-related brain potentials and human factors research. In J. W. Rohrbaugh, R. Parasuraman, and J. R. Johnson (Eds.), Event-related brain potentials: Basic issues and applications (pp. 279-300). New York, NY: Oxford University Press.

Parasuraman, R. (1993). Effects of adaptive function allocation on human performance. In D. J. Garland and J. A. Wise (Eds.), Human factors and advanced aviation technologies (pp. 147-157). Daytona Beach, FL: Embry-Riddle Aeronautical University Press.

Parasuraman, R., Bahri, T., Deaton, J. E., Morrison, J. G., and Barnes, M. (1992a). Theory and design of adaptive automation in aviation systems (Progress Report No. NAWCADWAR-92033-60). Warminster, PA: Naval Air Warfare Center.

Parasuraman, R., Bahri, T., and Molloy, R. (1992b). Adaptive automation and human performance: I. Multi-task performance characteristics (Final Report No. NAWCADWAR-92035-60). Warminster, PA: Naval Air Warfare Center.

Parasuraman, R., Bahri, T., Molloy, R., and Singh, I. (1991). Effects of shift in the level of automation on operator performance. In Proceedings of the 6th International Symposium on Aviation Psychology (pp. 157-218). Columbus, OH:

Parasuraman, R., Bahri, T., Molloy, R., and Singh, I. (1992c). Adaptive automation and human performance: II. Effects of shifts in the level of automation on operator performance (Final Report No. NAWCADWAR-92036-60). Warminster, PA: Naval Air Warfare Center.

Parasuraman, R., and Mouloua, M. (Eds.). (1995). Automation and human performance: Theory and applications. Hillsdale, NJ: Lawrence Erlbaum Associates.

Polson, M. C., and Richardson, J. J. (Eds.). (1988). Foundations of intelligent tutoring systems. Hillsdale, NJ: Lawrence Earlbaum Associates.

Rasmussen, J. (1986). Information processing and human-machine interaction: An approach to cognitive engineering. New York, NY: Elsevier.

Rasmussen, J., Pejtersen, A. M., and Goodstein, L. P. (1994). Cognitive systems engineering. New York, NY: John Wiley and Sons.

Rasmussen, J., and Vicente, K. (1989). Coping with human errors through system design: Implications for ecological

interface design. International Journal of Man-Machine Studies, 31, 517-534.

Reichman-Adar, R. (1984). Extended person-machine interface. Artificial Intelligence, 22, 157-218.

Rissland, E. (1984). Ingredients of intelligent user interfaces. International Journal of Man-Machine Studies, 21, 377-388.

Roth, E. M., Bennett, K. B., and Woods, D. D. (1987). Human interaction with an 'intelligent' machine. International Journal of Man-Machine Studies, 27, 479-526.

Rouse, W. B. (1981). Human-computer interaction in the context of dynamic systems. Computing Surveys, 13(1), 71-100.

Rouse, W. B. (1988). Adaptive aiding for human/computer control. Human Factors, 30(4), 431-443.

Rouse, W. B. (1994). Twenty years of adaptive aiding: Origins of the concept and lessons learned. In M. Mouloua and R. Parasuraman (Eds.), Human performance in automated systems: Current research and trends (pp. 28-32). Hillsdale, NJ: Lawrence Erlbaum Associates.

Rouse, W. B., Geddes, N. D., and Curry, R. E. (1987). An architecture for intelligent interfaces: Outline of an approach to supporting operators of complex systems. Human-Computer Interaction, 3, 87-122.

Rouse, W. B., and Rouse, S. H. (1983). A framework for research on adaptive decision aids (Tech. Report AFAMRL-TR-83-082). WPAFB, OH: Air Force Aerospace Medical Research Laboratory.

Sarter, N. B. (1991). The flight management system - Pilot's interaction with cockpit automation. In Proceedings of the 1991 IEEE International Conference on Systems, Man, and Cybernetics (pp. 1307-1310). New York, NY: IEEE.

Scallen, S. F., Hancock, P. A., and Duley, J. A. (in press). Evaluation of automation procedures for adaptive task allocation. Human Factors.

Scallen, S. F., Hancock, P. A., and Duley, J. A. (In Press). Pilot performance and preference for short cycles of automation in adaptive function allocation. Applied Ergonomics.

Sewell, D. R., Geddes, N. D., and Rouse, W. B. (1987). Initial evaluation of an intelligent interface for operators of complex systems. In G. Salvendy (Ed.), Cognitive Engineering in the design of human computer interaction and expert systems (pp. 551-558). New York, NY: Elsevier Science Publishers.

Shalin, V. L., and Geddes, N. D. (1994). Task dependent information management in a dynamic environment: Concept and measurement issues. In Proceedings of the IEEE International Conference on Systems, Man, and Cybernetics. New York, NY: IEEE.

Shalin, V. L., Mikesell, B. G., Geddes, N. D., and Ramamurthy, M. (1993). Performance effects of plan-based displays in commercial aviation. In Proceedings of the Seventh Suymposium on Aviation Psychology. Columbus, OH:

Shiffrin, R. M., and Schneider, W. (1977). Controlled and automatic human information processing: II Perceptual learning, automatic attending, and a general theory. Psychological Review, 84, 127-190.

Singh, I., Molloy, R., Deaton, J. E., and Parasuraman, R. (1993). Adaptive function allocation enhances pilot monitoring performance (Abstract only). In Proceedings of the 34th Annual Meeting of the Psychonomic

Society. Washington, DC:

Suchman, L. A. (1987). Plans and situated actions: The problem of human machine communication. New York, NY: Cambridge University Press.

Wickens, C. D. (1992). Engineering psychology and human performance. (2nd ed.). New York, NY: Harper Collins.

Wiener, E. L., and Curry, R. E. (1980). Flight-deck automation: Promises and problems. Ergonomics, 23(10), 995-1011.

Wiener, E. L., and Nagel, D. C. (Eds.). (1988). Human factors in aviation. San Diego, CA: Academic Press.

Woods, D. D. (1989). The effects of automation on the human's role: Experience from non-aviation industries. In S. Norman (Ed.), Flightdeck automation: Promises and realities. Moffett Field, CA: NASA Ames Research Center.

Woods, D. D. (1991). Representation aiding: A ten year retrospective. In Proceedings of the 1991 IEEE International Conference on Systems, Man, and Cybernetics (pp. 1173-1176). New York, NY: IEEE.

Woods, D. D., and Cook, R. I. (1991). Nosocomial automation: Technology-induced complexity and human performance. In Proceedings of the 1991 IEEE International Conference on Systems, Man, and Cybernetics (pp. 1279-1282). New York, NY: IEEE.

Woods, D. D., and Roth, E. M. (1988). Cognitive systems engineering. In M. Helander (Ed.), Handbook of human-computer interaction (pp. 1-41). Amsterdam: Elsevier Science Publishers B.V. (North-Holland).

Young, L. R. (1969). On adaptive manual control. IEEE Transactions on Man-Machine Systems, MMS-10, 292-331.

Zachary, W. (1986). A cognitively based functional taxonomy of decision support techniques. Human-Computer Interaction, 2, 25-63.

Appendix A

The computational aiding portion of the CFD HUD display was based on the B1 bomber navigation system, as described in Marshall (1983). The equations and portions of the following descriptions are taken directly from that publication.

The "centerline recovery" algorithm calculates the path back to the desired waypoint centerline in minimal time. The base equation is $\phi_c = K_\psi \psi_e + K_Y Y_e$, where ϕ_c is the directed bank angle for the pilot, ψ_e is the error between the aircraft heading and the waypoint centerline heading, Y_e is the horizontal error from the waypoint centerline, K_ψ is an arbitrary gain value (3.0) for heading error, and K_Y is an arbitrary gain value (0.0005) for position error (the gain values corresponded to angular errors measured in degrees and positional errors measured in feet). The first term ($K_\psi \psi_e$) can be thought of as heading correction, and the second term ($K_Y Y_e$) as position correction. The heading correction attempts to direct the aircraft parallel to the waypoint centerline, while the position correction makes adjustments to intercept the centerline. As the aircraft gets closer and closer to the waypoint centerline, the position correction term approaches zero, and the aircraft eventually will fly parallel to the centerline. A similar equation was used for altitude deviation, replacing horizontal error with vertical error, and waypoint centerline with desired glide slope. The gain values were set considerably higher ($K_\psi = 1.0$ and $K_Y = 0.04$) for the vertical equations, since the mission involved low-level flight navigation, and altitude error was deemed to be more critical than horizontal error.

The "turn short" algorithm calculates a desired flight path for transitioning between waypoints. The algorithm produces a path that will keep the aircraft as close as possible to both waypoint centerlines during a waypoint transition, by starting the turn before the upcoming waypoint so that the aircraft turn path is tangent to the next waypoint centerline. The algorithm consisted of the following two equations: $R = V^2 / (G * \tan 60)$ and $D = R \tan (Y / 2) + 4V$. "Y" is the heading change from the current waypoint centerline to the next waypoint centerline, "V" is the ground speed of aircraft (feet/sec), and "G" is the acceleration of gravity (feet/sec^2). "R" is calculated as the turning radius of the aircraft based upon a bank angle of 60 degrees, and "D" is the calculated turn short distance. Thus, the turn short distance is calculated based on the aircraft speed, desired bank angle, and the heading difference between the two waypoint centerlines. If the aircraft is closer than the turn short distance to the upcoming waypoint, then waypoint sequencing occurs and the pilot will be directed to begin turning.

The "90-degree test" algorithm serves as a backup waypoint sequencing method, if the aircraft is never closer to the upcoming waypoint than the turn short distance. In this case, the heading from the aircraft to the next waypoint is compared to the heading of the current waypoint centerline. If the difference is more than 90 degrees, waypoint sequencing occurs. The 90-degree test used the following logic: h = abs (Hc - Ha); if h > 180, h = 360 - h, else if h > 90, sequence to next waypoint. "Hc" is the current waypoint centerline heading (in degrees), and "Ha" is the heading from the aircraft to the upcoming waypoint (in degrees).

The "delta-limit filter" algorithm ensured a quick response time of the flight director output, but at the same time prevented the output from changing drastically within a very short time. When waypoint sequencing occurred, the flight director output could instantaneously change to drastically different angles, which might be disorienting to the pilot, especially if it takes the pilot a moment to relocate the flight director on the HUD. The delta-limit filter compares the directed angles at each update of the HUD with the directed angles at the last update. If the change (delta) is too large, it limits the displayed change to a maximum value. This method allows small changes to appear immediately, but forces larger changes to take several seconds to fully develop. The maximum change per HUD update was 0.5 degrees for the bank angle and 0.1 degrees for the pitch angle, which (at a 15 Hz update rate) results in a maximum change per second of 7.5 degrees and 1.5 degrees for the bank angle and pitch angle, respectively. Though less intuitive, the maximum change per second of the speed box of the CFD was .075, which represents a timing error of 3.375 seconds.

Alexander Bordetsky
Report not available at time of publication.

DEVELOPMENT OF FLUORESCENCE POST LABELLING ASSAY FOR DNA ADDUCTS

Joseph B. Guttenplan
Professor
Division of Basic Sciences Biochemistry Department

New York University
College of Dentistry
345 East 24th Street
New York, New York 10010

Final Report for:
Summer Faculty Research Program
Armstrong Laboratory

Sponsored by:
Air Force Office of Scientific Research
Bolling Air Force Base, DC

and

Armstrong Laboratory

February 1997

DEVELOPMENT OF A FLUORESCENCE POST LABELLING ASSAY FOR DNA ADDUCTS

Joseph B. Guttenplan
Professor
Division of Basic Sciences Biochemistry Department
New York University College of Dentistry

Abstract

DNA adducts likely to be formed by compounds of interest to the Air Force will probably fall into the class of smaller adducts. These are detected relatively inefficiently by most current methods. In this project a method of fluorescent labelling of adducts was adapted, that converted deoxynucleotides (dNMPs) to phosphoramidates (PAs), followed by derivitization of the free amino group with dansyl chloride and HPLC. A major difficulty with the method was interference from the hydrolysis product of dansyl chloride, and from the reaction product of ED (used to form the PA) with dansyl chloride. Methods were developed to reduce the concentration of residual ED. This not only reduced the concentration of the ED-dansyl chloride product, but also allowed a large reduction in the initial concentration of dansyl chloride. For known dNMPs published reports utilized an HPLC collection of the region where the dNMP eluted, and then reaction of the purified dNMP to form a PA. However, this procedure left substantial concentrations of ED. This method was improved upon by first forming a PA of the dNMP (or mix of dNMPs) and then applying to an HPLC and purifying the PAs of interest. It was determined using the PAs of normal and of the modified dNMP, $1,N^6$-etheno-dAMP, that the PAs were indeed stable enough to purify by HPLC and they reacted quantitatively with fluorescent reagents. Applying this method to DNA treated with chloracetaldehyde (which produces the $1,N^6$-etheno-dAMP) using published methods of enzymatic degradation of DNA led to a some conversion to nucleosides instead of nucleotides. Conditions were then established to minimize this conversion. A further improvement in the assay was the use of the more fluorescent label, Attotag, which increased sensitivity 30 x.

preclude dimer formation between phosphamidates instead of reaction of the imidazole phosphoramidate with ED. The entire set of reactions can be run in one mix containing all of the reagents and requires about one hr incubation at 37^0. The product is stable in the cold and can be reacted with any of a number fluorescent reagents under conditions specific for that reagent, but all within a one hour incubation at 37^0. A reaction scheme taken from ref (6) is depicted below.

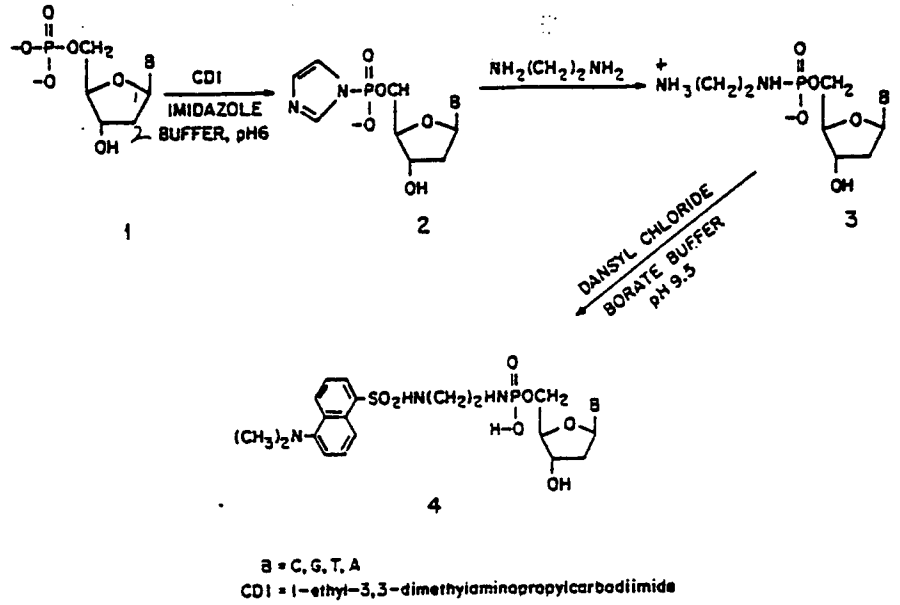

B = C, G, T, A
CDI = 1-ethyl-3,3-dimethylaminopropylcarbodiimide

FIG. 1. Scheme for the synthesis of fluorescent labeled nucleotides.

There are several possible applications of the fluorescence postlabelling assay depending on the level of sensitivity needed, the time and resources available and whether the identity of the DNA adduct is known:

1. If the identity of the modified dN is known and the fluorescent labelling is to be used to quantitate the products, then the DNA can be enzymatically digested to either 3' or 5' dNs (there appears to be little difference which is used, although certain separations may be easier with one or the other), fractionated by HPLC, and the fraction

corresponding to the retention time of the known modified nucleotide is collected, concentrated and labelled as above. It is then eluted by a second HPLC run under conditions specific for the that fluorescent dN. The method is more time consuming than method #2 (below) because it requires two HPLC runs, but probably more sensitive in practice because high sensitivity detection need only be focussed on the region of interest. A disadvantage with this method as with method #1, is the potential overlap of the peak of interest with the huge peaks resulting from the reactions of one or two of the amino groups of ED with the fluorescent reagent. At the time of initiation of this project only this method had been reported (7).

2. If a general screen for modified dNs is required, the DNA can be enzymatically digested to dNs, converted to PAs and the mixture of dNs can be derivatized with fluorophore and separated by HPLC. In this method all modified dNs are potentially detected, but overlap of adduct peaks with the large peaks resulting from the normal dNs is a potential problem, and overlap of the peak of interest with the huge peaks resulting from the reactions of one or two of the amino groups of ED with the fluorescent reagent. Also, one does not know <u>a priori</u> where the adducted nucleotides will elute, and therefore the entire chromatogram must be run with a long shallow gradient to ensure that minor peaks are not obscured by the rising baseline frequently observed with gradients. Interference by ED may be reduced by reducing or removing excess amine (see below) but this may involve an additional step.

3. A third application is similar to #1 in that, if the identity of the modified dN is known and the fluorescent labelling is to be used to quantitate the products, then the DNA can be digested, fractionated by HPLC, and, fraction corresponding to

the retention time of the known modified nucleotide is collected, concentrated and labelled as above. However, in this method the nucleotides are first converted to phosphoramidates and these are injected onto the HPLC, and the PA of the dN of interest is collected and reacted with fluorescent reagent and the fluorescent product is then analyzed by HPLC. The advantages of this method are similar to those of #2 and in addition, this method removes most of the large excess of ED. The method is more time consuming than method #2, (but not method #1) because it requires two HPLC runs. However, it is necessary to determine that the PA is stable enough to withstand injection onto the HPLC and then the drying step.

4. A fourth application is to digest the DNA, convert all of the nucleotides to phosphoramidates, inject onto an HPLC and collect all fractions except those containing the normal nucleotides. The collected fractions are then combined, concentrated, derivatized with fluorescent reagent with then analyzed in a second HPLC run. This method has the advantage that nearly all of the excess ED is removed by the HPLC fractionation, as well as the normal nucleotides (whose large areas might obscure adducted nucleotides). It has the disadvantage of requiring two HPLC runs and would require a long slow gradient elution to resolve new peaks. It also requires that PAs be stable enough to survive the HPLC elution and the concentration step.

METHODS

1. Preparation of chloracetaldehyde adducts of dAMP

Solutions of 5' or 3'-dNMPs (10mM) were treated with chloracetal (chloroacetaldehyde-diethylacetal, which is in equilibrium with chloroacetaldehyde) (0.3M) for 8 hr at 37^0 C at a pH of 6.0. The mixtures were then be applied to a C18 HPLC column

using a mobile phase of ammonium formate / acetonitrile. The elution was be monitored with UV and fluorescence detection (290 exc., 390 em). Peaks containing the new products were collected and lyophilized to dryness. In addition, regions of the chromatogram adjacent to those containing the putative products were collected and worked up in parallel with the those containing the new products. These fractions served as controls.

2. Preparation of DNA treated with chloroacetaldehyde

For the detection of adducts in DNA treated with chloroacetaldehyde a solution of calf thymus DNA (2mg/ml) was be treated with chloroacetaldehyde as described above and the DNA was precipitated with sodium acetate/ethanol, and washed several times with 70% ethanol.

3. Preparation of the phosphoramidates

As described in the literature (6) the PAs were prepared by incubating dNMPs, with CDI (0.15M) and ethylenediamine (0.20M) in 0.1M imidazole buffer for eight hours at room temperature (6) or one hr at 37^0 C. These first two steps of the reaction were carried out without isolating the intermediate product, and reactants and products were analyzed by analytical reverse phase HPLC in an aqueous buffer containing 0-10% methanol (depending on the dNMP).

4. Preparation of fluorescent derivatives of the phosphoramidates

After isolation and confirmation of efficiency of formation of phosphoramidates, solutions of the phosphoramidates were brought to a pH of 9 with sodium carbonate and allowed to react with fluorescent label, which was dissolved in DMSO or acetonitrile. In some cases the pH was first raised to 11 to release excess free ED, which was partially removed by drying. The labels employed were Dansyl chloride, Fluoram and Attotoag. The reaction with Fluoram was complete within seconds, but the other reagents were incubated at 37^0 for one hr and filtered if a precipitate formed. Attotag

reactions also required the addition of KCN.

5. Hydrolysis of DNA

DNA was be digested to 3'-deoxynucleotide monophosphates with micrococcal nuclease and spleen phosphodiesterase at a pH of 6 (5). Generally about 0.5 ug of each enzyme, per ug DNA was used (5). In later experiments the fraction of enzyme was reduced. Digestion of DNA to 5'-dNMPs with DNA polymerase I or DNAase was also carried out, but this digestion resulted in a significant conversion of DNA to nucleosides and was thus abandoned in favor of the former method. The fluorescence postlabelling assay can be employed with either the 3' or 5' monophosphates.

6. HPLC

Analyses were run on C18 reverse-phase columns (either 4 x 250 or 4 x 150, 5u particle) with ammonium formate buffer and varying concentrations of acetonitrile. Eluants were monitored with 254 absorbance (nonfluorescent peaks) and absorbance and fluorescence for fluorescent peaks. The excitation and emission wavelengths were optimized to the individual fluorescent products.

Results and Discussion

All of methods 1-4 described above require a fluorescent labeling reagent capable of derivatizing the amino group of the PA. In previous reports dansyl chloride was employed (5,6). This reagent is highly fluorescent, but is poorly soluble in water and the unreacted reagent decomposes to a highly fluorescent product (5,6). The reaction results in a large precipitate which must be separated from the mix, and the possibility exists that some of the product also precipitates and is thus underestimated. However, the product, dansyl sulfonic acid, elutes before the normal nucleotides and presumably before the modified nucleotides (which nearly always elute after the normal parent dN). The dansyl sulfonic acid then serves as an internal standard for retention

time. This reagent was used for the first group of experiments in this project. A convenient reagent later employed was Fluoram (fluorescamine). This reagent gives rise to similarly fluorescent products and is more soluble in water, but it reacts nearly immediately and quantitatively with primary amines, and the unreacted Fluoram has minimal fluorescence. However, the fluorescent product peaks were not as sharp as those of dansyl chloride making identification and quantification somewhat more difficult. A third type of fluorescent label employed was Attototag. This compound gives rise to a more fluorescent product than either of the other labels, is relatively water soluble and the unreacted reagent does not result in a significantly fluorescent product. However, the reagent is about 50x more expensive than the others (where cost is minimal) and in addition a large molar excess is needed. It was also found to be more sensitive to interference by other components in the reaction mixtures than the other reagents. When directly compared with Fluoram at the optimal wavelengths for both compounds, using a fluorometer, Attotag was about 30X more sensitive (results not shown). Thus, although this reagent seems to be the one of choice it was necessary to explore conditions to minimize its consumption. Although the vendor recommends a large molar excess of this reagent, it was found that reducing the volume and diluting the Attotag stock solution in DMSO allowed the reaction to proceed near quantitatively at only a several fold excess of the PA.

A problem common to most of the methods was reducing the concentration of unreacted ED after formation of the PA. The excess ED reacted with fluorescent labels in the same manner as the PA and led to two possible products (the mono and di fluorescent derivatives). These obscured the labelled modified dNs and the ED trapped large concentrations of the labelling reagent resulting in a requirement for even higher concentrations of reagent, which in turn, resulted in solubility problems and extra expense. Even in cases where the PAs were collected in HPLC fractions, the high concentrations of ED led to some tailing of the ED into the peaks

of interest. Thus, it was important to find methods to reduce the concentration of ED.

Initially the PA reaction mixtures were brought to a pH of 11 (to release the free base) after formation of the PA and then dried on a speed-vac. This reduced the concentration appreciably as assayed by total fluorescence of an aliquot of the mixture, but failed to remove significant quantities of ED. As shown in Fig. 2 for the reaction of 3'-dTMP-PA with Fluoram, a significant peak results from the residual ED-Fluoram compound. This peak can be reduced by lyophilization, as shown in Fig 3., although at much higher sensitivities (see below) it would still be observable. The PA was stable after one round of freeze drying but appeared to decompose after multiple cycles. The reason for the partial failure of the method is unclear. The free base was found to be completely volatile. Apparently the ED is reversibly bound (either covalently or noncovalently, possibly as a charge transfer or chelation complex) to one or more of the components in the incubation mix. Thus it still resulted in a high concentration of the ED-fluorescently labelled product.

Another approach was investigated. This approach took advantage of the fact that published methods of generating the PAs utilized a large molar excess of ED over PA (ca. 0.2M of ED for several mM PA (6). Also the usual concentration of phosphate groups was in the range of 3mM for a 1 mg/ml solution of hydrolyzed DNA. Therefore it might be possible to reduce the concentration of ED to a level closer to that of the dNs without affecting yield. The hypothesis was tested using the PA of 5'dAMP. It was found that concentration of ED could indeed be reduced many fold without appreciably affecting yield of PAs. The results shown in Fig. 4 demonstrate by HPLC analysis with UV absorbance detection that the ED concentration can be reduced ten fold with only a minor effect on yield of PA. Panels A-C depict the PA of dAMP and panel D shows a mixture of dAMP with the PA. In other experiments (not shown) the concentration of ED was reduced another two fold with little change in yield. However, it was also necessary to reduce the

concentration of the imidazole buffer or its high concentration in the reaction mix would preclude efficient reaction of the ED with the CDI intermediate.

It was also necessary to determine that the reduced ED concentration would not cause the PA to decompose in the presence of the labelling reagent by reversibly reacting any free ED in equilibrium with the PA. To test for this possibility the PA of 5'dAMP described above was reacted with dansyl chloride and the product yield analyzed by HPLC. As shown in Fig. 5 by HPLC with both absorbance and fluorescence detection, there was essentially no difference in the yield of dAMP-dansyl chloride at any of the concentrations of ED. The large peak preceding the dAMP-PA is the dansyl sulfonic acid (the fluorescent product resulting from dansyl chloride). However, a small peak of ED-dansyl chloride was still observable, even at the lowest concentration of ED. In order to emphasize the peak it is amplified 20X at the lowest concentration of ED. Although the concentration of this product seems small it must be remembered that the concentration of modified dNs will be orders of magnitude below that of the normal dN, dAMP shown here. Therefore, this method although useful, still leaves significant ED.

An additional method was employed to further reduce the level of ED. A small volume of the cationic exchange resin, Rexyn, was added to ED solutions to bind the ED. It was found that in solutions of ca. 0.1M M NaCl (or ionic strength equivalent) the concentration of ED could be significantly reduced (Fig. 6). Under these conditions the PA was not appreciably bound to the resin (results not shown). A second peak present in the dansyl chloride alone was also removed, suggesting it was a cationic impurity. This method, although relatively rapid (ca. 15 min contact time was employed), requires a centrifugation to remove the resin. It is possible that the whole step can be carried out in spin filter, but this has not yet been investigated.

Another factor which needed investigation was whether the two main steps of the reaction were quantitative. In this study the

formation of the PA of 5'dGMP was first monitored by HPLC with UV absorbance detection. As shown in Fig. 7A and 7B all of the dGMP was converted to the PA. Fig. 5C shows dGMP mixed with the dGMP-PA and then each compound mixed (separately) with the labelling reagent, Fluoram. The PA (panel E) but not the dGMP (panel D) was quantitatively consumed. Thus, both of the necessary steps of the labelling reaction are essentially quantitative.

If methods 3 and 4 were to be pursued it would necessary to demonstrate that the PA's were stable enough to be collected from the HPLC without decomposing. For this demonstration one of the modified dNMP's was prepared. This was this was the $1,N^6$-ethenoadenosine 3'-monophosphate (e-dAMP). This represents one of the classes of DNA adducts of interest to the Air Force, as it results from the reaction of a halogenated aliphatic compound with DNA. Although the 5'-monophosphate is available commercially, it was subsequently found (see below) that it was difficult to quantitatively digest the DNA to 5'- monophosphates, but not to 3'-monophosphates. The 3'e-dAMP was readily prepared by the reaction of chloracetaldehyde (CA) with 3'-dAMP and then converted to the PA. To prepare the PAs the reaction mix was dried (to remove excess CA), and reacted with 40mM ED and CDI (150mM). The mixture was applied to the HPLC and both the e-dAMP and the residual dAMP were converted to PAs (Fig 8A). The e-dAMP was collected, dried and reinjected. As seen in Fig 8C the e-dAMP-PA was recovered with apparently no decomposition to e-dAMP. Although the retention times of the e-dAMP and the residual dAMP were shifted after the reaction converting them to PAs, to further demonstrate they were truly PAs, the mixture was reacted with Fluoram, which should result in the loss of the PAs and the appearance of peaks with much longer retention times and different excitation and emission maxima. Fig. 8C shows the disappearance of the PAs. Although not detectable under these conditions, two new peaks were indeed detected under appropriate conditions (results not shown). This represented a crucial demonstration for the use of methods 3 and 4 above.

In the most recent experiments an attempt was made to digest CA-treated DNA, convert the dNMPs to PAs and separate them by HPLC. Results with a standards mix showed this should be possible (Fig.9) as the retention times of the 3'dNMPs changed after conversion to PAs, indicating the entire mix had reacted. However, digestion of the DNA to dNMPs proved inefficient under most standard conditions. The use of both DNA polymerase I or DNAase resulted in a large fraction of nucleosides (which cannot be labeled). The use of micrococcal nuclease and spleen diesterase under standard conditions (5) also led to significant conversion to nucleosides. However, it was possible to reduce the concentrations of these enzymes and use shorter incubation times to obtain near quantitative conversion. However, by the time this procedure was worked out the project period expired.

Conclusions

Fluorescent detection of modified DNA bases, nucleosides or nucleotide has the advantage that fluorescence can be extremely sensitive and does not require the use of large amounts of radioactivity as does the P^{32} post-labelling. It suffers from the disadvantages that most DNA bases, whether modified or not are not significantly fluorescent and there is no general reaction to derivatize nucleic acid bases with a fluorescent reagent, or to make them fluorescent. The method developed here results in highly fluorescent derivatives of modified dNMPs. A number of problems emerged before the method could be applied as general procedure to analyze actual DNA samples, but these have now been solved. Moreover, the methods here allow the user a choice of methods depending on the purpose of the assay.

References

1. Pilot, H.C. (1986) Fundamentals of Oncology. Chemical Carcinogenesis: Mechanisms, **Ed. 3, Marcel Decker (N.Y.)**

2. Boutwell, R.K, Verma, A.K., Ashendel, C.L., and Astrup, E. (1984) Mouse Skin: A Useful Model System for Stydying the Mechanism of Chemical Carcinogenesis. In: Carcinogenesis, **7**, pp. 1-12, Hecker, E., Fusenig, N.E., Kunz, W., Marks, F. and Thielmann, H.W. (eds.) Raven Press, New York.

3. Fearon, E.R. and Vogelstein, B. (1990) A Genetic Model for Colorectal Tumorigenesis. Cell, **61,** 759-767.

4. Hollstein, M.C., Sidransky, D., Vogelstein, B. and Harris, C.C. (1991) p53. Mutations in Human Cancer, Science (Washington, D.C.) **253**, 49-53.

5. Beach, A.C. and Gupta R.C. (1992) Human Biomonitoring and the ^{32}P-postlabeling Assay. Carcinogenesis, **13**, 1053-1074.

6. Azadnia, A., Cambell, R., and Sharma, M. (1994) The Scope of Dansyl vs Fluorescein Label in Fluorescence Postlabeling Assay for DNA Damage, Anal. Biochem., **218,** 444-448.

7. Jain, R. and Sharma, M. (1993) Cancer Res., **53**, 2771-2774.

8. Singer, B. and Grunberger, D. (1983) Molecular Biology of Mutagens and Carcinogens. *Plenum Press, N.Y.*, 15-44.

Figures

In figures of HPLC chromatographs injection points are indicated with arrows. New products are marked with a "P". The direction of the chromatograph is indicated with an arrow. In some cases, both fluorescence and UV absorbance are depicted on the same figure. In these cases the appropriate tracings are marked. Conditions are indicated in the Methods section.

Fig. 1. See text

Fig. 2. HPLC of Fluoram + dTMP-PA and an ED control

Fig. 3. HPLC of Fluoram + dCMP-PA, lyophilized before reaction

Fig. 4. Effect of contration of ED on yield of dAMP-PA

Fig. 5 Effect of concentration of ED on yield of dAMP-PA-dansyl chloride

Fig. 6 Effect of ion exchange treatment on concentration of ED

Fig. 7 Formation of dGMP-ED PA and reaction with fluoram

Fig. 8 Formation and e-dAMP-PA and its recovery from HPLC (Panel A, PAs of dAMP and e-dAMP; B, recovery of PA of e-dAMP-PA; C, A after reaction with Fluoram

Fig. 9 Formation of PAs of 3'-dNMPs

Fig. 2 A. dTMP - phosphoramidate - Fluoram
B. ED - Fluoram

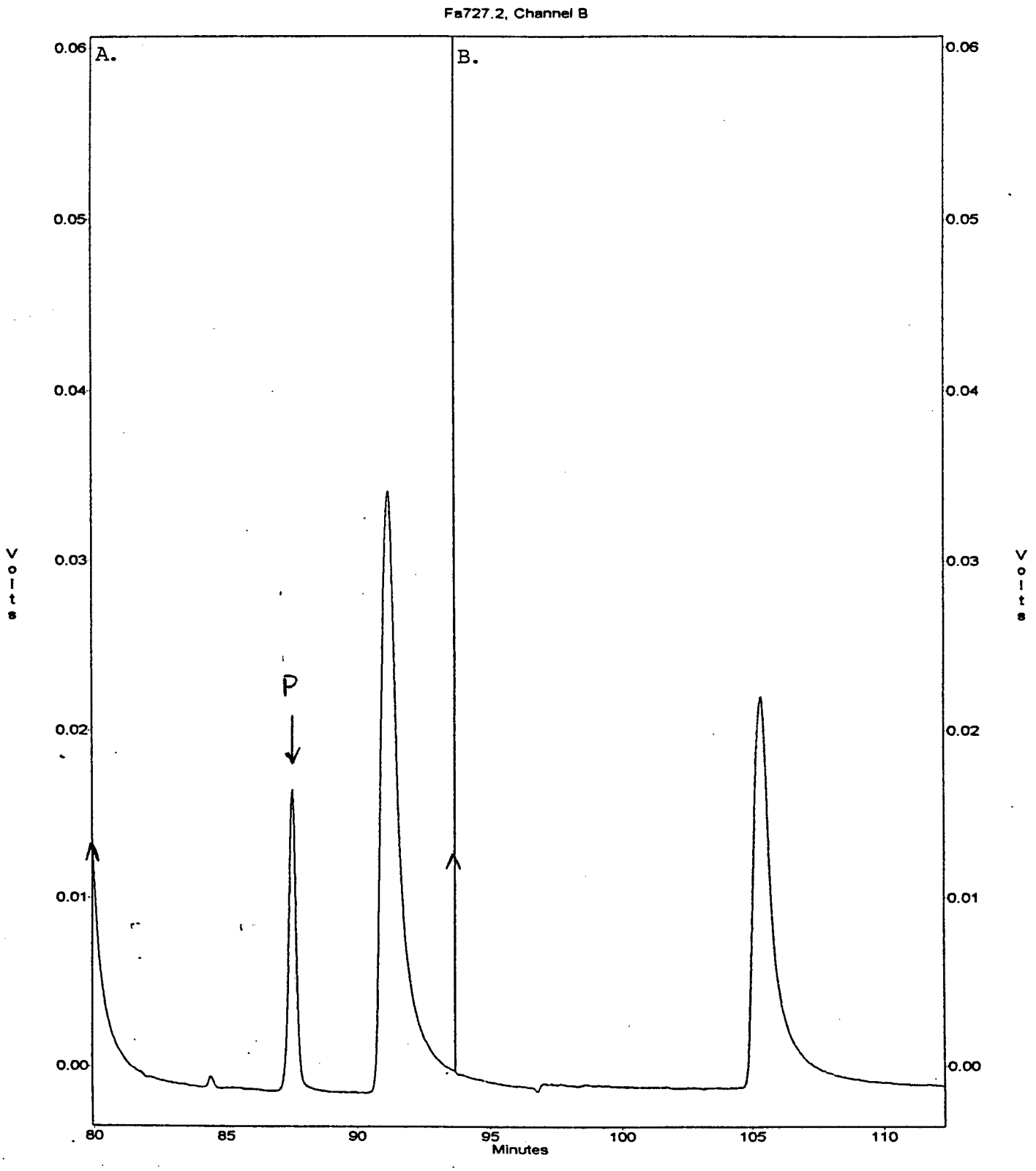

P = product

Fig. 3 dCMP - phosphoramidate - Fluoram
lyophilized before reaction

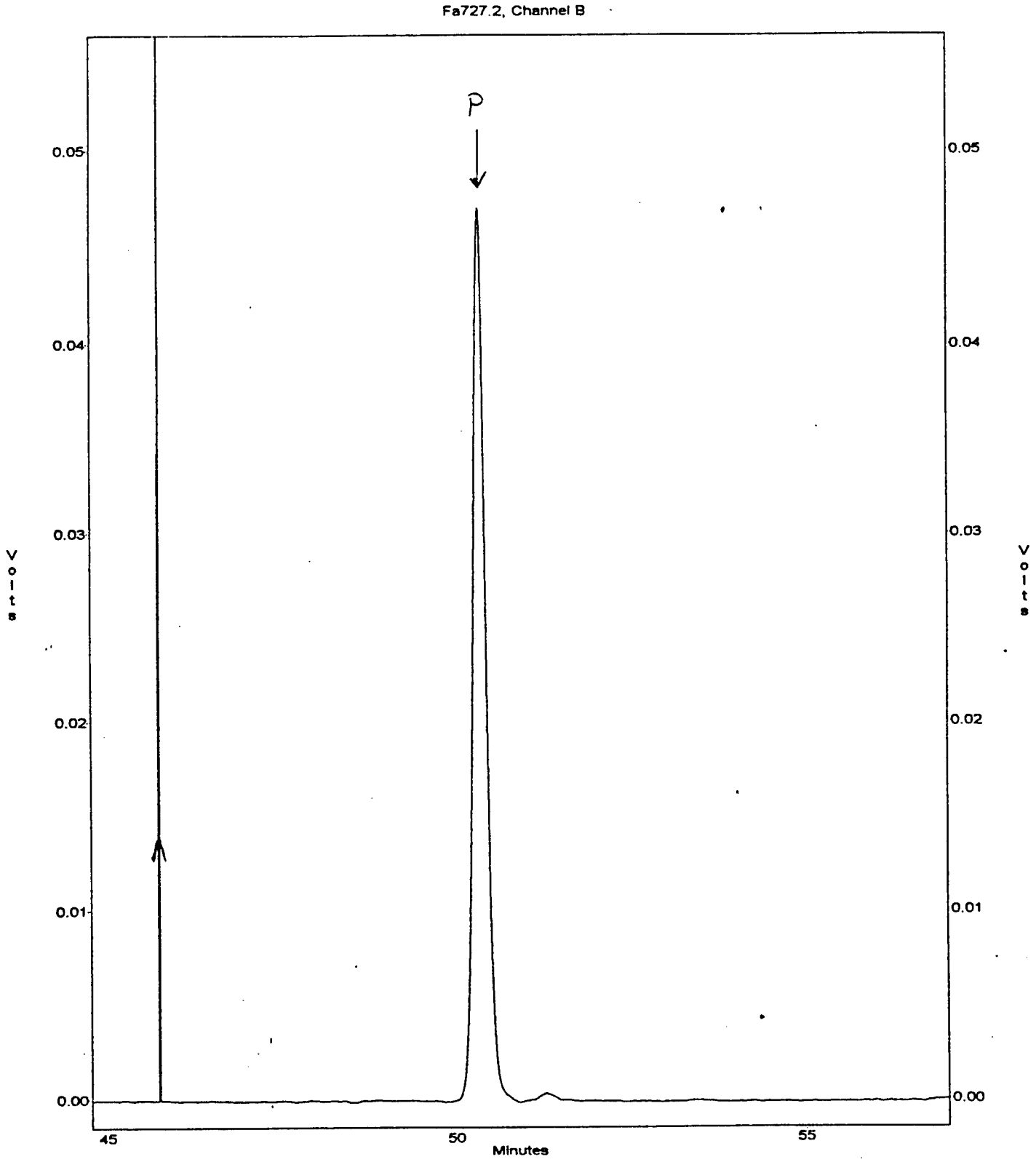

FORMATION OF PHOSPHORAMIDATE OF 5'dAMP AT DIFFERENT CONCENTRATIONS OF ED

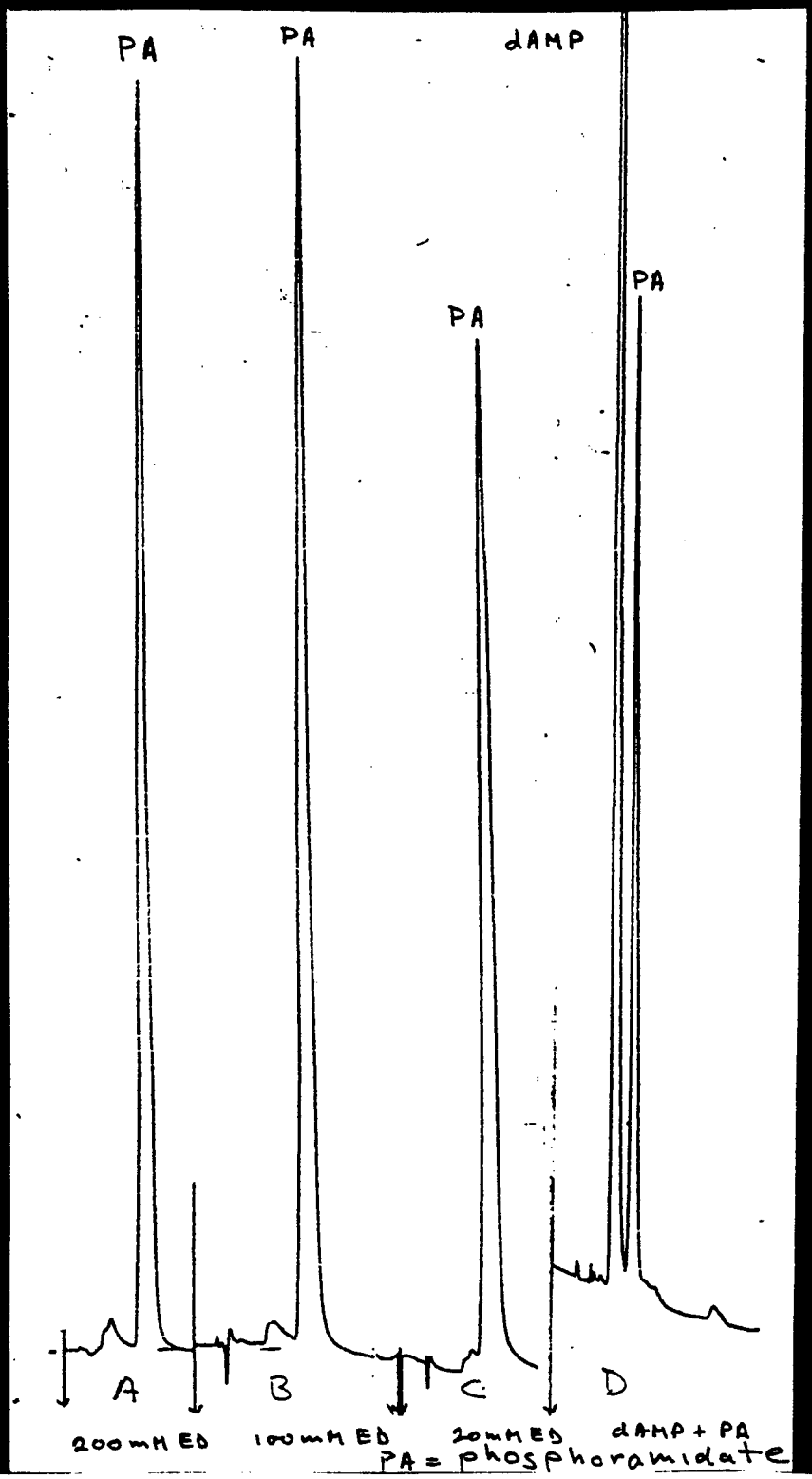

dAMP-PA prepared with +: A. 200mM ED; B. 100mM ED; C. 20mM ED; D. mix of dAMP with no ED and dAMP + 200mM ED (detection by u.v.)

FORMATION OF DANSYL CHLORIDE DERIVATIVE OF PHOSPHORAMIDATES FORMED AT DIFFERENT CONCENTRATIONS OF ED

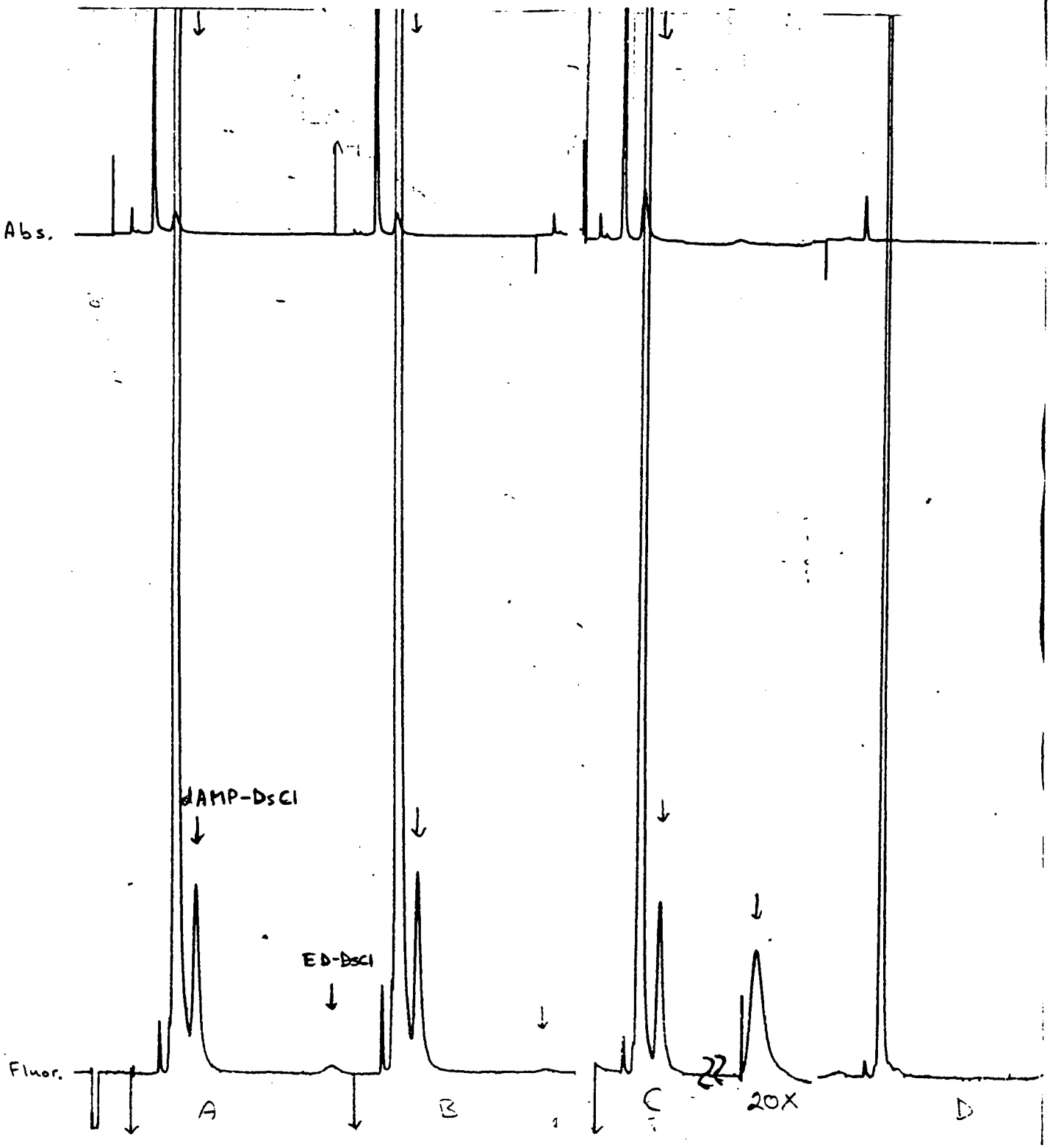

dAMP-PA-dansyl chloride prepared with: A. 200mM ED; B. 100mM ED; C. 20mM ED: D. no ED (detection by fluorescence)

EFFECT OF ION EXCHANGE TREATMENT ON THE CONCENTRATION OF ED-DANSYL CHLORIDE

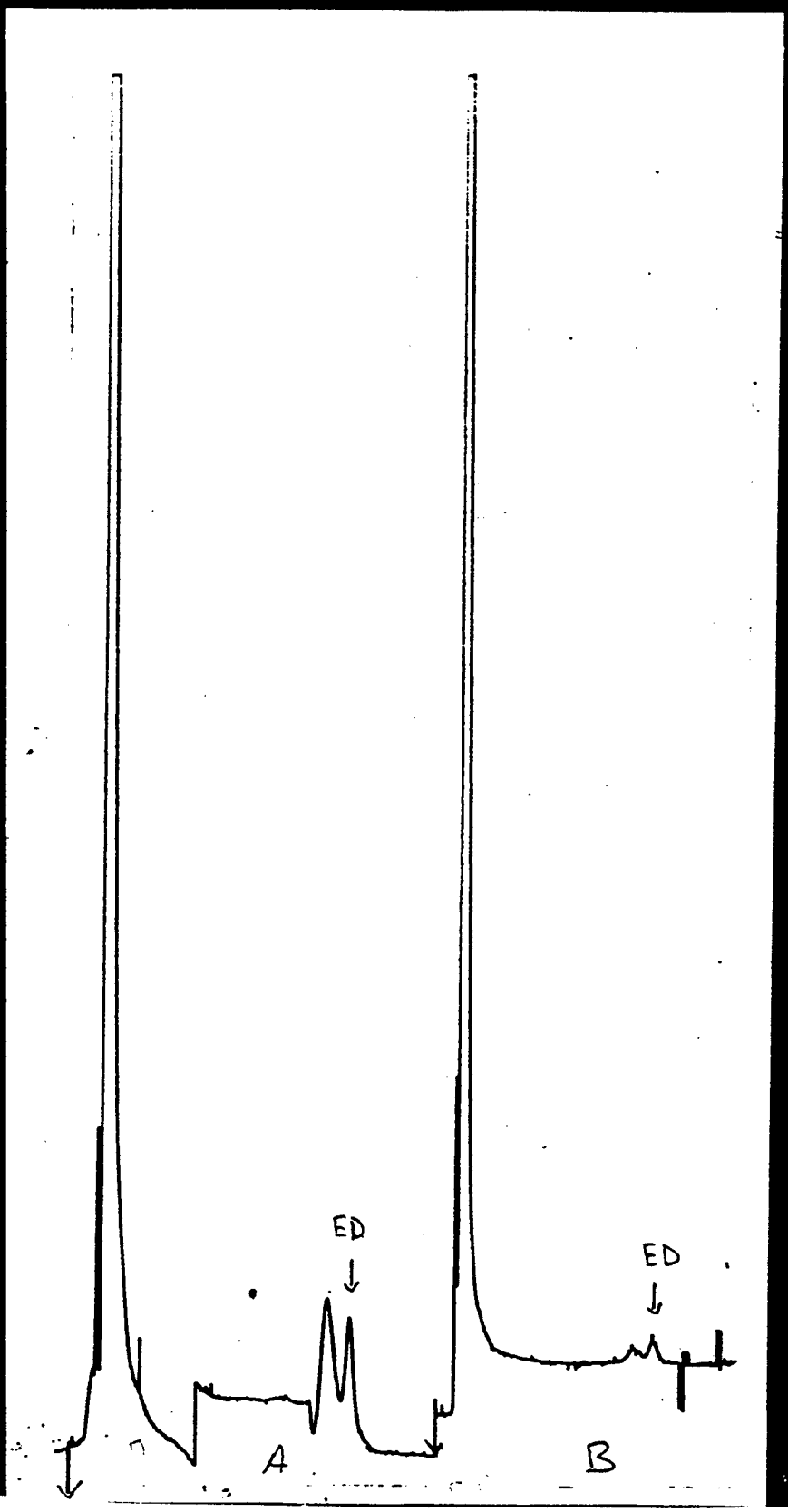

A. Dansyl chloride-ED B. SCX treated ED + dansyl chloride

FORMATION OF dGMP-ED PHOSPHORAMIDATE AND REACTION OF PHOSPHORAMIDATE WITH FLUORAM (detection by UV absorbance)

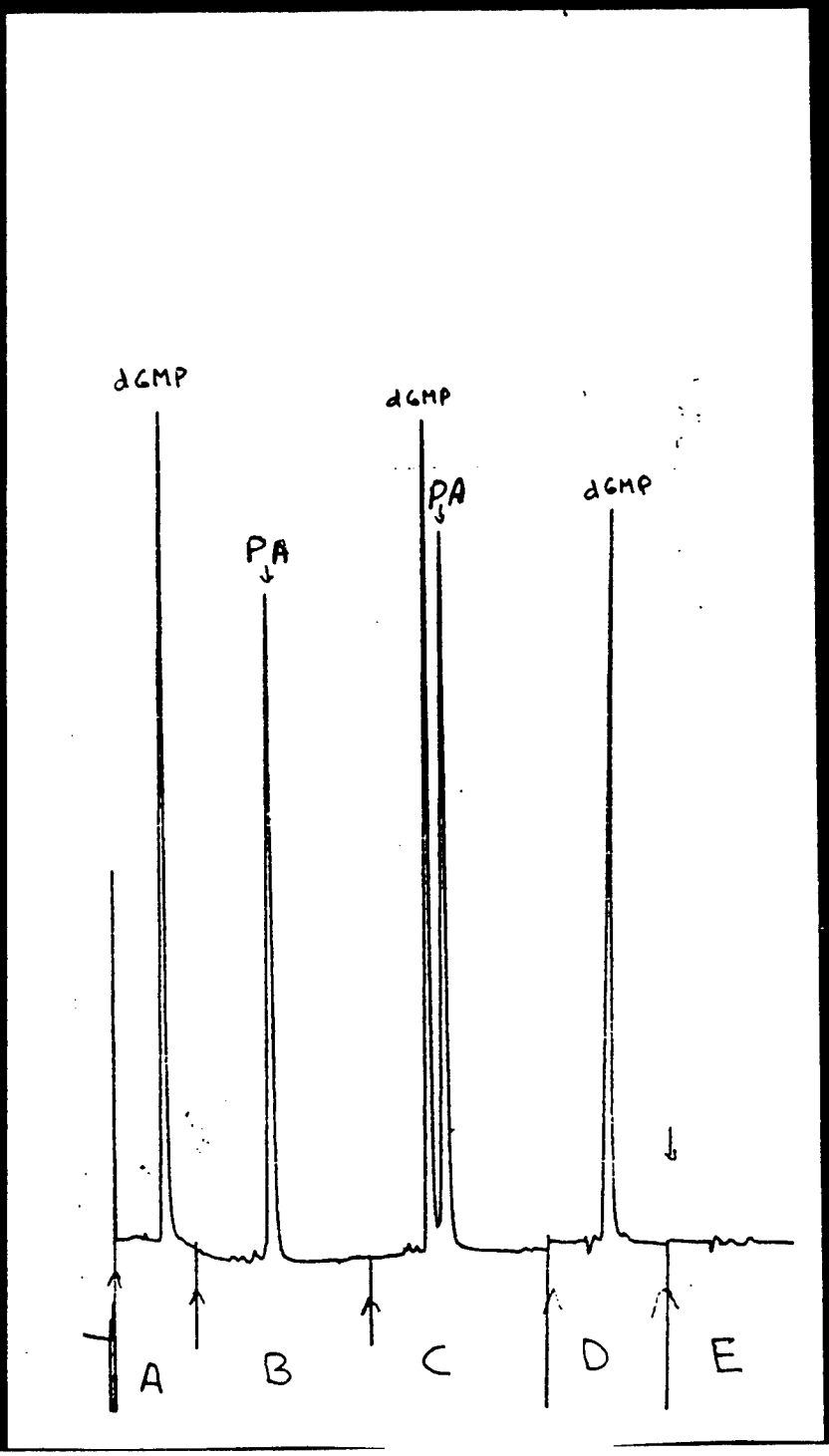

A. dGMP; B. dGMP-PA (dGMP + CDI + ED); C. A + B mixed; D. dGMP + Fluoram; E. dGMP-PA + Fluoram (detection by UV absorbance) PA = phosphoramidate

Fig. 8

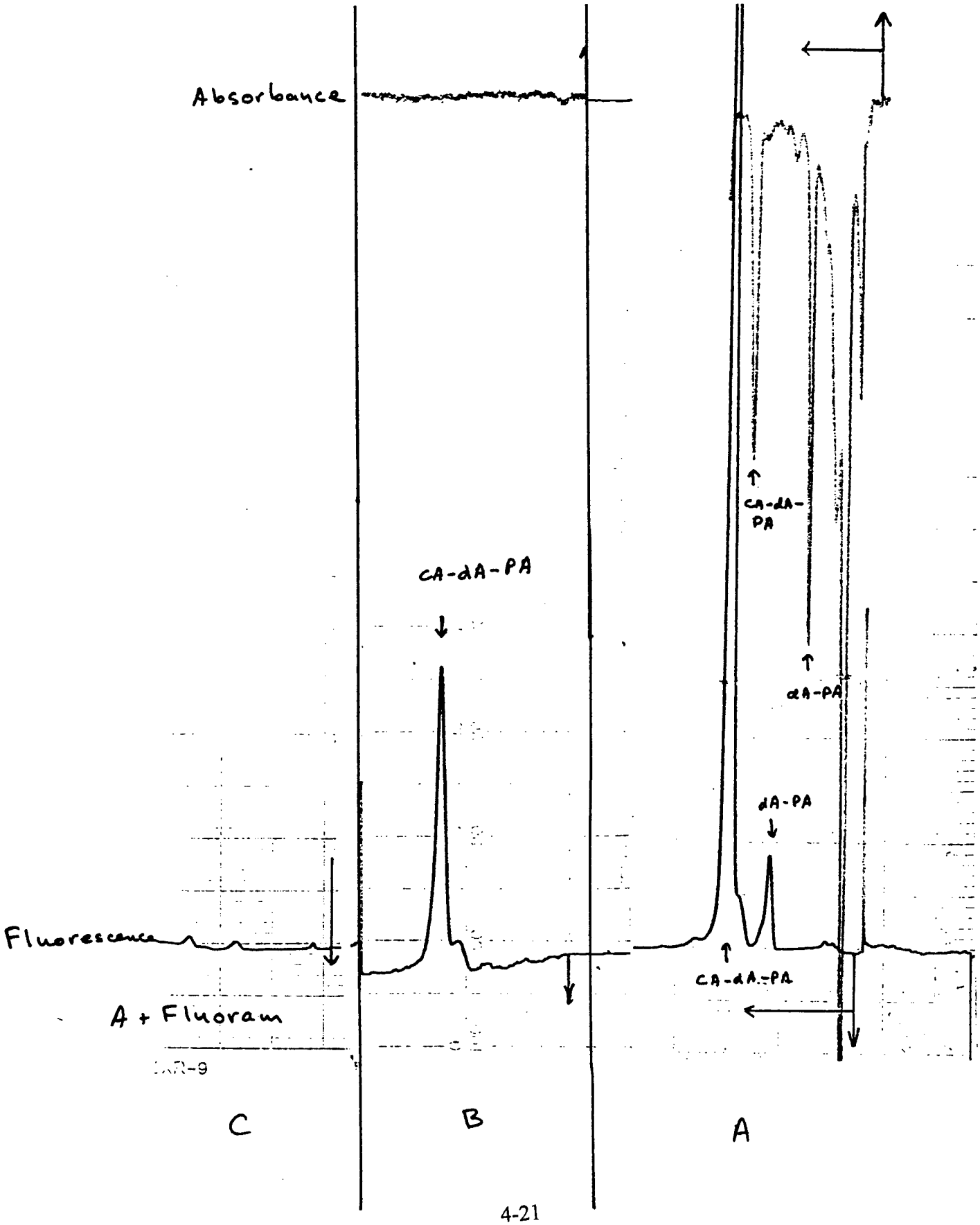
Absorbance
CA-dA-PA
CA-dA-PA
αA-PA
dA-PA
CA-dA-PA
Fluorescence
A + Fluoram
CXR-9
C
B
A

Fig. 9

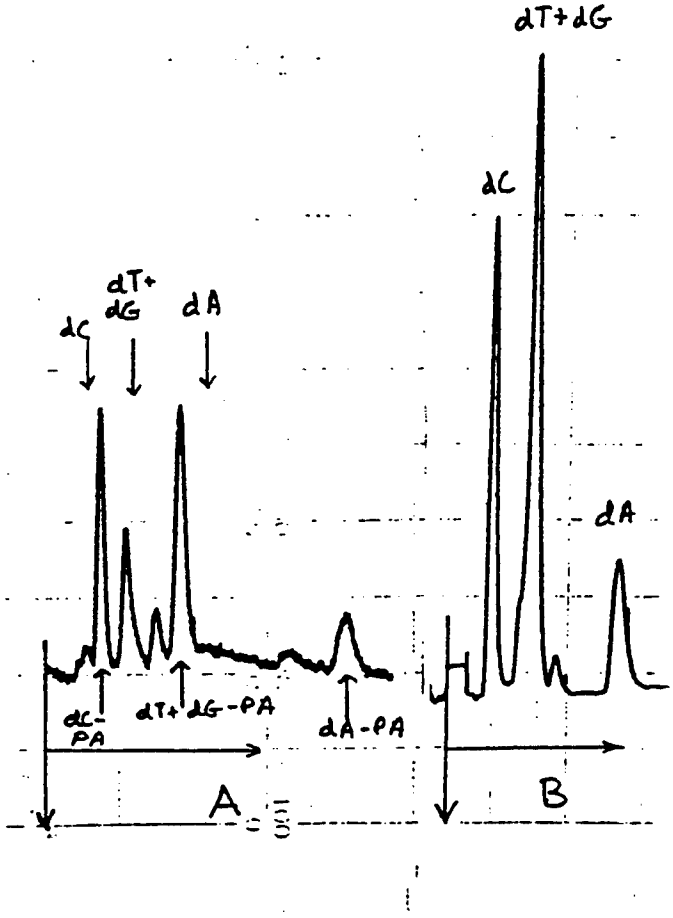

CORRECTION FOR BIAS INTRODUCED BY TRUNCATION IN PHARMACOKINETIC STUDIES OF ENVIRONMENTAL CONTAMINANTS

by

Joel E. Michalek
Epidemiologic Research Division
Armstrong Laboratory
Brooks Air Force Base, Texas 78235

Ram C. Tripathi
Department of Mathematics and Statistics
University of Texas at San Antonio
San Antonio, Texas 78249

Pushpa L. Gupta
Department of Mathematics
University of Maine
Orono, Maine

Kandansamy Selvavel
Department of Mathematics and Computer Science
Claflin College
Orangeburg, South Carolina 29115

and

Pandurang Kulkarni
Department of Mathematics and Statistics
University of South Alabama
Mobile, Alabama 36688

Final Report for: Summer Research Extension Program

Sponsored by: the Air Force Office of Scientific Research, Bolling AFB
and
Armstrong Laboratory, Brooks AFB

November 1996

CORRECTION FOR BIAS INTRODUCED BY TRUNCATION IN PHARMACOKINETIC STUDIES OF ENVIRONMENTAL CONTAMINANTS

Pandurang Kulkarni
Department of Mathematics and Statistics
University of South Alabama

Abstract

Pharmacokinetic studies of biomarkers for environmental contaminants in humans are generally restricted to a few measurements per subject taken after the initial exposure. Subjects are selected for inclusion in the study if their measured body burden is above a threshold determined by the distribution of the biomarker in a control population. Unless the data is properly conditioned, we show that ordinary weighted least squares estimate of the decay rate (λ) is biased due to regression toward the mean. We show that if the data is conditioned to lie above a line with slope $-\lambda$ on the log scale then the weighted least squares estimate of λ is unbiased. We give an iterative estimation algorithm that produces approximately unbiased estimates with commercially available software for fitting a repeated measures linear model. The estimate and its efficiency are discussed in the context of a pharmacokinetic study of 2,3,7,8-tetrachlorodibenzo-p-dioxin.

Key words: biomarker, half-life, least squares, regression toward the mean

CORRECTION FOR BIAS INTRODUCED BY TRUNCATION IN PHARMACOKINETIC STUDIES OF ENVIRONMENTAL CONTAMINANTS

Pandurang Kulkarni
Department of Mathematics and Statistics
University of South Alabama

1. INTRODUCTION

The Air Force is conducting a 20-year prospective study of health and exposure to 2,3,7,8-tetrachlorodibenzo-p-dioxin (dioxin) in veterans of Operation Ranch Hand, the unit responsible for aerial spraying of Agent Orange and other herbicides in Vietnam from 1962 to 1971[1]. Comparison veterans who served in Southeast Asia during the same period but who were not involved with spraying herbicides serve as referents. Physical examinations were administered in 1982, 1985, 1987 and 1992. Since 1987, exposure has been indexed by a measurement of dioxin in serum. In 1987, all willing Ranch Hand and Comparison veterans were asked to contribute blood for a dioxin assay; 870 Ranch Hands were assayed and received a quantifiable result[2]. As part of a pharmacokinetic study of dioxin, all 343 Ranch Hand veterans with dioxin levels above 10 parts per trillion (ppt) in 1987 and who had stored serum from the 1982 examination were selected. The initial dose in the Air Force study is unknown because the exposure occurred before the herbicides were known to be contaminated. The purposes of the pharmacokinetic study are to find an estimate of the half-life of dioxin in these veterans and to assess the significance of changes in half-life with covariates, such as body fat and age. In this report, we address only the problem of finding an estimate of the half-life.

We assume a one-compartment first order decay model, with decay rate λ, holds in subjects having body burdens above background levels defined by a threshold c. Subjects are selected for inclusion in the study if their measured body burden is above c at some point in time. The threshold is defined as a high quantile, such as 0.98, of the biomarker distribution in a control population with no known exposure. We assume that the biomarker data is log-normally distributed, which together with the first order model implies a repeated measures linear model relating the logarithm of the biomarker and time, with the slope being $-\lambda$. Unless the data is properly conditioned prior to analysis, we show that the ordinary weighted least squares estimate of λ is biased due to regression toward the mean. This regression to the mean phenomenon applies to any pharmacokinetic study in which subject selection is based on the magnitude of each subject's concentration of the contaminant. For example, in a recent study of the half-life of 2,3,7,8 tetrachlorodibenzo-p-dioxin (dioxin) in 48 occupationally exposed workers from a herbicide producing plant in Germany, researchers computed individual half-lives for workers whose blood levels of dioxin exceeded the 0.95 quantile of the German background concentration distribution[3]. In the study of dioxin half-life in veterans of Operation Ranch Hand[4], researchers reduced the sample to those veterans having dioxin levels greater than the 0.98 quantile of the dioxin background distribution, which was 10 ppt, in the population of unexposed control veterans.

To our knowledge, there have been no other studies of the effect of truncation on the bias and variance of weighted least squares estimation in the repeated measures linear model in the context of pharmacokinetic studies of the kind we consider. Earlier studies conducted by us, for example, did not take account of the truncated nature of the data and the associated bias in the least squares estimate of the decay rate[5]. Regression models in which the range of the dependent variable is constrained in some way have been called Tobit models and are also known as censored or truncated regression models. The model is called truncated if the observations outside a specified range are totally lost and censored if one can at least observe exogenous variables. Survival models are examples of censored regression models in biometry. Tobit models are used in econometrics to model phenomena in which the dependent variable is constrained to be positive. Amemiya[6] has surveyed Tobit models and the many associated parameter estimation procedures.

Because the usual weighted least squares estimate of the decay rate is biased due to regression toward the mean, our goal is to find a set of conditions under which the weighted least squares estimate would be unbiased. We present an iterative procedure to estimate the decay rate by conditioning the data set to include only those observations above a straight line in the log scale with slope equal to the negative of the decay rate passing through the threshold c at the last measurement time. With this procedure, existing commercially available software can be used to produce an unbiased estimate. We further want to describe the effect of the conditioning on the efficiency of the estimate.

We show, using the properties of the truncated normal distribution[7] that the resulting unbiased estimate is more efficient than the biased estimate produced by using all of the data in the Air Force study.

The results presented here do not apply to studies that do not require post hoc selection of subjects having concentrations above a threshold. For example, a study of persons exposed to dioxin in an industrial accident in Seveso, Italy[8], did not require post hoc subject selection based on the magnitude of the concentration of the contaminant, presumably because the subjects were so heavily exposed that none had background levels at the time of analysis. Similarly, a study of 5 individuals with paired serum levels of polychlorinated biphenyls, the first measured in 1977 and the second in 1984[9], did not require a post hoc selection based on measurements being above a threshold.

It may be possible that an alternative approach to our iterative conditioning procedure could be developed from first principles to accommodate the truncation[6] to provide unbiased estimates. However, a new approach using Tobit models, for example, does not appear straightforward, since much of the existing Tobit model theory does not address the repeated measures linear models we use. Actual implementation of such theory would require special computer programs and so would defeat our purpose, which was to provide a convenient way to eliminate bias while using commercially available statistical software for fitting the repeated measures linear model.

In Section 2, we express the weighted least squares estimate of the decay rate in closed form, find the bias, the variance and the mean squared error of the estimate conditioned on all measurements being greater than a constant and apply these results to data arising from the Air Force study[4]. In Section 3, we present an iterative estimation procedure that yields an approximately unbiased estimate of the decay rate and derive its variance. Application of these results to the Air Force study indicates the iteratively conditioned estimate is not only unbiased but also more efficient than the biased estimate based on all of the data. We discuss some extensions and remaining open issues in Section 4.

2. BIAS IN THE ESTIMATION OF THE DECAY RATE

We assume that k measurements per subject are available for each of n subjects, that the measurements were taken subsequent to the exposure and that the time between measurements (Δ) is fixed for all subjects, although the time between exposure and the first measurement for subject i (t_{i1}) varies between subjects. We assume that a single exposure produced an elevation of the body burden above background levels and that the first-order kinetics model

$$C_t=C_oe^{-\lambda t} \qquad (1)$$

holds in those subjects with body burdens above a threshold c. In (1), C_t is the concentration t years after exposure, C_o is the (unknown) initial concentration, and λ is a constant but unknown decay rate. Based on (1), the population half-life is $t_{½}=\log(2)/\lambda$, where log denotes the natural logarithm. If we take the natural logarithm of (1), we obtain

$$\log(C_t)=\log(C_o)-\lambda t. \qquad (2)$$

Thus, (2) can be regarded as a motivating equation for a linear model which accommodates multiple measurements per subject as well as covariates. Such a model, known as a fixed- effects repeated measures linear model, is given by

$$y_{ij}=\beta_0+\tau_i+\beta_1 t_{ij}+\varepsilon_{ij}, \qquad (3)$$

for i=1,2, ..., n and j=1, 2, ..., k, where i indexes n subjects and j indexes k measurements per subject, y_{ij} represents the natural logarithm of the jth measurement on the ith subject, $-\beta_1$ is the common decay rate (λ), $t_{ij}=t_{i1}+(j-1)\Delta$ is the time between exposure and the jth measurement, β_0 is the overall mean, τ_i is the effect of the ith subject and ε_{ij} is the residual error term for y_{ij}.

Because the first order model (1) holds only in exposed subjects with body burdens above background levels, subjects are included in the analysis only if $y_{ij} > \log(c)$, for all i and j. Given t_{ij}, j=1, 2, ..., k, prior to conditioning $\mathbf{y}_i=(y_{i1},y_{i2}, \ldots, y_{ik})'$ is k-variate normally distributed with covariance matrix Σ and mean $\mathbf{X}\beta$, where $\mathbf{X}$ is the design matrix for (3) and $\beta'=(\beta_0,\beta_1,\tau_1,\tau_2, \ldots, \tau_n)$. The weighted least squares estimate $\mathbf{b}$ of the vector of parameters β is

$$\mathbf{b}=(\mathbf{X}'\mathbf{V}^{-1}\mathbf{X})^{-1}\mathbf{X}'\mathbf{V}^{-1}\mathbf{y}, \qquad (4)$$

where $\mathbf{V}$ is a kn×kn block diagonal matrix with block Σ. When Σ is unknown, which is usually the case in practice, V is replaced by its estimate S, giving $\mathbf{b}=(\mathbf{X}'\mathbf{S}^{-1}\mathbf{X})^{-1}\mathbf{X}'\mathbf{S}^{-1}\mathbf{y}$. Under the normal distribution assumption, $\mathbf{b}$ is also the maximum likelihood estimate of β.

Here we first consider a special case of k=3 and Σ autoregressive of order one [AR(1)] given by

$$\Sigma = \sigma^2 \begin{bmatrix} 1 & \rho & \rho^2 \\ \rho & 1 & \rho \\ \rho^2 & \rho & 1 \end{bmatrix}.$$

Extensions to higher dimensions and other covariance models are discussed in Section 4.

k=3, AR(1)

The closed form weighted least squares estimate of λ, derived by solving equation (4), is

$$\hat{\lambda} = \frac{1}{\mathbf{n}} \sum_{i=1}^{n} \hat{\lambda}_{i13}, \qquad (5)$$

the sample mean of the individual decay rates $\hat{\lambda}_{i13} = (y_{i1} - y_{i3}) / 2\Delta$.

Because the sample is truncated based on the selection criterion that all measurements are greater than log(c), $\hat{\lambda}$ will be biased due to regression to the mean, regardless of the sample size. In this case, using the properties of the truncated normal distribution[7], we find that

$$E[\hat{\lambda} \,|\, y_{i1} > \log(c), y_{i2} > \log(c), y_{i3} > \log(c)] = \lambda + \text{BIAS}, \tag{6}$$

where

$$\text{BIAS} = \frac{\sigma(1-\rho^2)}{2n\Delta} \sum_{i=1}^{n} \frac{1}{\alpha_i} [\phi(a_{i1}) \Phi_2(A_{12i}, A_{13i}; \frac{\rho}{\sqrt{1+\rho^2}}) - \phi(a_{i3}) \Phi_2(A_{31i}, A_{32i}; \frac{\rho}{\sqrt{1+\rho^2}})], \tag{7}$$

and

$$a_{i1} = \frac{\log(c) - E(y_{i1})}{\sigma}, \; a_{i2} = \frac{\log(c) - E(y_{i2})}{\sigma}, \; a_{i3} = \frac{\log(c) - E(y_{i3})}{\sigma},$$

$$E(y_{i1}) = \beta_0 + \tau_i + \beta_1 (t_{i2} - \Delta), \; E(y_{i2}) = \beta_0 + \tau_i + \beta_1 t_{i2}, \; E(y_{i3}) = \beta_0 + \tau_i + \beta_1 (t_{i2} + \Delta),$$

$$A_{12i} = \frac{a_{i2} - \rho a_{i1}}{\sqrt{1-\rho^2}}, \; A_{13i} = \frac{a_{i3} - \rho^2 a_{i1}}{\sqrt{1-\rho^4}}, A_{31i} = \frac{a_{i1} - \rho^2 a_{i3}}{\sqrt{1-\rho^4}}, \; A_{32i} = \frac{a_{i2} - \rho a_{i3}}{\sqrt{1-\rho^2}}$$

σ^2=VAR(y_{ij}), j=1, 2, 3, ρ=corr(y_{i1},y_{i2}), $\alpha_i = P(x_{i1} > a_{i1}, x_{i2} > a_{i2}, x_{i3} > a_{i3})$,

x_{ij}=[y_{ij}-E(y_{ij})]/σ, i=1,2,...,n, j=1, 2, 3, ϕ is the standard normal density, and Φ_2(x,y;r) is the upper tail probability of a standard bivariate normal distribution with correlation r. To express the effect of this bias, we compute the mean squared error (MSE), defined by $\text{MSE} = \text{VAR}(\hat{\lambda}) + \text{BIAS}^2$, where the variance and bias are conditioned as in (6). To compute VAR($\hat{\lambda}$) and BIAS, we obtain the conditional first and second moments of x_{ij} when truncating at all three time points, given in the Appendix. Using these, we find that the conditional variance of $\hat{\lambda}$ can be written as

$$\mathrm{VAR}[\hat{\lambda}\,|\,y_{i1} > \log(c), y_{i2} > \log(c), y_{i3} > \log(c)] =$$

$$\frac{\sigma^2}{4n^2\Delta^2}\sum_{i=1}^{n}[\mathrm{VAR}(x_{i1}|x_{i1} > a_{i1}, x_{i2} > a_{i2}, x_{i3} > a_{i3}) + \mathrm{VAR}(x_{i3}|x_{i1} > a_{i1}, x_{i2} > a_{i2}, x_{i3} > a_{i3})$$

$$-2\mathrm{COV}(x_{i1}, x_{i3}|x_{i1} > a_{i1}, x_{i2} > a_{i2}, x_{i3} > a_{i3})], \qquad (8)$$

where $\mathrm{VAR}(x_{ij}|\, x_{i1}>a_{i1},\ x_{i2}>a_{i2},\ x_{i3}>a_{i3})$ and $\mathrm{COV}(x_{i1},x_{i3}|\, x_{i1}>a_{i1},\ x_{i2}>a_{i2},\ x_{i3}>a_{i3})$.

Example

In the Air Force study, the threshold c is 10 ppt, the 98th percentile of the Comparison dioxin distribution, and is the value we regard as the upper threshold for background exposure. Of the 343 subjects, 240 had a dioxin result greater than 10 ppt in 1982, 1987 and 1992[4]. These data, after log transformation, are summarized in Table 1. In summarizing the total population in 1987, we excluded 9 Ranch Hands with nondetectable dioxin levels (equal to 0 ppt) to preserve normality, reducing the sample size in 1987 to 861.

INSERT TABLE 1 HERE

The estimated within-subject correlation matrix, based on the subset of 240 subjects having all three dioxin measurements above the threshold of c=10 ppt in 1982, 1987 and 1992, is

$$\begin{bmatrix} 1.00 & 0.87 & 0.79 \\ 0.87 & 1.00 & 0.84 \\ 0.79 & 0.84 & 1.00 \end{bmatrix},$$

which appears to follow the AR(1) model. We included all 240 subjects with all three dioxin measurements above 10 ppt and corrected for background levels by subtracting 4 ppt from each dioxin measurement before taking the logarithm[10]. Specifying an AR(1) within-subject covariance matrix, we applied SAS™ PROC MIXED[11] to the log-transformed dioxin results to fit the repeated measures linear model (3) and found that $\hat{\lambda} = 0.0777$. To compute the bias (7), variance (8) and MSE, we used an estimate of the autocorrelation (ρ) of the untruncated data using the algorithm of Mee and Chua[12], which gave $\hat{\rho} = 0.8577$. Using this value of ρ, we found that BIAS=-0.00184, VAR($\hat{\lambda}$)=2.21×10^{-5} and MSE=2.55×10^{-5}.

3. UNBIASED ESTIMATION OF THE DECAY RATE

Inspection of (7) shows that the bias can be made equal to zero by truncating the data such that $a_{i1}=a_{i2}=a_{i3}$, or, equivalently, such that the observations lie above a straight line with slope $-\lambda$, with $y_{i1}>\log(c)+2\lambda\Delta$, $y_{i2}>\log(c)+\lambda\Delta$, $y_{i3}>\log(c)$. Because λ is unknown, we accomplish this truncation with the following iterative procedure.

The first step is to truncate the data at $\log(c)$ at each time point and estimate λ using weighted least squares. The second step is to truncate the first measurement at $\log(c)+2\hat{\lambda}\Delta$, the second at $\log(c)+\hat{\lambda}\Delta$ and the third at $\log(c)$, where $\hat{\lambda}$ is the estimate from the previous step, and update the estimate of λ using weighted least squares. The third step is to repeat step two using the updated value of $\hat{\lambda}$. The process is repeated until the estimated value of λ is equal to the value used for truncation in the previous step.

When applied to the Air Force data and again using PROC MIXED with AR(1) covariance structure, the procedure converged in two steps. At the first step, $\hat{\lambda}=0.0777$, giving $\hat{t}_{1/2}=8.9$ years, based on 240 subjects with all three measurements greater than $\log(10)$. In the second and final step, $\hat{\lambda}=0.0812$, giving $\hat{t}_{1/2}=8.5$ years, with $\mathrm{VAR}(\hat{\lambda})=2.34\times10^{-5}$, given by equation (8), based on 213 subjects. In original units, the data was truncated at the final step with the first dioxin level above 22.5 ppt, the second above 15.0 ppt, and the third above 10.0 ppt. The relative efficiency, defined as the ratio of the variance of the unbiased estimate to the MSE of

the biased estimate, is 0.91, indicating that the unbiased estimate is more efficient than the biased estimate. Thus, the removal of 27 subjects from the data base has served the dual purpose of reducing the variation and correcting the estimate.

4. EXTENSIONS

The results of the previous two sections generalize to any number, k, of measurements per subject when Σ has AR(1) structure. When $k \geq 4$, the weighted least squares estimate of λ can be written as a weighted average of pairwise decay rates,

$$\hat{\lambda} = \frac{1}{n}\sum_{i=1}^{n}\left\{ w_{1k}\hat{\lambda}_{1k} + \sum_{j=L(k)}^{k-1} w_{j,k+1-j}\hat{\lambda}_{j,k+1-j} \right\}, \tag{9}$$

where L(k) is the least integer greater than (k+1)/2,

$$\hat{\lambda}_{1k} = \frac{y_{i1} - y_{ik}}{(k-1)\Delta}, \quad \hat{\lambda}_{j,k+1-j} = \frac{y_{ij} - y_{i,k+1-j}}{(k+1-2j)\Delta},$$

$$w_{1k} = [2 + (k-3)(1-\rho)](k-1)/D, \quad w_{j,k+1-j} = (1-\rho)^2 \sum_{j=L(k)}^{k-1}(2j-k-1)^2 / D,$$

and

$$D = (k-1)\left\{ 2 + (k-3)(1-\rho) + (1-\rho)^2 \frac{(k-2)(k-3)}{6} \right\}.$$

The weights in (9) sum to one and the expectation of (9), given that $y_{ij} > \log(c)$, i=1,2, ..., n, j=1,2, ..., k, can be written in the form (6), where the bias is of the form (7) and the variance is of the form (8). The bias is zero when the data is conditioned to lie above a straight line with slope $-\lambda$ in log units, or, in particular, when $y_{i1} > \log(c) + (k-1)\lambda\Delta$, $y_{i2} > \log(c) + (k-2)\lambda\Delta$, ..., $y_{ik} > \log(c)$. This is because symmetries in the coefficients of the standardized y_{ij}, and the partial correlations together with alternating signs in the bias term cause all of the summands in the bias to be identically zero when the standardized cut points, a_{ij}, are equal for all j.

We have also considered the more general Toeplitz covariance model and have found that the results hold for k=3 and k=4. In this case the elements of Σ satisfy $\sigma_{ij}=\theta_r$, $r=1+|i-j|$, i=1, 2, ..., k and j=1, 2, ..., k. These results are summarized below.

k=3, Toeplitz

In this case, $\hat{\lambda}$ is the same as that given by equation (5).

k=4, Toeplitz

In this case, $\hat{\lambda}$ has the same form as in the case k=4, AR(1), with weights

$$w_{14} = \frac{3(\theta_3 - 4\theta_2 + 3\theta_1)}{(15\theta_2 + \theta_4 - 6\theta_3 - 10\theta_1)} \text{ and } w_{32}=1-w_{14}.$$

When Σ is Toeplitz and k=3 or k=4, $\hat{\lambda}$ is biased if the data is truncated to lie above $\log(c)$ at every point in time and is unbiased if the data is truncated to lie above a straight line with slope $-\lambda$ in log units. We have been unable to prove this result for general values of k under the Toeplitz covariance assumption, however, we conjecture that these results do hold for general values of k under this model.

When the covariance assumptions are further weakened, the result fails to hold. For example, the weighted least squares estimate of the decay rate cannot be made unbiased by truncation above a straight line with slope $-\lambda$ when Σ is equivariant

($\sigma_j^2 = \sigma_k^2, j \neq k$, σ_{jk} arbitrary).

5. CONCLUSION

Without knowing the actual formula for the weighted least squares estimate of λ, it is clear from the underlying model (3) that the estimate will be biased under truncation because the conditional expectation of the error term, given that the response is greater than a constant at every time point, is nonzero. The existence of this bias is caused by selecting subjects whose values are greater than a threshold, a criteria that will apply to any study in which the exposures are moderate enough so that when the study is begun, presumably at least one half-life after the exposure, some subjects have background levels and so must be excluded from the pharmacokinetic study.

The properties of our heuristic iterative decay rate estimate remain largely unexplored. In the Air Force example, the weighted least squares estimate based on all of the data under estimated the decay rate. General statements regarding the direction of the bias are not easily made, however, even when $k=3$, because the bias involves all of the parameters. Finally, although our iterative procedure converged in two steps in the example, its rate of convergence has not been worked out in terms of the parameters. We found that the unbiased estimate produced by our iterative procedure is more efficient than the biased estimate produced by simply truncating the data above 10 ppt at every time point. This increased efficiency is intuitively reasonable because, by truncating above a line with slope $-\lambda$ in the log scale, we are removing low values at the earlier time points

that contribute to bias. This removal serves the dual purpose of reducing the variation and correcting the estimate. Thus, in spite of the reduced number of observations, the efficiency of the final (unbiased) estimate is increased.

REFERENCES

1. Wolfe, W.H., Michalek, J.E., Miner, J.C., Rahe, A.J., Silva, J., Thomas, W.F., Grubbs, W.D., Lustik, M.B., Karrison, T.G., Roegner, R.H., and Williams, D.E. 'Health status of Air Force veterans occupationally exposed to herbicides in Vietnam', *Journal of the American Medical Association,* **264**, 1824-1831 (1990).

2. Roegner, R.H., Grubbs, W.D. Lustik, M.B., Brockman, A.S., Henderson, S.C., Williams, D.E., Wolfe, W.H., Michalek, J.E. and Miner, J.C. 'The Air Force Health Study. An epidemiologic investigation of health effects in Air Force personnel following exposure to herbicides. Serum dioxin analysis of 1987 examination results', National Technical Information Service (AD A 237 516-524), Springfield, Virginia, 1991.

3. Flesch-Janys D., Gurn, P., Jung, D., Konietzko, J. Manz, A. and Papke, O. 'First results of an investigation of the elimination of polychlorinated dibenzo-p-dioxins and dibenzofurans (PCDD/F) in occupationally exposed persons', *Organohalogen Compounds,* **21,** 93-99 (1994).

4. Michalek, J.E., Pirkle, J.L., Caudill, S.P., Tripathi, R.C., Patterson Jr, D.G. and Needham, L.L. 'Pharmacokinetics of TCDD in veterans of Operation Ranch Hand: 10-year follow-up', *Journal of Toxicology and Environmental Health* **,47,** 209-220 (1996).

5. Michalek, J.E., Tripathi, R.C, Caudill, S.P. and Pirkle, J.L. 'Investigation of TCDD half-life heterogeneity in veterans of Operation Ranch Hand', *Journal of Toxicology and Environmental Health,* **35**, 29-38 (1992).

6. Amemiya, T. 'Tobit models: a survey', *Journal of Econometrics,* **24,** 3-61 (1984).

7. Tallis, G.M. 'The moment-generating function of the truncated multinormal distribution', *Journal of the Royal Statistical Society B,* **23,** 223-229 (1961).

8. Needham, L.L., Gerthoux, P.M., Patterson Jr, D.G., Brambilla, P., Pirkle, J.L., Tramacere, P.L., Turner, W.E., Beretta, C., Sampson, E.J. and Mocarelli, P. 'Half-life of 2,3,7,8-tetrachlorodibenzo-p-dioxin in serum of Seveso adults: Interim report', *Organohalogen Compounds.* **21**, 81-85 (1994).

9. Steele, G., Stehr-Green, P. and Welty E. 'Estimates of the biological half-life of polychlorinated biphenyls in human serum', *The New England Journal of Medicine,* **314**, 926-927 (1986).

10. Pirkle, J.L., Wolfe W.H., Patterson Jr, D.G., Needham, L.L., Michalek, J.E., Miner, J.C. and Peterson, M.R. 'Estimates of the half-life of 2,3,7,8-tetrachlorodibenzo-p-dioxin in Vietnam veterans of Operation Ranch Hand', *Journal of Toxicology and Environmental Epidemiology,* **27**, 165-171 (1989).

11. 'SAS™ Technical Report P-229. SAS/STAT™ Software: Changes and Enhancements'. SAS Institute, Cary, North Carolina, 1992.

12. Mee, T.W. and Chua, T.C. 'Regression toward the mean and the paired sample t test', *The American Statistician.* **45**, 39-42 (1991).

APPENDIX

Conditional moments are given below for the special case that k=3 and Σ is AR(1) using the notation of Section 2.

$$\alpha_i E(x_{i1}) = \phi(a_{i1})\Phi(A_{i12}, A_{i13}; r) + \rho\phi(a_{i2})\Phi(A_{i21}, A_{i23}; 0) + \rho^2\phi(a_{i3})\Phi(A_{i31}, A_{i32}; r)$$

$$\alpha_i E(x_{i3}) = \rho^2\phi(a_{i1})\Phi(A_{i12}, A_{i13}; r) + \rho\phi(a_{i2})\Phi(A_{i21}, A_{i23}; 0) + \phi(a_{i3})\Phi(A_{i31}, A_{i32}; r)$$

$$\begin{aligned}\alpha_i E(x_{i1}^2) = {} & \alpha_i + a_{i1}\phi(a_{i1})\Phi(A_{i12}, A_{i13}; r) + \rho^2 a_{i2}\phi(a_{i2})\Phi(A_{i21}, A_{i23}; 0) + \rho^4 a_{i3}\phi(a_{i3})\Phi(A_{i31}, A_{i32}; r) \\ & + \rho(1-\rho^2)\phi(a_{i1}, a_{i2}; \rho)\Phi(A_{i13}^2) + \rho^2(1-\rho^4)\phi(a_{i1}, a_{i3}; \rho^2)\Phi(A_{i12}^3) \\ & + \rho^3(1-\rho^2)\phi(a_{i2}, a_{i3}; \rho)\Phi(A_{i21}^3)\end{aligned}$$

$$\begin{aligned}\alpha_i E(x_{i3}^2) = {} & \alpha_i + \rho^4 a_{i1}\phi(a_{i1})\Phi(A_{i12}, A_{i13}; r) + \rho^2 a_{i2}\phi(a_{i2})\Phi(A_{i21}, A_{i23}; 0) + a_{i3}\phi(a_{i3})\Phi(A_{i31}, A_{i32}; r) \\ & + \rho^3(1-\rho^2)\phi(a_{i1}, a_{i2}; \rho)\Phi(A_{i23}^1) + \rho^2(1-\rho^4)\phi(a_{i1}, a_{i3}; \rho^2)\Phi(A_{i32}^1)) \\ & + \rho(1-\rho^2)\phi(a_{i2}, a_{i3}; \rho)\Phi(A_{i31}^2)\end{aligned}$$

$$\begin{aligned}\alpha_i E(x_{i1}x_{i3}) = {} & \rho^2\alpha_i + \rho^2 a_{i1}\phi(a_{i1})\Phi(A_{i12}, A_{i13}; r) + \rho^2 a_{i2}\phi(a_{i2})\Phi(A_{i21}, A_{i23}; 0) \\ & + \rho^2 a_{i3}\phi(a_{i3})\Phi(A_{i31}, A_{i32}; r) + \rho(1-\rho^2)\phi(a_{i1}, a_{i2}; \rho)\Phi(A_{i23}^1) \\ & + (1-\rho^4)\phi(a_{i1}, a_{i3}; \rho^2)\Phi(A_{i32}^1) + \rho(1-\rho^2)\phi(a_{i2}, a_{i3}; \rho)\Phi(A_{i31}^2),\end{aligned}$$

where $r = \rho/\sqrt{1+\rho^2}$, $\phi(x)$ is the standard normal density, $\Phi(x)$ is the standard normal survival function, $\phi(x,y;s)$ is the bivariate standard normal density with correlation s, $\Phi(x,y;r)$ is the bivariate upper tail probability of the bivariate standard normal distribution with correlation r,

$A_{i23}^1 = A_{i13}^2$, $A_{i12}^3 = A_{i32}^1$, $A_{i21}^3 = A_{i31}^2$ and

$$A_{i13}^2 = \frac{a_{i3} - \rho a_{i2}}{\sqrt{1-\rho^2}}, \quad A_{i12}^3 = \left(a_{2i} - \frac{\rho a_{3i}}{1+\rho^2} - \frac{\rho a_{1i}}{1+\rho^2}\right)\sqrt{\frac{1+\rho^2}{1-\rho^2}}, \quad A_{i31}^2 = \frac{a_{i1} - \rho a_{i2}}{\sqrt{1-\rho^2}}.$$

Table 1

Summary of Log Transformed Dioxin Distributions in the Air Force Health Study

	Half-Life Study		Entire Population	
Year	**N**	**Mean (SD)**	**N**	**Mean (SD)**
1982	240	3.9 (0.7)		
1987	240	3.7 (0.8)	861	2.7 (1.04)
1992	240	3.2 (0.7)		

INDUCTION OF NITROBENZENE NITROREDUCTASE AND TRANSFORMATION OF NITROARMATIC COMPOUNDS BY *PSEUDOMONAS PSEUDOALCALIGENES* JS45

Michael P. Labare

Assistant Professor

Department of Chemistry

United States Military Academy

West Point, NY 10996

Final Report for:

AFOSR Summer Research Extension Program

Armstrong Laboratory

Sponsored by:

Air Force Office of Scientific Research

Bolling Air Force Base, D.C.

and

Armstrong Laboratory

June 1997

Abstract

Pseudomonas pseudoalcaligenes JS45 uses nitrobenzene as the sole source of C, N and energy via incomplete reduction to hydroxylaminobenzene. This study determined that induction of the nitroreductase responsible for the initial reduction of nitrobenzene is dependent on the growth history of JS45. When JS45 is transferred from cultures grown on succinate to a nitrobenzene containing medium, the lag phase can last from 12 to 48 hours. The length of the lag phase is dependent upon the number of generations JS45 was grown on succinate in a sigmodal fashion. It was also determined that prolonged growth of JS45 on nitrobenzene selects for strains in which reductase expression changes from inducible to constitutive. JS45 was also shown to transform a number of nitroaromatic compounds (nitrophenols, dinitrotoluenes, 4-nitrotoluene, 4-nitrobenzylalcohol and 4-nitrobenzaldehyde) in the presence or absence of nitrobenzene. However, the growth of JS45 is decreased by these transformations. The exception was 2,3-DNT which increased the growth of JS45 as measured by optical density.

Introduction

Nitroaromatic compounds are byproducts of the synthesis of solvents, dyes, and explosives and are commonly found as environmental contaminants. Some (e.g. nitrobenzene and 2,4-dinitrotoluene) are listed as priority pollutants by the Environmental Protection Agency (Keith and Telliard, 1979). Most nitroaromatic compounds are biodegradable and many can be completely mineralized by bacteria which utilize them as sole sources of carbon, nitrogen, and energy (Gorontzy et al, 1994). The initial step in the mineralization of nitroaromatic compounds may follow one of four routes: 1) oxygenation of the aromatic ring with the release of nitrite; 2) reduction of the aromatic ring with the release of nitrite; 3) reduction of the nitro group to an amine; or 4) incomplete reduction of the nitro group to a hydroxylamino derivative (Spain, 1995).

Until recently little was known about the degradative pathways for nitrobenzene (NB). Nishino and Spain (1993) isolated *Pseudomonas pseudoalcaligenes* JS45, which uses NB its sole source of carbon, nitrogen, and energy. The degradative pathway proceeded via incomplete reduction to hydroxylaminobenzene. The enzyme responsible for initial reduction is nitrobenzene nitroreductase. The nitroreductase has been purified and characterized. It is an oxygen-insensitive (Type 1) flavoprotein (2 moles of FMN per mole of protein) and is active as a monomer of 30-33 kDa. The reductase does not require metal cofactors and its production is induced by NB (Somerville et al, 1995).

P. pseudoalcaligenes JS45 grows on NB, hydroxylaminobenzene, and 2-aminophenol but not on other aromatic compounds. The compounds tested were dinitrobenzenes, nitrobenzoates, nitrotoluenes, nitrophenols, catechol, nitrocatechols,

aminophenols, aniline, benzene, phenol, toluene, nitrosobenzene, and picolinic acid (Nishino and Spain, 1993). Although JS45 does not grow on these compounds, their transformation has not been studied. It is not known if these compounds serve as substrates for the enzymes of the nitrobenzene degradation pathway. If the compounds are substrates, transformation may produce toxic or metabolically inert intermediates. Alternatively, these nitroaromatics may not induce production of the reductase or the subsequent enzymes.

This study was conducted to determine if the nitroreductase is induced by nitroaromatics other than nitrobenzene and to examine the transformation of nitroaromatics by JS45.

Material and Methods

Culture conditions. *Pseudomonas pseudoalcaligenes* strain JS45 was in grown at 25 $\pm$ 2 ^{o} C on a rotary shaker (150 rpm) in minimal medium (MSB; Stanier et al, 1966) amended with a suitable carbon source.

Effects of JS45 growth history on NB nitroreductase induction. Two strains of JS45 with different growth histories were established. The strains differed with respect to exposure to NB. Both strains originated from JS45 grown on MSB amended with 3 mM succinate in a chemostat. The growth conditions in the chemostat were: 25^{o} C, agitation of 150 rpm, and a dilution rate of 60 ml/h. The chemostat was allowed to run for 30 days.

The first strain, termed JS45-NE, was taken directly from the chemostat and grown in a 50 ml batch culture of MSB amended with 3 mM succinate. JS45-NE was maintained on succinate only for at least 10 generations.

The second strain, JS45-RE, was established by using an aliquot of the chemostat culture to inoculate a 50 ml batch culture of MSB amended with 1.0 mM NB. This strain exhibited a 48 hour lag phase when it was transferred from the chemostat to NB.

Both strains were grown over night on 3 mM succinate and used to inoculate the following media: MSB, and MSB amended with 3 mM succinate, 2 mM NB, 2 mM NB and 3 mM succinate, or 2 mM NB and 0.1 mM succinate. Growth was monitored by optical density (600 nm). At subsequent times post inoculation samples were removed and analyzed for NB by HPLC.

JS45-RE was also used to inoculate an additional 50 ml batch culture growing on 1.0 mM NB to produce a strain with a constant exposure to NB. This strain, JS45-CE, was only used to inoculate 2 mM NB plus 3 mM succinate.

The OD density of the cultures was monitored and based on prior studies (Labare 1996) induction was assumed to occur 4 hours prior to measurable growth. In addition, the concentration of NB in the cultures was determined via HPLC analysis.

Nitroreductase resting cell assay. JS45 was grown overnight on MSB amended with 1 mM NB, harvested by centrifugation (10 minutes, 10,000 g), washed 2 times in MSB and transferred to 50 ml of 3 mM sodium succinate in MSB. JS45 was grown overnight, harvested, washed twice in MSB and transferred to 50 ml of MSB amended with 1 mM NB, 0.25 mM 2-NP, or 1 mM NB and 0.25 mM 2-NP. All cultures were carried out in triplicate. After 15 hours the cultures had reached ODs of 0.0897 (NB) and 0.0080 (2-NP). The cells were harvested and washed twice with MSB. Due to the low cell density, the three cultures exposed to 2-NP were combined. The cells were resuspended in MSB at an OD of 0.06. Each reaction vessel received 495 µl of the cell suspension and 5 µl of 10 mM NB (0.1 mM NB final concentration). The reaction vessels were statically incubated for 5 minutes and centrifuged for 5 minutes. The reaction was stopped by mixing 0.4 ml of the reaction mixture with 0.4 ml of acetonitrile: 0.1% trifluroacetic acid (40:60; v:v). The NB concentration was determined by HPLC. The reductase activity was expressed as mmol NB consumed per minute with each reaction mixture receiving the same number of cells.

Nitroreductase enzyme assay. JS45 was grown as described above with the following exception. After growth on 3 mM succinate, JS45 was transferred to MSB amended with 1 mM NB, 3 mM succinate, 0.25 mM 2-NP or nothing. After an additional 24 hours, the cells were harvested, washed twice in MSB and resuspended in 1 ml of phosphate buffer (20 mM, pH 8). The cells were broken by sonication with a Ultrasonic processor (Heat Systems, Inc., Farmingdale, NY) equipped with a microtip at output level 5. Total sonication time was 3 minutes. The sonicator was run in 0.25 second bursts for 30 seconds on and 30 seconds off while in an ice bath. The enzyme extract was then centrifuged to remove intact cells. The reaction mixture received 100-300 µl of enzyme extract.

Reductase activity was measured spectrophotometrically as the decrease in A_{340} due to the oxidation of NADPH in the reaction mixture. Unless otherwise stated the reaction mixture contained enzyme extract, 0.1 mM NB, 0.5 mM NADPH, and 20 mM (pH 8) phosphate buffer in a volume of 1 ml. Specific activity was expressed as µmol of NADPH oxidized per minute per mg of protein. All tests were run in triplicate.

Cometabolism of nitroaromatic compounds by JS45. JS45 was grown as described above. Washed cells were transferred to 50 ml of MSB amended with 1 mM NB, 0.25 mM of the test compound or 1 mM NB plus 0.25 mM of the test compound. All cultures were carried out in triplicate. The compounds tested were 2-, 3-, and 4-nitrophenol (NP); 2,3-, 2,4-, and 2,6-dinitrotoulene (DNT); 4-nitrotoluene; 4-nitrobenzoate; and 4-nitrobenzaldehyde. At times post inoculation, 0.7 ml aliquots were removed, centrifuged and 0.4 ml of cell-free, spent broth mixed with 0.4 ml of the HPLC mobile phase. The

concentration of NB and the test compound was determined by HPLC analysis. The growth was monitored by OD.

HPLC analysis. Aliquots (50 µl) of samples were analyzed on a 250 mm Allsphere octyl C8 column (Alltech, Deerfield, IL) with a gradient of acetonitrile and trifluroacetic acid (0.1% in distilled water) as mobile phase. Elution started at 60:40 (trifluroacetic acid:acetonitrile; v:v) with a gradient to 40:60 over 8 minutes. The flow rate was 1.0 ml/minute. Products were detected at UV A_{210} with a Waters 996 Photodiode Array Detector (Milford, MA).

RESULTS

Effects of JS45 growth history on NB nitroreductase induction. None of the strains grew in the presence of MSB alone. JS45-NE and JS45-RE both grew on MSB amended with 3 mM succinate without a lag phase. Maximum OD (0.32-0.34) was reached within 5 hours.

Both strains had extended lag phases when grown on MSB amended only with 2 mM NB. JS45-RE had a lag phase of 12-14 hours and NB was undetectable by 28 hours. The lag phase for JS45-NE was 19 to 23 hours. NB started to decrease between 15 to 20 hours and was gone by 28 hours (Figure 1).

The two strains exhibited different growth patterns on MSB amended with 2 mM NB and 0.1 mM succinate. JS45-RE had a 3 hour lag phase and NB was undetectable by 9 hours post inoculation. JS45-NE had a 20-22 hour lag phase and the concentration of NB started to decrease around 15-20 hours post-inoculation. NB undetectable by 30 hours (Figure 2).

All three strains grew without a lag phase on MSB amended with 2 mM NB plus 3 mM succinate. JS45-CE degraded all the NB within 8 hours. NB was undetectable within 11 hours for JS45-RE (Figure 3). JS45-NE exhibited biphasic growth reaching a plateau by 10 hours with growth resuming at 23 hours. The NB started decreasing within 5 hours. The rate of NB disappearance from 5 to 23 hours was 0.00032 mmol of NB per hour. At 23 hours the rate of disappearance of NB increased to 0.0095 mmol of NB per hour (23-33 hours). Thus the rate of NB disappearance increased over 29 times and was

undetectable by 33 hours. The switch to the faster rate of NB disappearance coincided with the renewed growth of JS45 (Figure 3).

Nitroreductase resting cell assay. After growth of JS45 on succinate, the cells were exposed to 1 mM NB or 0.25 mM 2-NP. The reaction mixtures received approximately equal number of cells as determined by the OD of the reaction mixture. The cells grown on NB alone had an average OD of 0.764 whereas the combined cultures exposed to 2-NP had an average OD of 0.873. The rate of NB reduction was 0.00040 and 0.00012 mmol of NB per minute for JS45 exposed to NB and 2-NP, respectively. This rates were significantly different ($p < 0.05$) as measured by the student's t test.

Nitroreductase enzyme assay. The nitroreductase activities of JS45 cells exposed to 1 mM NB, 3 mM succinate, 0.25 mM 2-NP or MSB alone were 0.021, 0.029, 0.032 and 0.007 μmol of NADPH oxidized per minute per mg of protein, respectively. The specific activity of the cells exposed to NB was significantly lower than the specific activity in any of the other treatments ($p < 0.05$) as measured by the student's t test.

Cometabolism of nitroaromatic compounds by JS45. The cometabolism of nitroaromatic compounds was examined under two conditions, in the presence or absence of NB. In the absence of NB only 3- and 4-NP were not transformed. The addition of NB increased the extent of transformation for all nitroaromatics tested save 4-nitrobenzaldehyde. The amount transformed ranged from 1.7 to 100 % for 3-nitrophenol and 4-nitrotoluene, respectively (Table 1). A number of intermediates were detected by the HPLC for all the nitroaromatics except 4-nitrobenzaldehyde and 4-nitrobenzoate. In

general there were more detectable intermediates when both NB and the test compound were present together.

Growth of JS45 on nitroaromatic mixtures. The presence of 0.25 mM 2-NP, 3-NP, 4-NP, 4-NT, 4-NBA, or 4-nitrobenzaldehyde (NB plus test compound) decreased the growth (OD) of JS45 when compared to growth on NB alone ($p < 0.05$). 2,4-DNT or 2,6-DNT appeared to decrease the amount of growth but not by a statically significant amount. Only 4-nitrobenzoate had no effect on growth. In one case, 2,3-DNT, there was an increase in the maximum OD. However, maximum growth did not occur until 24 hours later and was only significant at the $p < 0.10$ level.

DISCUSSION

Effects of JS45 growth history on NB nitroreductase induction. The growth history of JS45 has a significant effect on the induction of nitroreductase. When JS45 is transferred from succinate to NB there is a lag phase lasting at least 14 hours and frequently greater than 20 hours. This study and others have shown there is a sigmodal correlation between the number of generations that JS45 had not been exposed to NB and the length of the lag phase when transferred to NB (Somerville, personal communication). Conversely, cells transferred to NB from NB have no lag phase.

The lag phase can be reduced by the addition of succinate (0.1 mM) to MSB amended with 2 mM NB for JS45 that has been recently exposed to NB. The lag phase for JS45-RE decreased from 14 to 3 hours. However, succinate did not alter the lag phase for JS45-NE, a strain that had not been recently exposed to NB. When 3 mM succinate was added, JS45-NE did grow immediately but exhibited biphasic growth, indicating the succinate was being preferentially used. In fact the resumption of growth coincided with the lag phase of JS45-NE growing on 2 mM NB alone (Figures 1 and 3). These results are consistent with previous induction studies (Nishino and Spain, 1993) but also indicate that the lag phase exhibited by JS45-RE, but not JS-NE, was partially due to energy limitations. This, combined with the long lag phase and biphasic growth of JS45-NE on mixtures of NB and succinate indicates that the lag phase may not be completely due to enzyme induction but is limited by some other factor, possibly transport limitations.

Induction of nitroreductase by nitroaromatics. Nitroreductase activity was demonstrated in JS45 growing on NB, succinate, or cells exposed to 2-NP. These results show the strain used for the induction experiments has mutated and is clearly different then the strain used for the growth history experiments.

Cometabolism of nitroaromatic compounds by JS45. Nitrobenzene nitroreductase purified from JS45 was previously shown to reduce a number of nitroaromatic compounds (Labare, 1995). This study has demonstrated that intact cells which expressed the inducible form of the nitroreductase are also capable of transforming many of these nitroaromatics both in the presence and absence of NB (Table 1). However, the transformation of these nitroaromatics is detrimental to the growth of JS45. All the compounds examined, save 2,3-DNT, decreased the maximum optical density of JS45 growing on the mixture of nitroaromatics as compared to growth on NB alone. It is probable that some of the intermediates detected by HPLC analysis were toxic or the parent compound were inhibiting the nitroreductase or that reducing equivalents were being wasted in non-productive reactions.

Future plans. Additional studies are planned to examine the cometabolism of nitroaromatics by JS45. Specially, the intermediates will be identified and tested for toxicity. These studies will also focus on the transformation of 2,3-DNT since it was the only nitroaromatic compound that consistently increased the growth of JS45. Experiments will be conducted to examine this increased growth and determine if JS45 is in fact obtaining some benefit from the transformation of 2,3-DNT.

ACKNOWLEDGMENTS

I would like to acknowledge the assistance and guidance of Drs. Jim Spain, Charles Somerville, and Dave Loehle. This work was supported by a grant (95-0034) from the Air Force Office of Scientific Research.

REFERENCES

Keith, L.Y. and W.A. and Telliard. 1979. Priority pollutants. I. A perpective view. Environ. Sci. Technol. **13:**416-423.

Gorontzy T., O. Drzyzga, M.W. Kahl, D. Bruns-nagel, J. Breitung, E. von Loew, and K.-H. Blotevogel. 1994. Microbial degradation of explosives and related compounds. Critical Reviews in Microbiol. **20:**265-284.

Nishino, S.F. and J.C. Spain. 1993. Degradation of nitrobenzene by a *Pseudomonas pseudoalcaligenes* Appl. Environ. Microbiol. **59:**2520-2525.

Somerville, C.C., S.F. Nishino, and J.C. Spain. 1995. Isolation and characterization of nitrobenzene nitroreductase from *Pseudomonas pseudoalcaligenes* JS45. J. Bacteriol. **177:** 3837-3842.

Spain, J.C. 1995. Bacterial degradation of nitroaromatic compounds under aerobic conditions. p. 19-35. *in* J.C. Spain (ed.), Biodegradation of nitroaromatic compounds. Plenum Press, NY, NY.

Stanier, R.Y., N.J. Palleroni and M. Doudoroff. 1966. The aerobic pseudomonads: a taxonomic study. J. Gen. Microbiol. **43**:159-271.

Table 1. Cometabolism of nitroaromatic compounds by JS45

Substrate (0.25 mM)	Without NB		With NB	
	µmol lost	% lost	µmol lost	% lost
4-nitrotoluene	12.0[A]	89.4	13.0[A,B]	100
4-nitrobenzylalcohol	0.6[A]	5.0	4.2[A,B]	31.8
4-nitrobenzaldehyde	10.0[A]	73.3	1.0[A,B]	52.1
2-NP	2.8	19.7	14.0 [A,B]	100
3-NP	none	0	0.2[A]	1.7
4-NP	none	0	0.8 [A]	6.6
2,3-DNT	0.7 [A]	6.1	4.0 [A,B]	42.0
2,4-DNT	2.3 [A]	18.7	6.5 [A,C]	56.2
2,6-DNT	2.8 [A]	22.5	3.8 [A]	30.9

[A] The concentration of the nitroaromatic is significantly lower than the initial concentration ($p < 0.05$).
[B] The concentration of the nitroaromatic compound in the presence of nitrobenzene is significantly lower than in the absence of nitrobenzene ($p < 0.05$).
[C] The concentration of the nitroaromatic is significantly lower than the initial concentration ($p < 0.10$).

Figure 1. Growth of JS45-RE and JS45-NE
on 1 mM NB

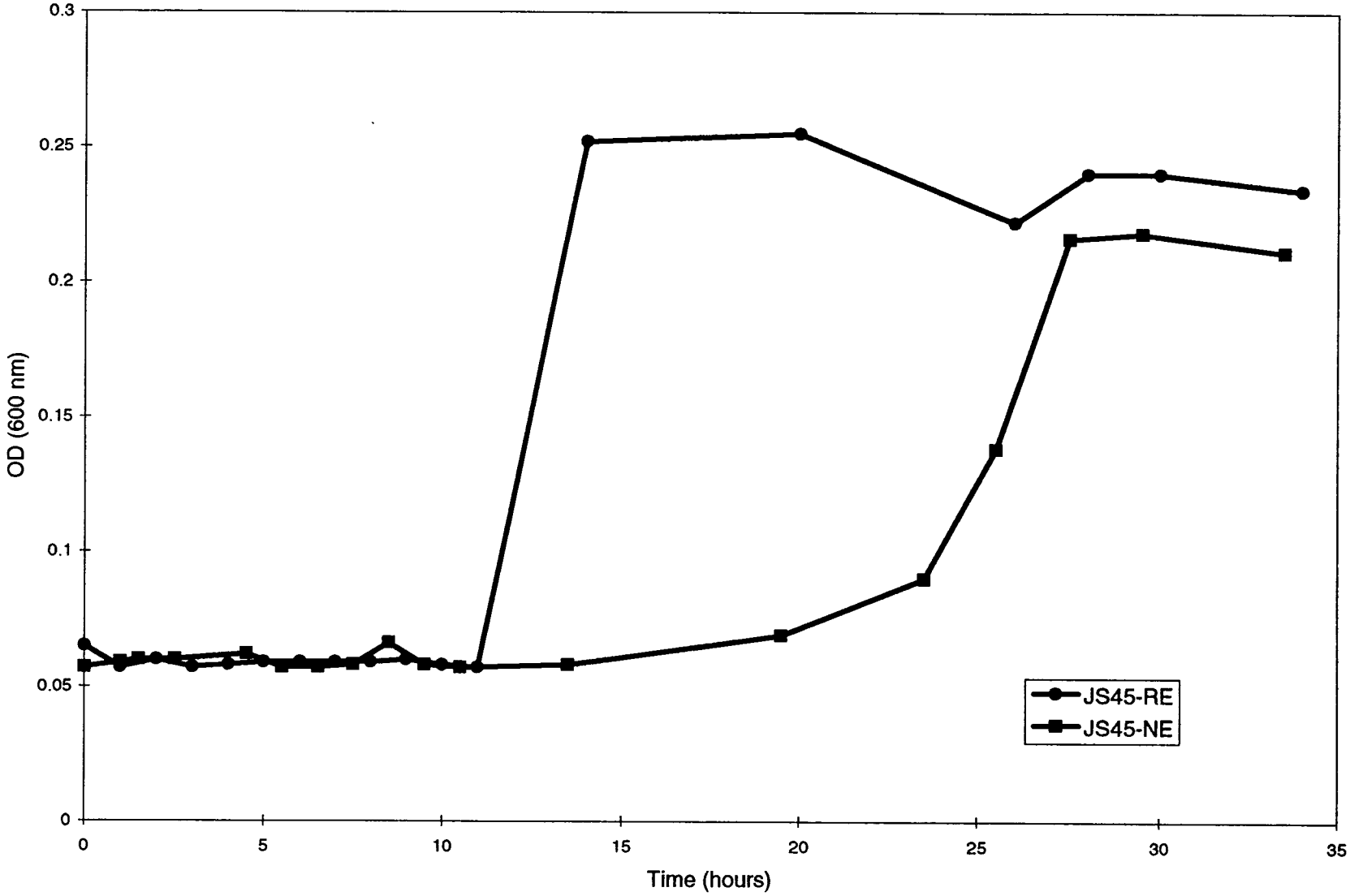

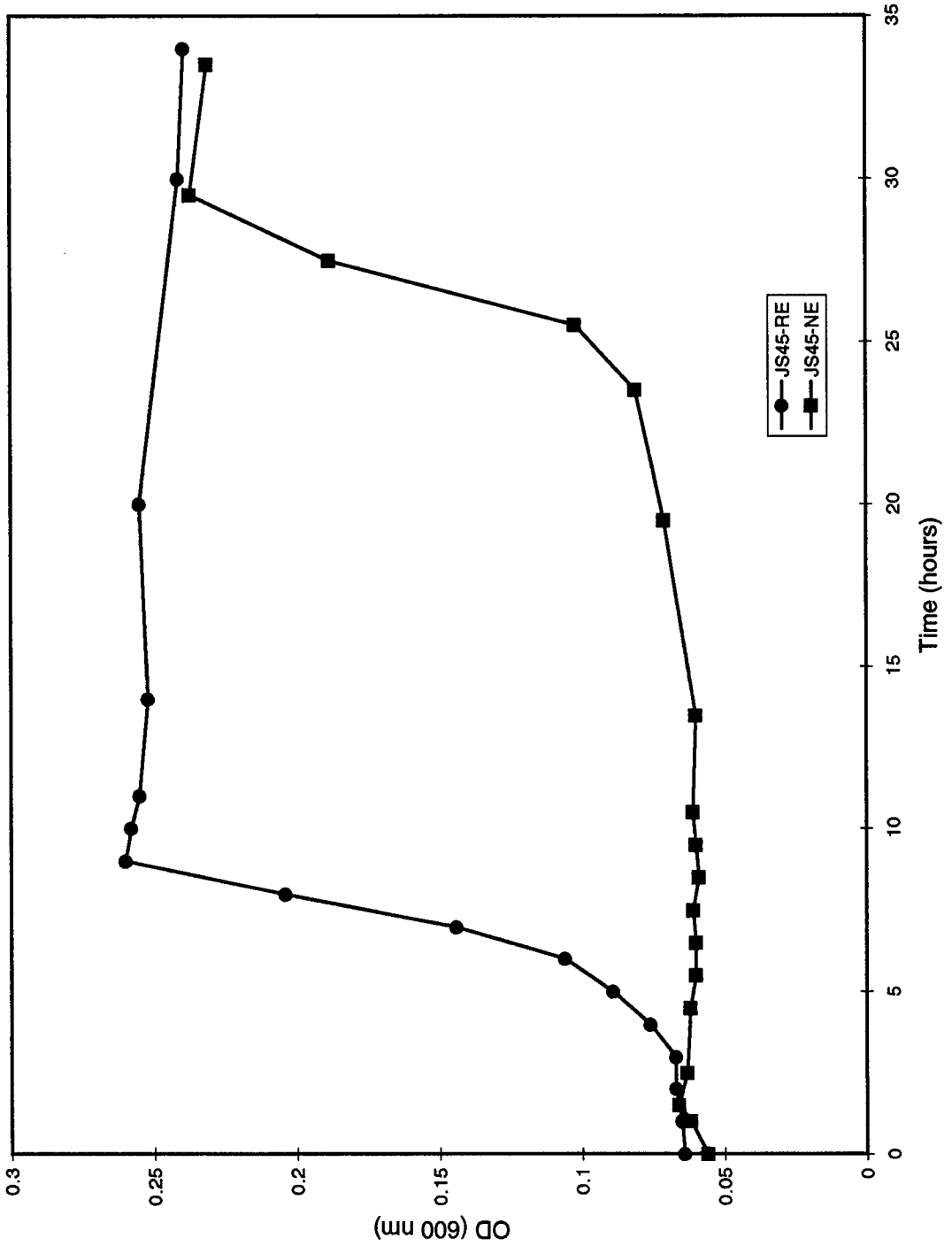

Figure 2. Growth of JS45-RE and JS45-NE on 1 mM NB plus 0.1 mM succinate

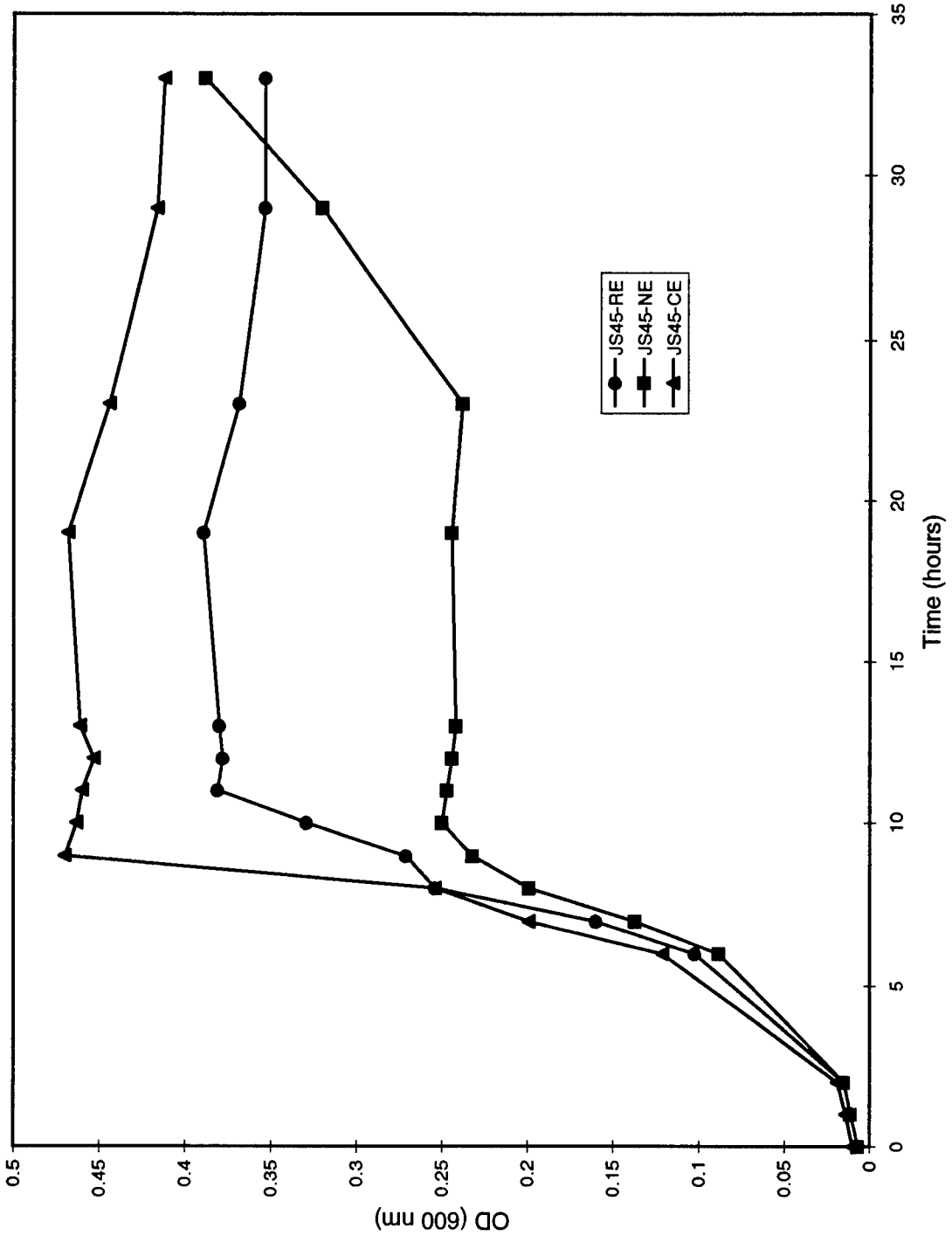

Figure 3. Growth of JS45-RE, JS45-NE and JS45-CE on 2 mM NB plus 3 mM succinate

TUNED SELECTIVITY SOLID PHASE MICROEXTRACTION: COMPUTER ASSISTED METHODS DEVELOPMENT FOR CHARACTERIZING FUEL SPILLS

Barry K. Lavine
Associate Professor
Department of Chemistry

Clarkson University
Box 5810
Potsdam, NY 13699-5810

Final Report for:
Summer Research Extension Program
Armstrong Laboratory

Sponsored by
Air Force Office of Scientific Research
Bolling Air Force Base, DC

and

Clarkson University

December 1996

TUNED SELECTIVITY SOLID PHASE MICROEXTRACTION: COMPUTER ASSISTED METHODS DEVELOPMENT FOR CHARACTERIZING FUEL SPILLS

Barry K. Lavine
Department of Chemistry
Clarkson University

Abstract

The volatile components of jet fuels have been examined by solid phase microextraction (SPME). Gas chromatograms of the microextracts of the headspace of neat and weathered jet fuels yielded reproducible and well resolved chromatographic profiles. Utilizing pattern recognition methods, the chromatograms of jet fuels that had undergone weathering in an aquatic environment could be identified by type using discriminants developed from the gas chromatograms of neat jet fuels. This approach to fuel spill identification was taken because the physical and chemical interactions of jet fuel components with subsurface environments are not yet fully understood.

TUNED SELECTIVITY SOLID PHASE MICROEXTRACTION: COMPUTER ASSISTED METHODS DEVELOPMENT FOR CHARACTERIZING FUEL SPILLS

Barry K. Lavine

Introduction

More than half of the individual households and communities in the United States rely on groundwater as their primary potable water resource (1). Possible contamination of this important natural resource by jet fuels stored in leaking underground tanks and pipelines is a serious environmental problem, prompting the development of new methods for the identification of fuel materials recovered from subsurface environments (2-3). Growing interest in techniques that can establish the type of fuel responsible for the contamination of an underground well or aquifer is motivated in part by the clean-up costs, legal fees and fines incurred by the polluter.

Water samples that are collected from underground wells contaminated by leaking fuels exist in one of two forms. Either water collected from the well shows layers of floating fuel or the water contains dissolved hydrocarbons from the leaking fuel. On-site chemical analysis of the fuel materials by solid phase microextraction (SPME) and gas chromatography (GC) is attractive because many of the problems (4-7) associated with collecting and transporting the samples (e.g., representative sampling, contamination, loss of volatiles, storage, lack of temporal resolution, etc.) are eliminated. Furthermore, on-site chemical analysis by SPME/GC possesses significant potential to circumvent the bottleneck caused by standard analytical practices.

In this report, headspace SPME/GC as a possible alternative to conventional chromatographic methods is discussed. Although SPME enjoys widespread application in analysis of semi-volatile organic compounds in water (8-9), the technique can also be applied to headspace and other vapor phase samples. For example, headspace SPME extractions have been reported for flavor components in food and beverages (10) and for environmental contaminants in water (11). The headspace technique is advantageous when the volatility of the analytes permits a headspace determination or

when undesirable components in the bulk sample make direct SPME undesirable. Headspace sampling also prolongs fiber life, and is faster than direct sampling (12). Finally, recovered fuels cannot be analyzed by direct SPME because of irreversible fiber damage caused by excessive swelling of the polymer coating, which is a direct result of the fiber being in intimate contact with the fuel layer (13).

Solid Phase Microextraction

SPME is a microscale analytical extraction technique designed for use with gas chromatography. SPME employs a fused silica fiber coated with a polymer to extract organic compounds from aqueous samples. The fiber is attached to a modified syringe as shown in Figure 1. The organic analyte is extracted by introducing the syringe into the headspace of the sample for a period of time. When the plunger is depressed, the fiber is in contact with the sample, and organic compounds are absorbed by the polymeric coating. The extraction efficiency of the polymer coating for an analyte is a function of the partition coefficient of the compound.

Following the extraction period, the plunger is retracted, and the SPME device is inserted directly into the injection port of the gas chromatograph. The plunger is then depressed, exposing the polymeric coating to the high temperature of the injector port, which ensures thermal desorption of the absorbed molecules. The absorbed molecules are immediately released into the carrier gas stream, where they are swept onto the column for separation and subsequent identification.

Methods

173 fuel samples representing six different types of jet fuels (JP-4, Jet-A, JP-7, JPTS, JP-5, and JP-8) were analyzed by headspace SPME/GC (see Table 1). The fuel samples were obtained from Wright Patterson Air Force Base or Mukilteo WA Energy Management Lab and were splits from regular quality control standards used by these laboratories to verify the authenticity of manufacturer's claims. The control standards constituted a representative sampling of the fuels. In

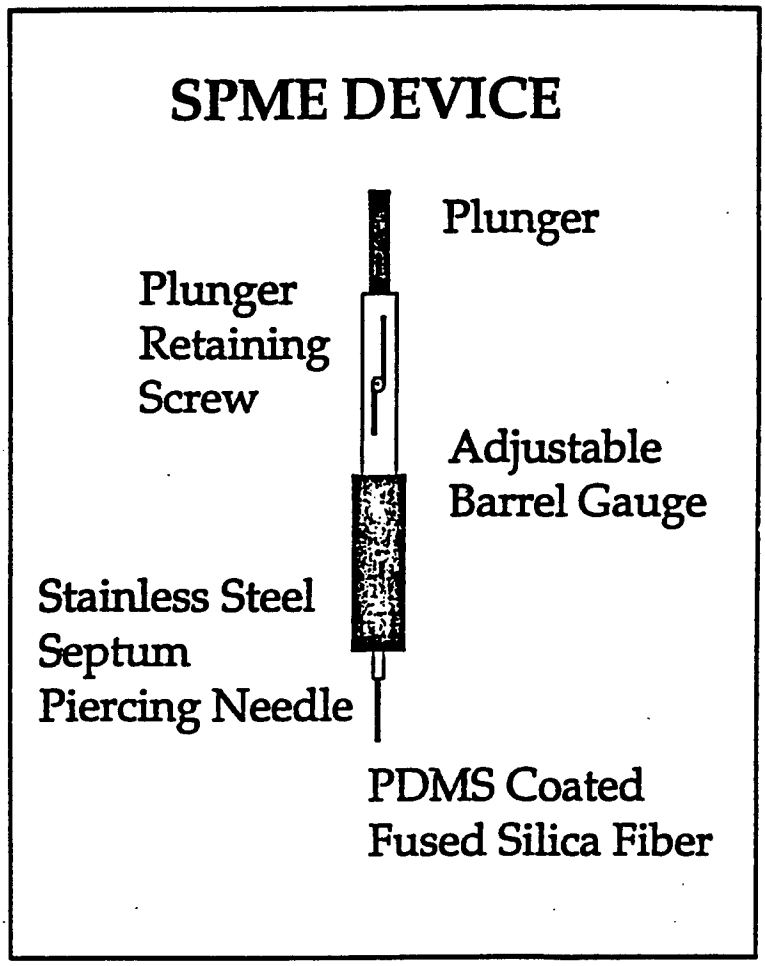

Figure 1. SPME Device.

additon, 19 fuel samples (11 JP-4, 2 JP-5, 2 Diesel, 4 JP-8) recovered from the subsurface environment near Air Force and Navy airfields were also analyzed by headspace SPME.

Table 1. Neat Jet Fuel Data

Fuel Type	Number of Samples
JP-4	46
Jet-A	45
JP-7	09
JPTS	15
JP-5	14
JP-8	44
Total	173

The following experimental protocol was used to obtain GC profiles of the volatile components of a jet fuel. Four milliliters of a neat jet fuel were placed in a 40 ml VOA bottle. A micro-stirring bar was also placed in the VOA bottle prior to the introduction of the fuel sample to permit stirring of the sample during the SPME sampling period which was 10 minutes. In a previous study, we found that 10 minutes was sufficient to obtain a representative sampling of the volatile compounds present in a jet fuel (12). Gas chromatograms of the microextracts were analyzed using a high efficiency fused silica capillary column 10 meters long with an internal diameter of 0.10 mm and coated with 0.34 μm of a bonded and cross-linked 5% phenyl-substituted polymethylsiloxane phase. The column was temperature programmed from 60 to 270^0 degrees Centigrade at 10^0 per minute.

Results & Discussion

Figure 2 shows GC profiles representative of the volatile components of neat jet fuels. The headspace of the neat jet fuels was sampled by SPME, and gas chromatograms are shown in Figure 2 representative of the prototypical vector for the six fuel classes. JP-4 and Jet-A fuels can be readily differentiated from the other fuels on the basis of their GC profiles. In fact, JP-4 fuel materials recovered from several monitoring wells at Tyndall could be identified as to fuel type by comparing the gas chromatograms of the recovered fuels to the gas chromatograms of the neat jet fuels, in order

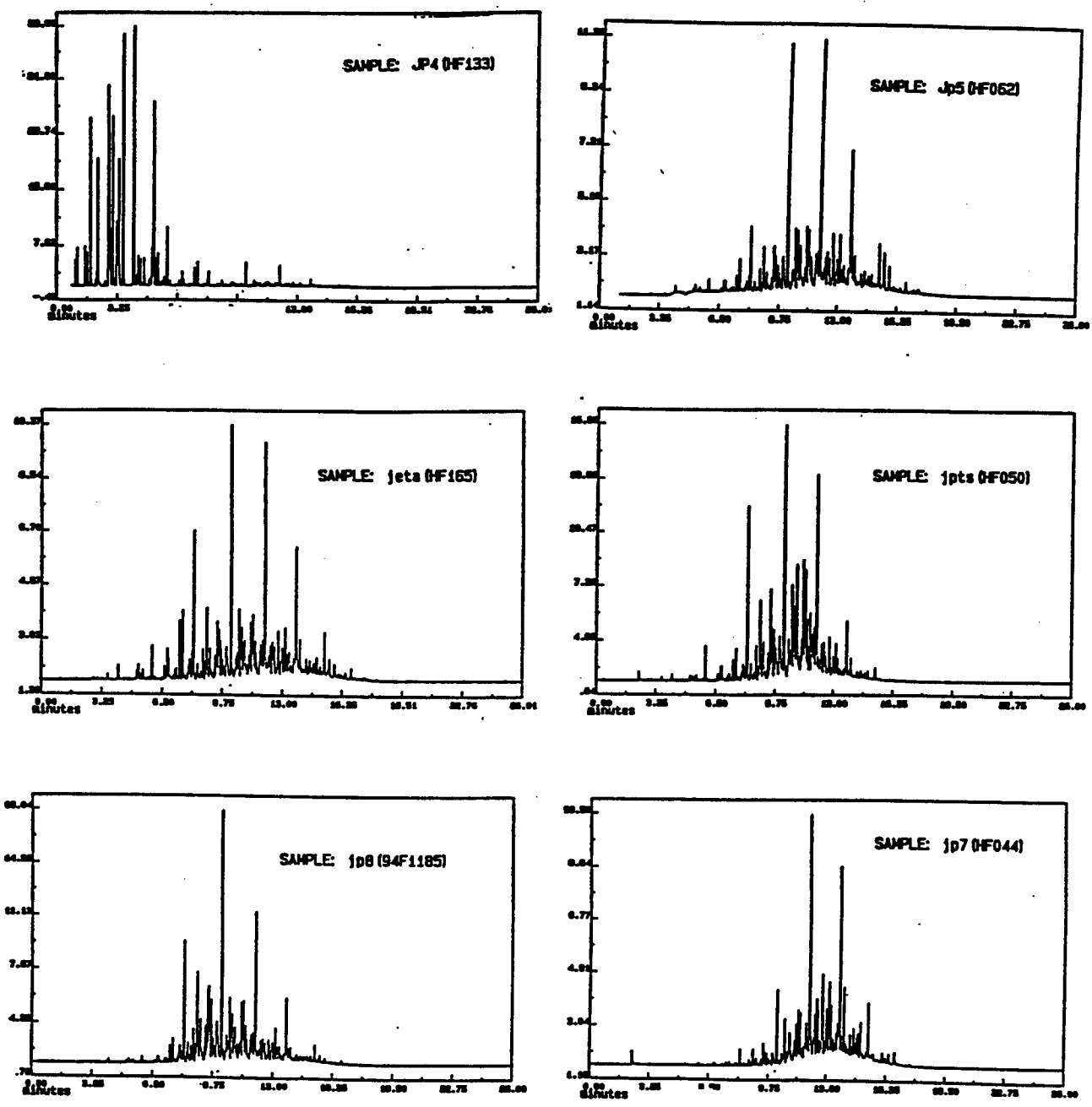

Figure 2. Headspace SPME/GC profiles of neat jet fuels.

to seek a best match (see Figure 3). On the other hand, it is apparent from an examination of Figure 2 that GC profiles of JP-7, JPTS, JP-8 and JP-5 fuels share a similar set of attributes which suggests the use of pattern recognition methods to identify fingerprint patterns in the chromatograms that are characteristic of fuel type.

For pattern recognition analysis, each gas chromatogram was initially represented as an 84-dimenisonal data vector. These standardized retention time windows were identified in each gas chromatogram using special peak matching software (14). Figure 4 shows a plot of the two largest principal components (15) of the 84 GC peaks. It is evident from the plot that JP-4 can be readily differentiated from the other fuels. However, the gas chromatograms of the other fuels cannot be readily identified when all 84 GC peaks are used. Figure 5 shows a plot of the two largest principal components of 34 GC peaks that were selected on the basis of their variance weights (16). It is evident that fingerprint patterns indicative of fuel type exist in the data. Using principal component analysis and variance feature selection, it is possible to identify these fingerprint patterns in the data. Hence, SPME/GC coupled with pattern recognition methods can be used to differentiate aviation fuels on the basis of fuel type. The technique of headspace SPME can also be readily adapted to the field and clearly possesses significant potential which can be exploited by the Air Force in its current fuel spill identification program.

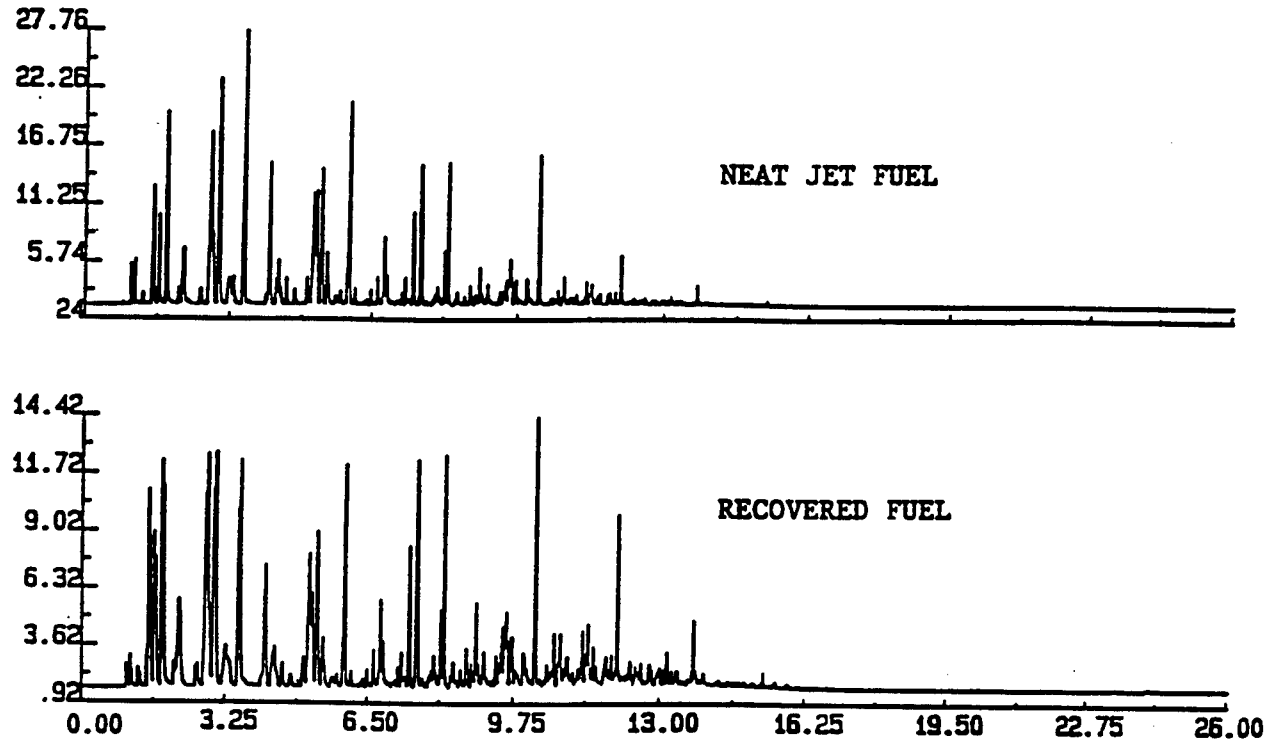

Figure 3. Comparison of the SPME/GC profile of a JP-4 fuel and a recovered fuel.

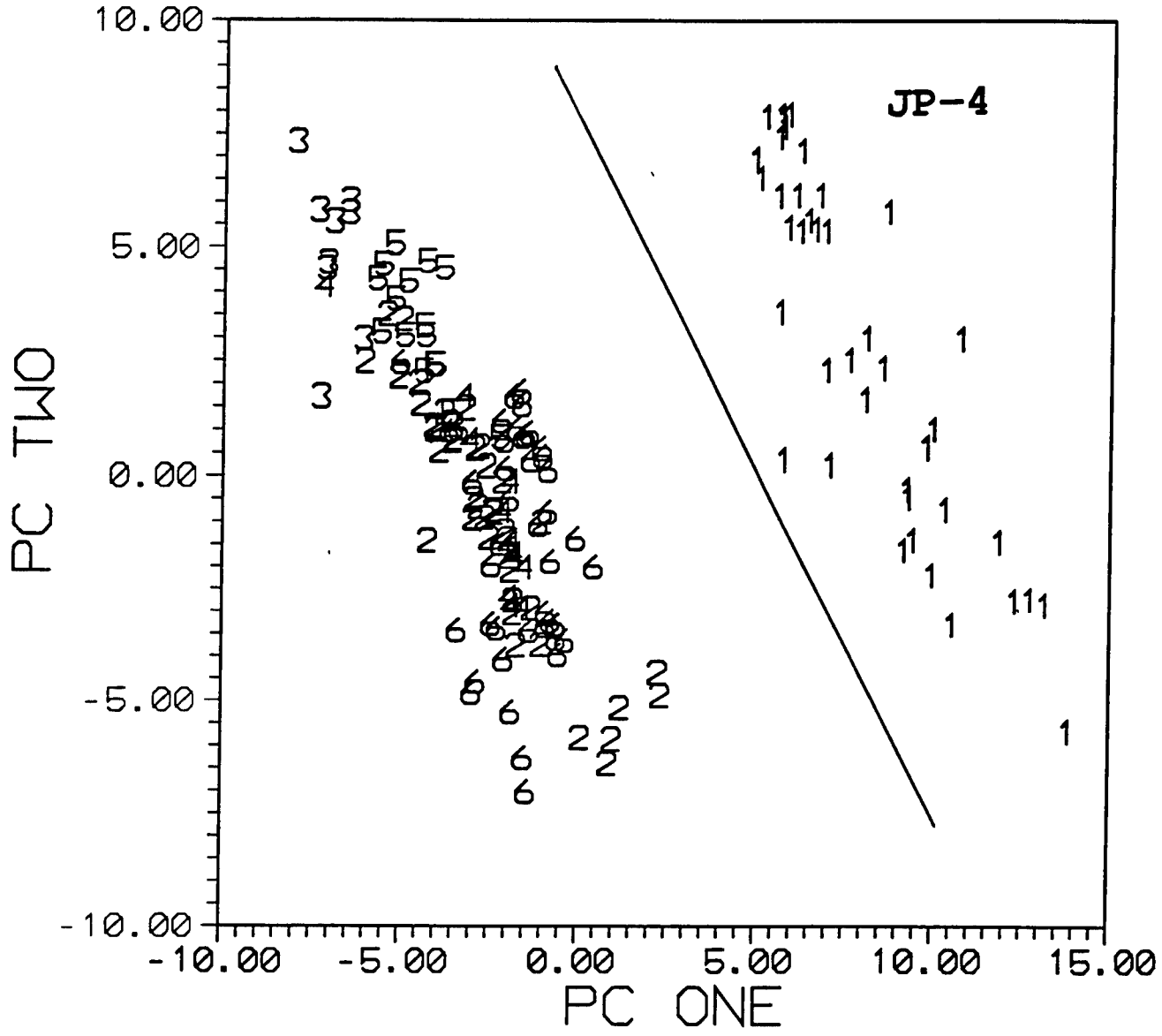

Figure 4. A plot of the two largest principal components of the 84 GC peaks.

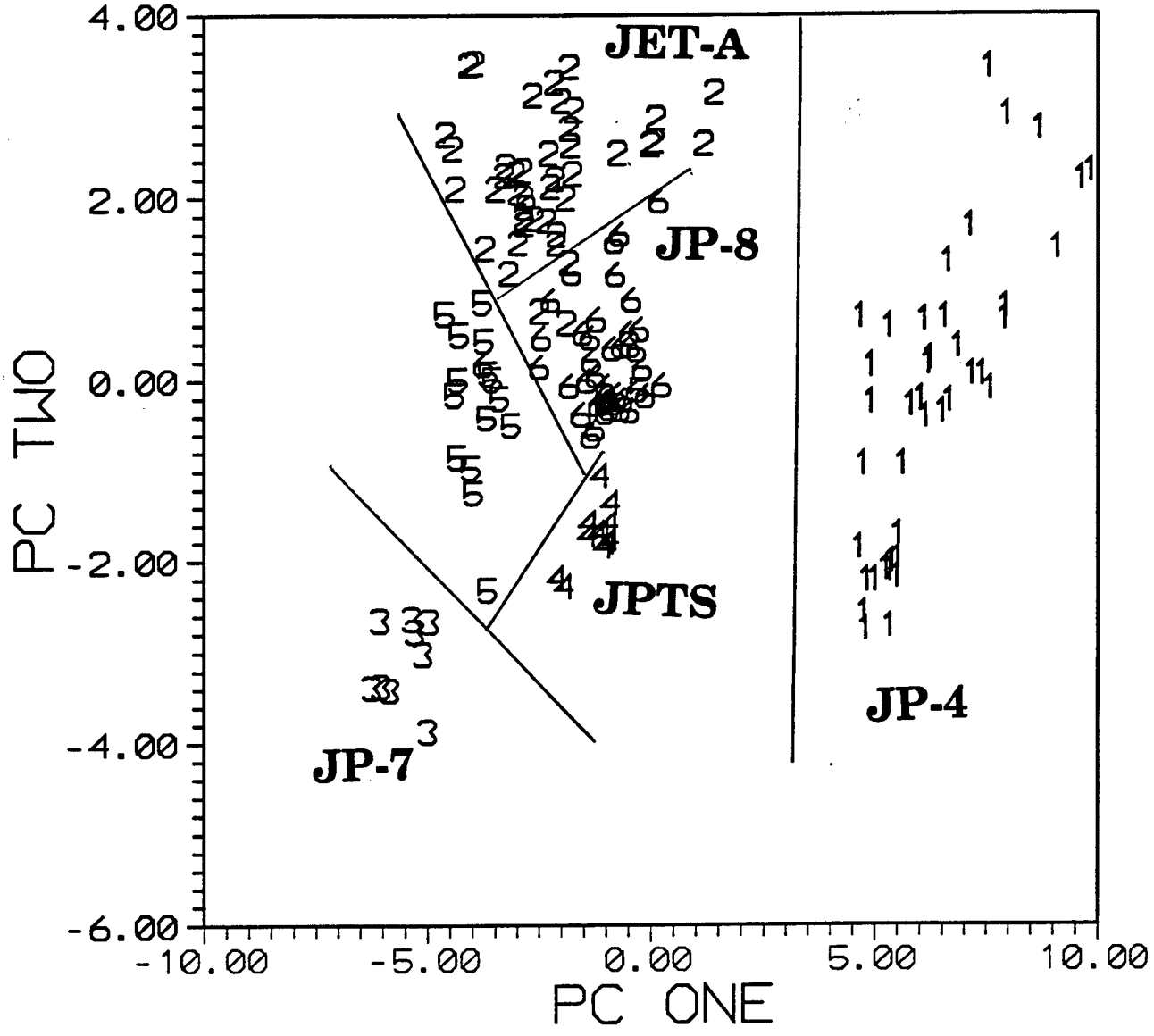

Figure 5. A plot of the two largest principal components of the 34 GC peaks.

Robert Mahan
Report not available at time of publication.

Sandra McAlister
Report not available at time of publication.

Alan Musicant
Report not available at time of publication.

Neck Models for Predicting Human Tolerance to G-Y Acceleration

Ali M. Sadegh
Professor
Department of Mechanical Engineering

The City College of
The City University of New York
New York, NY

Final Report for:
Summer Research Extension Program
Armstrong Laboratory

Sponsored by:
Air Force Office of Scientific Research
Bolling Air Force Base, DC

and

Armstrong Laboratory

January 1997

NECK MODELS FOR PREDICTING HUMAN TOLERANCE TO G-Y ACCELERATION

Ali M. Sadegh

1. INTRODUCTION

Advancements in aerospace technology have made the increase in airspeed of aircraft possible. Increased airspeed has made the safe ejection of crew members from disabled aircraft difficult. In an emergency situation requiring ejection from the cockpit, a fighter pilot's torso is subjected to a high acceleration on the order of 15 G's (this is representative for a B52 aircraft ejection seat [1]). The time required for an ejection is on the order of milliseconds. This high acceleration, which is achieved in an extraordinarily brief period of time, applies an extremely high magnitude of load to the spinal column, particularly the cervical spine. This load often causes injuries; many of which occur in the lumbar and thoracic regions of the spine, but more frequently in the cervical spine and the neck [1].

In recent years pilots have been equipped with night vision goggles and helmet-mounted displays that have significant advantages over panel-mounted instruments. This additional instrumentation has increased the mass of the helmet system, which also increases the risk of a major neck injury in an emergency escape situation. Scientists and investigators at the Armstrong laboratory at Wright-Patterson Air Force Base have started a program to determine parameters for helmet design [2].

Recent advances in seat design and pilot training have added more restraint to the pilot's lumbar and thoracic regions, thereby reducing the risk of lower back injuries. However, the lack of restraint in the neck and head regions has made the pilot's cervical spine vulnerable to injuries. This is due to the fact that the pilot's head must have a reasonable freedom of motion in order to ensure an adequate field of view. In the ejection process, the initial orientation of the head and the direction of the acceleration vector plays an important role in the magnitude of the load that would be applied to the neck. That is, the head acceleration varies considerably when the airplane is in roll or spin conditions.

Experimental studies have been performed to better understand the factors underlying injury and to improve ejection devices and seat design. These experimental studies have limited usefulness due to the low tolerance limits of human volunteers. Even cadavers and mannequins are only subjected to near-tolerance limits. Thus, there is a gap between low G amplitude human volunteer tests and the actual high amplitude acceleration to which pilots are subjected. Computer models are an appropriate means for closing the gap. They are reliable tools for analytical prediction of the dynamic response of the neck and the head and determining the human tolerance level.

The goal of this study was to develop three dimensional finite element models of the cervical spine capable

of simulating the response of the musculo-skeletal structures of the neck when subjected to the forces resulting from G-y and G-z accelerations in an ejection process. The model predicted the local loads due to the accelerations which could not be provided by the global rigid dynamic model developed in the previous studies. This study employed the forces and torques reported by Sadegh [5] and Perry [1] and applied them to the neck models where the stresses and deformations of each cervical vertebra and disc were determined.

In this investigation, two types of finite element models were developed: (a) a layered elastic and viscoelastic bulk models of the neck, and (b) a continuum model of the cervical spine with ligaments and two major muscles attachments. The latter model provides a more realistic representation of the neck. In each model the stresses and displacements at each vertebra and disc were determined. The second model, the continuum model, is an improvement on the first model in which the effect of the muscles and the ligaments attachments on the stress and strain fields of each layer was studied. The stresses determined from these models could be compared to the human tolerance level.

This study was a first step towards an understanding of the local stresses in each vertebra and an estimation of the tolerance limiting range of the vertebrae corresponding to G-y and G-z accelerations. In the next section the background on the experimental data and the rigid body dynamics of the head/neck/torso is presented. The anatomy of the cervical spine is presented in Section 3. The three models and cases are described in section 4. Validation of the model is presented in section 5. Results and discussions and conclusion are presented in sections 6 and 7, respectively.

2. BACKGROUND AND EXPERIMENTAL DATA

There have been some studies and analyses of the head acceleration due to the acceleration in z and x directions, (G-z and G-x), [3, 4]. Sadegh [5] reported the validation of the test results for G-y acceleration and determined the forces and torques at the neck/head joint, Occipital Condyle, OC. Since this research represents the continuation of the work presented by Sadegh [5], for completeness, a summary of his report is presented.

Sadegh [5] employed experimental data that were collected from the biodynamic responses of human volunteers during an acceleration in the Y direction at the sled track facility located at the Armstrong Laboratory at WPAFB. This facility employs an Impulse Accelerator [Shaffer 1976], which is a gas powered actuator that accelerates a sled on a two-rail track. The volunteers were placed in a chair mounted on a sled facing perpendicular to the direction of the track. Two sets of three orthogonal linear accelerometers were located in a chest pack and a mouth pack. These accelerometers collected the x, y and z accelerations of the torso and head as a function of time during the acceleration impulse. The coordinate system of the acceleration and the chair is shown in Figure 1a. The sled was subjected to the acceleration pulse of a half-sine with peak acceleration ranging from 4G to 7G and a duration ranging from 31 ms to 250 ms.

To validate and analyze the data Sadegh [5] employed a head/neck model consisting of three segments, namely, Head, Neck, and Upper Torso. Based on the weight and sex of the subject, the appropriate physical and geometric parameters for each segment were supplied by GEBOD software. The GEBOD program is an interactive computer program that produces the human and dummy body description data used by the ATB model. In this model the head segment is joined to the neck by "Head Pin" (HP) joint and the neck is connected to the upper torso by the "Neck Pin" (NP) joint, see figure 1b. Both joints were of the ball-and-socket type. However, at the neck pin, NP, a viscoelastic slip joint composed of parallel spring and dashpot (Voigt Model) was added. This joint allows relative axial motion between the neck and the upper torso which simulates "compression" at this joint. The spring stiffness was modeled by linear spring coefficient, K1 (lb/in) and a quadratic spring coefficient, K2 (lb/in2), while the dashpot was given only a linear damping coefficient, c (lb-sec/in). Coulomb friction was assumed to be zero. The Articulated Total Body (ATB) program was employed and the rigid body response of the model and the forces and torques were determined. The chest acceleration of the subject was used as the input to the ATB model. Sadegh validated the model by selecting parameters such that the ATB model predicted and duplicated the experimental data collected at the mouth piece.

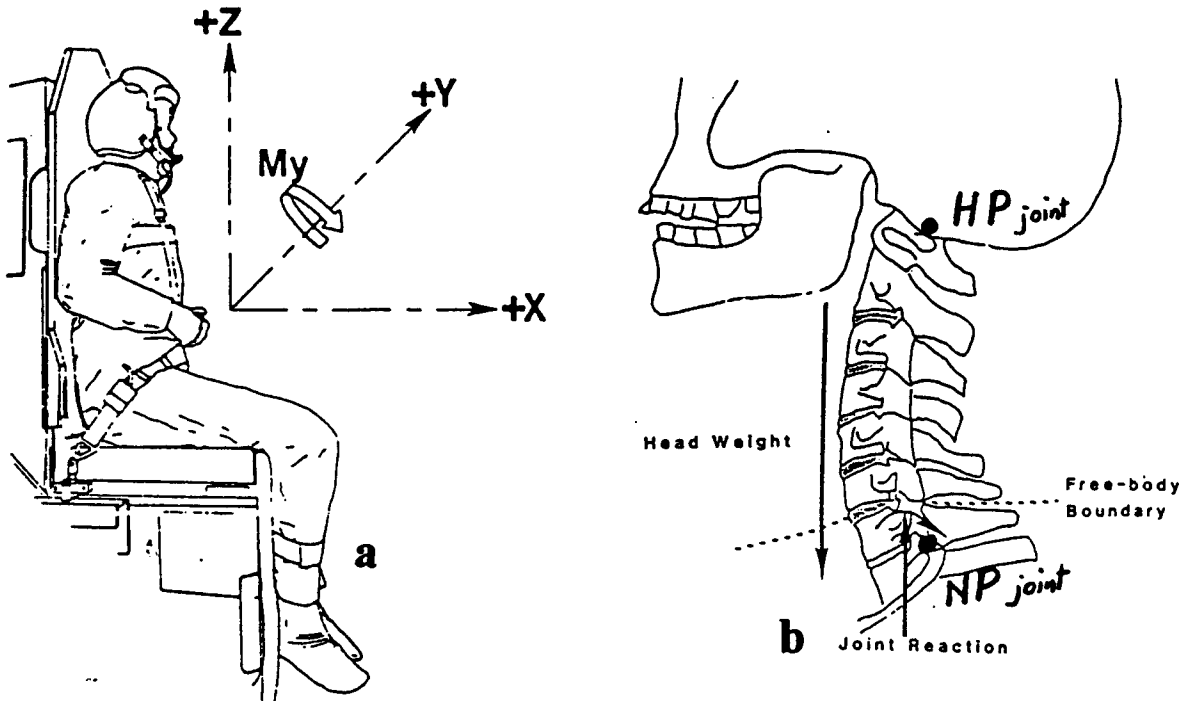

Figure 1. a: The orientation of the pilot seat
b: The head-neck-torso model

The forces and the torques at the head-pin, HP, and neck-pin, NP, joints in the X, Y and Z directions, Fx, Fy and Fz, and Tx, Ty and Tz, respectively, were determined. A sample of the results, for test #4185 is shown in Figures 2. This Figure has two plots of loads and torques for the HP joint and two plots of loads and torques for the NP joint. As expected, the force in the y direction, Fy, is the dominating load at both the neck pin NP and the head pin HP joints. The force Fx in the neck pin NP is almost zero because of the restraint of the chest. However, at the head joint HP, the magnitude of the forces in y and z directions are relatively high compared to the x direction. This indicates that the head is moving in the three directions. The torque in the x direction Tx is the dominating load at both the neck pin, NP, and the head pin, HP joints. It is important to note that the magnitude of the Tx in NP joint is almost twice that of the HP joint.

The maximum loads and torques applied to the joints play an important role in neck injuries. Figures 3 depicts the variation of the maximum compressive forces at the NP and HP joints with respect to the change in amplitude of the acceleration of the test cells. Figure 4 depicts the change of the maximum torques at the NP and the HP joints versus the change in duration of the acceleration of the test cells. These curves were drawn using a least square curve fitting program.

Figure 3 indicates that at the NP joint the maximum force and the maximum torque increases with an increase in amplitude of the input acceleration. However, the maximum compressive force at the HP joint has a minimum. This is due to the fact that the mass inertia of the head has some time lag and back lash with respect to the input acceleration. On the other hand, Figure 4 indicates that the forces and the torques on both joints will increase when the time duration of the input acceleration increases. However, slopes of the curves for the maximum forces and torques is reduced after about 190 ms. This could be due to the fact that the muscles responded to the input acceleration and began to absorb some of the load.

Similar studies were done for the G-z acceleration by Buhrman and Perry [15] and Perry [16] in which the drop tower at the Escaped and Impact Protection Branch at Armstrong Laboratory at WPAFB was utilized. The subject on the drop tower was subjected to an acceleration pulse of +10 G-z. They then determined the forces and torques at the head point, OC.

Because of safety rules the test subjects were not subjected to an acceleration of more than 10G. However, cadavers were used to estimate the maximum tolerance and the injury region of the cervical spine. Buhrman and Perry [15] reported that for the neck in flexion based on the +G-x direction, the maximum responses of a cadaver without producing ligament or bone damage at the Occipital Condyle were estimated as: M-y of approximately 1700 in-lb, shear load Fx of 450 lb and compression load Fz of 400 lb. Although a great number of cases for G-z and G-y were available, due to the lack of time and large volume of data to be processed, only four cases for the G-z acceleration and four cases for the G-y acceleration were considered. In this analysis, ten cases were considered. The first two cases were studied

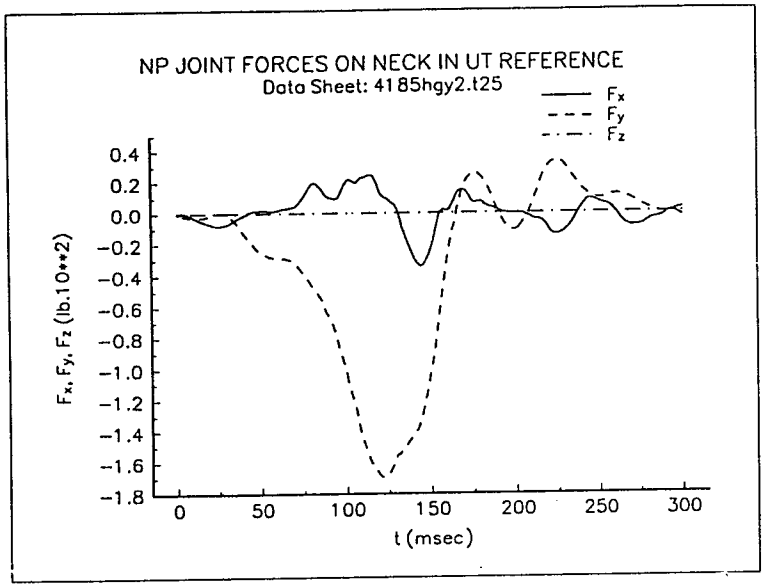

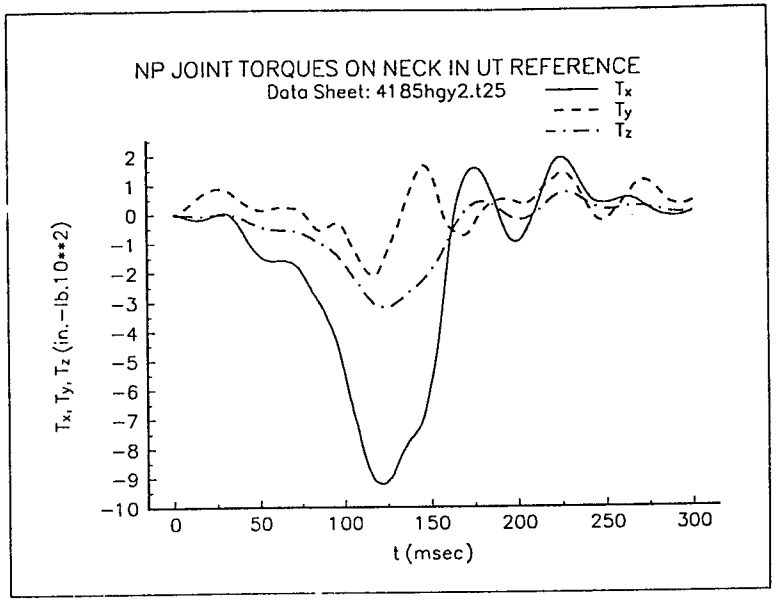

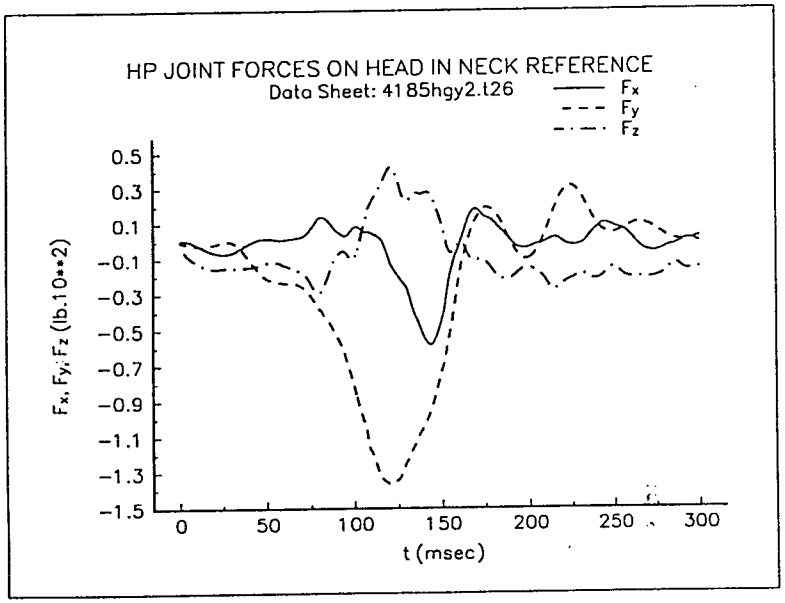

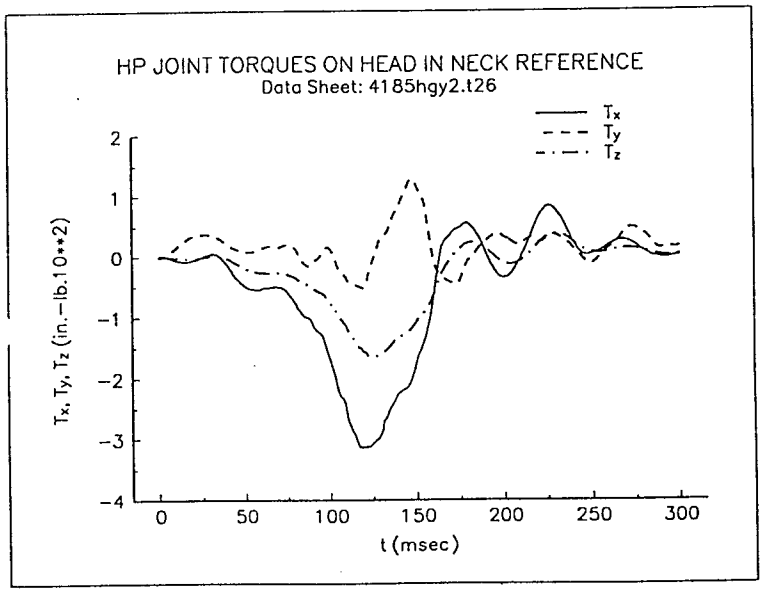

Figure 2- Forces and Torques at NP and HP Test #4185

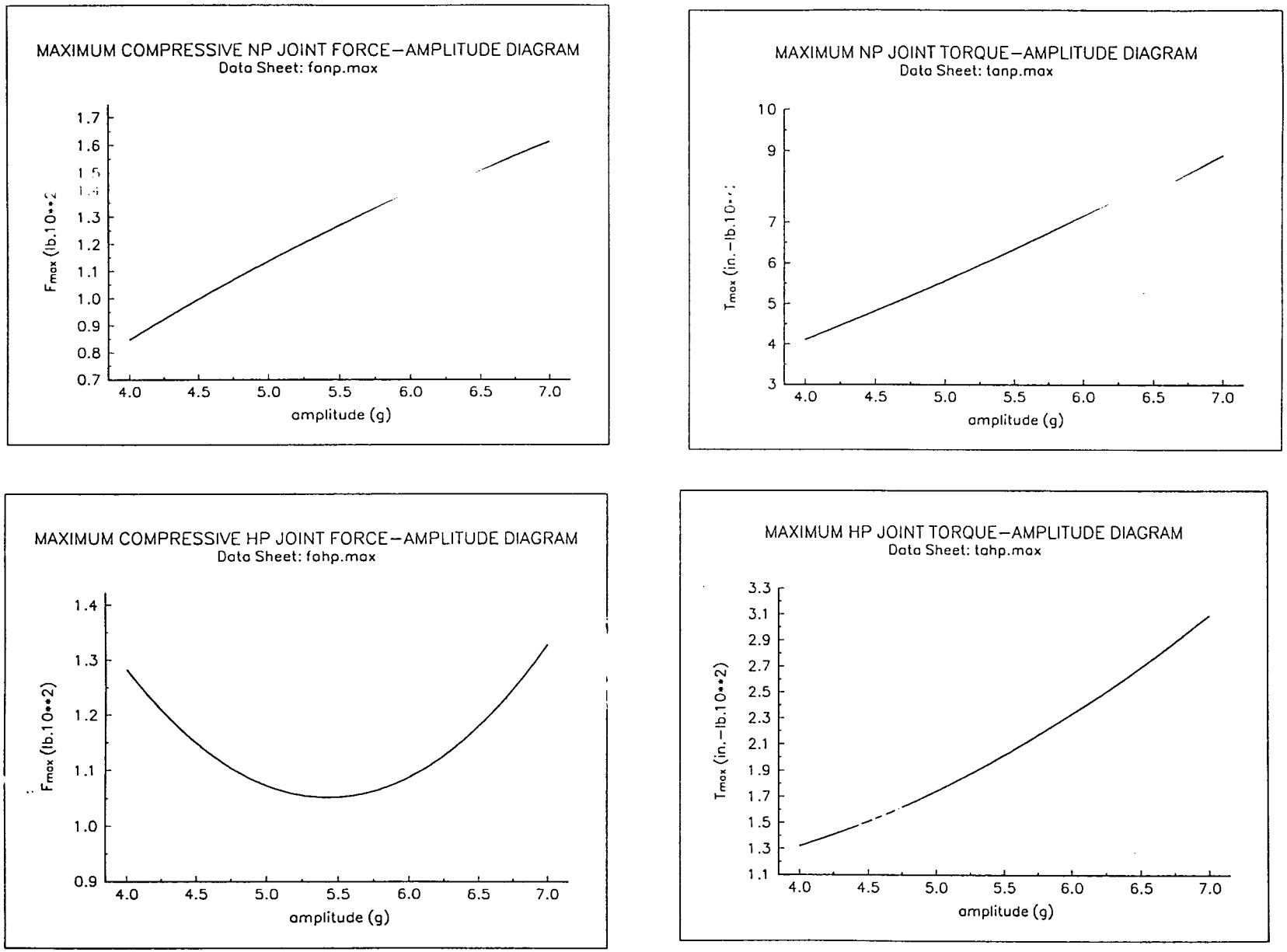

Figure 3 - Maximum Force and Torque vs. Amplitude

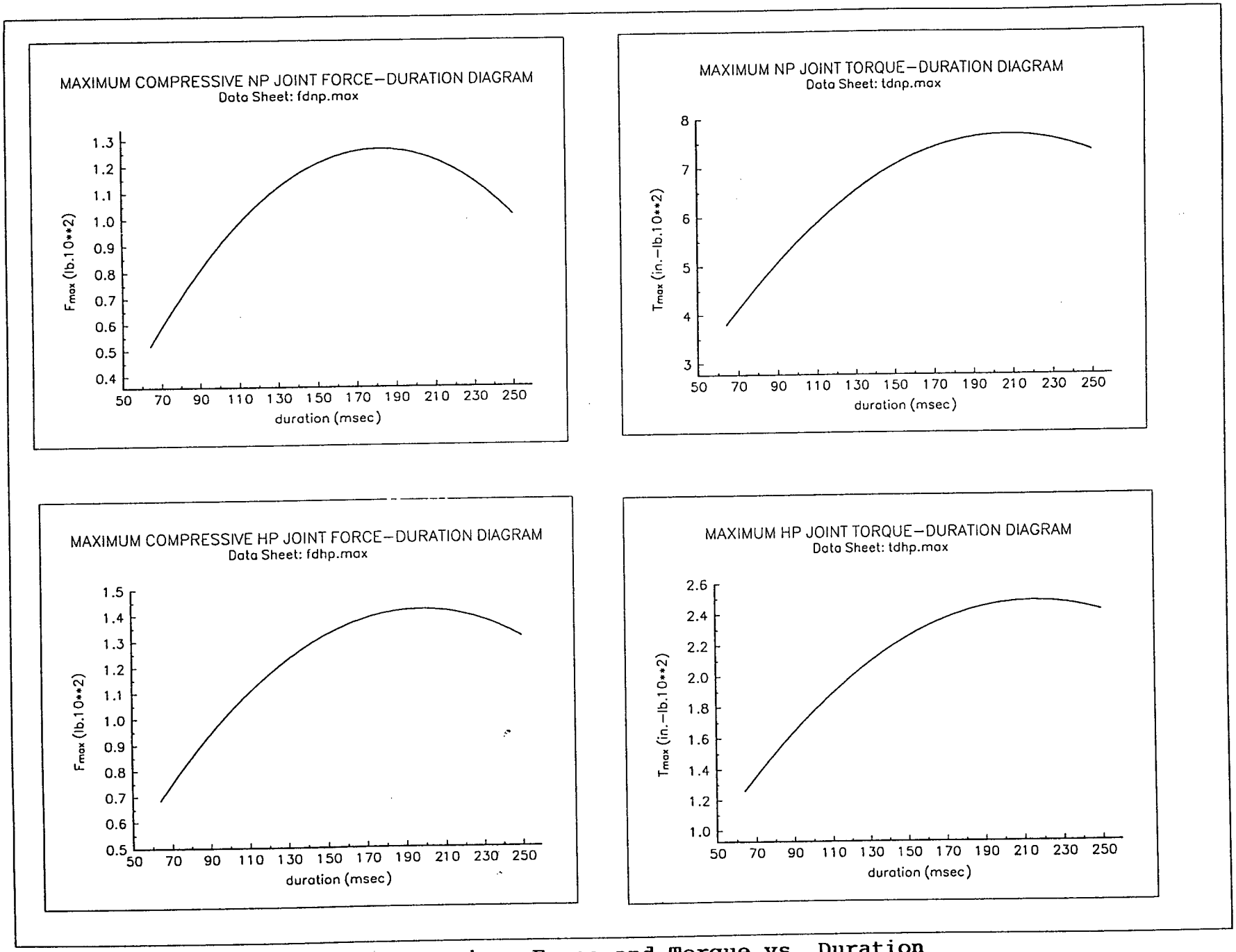

Figure 4 - Maximum Force and Torque vs. Duration

using the bulk elastic and viscoelastic models. The third continuum model was used for the remaining eight cases that involved detailed geometric descriptions of the vertebrae and the discs. The calculated loads and moments used in these analyses are shown in Table 1.

3. ANATOMY OF THE CERVICAL SPINE

To better understand the effects of the external global loads on the local vertebrae, the anatomy of the neck, including muscles and ligaments, was first studied. A typical cervical vertebra is shown in Figure 5. The characteristic feature of the cervical vertebrae is a foramen in the transverse processes for the passage of the vertebral artery, vein and sympathetic nerves. The complete cervical vertebrae in sagittal and posterior views are shown in Figure 6 and 7. The first cervical vertebra, known as the atlas, supports the skull. It has no vertebral body and no spinous process, but is made up of two lateral masses and two arches. The second vertebra, called the axis or epistropheus, has a toothlike process, conical in shape. The third to sixth vertebrae have the typical, standard shape shown in figure 5. They have small vertebral bodies that are broader from side to side than they are from front to back. The seventh vertebra has a long, nearly horizontal spinous process which serves as an attachment point for many neck muscles. The ligaments of the cervical spine bind the vertebrae together as they do in the rest of the spine, and together with the paracervical muscles prevent any motion that would injure the spinal cord and nerve roots. Most of the axial rotation of the head on the neck occurs between the first two vertebrae, the atlas and the axis.

Extension in the cervical spine is limited at the upper end by the superior facets of the atlas whose posterior edges lock into the occipital condylar fossae. Flexion is stopped just after the cervical convexity is straightened; the limiting factor is the contacting of the overhanging lops of the bodies of the vertebrae with the wall of the subjacent vertebral bodies. In this study our interest is in the lateral flexion. The lateral flexion in the lower cervical spine (C2-C7) is always coupled with a certain amount of axial rotation. This coupling is such that during lateral bending to the left the spinous processes go to the right, and during lateral bending to the right they go to the left.

The muscles of the neck can be classified as either flexors or extensors. The primary neck flexor is the sternomastoid, which is a single muscle. The neck extensors, which prevents flexion of the neck and forward rotation of the head, are located to the posterior of the vertebral bodies. Vertebral balance is maintained by a continuous adjustment of ligamentous and muscular forces in the spine as shown in Figure 7. The short muscles of the back function, for the most part, as postural muscles, which steady adjoining vertebrae and control the movements of the vertebrae with respect to each other, and to the column as a whole.

Foust, et. al. [6] measured the stretch and reflex times of neck muscles. The stretch reflex time is the time between the onset of the acceleration and the beginning of muscle activity, as measured by electromyography. The extensor muscles were consistently slower than flexor muscles. Average neck muscles reflex times ranged from 52 to

TABLE 1 : CASES DESCRIPTION

Case	Subject	Cell	Accel.	Fx in lb (N)	Fy in lb (N)	Fz in lb (N)	Mx in lb-in (Nmm)	My in lb-in (Nmm)	Max. Displ. (mm)	Max. Pr. σ in Mpa	V. Mises σ in MPa
1 Cadaver	Cadaver	CB		450 (2034)		-400 (-1818)		1700 (195075)	354.5	+ 230 - 140	190
2 # 2368	C-8	CB	10 gz	25 (113)		-200 (-909)		320 (36945)	57	+ 30 - 20	30
3 # 2619	B-9	AB	8 gz	25 (113)	10 (45)	-160 (-723)		210 (24850)	42	+ 23 - 14.8	23
4 # 2760	B-1	AB	6 gz	23 (104)	6.5 (29.5)	-98 (-443)		150 (17250)	31	+ 17.3 - 10.7	16
5 # 4128	A-5	A	4 gy	20 (90)	-55 (-248)		-120 (-13800)	-80 (-9200)	6.5	+ 23 - 3.5	23
6 # 4147	A-5	B	5 gy	30 (135)	-100 (-452)		-200 (-28000)	-90 (-10350)	13.82	+30 -6.5	35
7 # 4165	A-5	C	6 gy	40 (180)	-110 (-497)		-250 (-26450)	-90 (-10350)	13.88	+38 -8	40
8 # 4185	A-5	D	7 gy	55 (248)	-130 (-587)		-310 (-35650)	-120 (-13800)	14.08	+45 -10	48

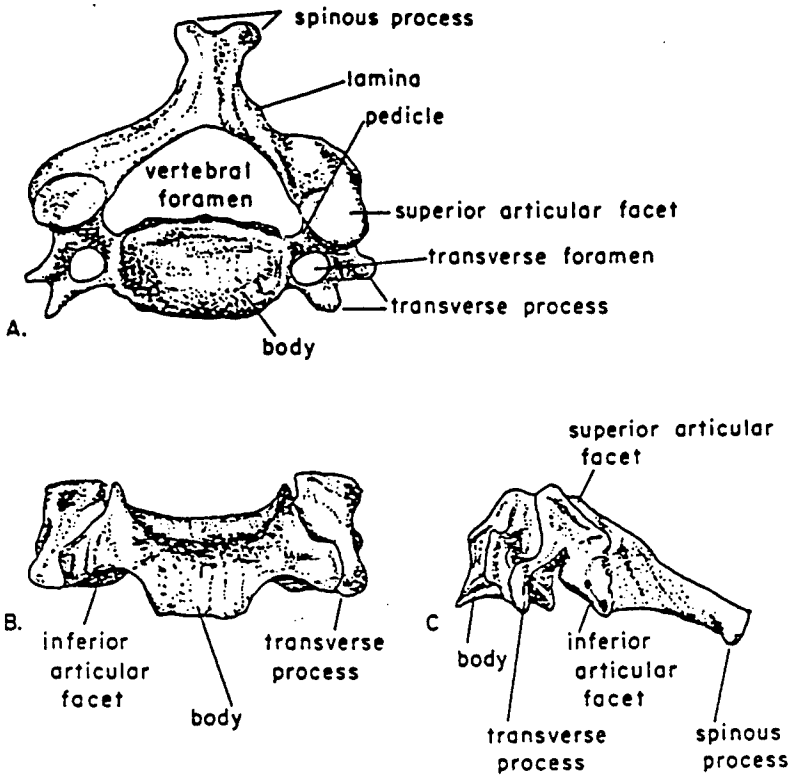

Typical Cervical Vertebra

a

A. Top view
B. Front view
C. Side view

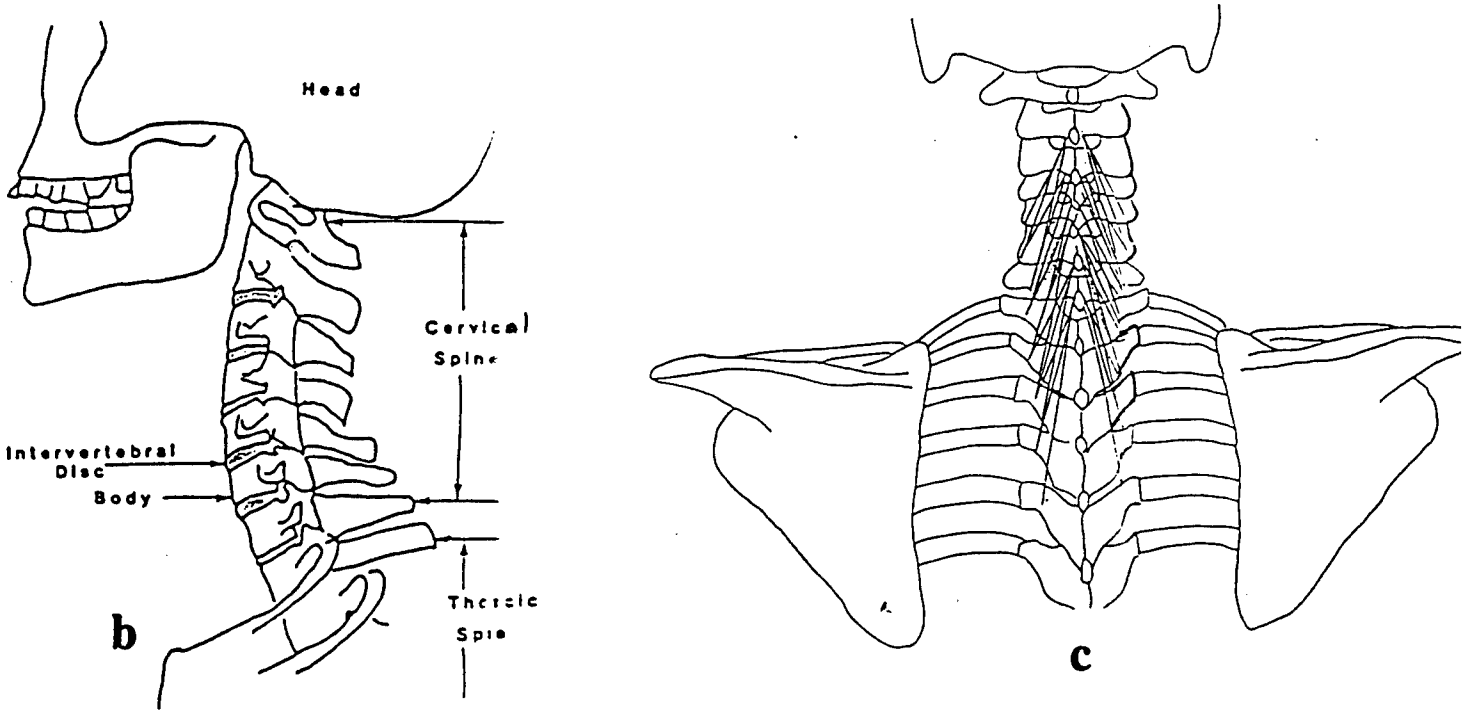

Figure 5: a: Typical cervical vertebra, b: Sagittal view and c: Posterior view of the cervical spine

92 msec for flexure and 54 to 87 msec for extensors. The average time needed for the muscles to activate fully has been estimated to be from 54 to 66 msec for flexure and from 64 to 86 msec for extensors in an 18-44 year old male, Foust, et. al. [6]. The neck muscle strength was also estimated by Foust, et. al. [6]. For males, aged 18-44 years, the neck flexures could exert a total force of about 123-162 N and the extensor a force of 149-206 N.

Muscles can act as active or as passive elements. In an unanticipated car accident it may be assumed that a person's muscles are relaxed at the time of impact and that they act as passive elements during the first 60-200 msec. However, in the pilot ejection situation, especially for a pilot with ejection training, many of the neck muscles needed to resist neck flexion are probably tensed from the start of acceleration. On the other hand, because of their great magnitude, the forces of the ejection are impossible to resist as far as forward rotation of the head is concerned.

4. THE MODELS

Three models were developed. These models were generated using I-DEAS software from SDRC Inc., running on a DEC workstation. I-DEAS is a large solid modeler, with pre- and post-processor software that interacts with ABAQUS software. ABAQUS software is a research oriented nonlinear finite element solver with a wide variety of linear and nonlinear elements for many different kind of engineering analyses.

In the first model, the cervical spine including the soft tissue and the muscles were considered as a bulk column of seven vertebrae and six discs. However, in order to apply the loading and the boundary conditions to the model, and minimize the stress concentration, one extra disc was added to both the top and the bottom of the model. The top disc was a thin rigid material that was included in the model for better distribution of the applied loads and the torques. The bottom thick disc represented the T1 vertebra. The cross section of the body of a vertebra is an ellipse that is very close to a circle, with an average radius of 9 mm, as given in Williams and Belytschko [9]. However, to compensate for the arch and processes of the vertebrae and the soft tissues, the radius of the column was assumed to be 15.8 mm, which is larger than the actual radius of the body of a vertebra. In this model 589 quadratic ten-noded tetrahedral elements and 1568 nodes were used. The model was constrained at T1 at the inferior of the seventh cervical vertebra. The loads were applied to a rigid plate on top of the C1 in order to avoid a stress concentration. The maximum force and torque at the head point, shown in Figure 2, were used for this model. The loads are Fz = 133 lb and My = -310 lb-in. The material properties of bone used in this model are given in Table 3.

In the second model the same bulk column of seven vertebrae and six discs described above was employed; only the material properties of the discs were changed to a viscoelastic material. To compare the elastic model and the viscoelastic model, the same loads as in the first model were used. However, unlike the first model, the time history of the force Fz and the torque My, ranging from 10 to 200 msec, as shown in Figure 2 were employed. The phenomenological material model was employed for this geometry, Visarius [12]. The phenomenological model uses

quasi-linear viscoelastic theory (QLV), Johnson [7]. This material model has been proven to be a realistic model for biological materials, Johnson [7]. The quasi-linear viscoelastic theory can be derived from the classical linear theory of viscoelasticity. The material properties are defined by a Prony series representation of the normalized shear and bulk relaxation moduli, see ABAQUS [8]. The viscoelastic properties of the muscles and ligaments are given in Williams and Belytschko [9] and Woo, et. al. [14]. The viscoelastic coefficients of the materials used in this model are given in Table 3.

The third model was a detailed anatomical description of the cervical spine as shown in Figure 6. The complete cervical vertebrae in sagittal and posterior views are shown in Figure 7 and 8, respectively. The solid model of each vertebra and disc was carefully created using the true anatomical dimensions given in the Cervical Spine Research Society Book [17] and as shown in Table 5. Also, the relative orientation of the vertebrae and the discs were carefully generated to resemble the anatomical orientation as given in [17]. To minimize the stress concentrations on vertebrae C1 and C7, and to represent the head and the T1, an additional thin disc was added to the top of the C1 and a plate was added to the bottom of C7, respectively. Relatively rigid material properties were taken for the thin disc and the plate. Initially, nearly 3000 quadratic ten-node tetrahedron elements and in excess of 5000 nodes were used. When the model was processed, however, it was found that ABAQUS solver took a rather long time to complete the calculation, probably due to the nonlinear elements (such as viscoelastic beam elements). A simpler model with linear tetrahedral elements was then developed. The new model employed 1143 four-noded tetrahedral elements with 599 nodes.

In order to simulate the articular facets, ligaments and muscles, 57 beam elements with various material properties were used to connect the inferior section of each vertebra to the superior section of the adjacent vertebrae. These soft tissue connections are described below. There are nine beam elements connecting the inferior plane of a vertebra, Ci, to the superior plane of the Ci-1, as shown in Figure 9. Beam elements 1 to 5 were used to simulate spinous process ligaments connecting the two adjacent posterior arches. Beam elements 6 and 7 were used to simulate the articular facets. Beam elements 8 and 9 were used to simulate the anterior and posterior longitudinal ligaments. To simulate the major muscles of the cervical spine that are used for extension, flexion and lateral movements, that is, the Semispinalis Capitis and Splenius Capitis muscles, two major beam elements connecting the T1 to the OC were used. By selecting the right material properties for these beam elements we simulate the ligaments, muscles and articular facets around the bodies and the posterior arch of the vertebrae.

As the boundary conditions for this model the nodes on the inferior surface of the lower plate representing the body of the T1 were constrained. The loads were distributed over the superior surface of the thin plate located on top of C1. To simulate the local stresses in discs and vertebrae due to the G-z and G-y accelerations eight loading cases, shown in Table 1, were considered.

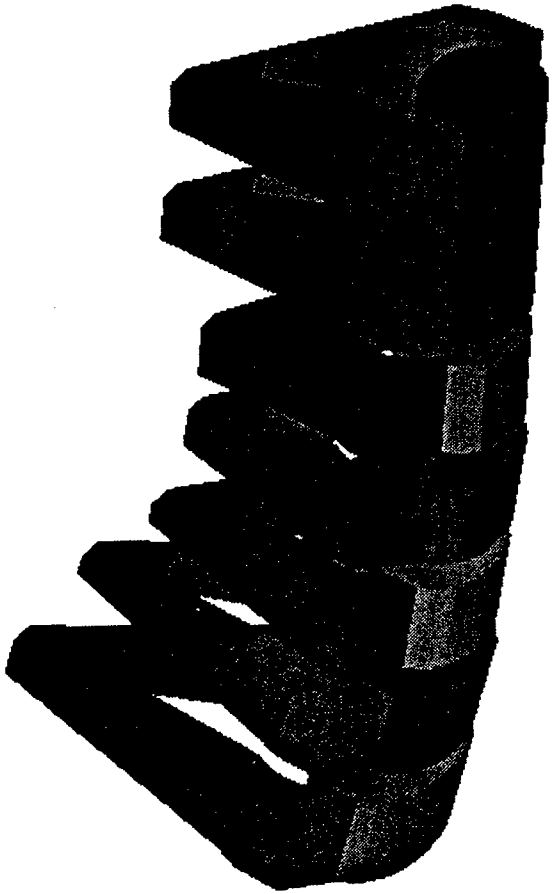

Figure 6: Oblique view of the third model

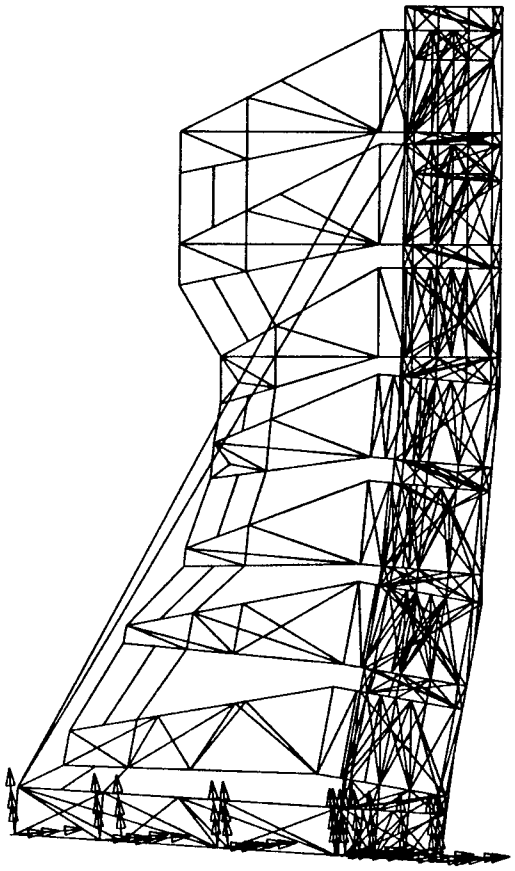

Figure 7: Sagittal View of the third model

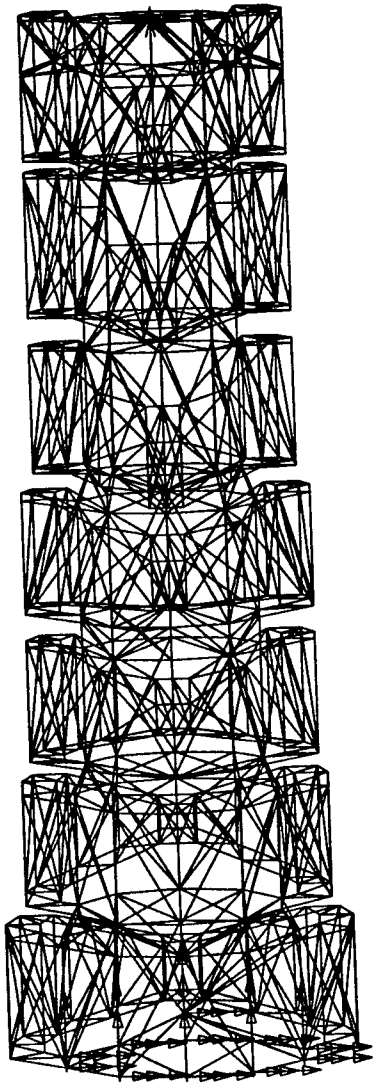

Figure 8: Posterior view of the third model

5.VALIDATION OF THE MODEL

Recognizing the fact that the third anatomical finite element model is by no means an exact model of cervical spine, additional validation of the model is necessary. The majority of the models that have been used are concerned with the biodynamic and global motion of the head and neck, and can be easily validated by the sled or drop tower test results. However, a validation of a finite element model which involves the local stresses at the vertebral levels, as does the third model, is a difficult because there are no corroborative experimental results other than in vitro cadaver tests. Therefore the third finite element model was validated with the load-displacement (motion segments) of cervical vertebrae reported in [17]. It is assumed that under 10 G-z acceleration the flexion (deflection) of the cervical spine would achieve a magnitude equal to its limit of mobility. This is due to the fact that up to 10 G-z accelerations human subjects are safe and do not suffer permanent injury. Therefore, case 2, with an acceleration of 10 G-z was employed to validate the model.

To validate the model, the material properties of case 2 (10 G-z) were varied and the deflection of each vertebra was determined, as shown in Table 2. The maximum total (flexion) deflection of the C1 was measured and compared to the mobility range shown in Table 5. It was found that the flexion of the case shown by " *" in Table 2, that is 57.09 mm, matched the motion range and thus was selected. The deflection of the validated case is shown in Figure 10. The final selected material properties are also shown in Table 3.

6. RESULTS AND DISCUSSIONS

The elements, nodes, boundary conditions and the loads of different models created in I-DEAS were used to create the input files for ABAQUS finite element method program. The results of each run, i.e., the stresses and displacements of each layer representing the discs and the vertebrae, were tabulated and analyzed. Due to the large number of tables and graphs generated and the page limitation for this report only a representative selection numbers of graphs and figures are presented here.

The maximum tensile stress and compressive stresses on the vertebrae of the first bulk elastic model are shown in Figures 11 and 12, respectively. As indicated in the modeling section, the first and the last points on these figures are not part of the cervical spine and should be ignored. The overall deflection of the model due to the load is shown in Figure 13. This deflection was validated by the motion range of the cervical spine. The maximum tensile stress and compressive stresses on the vertebrae of the second viscoelastic bulk model are shown in Figures 14 and 15, respectively. These curves are similar to that of Figures 11 and 12, except that the magnitude of the stresses are lower for the viscoelastic model. This is due to the fact that the shock effect of the load is absorbed by the viscoelastic properties of the discs. Clearly, as the relaxation time tends to go to infinity the stresses predicted by the two models approaches equality.

TABLE 2 : VALIDATION OF THE MODEL USING CASE 2 (10 G-z ACCELERATION)

Muscles			Ligaments			Vertebrae (E in MPa)		Discs (E in MPa)		Displ. (mm)
E - Modul (MPa)	Poisson's Ratio ν	Diameter ϕ (mm)	E - Modul (MPa)	Poisson's Ratio ν	Diameter ϕ (mm)	E - Modul (MPa)	Poisson's Ratio ν	E- Modul (MPa)	Poisson's Ratio ν	Max. Flexion
35	0.45	20	25	0.45	4	2000	0.3	100	0.4	32.5
35	0.45	20	15	0.45	4	2000	0.3	90	0.4	35.5
30	0.40	15	10	0.40	4	2000	0.3	90	0.4	50.57
20	0.40	15	20	0.40	4	2000	0.3	90	0.4	48
20	0.40	15	20	0.40	4	1800	0.3	90	0.4	49.3
15	0.40	15	15	0.40	4	1800	0.3	90	0.4	50.37
10	0.40	15	15	0.40	4	1800	0.3	80	0.4	54.4
10	0.40	15	10	0.40	4	1600	0.3	80	0.4	57.65
10	0.38	15	10	0.38	4	1600	0.3	80	0.4	63
10	0.38	15	10	0.38	2	1600	0.3	80	0.4	65.5
10	0.38	15	15	0.38	2	2000	0.3	90	0.4	56.3
10	0.38	15	15	0.38	2	1800	0.3	90	0.4	58
10	0.38	10	15	0.38	1.5	1800	0.3	90	0.4	58.5
10	0.38	10	10	0.38	1.5	1800	0.3	90	0.4	58.72
10	0.38	10	10	0.38	1.5	1600	0.3	80	0.4	66
*10	0.38	10	15	0.38	1.5	2000	0.3	90	0.4	57.09 *
10	0.38	10	10	0.38	1.5	2000	0.3	90	0.4	57.09

* * **Validated case**

TABLE 3 : MATERIALS AND PHYSICAL PROPERTIES

Muscles			Ligaments			Vertebrae		Discs	
E - Modul (MPa)	**Poisson's Ratio ν**	**Diameter ϕ (mm)**	**E - Modul (MPa)**	**Poisson's Ratio ν**	**Diameter ϕ (mm)**	**E - Mod. (MPa)**	**Poisson's Ratio ν**	**E - Mod. (MPa)**	**Poisson's Ratio ν**
10	0.38	10	15	0.38	1.5	2000	0.3	90	0.4

Viscoelastic properties

Shear relaxation	Bulk relaxation	Relaxation time
g1 = 0.3991	k1 = 0.700	t1 = 3.4519
g2 = 0.3605	k2 = 0.149	t2 = 2000
g3 = 0.1082	k3 = 0.150	t3 = 7000

Figure 9: Positions of soft tissue attachments in the top and oblique views of a vertebra

TABLE 4 : LIGAMENTS, FACETS AND MUSCLES ATTACHMENTS

Vertebrae	Ligaments positions								
C1 - C2	1	2	3	4	5	6	7	8	9
C2 - C3	1	2	3	4	5	6	7	8	9
C3 -C4	1	2	3	4	5	6	7	8	9
C4 - C5	1	2	3			6	7	8	9
C5 - C6	1	2	3			6	7	8	9
C6 - C7	1	2	3			6	7	8	9
C7 - T1	1	2	3			6	7	8	9
T1 - C1	2 muscles attached : left & right								

Positions	Explanation
1 to 5	Spinous process ligaments
6 & 7	Articular facets
8 & 9	Anterior and posterior ligaments

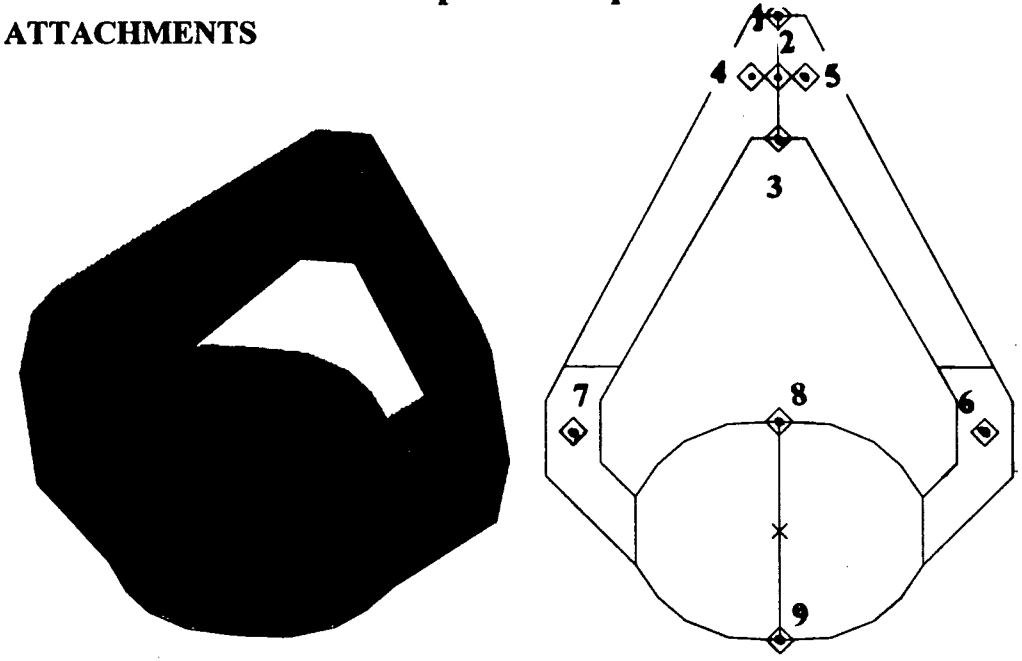

TABLE 5.1 : ANATOMICAL DIMENSIONS OF DISCS AND VERTEBRAE

Vertebrae	d1	d2*	a	b	c	α
C1	16	20	14	37	7	11°
C2	16	20	14	37	7	11°
C3	16	20	12	30	8	14.5°
C4	16	21	12	30	6	12°
C5	16	22	11	33	3	6°
C6	17	25	11	40	3	4°
C7	17	30	12	46	6	7.5°

* d2 = second diameter of the elliptical shape

TABLE 5.2 :MOBILITY OF CERVICAL SPINE

Flexion - Extension	
Vertebrae	Average range
Occiput	15°
C1 - C2	13°
C2 - C3	12°
C3 - C4	18°
C4 - C5	20°
C5 - C6	20°
C6 - C7	15°

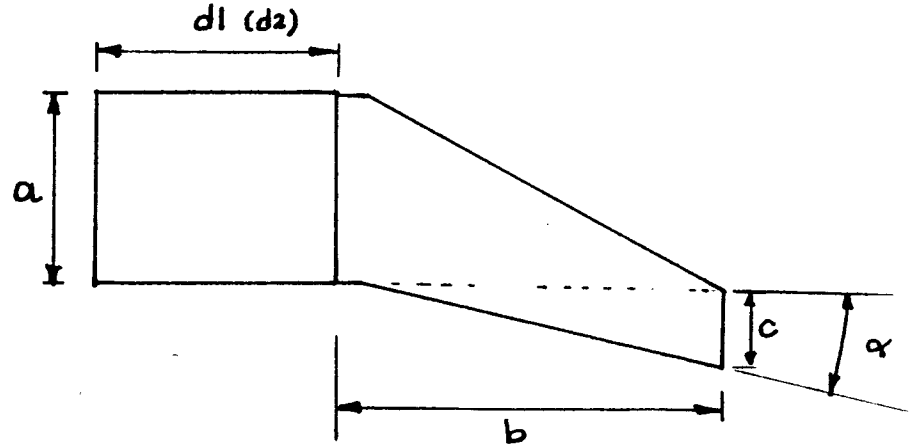

The oblique view of the third model given by solid modeling is shown in Figure 6. The sagittal view and the posterior views of the finite elements of the model are shown in Figures 7 and 8, respectively. The beam elements representing the ligaments, articulate facets and muscles are shown in Figure 7 as connecting lines between the two nodes of the posterior arches of adjacent vertebrae.

The results, including the maximum principal stress S33, the maximum Von Mises stress and maximum deflection of the third model, for the cases 1 through 8, are shown in Table 1. Because of the large number of figures only three views (anterior, posterior and oblique) of the maximum principal stress field of cases 1, 2 and 8 are presented in figures 11, 12 and 13, respectively. This selection was due to the fact that the stress fields of cases 3 and 4 were similar to that of case 1, and the stress fields of cases 5, 6 and 7 were similar to that of case 8, and only the magnitude were different. The maximum principal stress field that is more often used as a failure criterion for bones has been employed in this analysis. The stress concentrations areas of Figures 16-18 are predominantly at the top disc, representing the head and the bottom plate representing T1 and were neglected. The top disc and the bottom plate were created to offset the stress concentration on C1 and C7, respectively.

The principal stress field of case 1 (cadaver), shown in Figure 16, indicates that the maximum compressive stress occurs on the anterior side of the cervical spine while the tensile stress occurs at the posterior side of the vertebral bodies. In this case the maximum compressive stress occurs at C4 and is 105 MPa., as shown in Figure 19a, while the maximum stress on discs occur in disc 45, between C4 and C5, as shown in Figure 19b.

Figure 17 shows the principal stress field of case 2 (10 G-z). Similar to the case 1 the maximum compressive stress occurs on the anterior side of the body of the vertebrae of the cervical spine while the tensile stress occurs at the posterior side of the vertebral bodies. The principal stress field of cases 3 and 4, for 8 G-z and 6 G-z, respectively, were similar to that of case 2 and thus were not presented. However, the stresses in the discs and vertebrae are compared for cases 1 to 4 and are shown in Figures 19a and 19b.

The principal stress field of case 8 (7 G-y) acceleration is shown in Figure 18. The maximum compressive stresses occur on the anterior-lateral side of the body of the vertebrae of the cervical spine while the tensile stress occurs at the posterior-medial side of the vertebral bodies. The principal stress field of cases 5, 6 and 7, for 4 G-y, 5 G-y and 6 G-y, respectively, were similar to that of case 8, 7 G-y, and therefore were not presented. As for G-z, the stresses in discs and vertebrae for G-y are compared for cases 5 to 8 and are shown in Figures 20a and 20b.

Each vertebra and disc of every case was analyzed. The variation of maximum compressive stress for each vertebra and disc in all the cases of accelerations, are shown in Figures 19 and 20. The maximum compressive stress of each model was plotted against the accelerations, as shown in Figure 21. For G-y acceleration, the stress level gradually increases, while for G-z acceleration the stress is linear up to 10 G. Since there were no data points between the 10 G and the Cadaver case 1, a broken line is used in the figure.

Neck Model 2 /TCH

LOAD SET: 1 - LOAD SET 1
DISPLACEMENT - NORMAL MIN: 0.00 MAX: 57.09

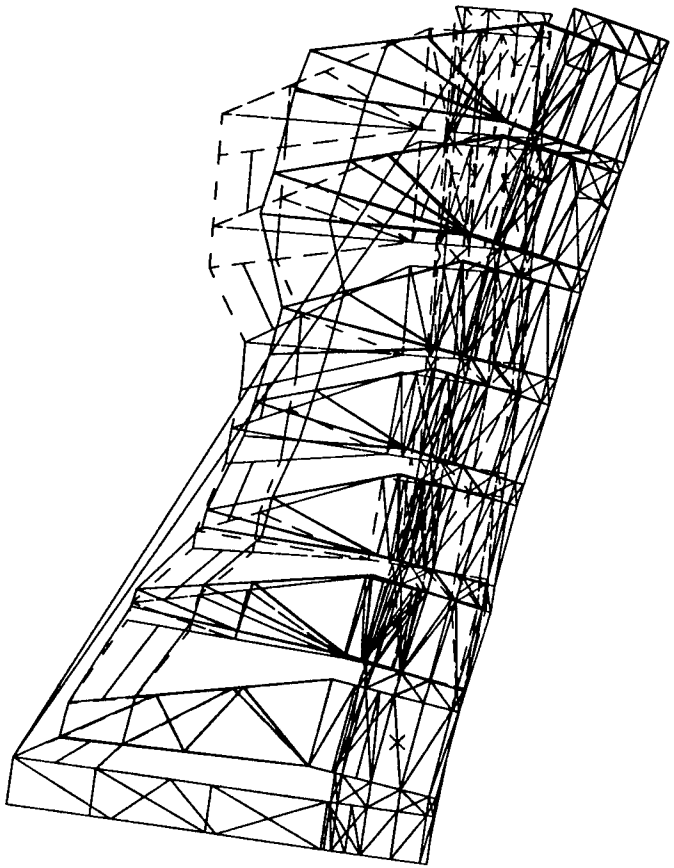

Figure 10. Deflection of validation (case 2 10G-z)

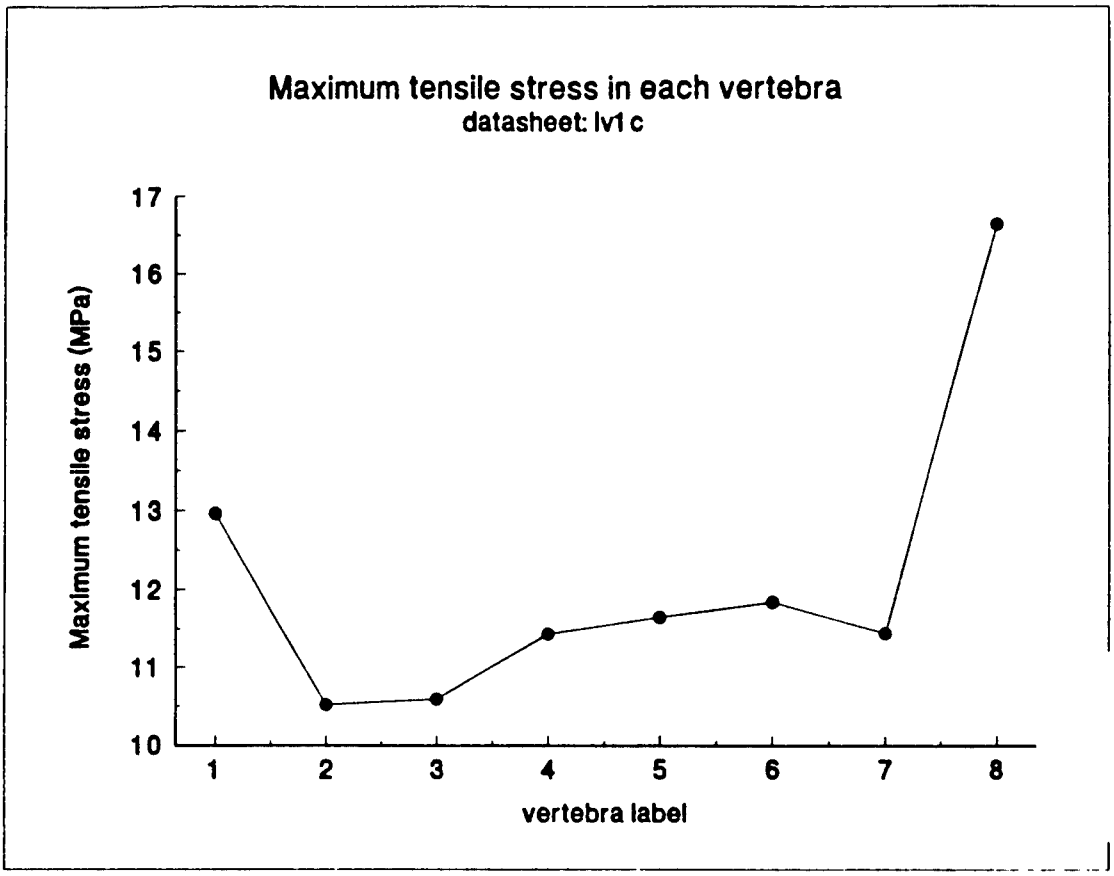

Figure 11: Bulk elastic model, tensile stress vs. vertebra

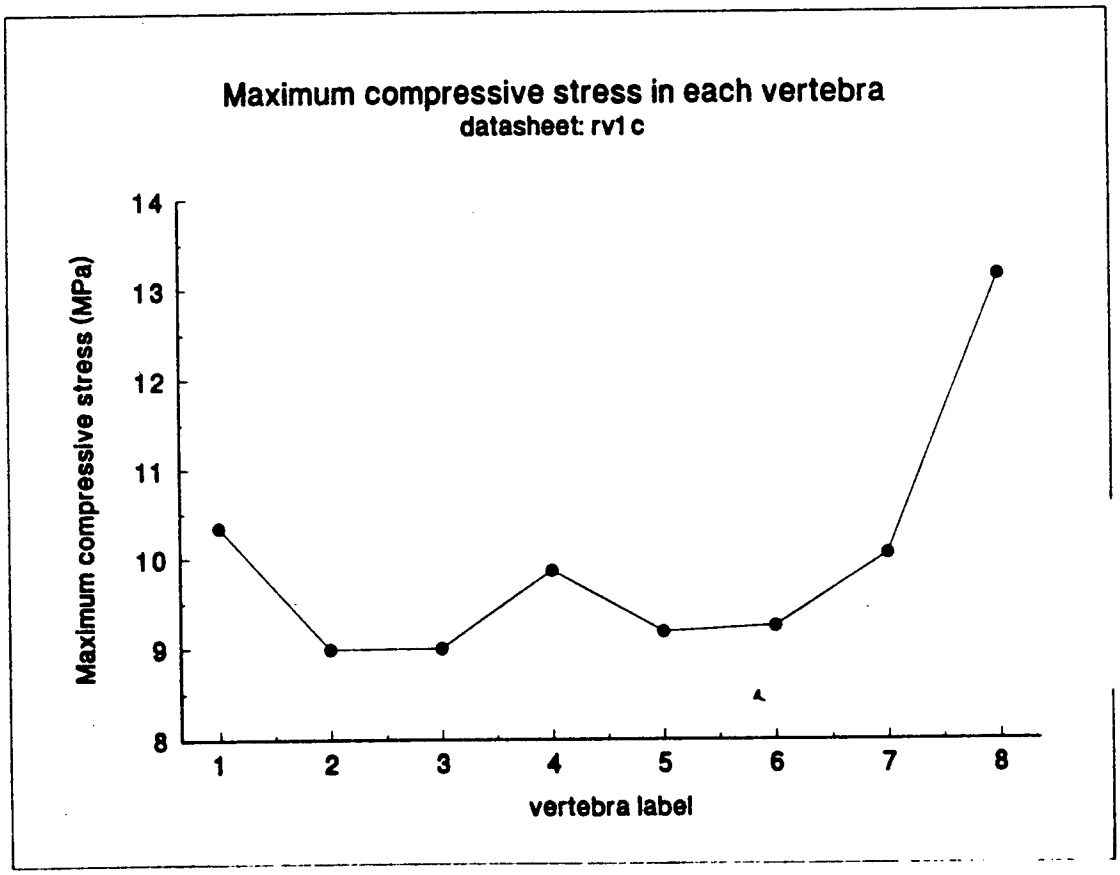

Figure 12 : Bulk elastic model, compressive stress vs. vertebra

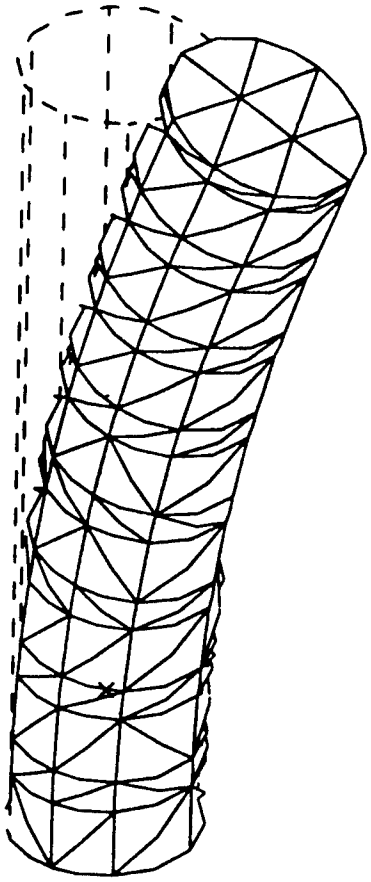

Figure 13: Deflection of the bulk elastic model

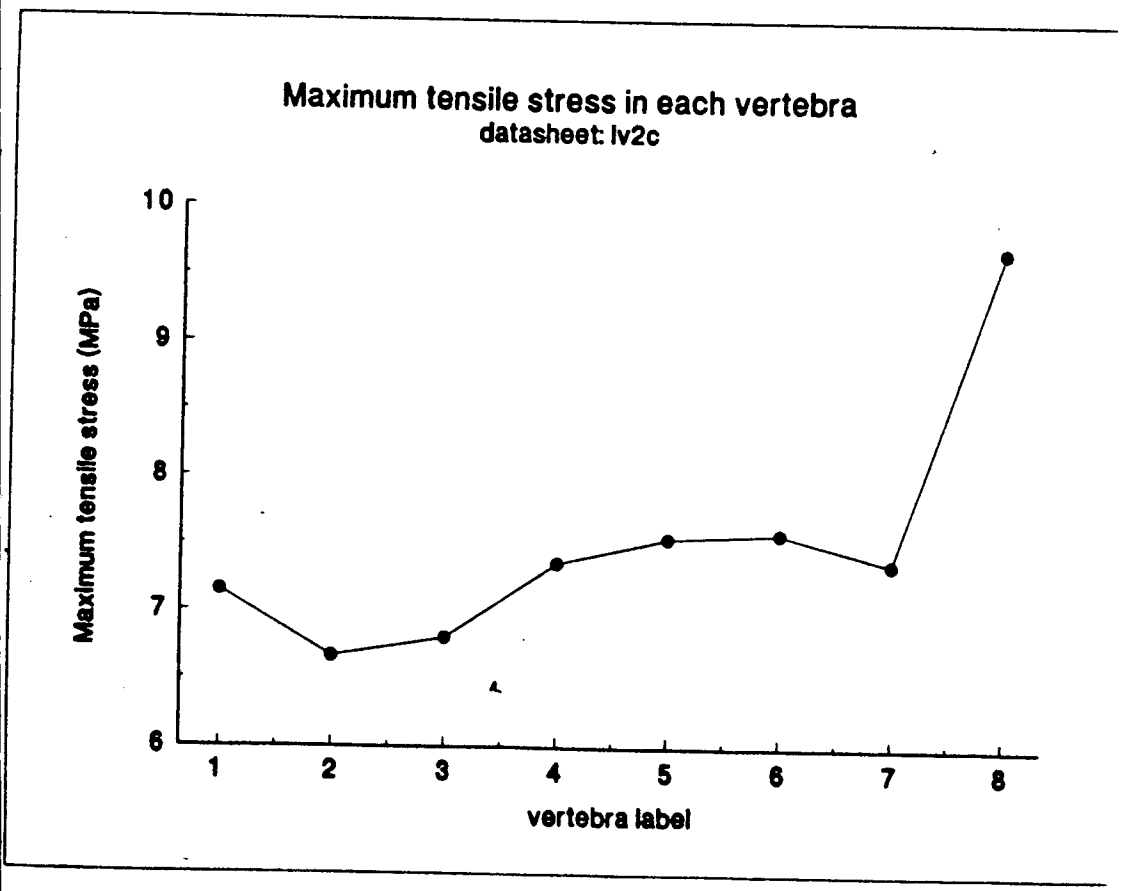

Figure 14 Bulk viscoelastic model, tensile stress vs. vertebra

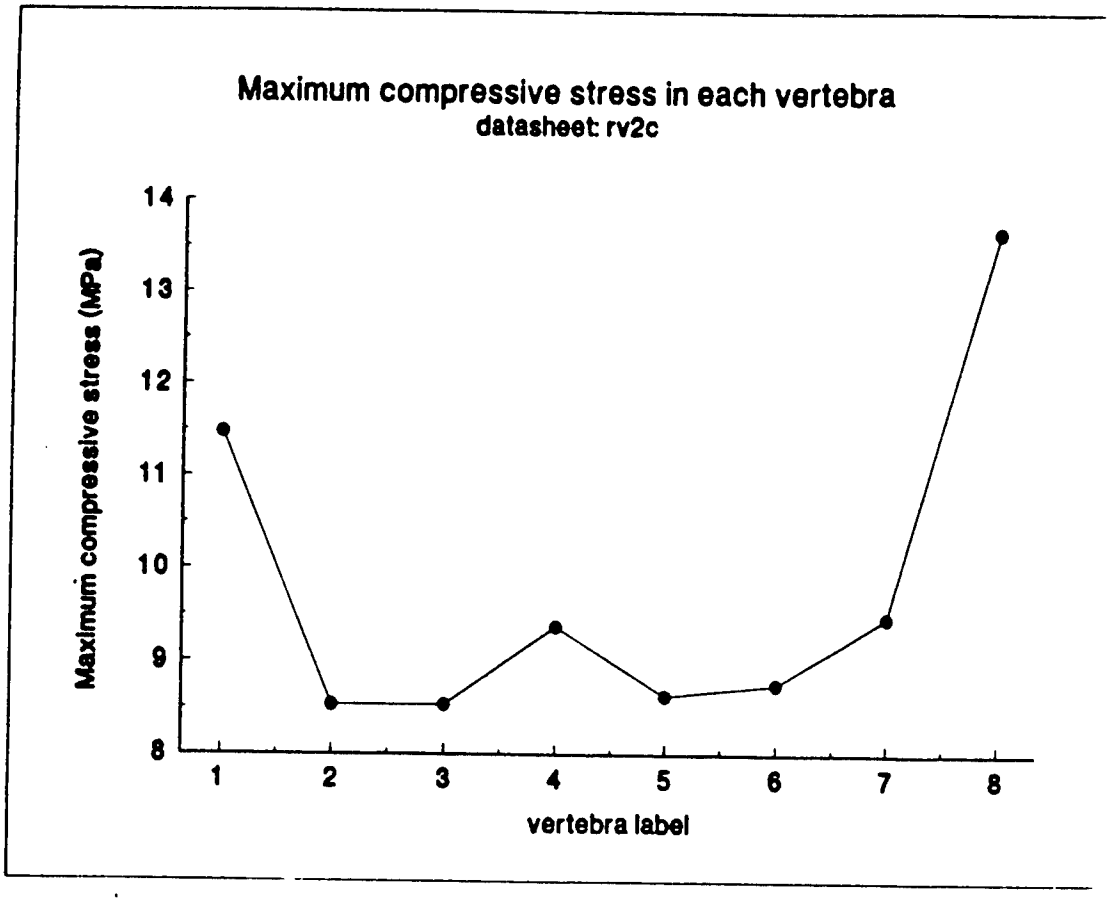

Figure 15. Bulk viscoelastic model, compressive stress vs. vertebra

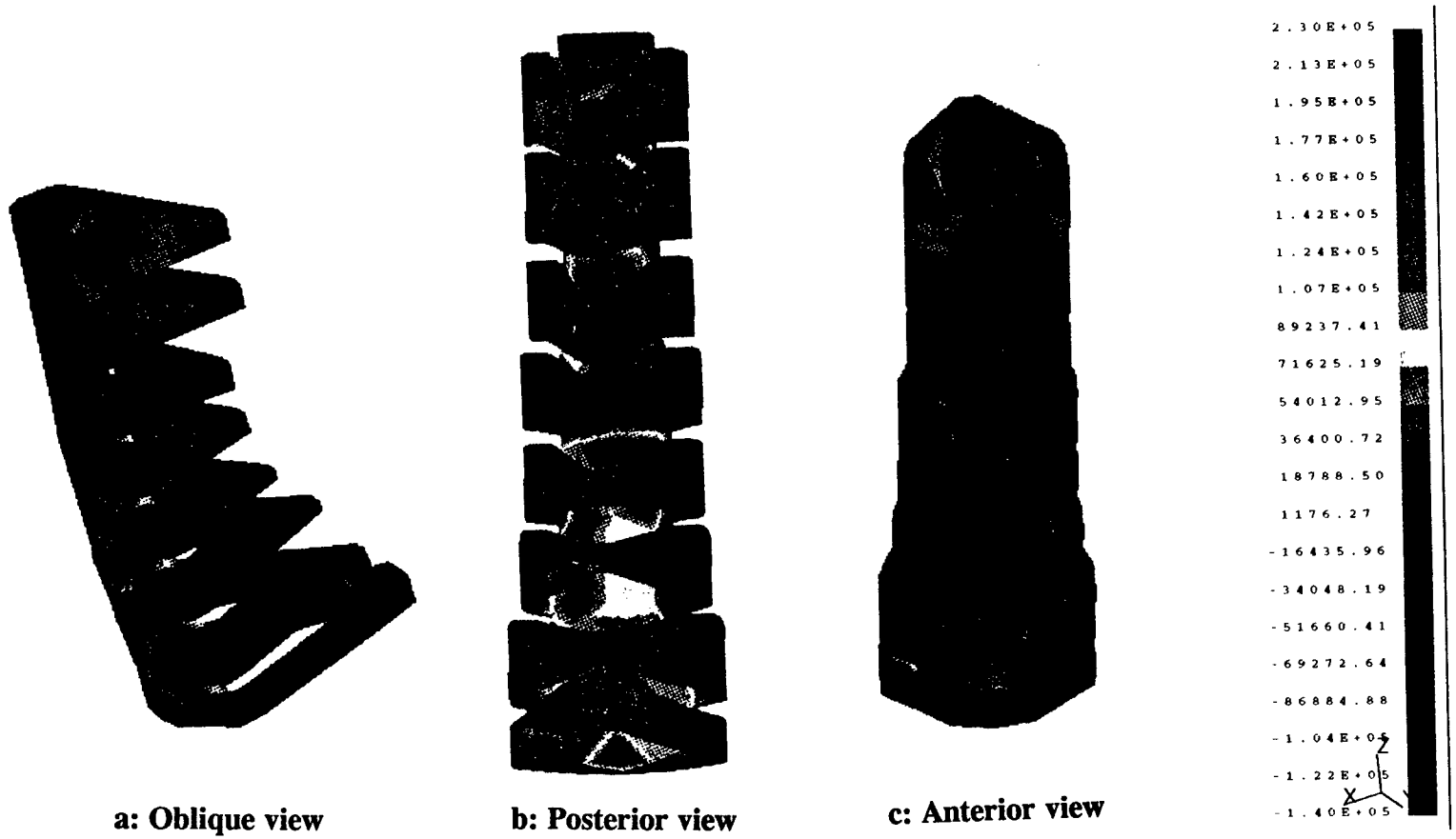

a: Oblique view b: Posterior view c: Anterior view

Figure 16: Principal stress field of the third model, cadaver, case 1, G-z Acc.

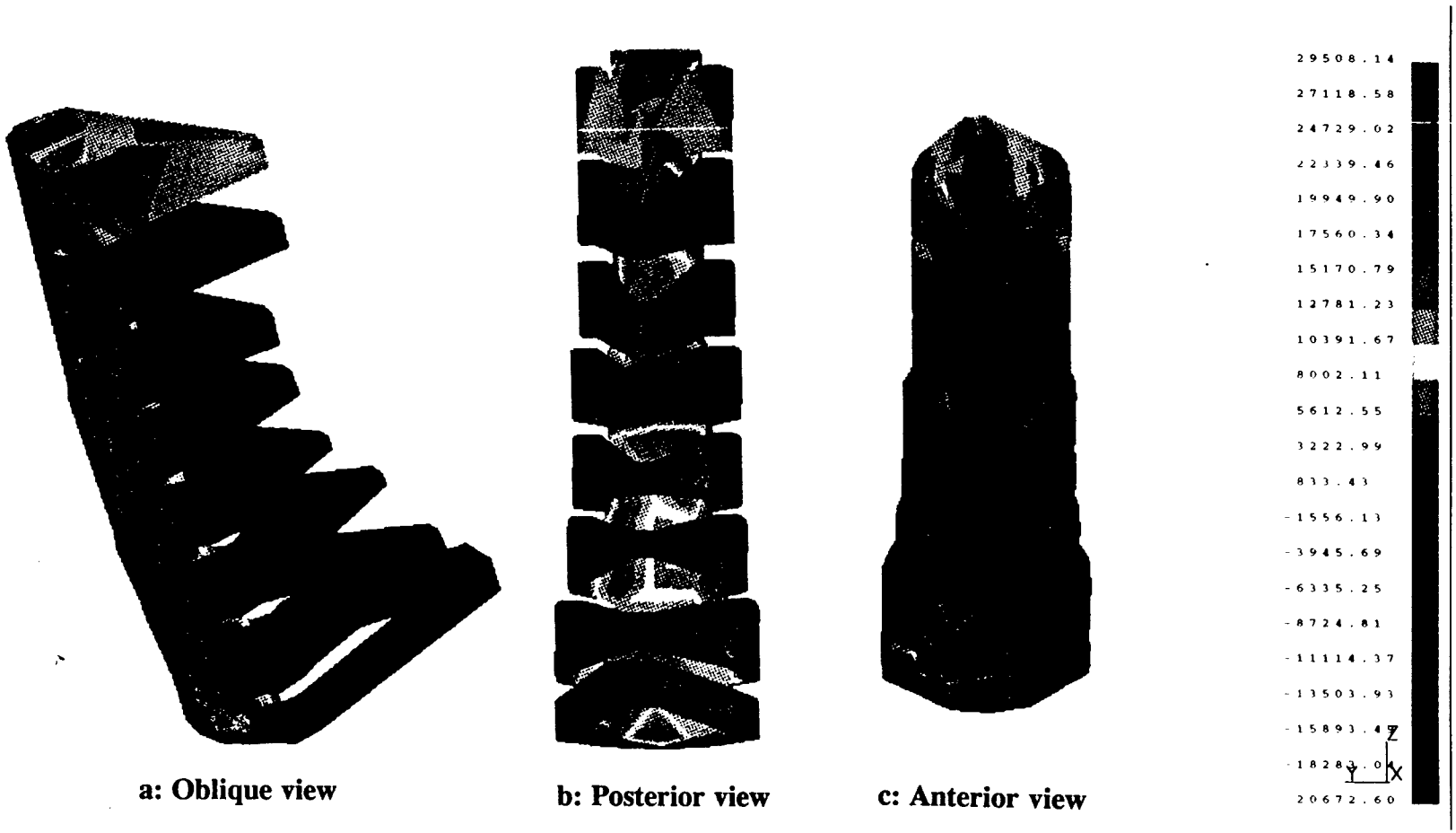

a: Oblique view b: Posterior view c: Anterior view

Figure 17: Principal stress field of the third model, case 2, 10 G-z Acc.

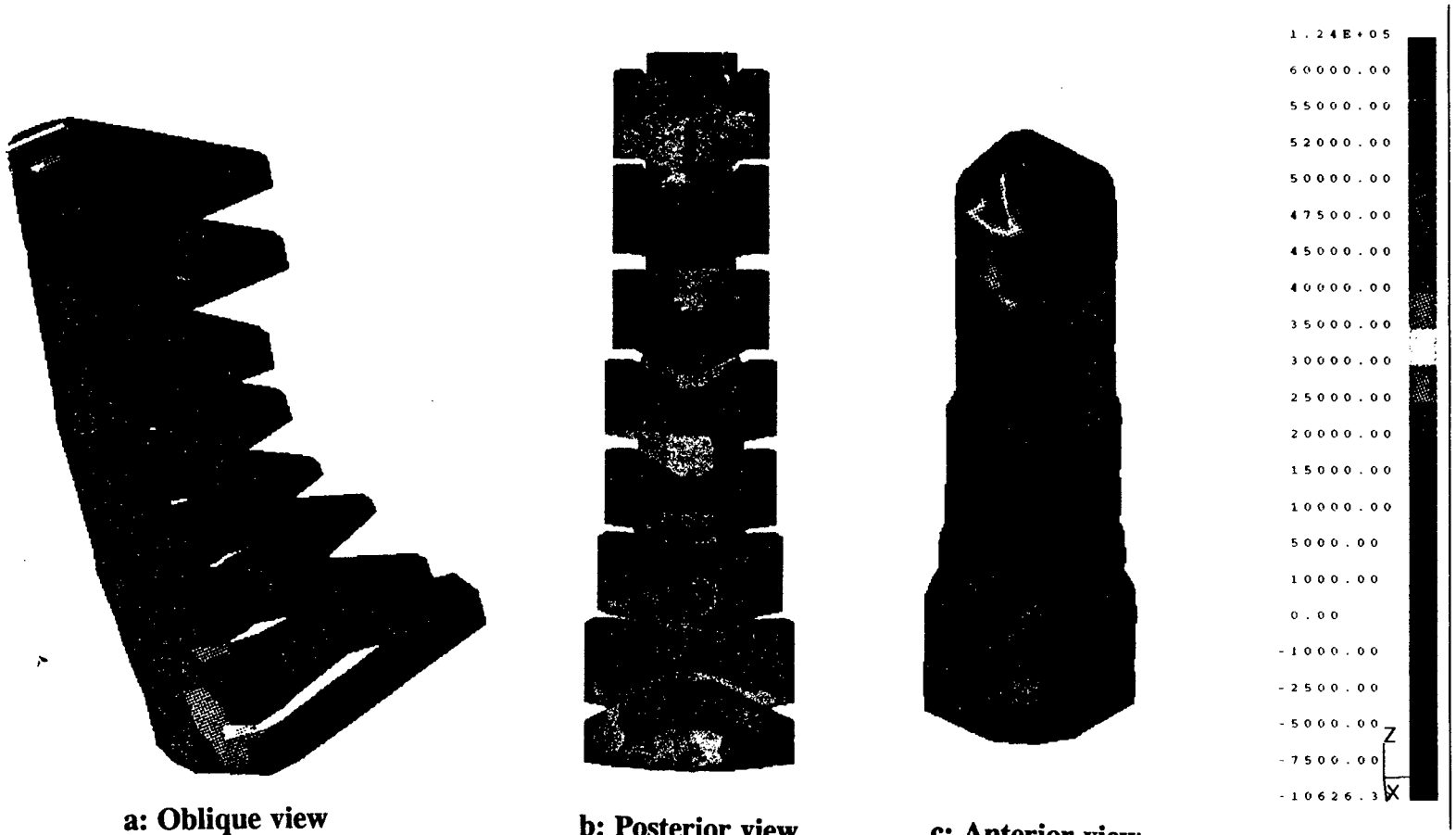

a: Oblique view

b: Posterior view

c: Anterior view

Figure 18: Principal stress field of the third model, case 8, 7 G-y Acc.

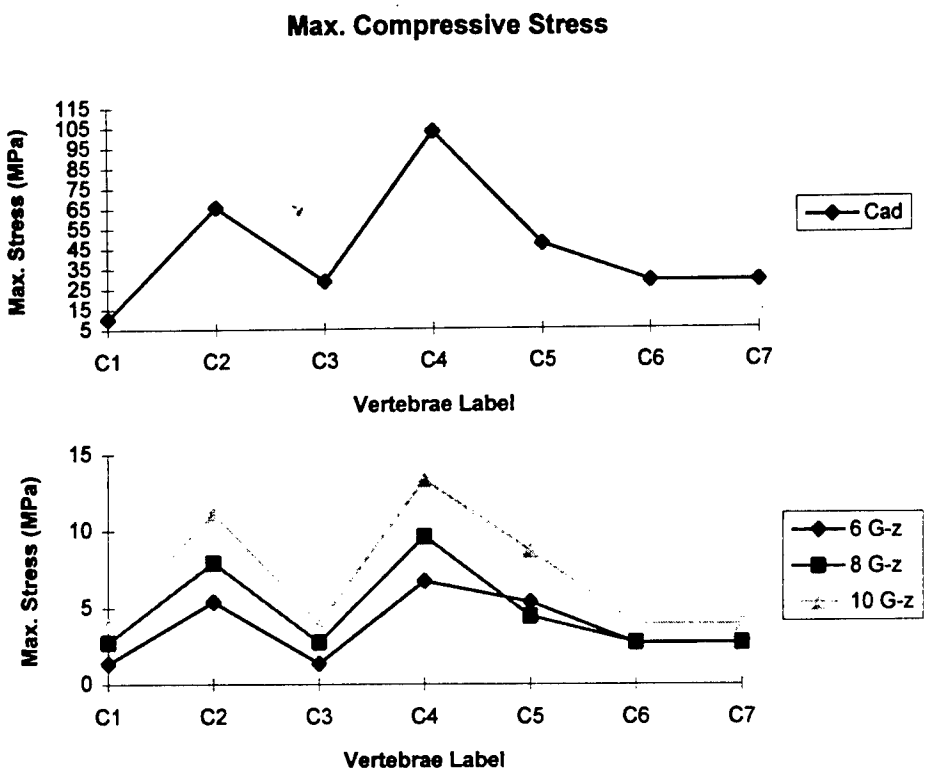

a

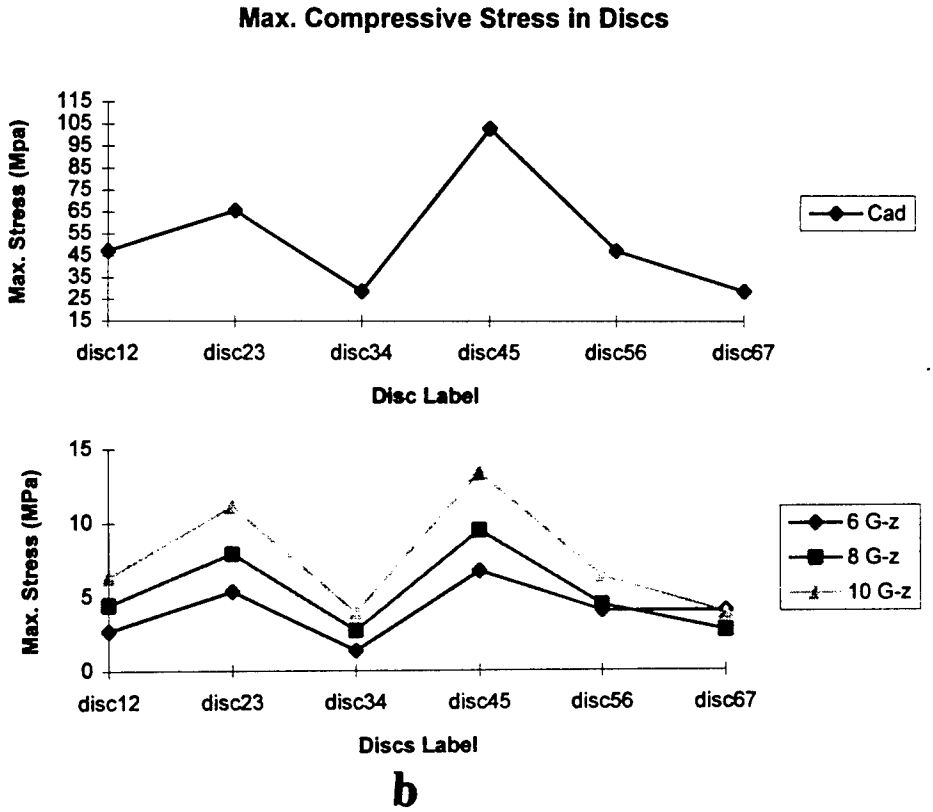

b

Figure 19: Variation of max. compressive stress v.s. vertebrae or discs in G-z

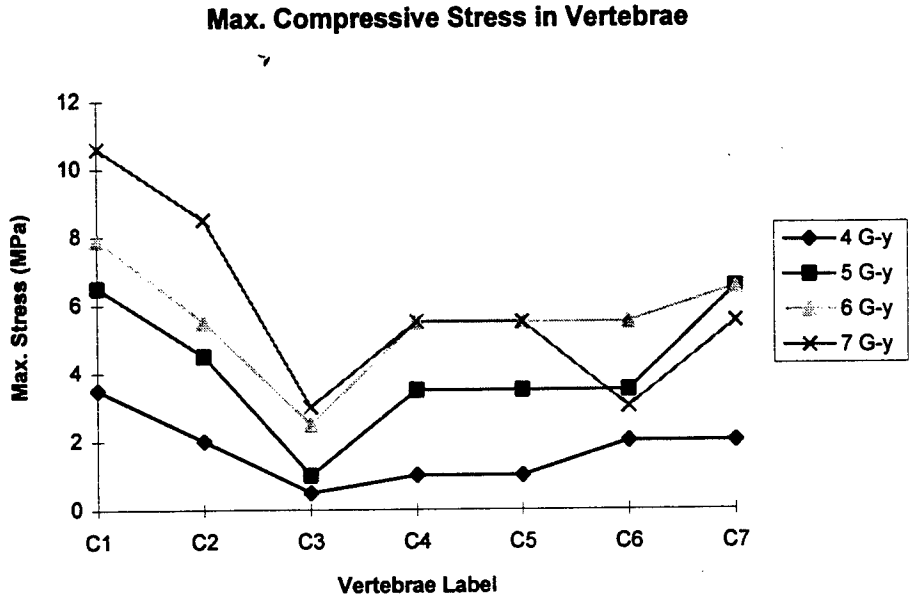

a

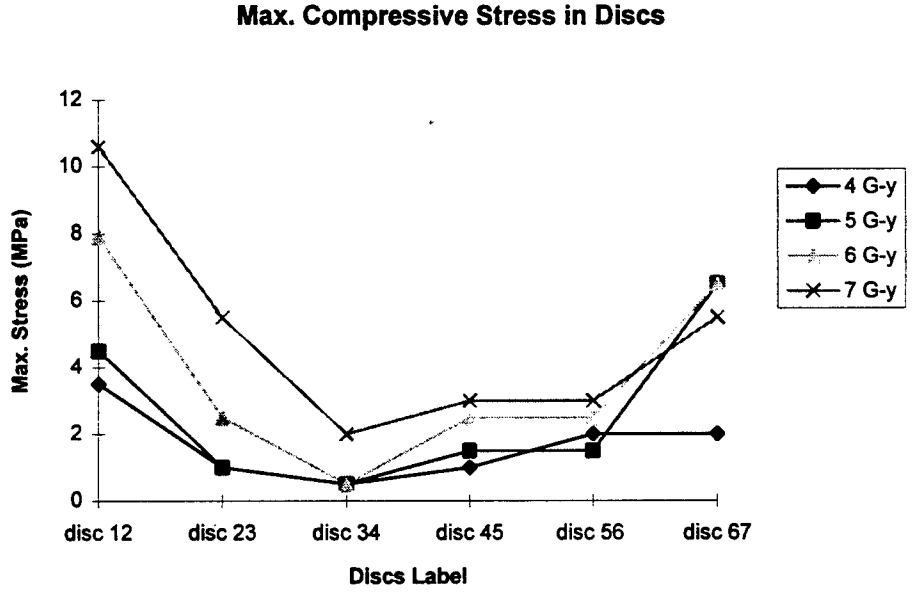

b

Figure 20: Variation of max. compressive stress v.s. vertebrae or discs in G-y

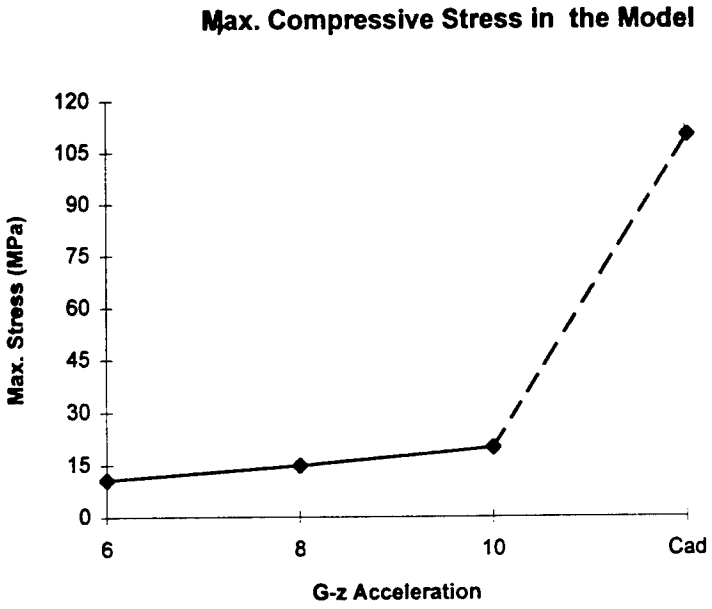

a

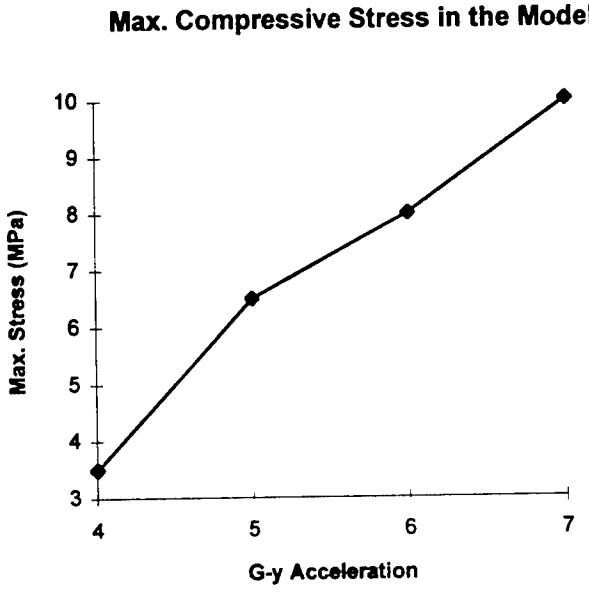

b

Figure 21: Variation of max. compressive stress v.s. G-y or G-z Acc.

6.CONCLUSIONS

The first bulk elastic model was a gross approximate model of the neck. The enlarged radius of 15.8mm was a geometrical average of the vertebrae including the arches and the processes. While the stress levels of the model and the stress variation seem reasonable, the use of the enlarged radius in the model is difficult to justify. This is due to the fact that actual compensation for the soft tissue and the muscles attachment was not analyzed. However, the model is appropriate as a quick, first approximation model to find the critical accelerations and stresses.

In the second model, viscoelastic material properties were used. While the maximum stresses for each vertebra and disc for viscoelastic bulk model, shown in Figure 14 and 15, are similar to that of Figures 11 and 12, the magnitude of the stresses are lower for the viscoelastic model. This is due to the fact that the damping effect of the disc materials absorbs some of the impulse loads. If the time is extended to infinity the final loads, after relaxation, will approach the level of the first model.

Geometrically, the third model is a relatively accurate model of the cervical spine. While the effect of the soft tissues, the ligaments, articular facets and muscles, were compensated by the beam elements in the model, more detailed nonlinear spring and dashpot elements could be used to simulate the neck model more realistically.

Comparison of the maximum principal stresses in each disc and vertebra for G-z accelerations, as shown in Figure 19, indicates that: (a) all the G-z cases exhibit a similar stress pattern, (b) the maximum stresses occur at C4. These results are consistent with the results of the first model (bulk elastic) and the second models (viscoelastic), as shown in Figures 12 and 15. It is also important to note that C2 and its inferior disc 23 have the second highest maximum stress, as shown in Figure 19. The pattern of maximum stresses in vertebrae and discs in G-y acceleration, as shown in Figure 20, indicates that maximum stress occurs in C1 and its inferior disc 12. The second highest stress level occurs at vertebrae C4 to C7.

All the results shown in Figures 19 and 29 indicate that the maximum stress in all cases increased as the magnitude of the acceleration increased. However, the stresses in the vertebrae fluctuate. For the G-z acceleration cases, the vertebrae C2 and C4 and their corresponding discs experienced higher stresses compared to others. In the G-y acceleration cases the vertebrae C1 and C7 and their corresponding discs experienced higher stresses compared to others. The stresses in the 10 G-z case and 7 G-y case were acceptably below the injury region as determined by the cadaver tests.

The reason for nonlinear distribution of the maximum stresses shown in Figures 19 and 20 is that the geometry of the cervical spine is complex and nonlinear. It resembles a curved beam that is subjected to axial and bending loads. Since the points of application of the loads are not at the centroid of the cross-section, the stresses found in the vertebral bodies were not uniform.

Figure 21 depicts the variation of the maximum principal stress against the accelerations. This figure indicates

that the stress level increases with the increase in G acceleration. There was no data between the 10 G-z acceleration and the cadaver case, thus a linear increase is assumed and shown as the dashed line in Figure 21a. One may estimate the threshold of safe and non-injury level of the stress and the acceleration by linear extrapolation of the curves beyond 10 G-z and 7 G-y, as shown in Figure 21.

There are five major mechanisms resulting in cervical injuries: compression, flexion, extension, rotation, and lateral flexion. However, upper cervical spine (C1 and C2) injuries are mainly due to hyperextension, and their dislocations are fatal. The intervertebral discs, joints and ligaments are very resistant to compression, dislocation, flexion and extension, but very vulnerable to rotation and horizontal shearing forces such as in G-y accelerations, Roaf, [10]. According to Roaf [10], the clinical approach of a cervical dislocation or fracture-dislocation, usually attributed to hyperflexion, is really the result of rotation. Belytschko, et. al., [11] reported that the maximum voluntary static neck reaction is about 1.13×10^8 dynes in tension and 1.11×10^8 dynes in compression. A limited amount of strength data for individual components of the neck can be found in the literature.

While the results of the three models give a better understanding of the load and torque distributions in the vertebrae due to G-y and G-z acceleration, there are still many other aspects of cervical spine injuries that require further investigation. In fact, the third model should be further modified to include dashpot and spring elements. Additional studies are needed to compare these maximum stresses to the soft tissue damage since the stresses are substantially below the cadaver stresses. Further, the issue of the dynamic response of the neck to the impulse load should be addressed. These analyses were beyond the time limitation and scope of this study and are deferred to the next report.

7. REFERENCES

1. Guill, F.C. and Herd, G.R., "Aircrew Neck Injuries: A new, or an existing misunderstood phenomenon?", Neck Injury in Advanced Military Aircraft Environment, AGARD, conference Proceedings No. 471, pp 9.1-12, 1990.

2. Knox, F. S., Buhrman, J. R., Perry, C. E., Kaleps, I. "Interim Head/Neck criterion", Armstrong Laboratory Consultation report, WPAFB, OH, Dec., 1991.

3. Miller, H. L. and Schneck D. J., "Biodynamic responses to emergency ejections under conditions of added head mass", WPAFB, research contract, 1993.

4. Perry, C. E., "Vertical impact testing of two helmet-mounted night vision systems", AL/CF-SR, 1994-0013

5. Sadegh, A. "Analysis of loads on the neck and head joints due to G-y acceleration" SFRP report, AL/CFBE, WPAFB, 1995.

6. Foust D. R., Chaffin, D. B., Snyder, R. G. and Baum, J. K., "Cervical range of motion and dynamic response and strength of cervical muscles," Proceedings of 17th Stapp car conference, paper #730975, 285-309, 1973.

7. Johnson , RW., Crelin, E. S., White III, A. A., Panjabi, M. M. and Southwick, W. O., "Some new observations on the functional anatomy of the lower cervical spine", Clin. Orthop: 3, 192-200, 1975.

8. ABAQUS User Manual, 1995.

9. Williams J. and Belytschko T., "A Dynamic model of the cervical spine and head", AFAMRL-TR- 81-5.

10. Roaf R. "A Study of the Mechanics of Spinal Injuries", J. Bone Joint Surg., 42B, 810-823, 1960.

11. Belytschko T. Rencis M. and Williams, "Head-Spine structure modeling: enhancements to secondary loading path model and validation of head-cervical spine model" AAMRL-TR-85-019, 1985.

12. Visarius H., "On the experimental and mathematical modeling of the viscoelastic behavior of the human spine", Dissertation, Wayne State Univ., 1994.

13. Farfan H., Gracovetsky, S., and Helleur C." Cervical spine analysis for ejection injury prediction", US AFOSR #81-0012, 1982.

14. Woo SLY, Johnson GA., Smith B." Current concepts in modeling of ligaments and tendons, ASME Bioeng. Conf. 1993, BED-Vol 24, 298, 1993.

15. Buhrman, J. and Perry, C. "Human and Manikin Head/Neck Response to +Gz Acceleration when encumbered by helmets of various weights", Aviation, Space, and Environmental Medicine, P 1086-1090, December, 1994.

16. Perry, C. "Gz Impact acceleration test results for human subjects and manikin", internal communications of the test results., 1996.

17. The Cervical Spine", The Cervical Spine Research Society, Second edition, Lippincott Company, 1995.

18. White A. and Panjabi M. "Clinical biomechanics of the Spine", Lippincott Company, second edition, 1995.

19. Sadegh, A. "Investigation of neck models for predicting human tolerance to accelerations", SFRP report, AL/CFBE, WPAFB, 1996.

20. Yaganadan N., Kumaresan S. Voo L. and Pintar F., "Spine update finie element applications in human cervical spine modeling", SPINE Vol. 21 N.15 pp 1824-1834, 1996.

Two-Phase Flow Patterns in Porous Media: An Investigation Relating to IN-SITU Air Sparging

William R. Wise
Associate Professor
Department of Environmental Engineering Sciences

Michael C. Brooks
Graduate Student

University of Florida
Gainesville, FL

Final Report for:
Summer Extension Research Program
Armstrong Laboratory

Sponsored by:
Air Force Office of Scientific Research
Bolling AFB, Washington, DC

and

Armstrong Laboratory

December 1996

TWO-PHASE FLOW PATTERNS IN POROUS MEDIA: AN INVESTIGATION RELATING TO IN-SITU AIR SPARGING

Michael C. Brooks
Graduate Student

William R. Wise
Associate Professor

Department of Environmental Engineering Sciences
University of Florida

Abstract

In-Situ Air Sparging (ISAS) is a technique to remedy groundwater contamination. It consists of injecting air below the saturated zone for the purpose of either volatilizing contaminants or promoting bioremediation. Both of these treatment processes rely on mass transfer between phases. Interphase mass transfer is dependent on the interfacial area between the phases, which in turn, is dependent on the type of flow pattern.

Two types of gas-flow patterns have been discussed in the ISAS literature: air bubbles in a continuous liquid phase (bubble flow), and a continuous air phase displacing the liquid phase along paths of least resistance (air channels). For the wide range of subsurface conditions, both bubble flow and air channels are possible.

Two competing forces govern the flow domain resulting in a given system: buoyancy forces lifting the air and capillary forces that must be overcome for the air to penetrate pores. When the former dominates, bubble flow results; the latter dominates during channel flow. The competition between these forces may be described using a bond number that is related to the physical size of the grains of the porous medium of interest, the density disparity between phases (air and water), gravity, and the interfacial tension. When this bond number is modified to include the aspect ratio (ratio of pore throat to pore body size), the transition from channel flow to bubble flow is seen to occur near a modified bond number of unity. This result holds for various experimental results reported in the literature, as well as for glass bead experiments, performed during this project, designed specifically to test the modified bond number's ability to characterize the transition. The aspect ratio is important because the buoyancy forces are governed by the size of the pore body, while the capillary forces are related to the restrictive nature of pore throats.

TWO-PHASE FLOW PATTERNS IN POROUS MEDIA: AN INVESTIGATION RELATING TO IN-SITU AIR SPARGING

Michael C. Brooks
Graduate Student

William R. Wise
Associate Professor

INTRODUCTION

In-Situ Air Sparging (ISAS) is a relatively new technique to remedy groundwater contamination. It consists of injecting air into the saturated zone for the purpose of either volatilizing contaminants or promoting bioremediation. First introduced in the mid 1980's (Middleton and Hiller, 1990), it did not receive considerable attention until this decade (Ardito and Billings, 1990; Brown and Jasiulewics, 1992; Brown et. al., 1991; Kerfoot and Evans, 1993; Marley, 1991; Marley et al., 1992a; Loden, 1992; Pankow et al., 1993; Roberts and Wilson, 1993; Sellers and Schreiber, 1992; Wilson et al., 1992; Wilson, 1992; Lundegard, 1994; Leeson et al., 1995; Acomb et al., 1995). conceivably because recognition of pump-and-treat limitations motivated the development of alternative treatment techniques. Both of the treatment processes (volatilization and bioremediation) rely on mass transfer from one phase to the other. Mass transfer from one phase to the other is dependent on the interface between the phases. which is dependent on the type of flow pattern. However, as pointed out previously by Loden (1992), the exact spatial distribution of the gas phase in the subsurface is unknown. The ability to predict the flow pattern resulting from ISAS, at least in some average sense, is a necessary first step to modeling remedial treatment potential.

Two types of gas-phase flow patterns have been discussed in the ISAS literature. The first pattern consists of bubble flow (Wehrle, 1990; Brown and Fraxedas, 1991; Brown and Jasiulewics, 1992; Ardito and Billings, 1990; Sellers and Schreiber, 1992; Kerfoot, 1992; Juncosa, 1993; Ji et al., 1993). Wehrle (1990) identifies bubble flow in ISAS laboratory experiments using water, air, and fine gravel with a median size (D_{50}) of 3 millimeters (mm). Air was reported to travel upward in a limited area around the injection point. Ji et al. (1993) observed bubble flow in ISAS laboratory experiments using water, air, and 4-mm glass beads. Bubble flow and air channels were reported using 2-mm glass beads. Juncosa (1993) noted similar observations for ISAS laboratory experiments using water, air, and 4-mm glass beads, however, only air channels were observed using 2-mm glass beads. Tung and Dhir (1988) report observations of bubbly, slug, and annular two-phase flow patterns in two-phase flow

experiments using air, water, and porous media composed of particles with diameters greater than or equal to 6 mm.

The second pattern reported in the ISAS literature is channel flow, in which continuous air displaces liquid along paths of least resistance (Marley, 1991; Marley et. al., 1992a; Middleton and Hiller, 1990; Johnson et al., 1993; Ahlfeld et al., 1994; Leeson et al., 1995). Ji et. al. (1993) observed air channels in laboratory models using water, air, and 0.75-mm glass beads. Injected air was reported to travel in a few narrow channels through the porous media. Juncosa (1993) observed air channels in ISAS experiments using 2-mm glass beads. Likewise, air was reported to travel in preferred pathways during other ISAS experiments composed of sand ($D_{50} \approx$ 1.5 mm), loam ($D_{50} \approx$ 0.4 mm), and silty sand ($D_{50} \approx$ 0.4 mm).

Figure 1 summarizes the flow patterns discussed above as a function of the reported porous media sizes. It is noted that a transition from air channels to bubble flow is observed as the porous media size increases. It is evident from this figure that a change in the observed flow patterns occurs around 1 mm to 2 mm for air-liquid systems. Ji et al. (1993) identify the transition size as 2 mm. Wehrle (1990) identifies the differences in air-phase distribution patterns for coarse-grain soils and fine-grain and cohesive soils in his model-scale experiments. For coarse-grain soils the vertical motion of the air is described as "pulsating bubbles" and "groups of bubbles," and the motion was attributed to hydraulic uplift. For fine grain and cohesive soils it was reported that the air only escaped the saturated zone at a limited number of points, and that the air was opposed by the entry pressure associated with the pore spaces. Wehrle (1990) states that a coarse grain soil with D_{50} = 0.8 mm forms the demarcation between the two cases.

Using the Uniform Soil Classification System (ASTM, 1993), the transition zone falls in the medium to coarse sand classification. Therefore, as a gross predictive tool, ISAS in a porous media characterized by medium sand or smaller will have air channels, while the flow pattern in porous media composed of coarse sand or larger will have bubble flow. Actually, several patterns as identified from the chemical and petroleum engineering literature should be possible (i.e., bubble flow, slug flow, mixed flow, etc.). However, for the sake of brevity, bubble flow will be used to refer to these two-phase flow patterns.

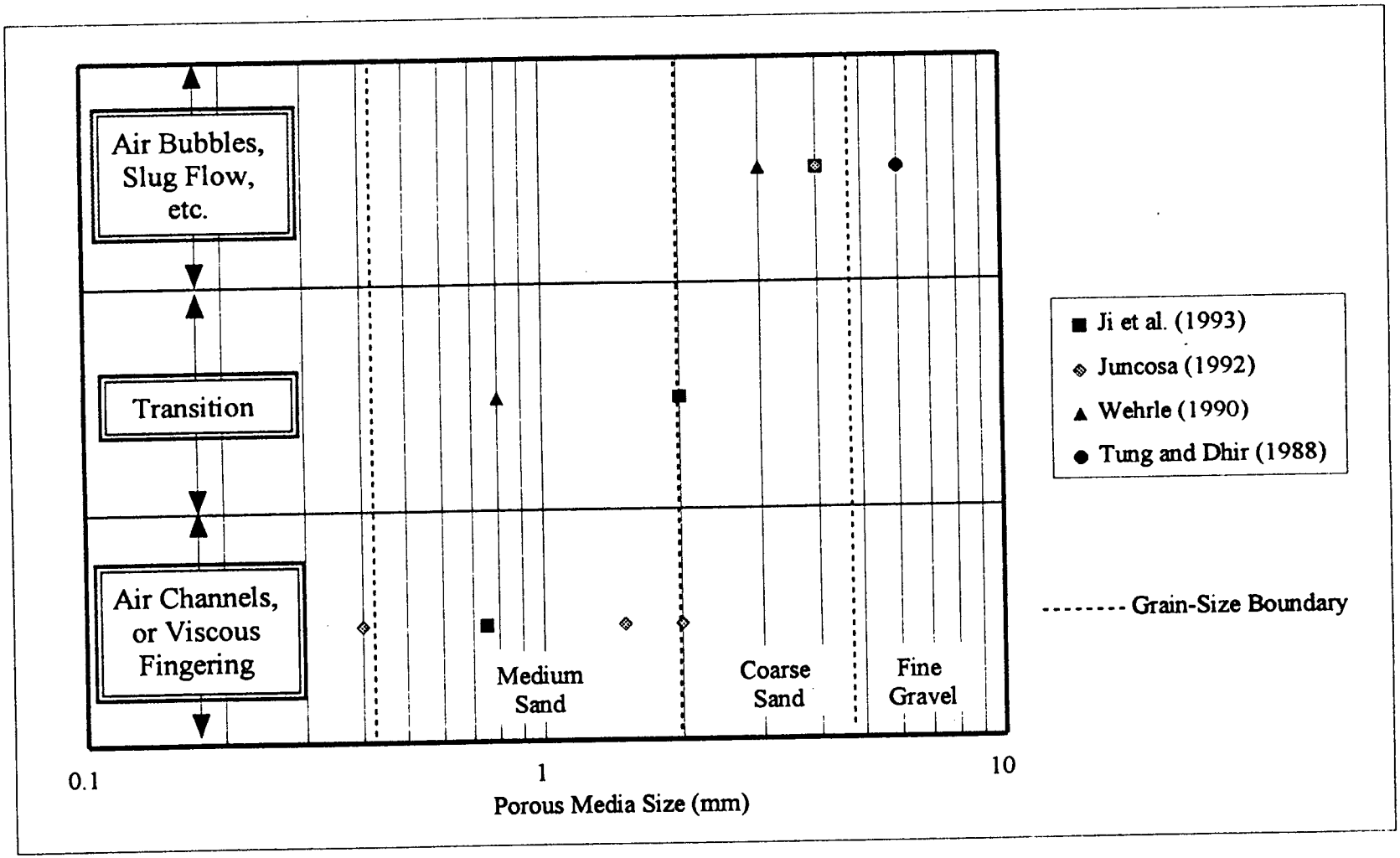

Figure 1 Two-phase flow pattern observations versus porous media size. The grain size classifications are based on the Unified Soil Classification System.

For the wide range of subsurface conditions which may occur, both bubble flow and air channels are possible, and with changing properties within an aquifer, one flow pattern may evolve to the other, or to an intermediate two-phase flow pattern. Furthermore, the flow pattern is primarily a function of the size of the porous media. It is the intent of this work to investigate two-phase flow patterns in porous media, discuss factors affecting the patterns, and present a qualitative tool for predicting the flow patterns resulting from ISAS as a function of porous media size.

THEORY

Since multiple two-phase flow patterns may be possible in porous media, it is important to predict which two-phase flow pattern may exist for a set of subsurface and ISAS operating conditions. Unfortunately, this is not a trivial problem. To begin developing a predictive tool, a review is made of the forces affecting fluids at an air-liquid interface. These include, among others, gravity or buoyancy, pressure, viscous forces, and surface tension or capillary forces (Daugherty et al. pg. 187, 1985). With respect to the movement of NAPL within the subsurface environment, Conrad et al. (1992) stated that the major forces controlling the behavior of organic liquids are capillary forces, viscous forces, and buoyancy forces. Their observations have application in the study of ISAS. The importance of buoyancy and capillary forces in ISAS were stated by Ahlfeld et al. (1994).

To understand the apparent transition in flow patterns which occur at a grain size of 1 to 2 mm, a quantitative investigation of capillary and buoyancy forces was conducted. The general equation which describes the pressure difference across a gas-liquid interface is the Laplace equation of capillarity:

$$P_c = \sigma\left(\frac{1}{r_1}+\frac{1}{r_2}\right) \tag{1}$$

where,

σ = air-water interfacial tension [$M\text{-}T^{-2}$],

r_1 and r_2 = principle radii of curvature [L], and

P_c = capillary pressure [$M\text{-}T^{-2}\text{-}L^{-1}$].

It can be seen from equation (1) that the capillary pressure is inversely proportional to the radii of curvature. Buoyancy forces on an object are equal to the difference between the weight of the fluid displaced by the object and the weight of the object itself (Daugherty et al., pg. 46, 1985). For a gas bubble in a liquid, the buoyancy force, F_b, is defined as:

$$F_b = \left(\frac{4}{3}\pi r_b^3\right) g\Delta\rho \tag{2}$$

where,

r_b = radius of bubble [L],

g = gravitational acceleration [$L\text{-}T^{-2}$], and

$\Delta\rho$ = density difference between the object and the surrounding fluid [$M\text{-}L^{-3}$].

Equation (2) shows the direct relationship between the buoyancy force and the bubble radius. Buoyancy forces and capillary forces can be compared through the use of a dimensionless number called the Bond number (N_B). The Bond number has been used by several researchers to investigate multiphase-flow in porous media (Marrow and Songkran, 1981; Wilson and Conrad, 1984, Pennel et al., 1995). Marrow and Songkran (1981) define the Bond number as:

$$N_b = \frac{\Delta\rho g r^2}{\sigma} \tag{3}$$

where,

r = particle radius [L].

Equation (3) assumes a contact angle of zero, and that r is a measure of the pore space. Capillary forces are dominant if N_B is less than unity, and buoyancy forces are dominant if N_B is greater than unity. Figure 2 shows a plot of N_B versus porous media size for two liquid-gas mixtures: one representing water-air-glass, and the other representing water-air-soil. Values of σ used to create the plot were taken from Corey (1990).

It is suspected that N_B should be approximately unity at the transition zone, which, based on previous work is approximately 1 to 2 mm (Figure 1). Note in Figure 2 that N_B passes through unity at approximately 5 to 6

mm. This suggests one of two possibilities: the buoyancy force is underestimated, or the capillary force is overestimated by the present definition of N_B. The Bond Number in Figure 2 uses the grain size as the value of r in equation (3), thereby approximating the pore space by the porous media particle size. This r represents the spatial dimension for estimating the buoyancy force and the spatial dimension for estimating the capillary force.

The discrepancy between Figures 1 and 2 may be due to the inability of r^2 to characterize both spatial dimensions. Even for porous media composed of a single grain size with uniform packing, the pore space dimensions will vary. Pore spaces can be characterized by larger pore bodies interconnected by smaller pore throats. For example, Conrad et al. (1992) and Chatzis et al. (1983) conducted experiments on the morphology of NAPL residual saturation by injecting an organic liquid (styrene monomer) into a saturated porous media. The organic liquid hardened in place, allowing subsequent analysis on the NAPL blob shape and size. Both papers described shapes corresponding to the concept of a pore space characterized by pore bodies and pore throats. The pore throat dimension will dictate the largest capillary force (see equation (1)), and the pore body dimension will dictate the largest buoyancy force (see equation (2)). Conrad et al. (1992) reported that the pore bodies of NAPL blobs correlated well to the grain size. The ratio of pore throat size to pore body size, referred to as the aspect ratio (Chatzis et al., 1983), ranged from 0.1 to 0.5 in the research with Sevilleta sand by Conrad et al. (1992). The aspect ratio ranged from 0.05 to 0.25 in the research with Berea sandstone by Chatzis et al. (1983). Based on this information, the radius associated with capillary forces should be between 0.05 and 0.5 times smaller than the radius associated with buoyancy forces.

Assuming that a single r value cannot describe the spatial dimension for both the buoyancy and capillary forces, equation (3) can be expanded to reflect the relative influences of the pore throat and pore body sizes (Brooks, 1995):

$$N_B^* = \left(\frac{\Delta\rho g}{\sigma}\right)\left(\frac{r_b^3}{r_c}\right) \tag{4}$$

where,

N_B^* = Modified Bond Number, and

r_c = radius associated with capillary force [L].

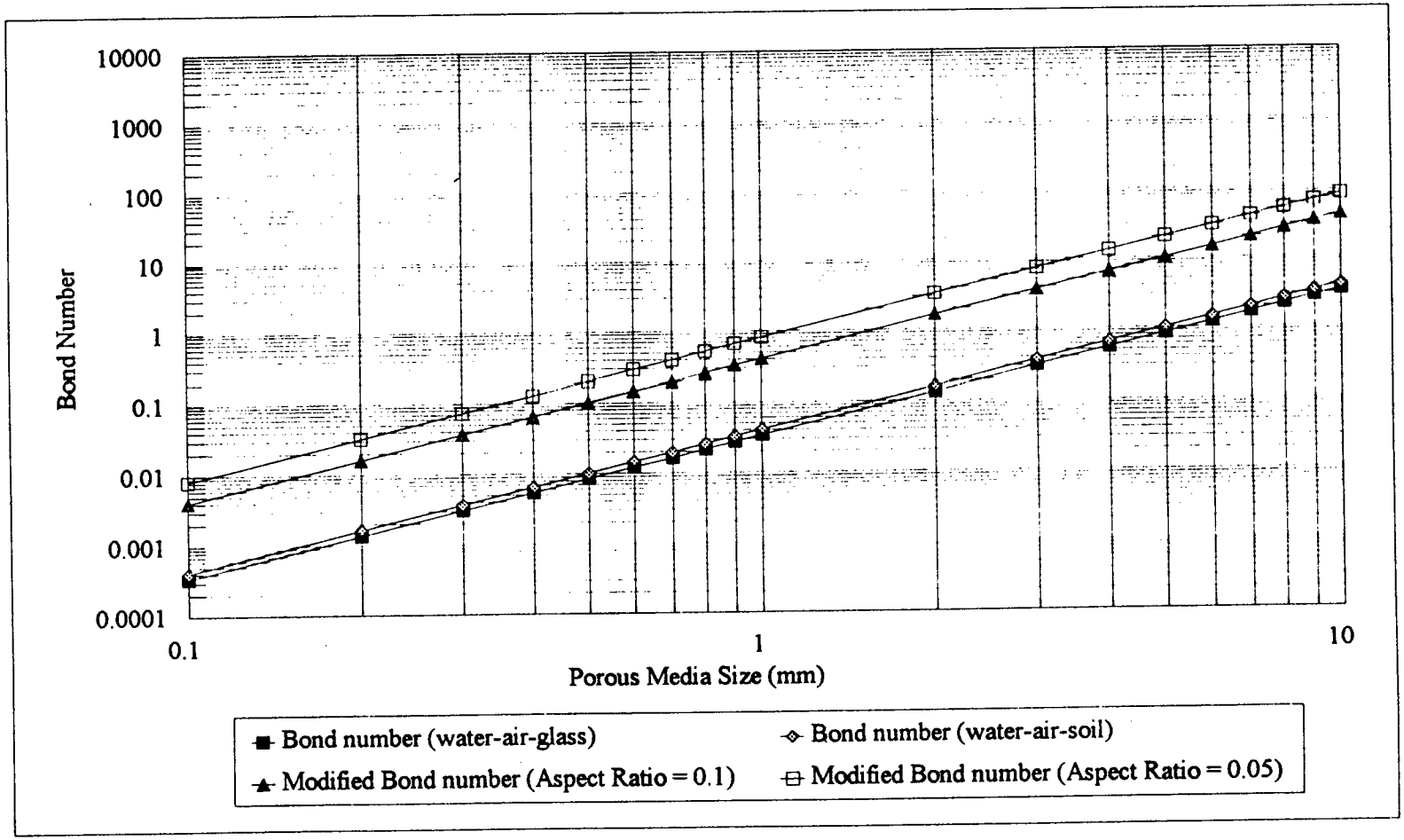

Figure 2 Bond number and Modified Bond number versus porous media size. Surface tension estimates for water- air-glass, and for water-air-soil were taken from Corey (1990). Modified Bond numbers are based on a surface tension for water- air-soil, and use aspect ratios of 0.1 and 0.05.

Based on the observations of Conrad et al. (1992), r_b will be assumed equal to r (the grain size), and r_c is assumed equal to r times the aspect ratio, α. Therefore, the modified Bond number may be defined as:

$$N_B^* = \frac{N_B}{\alpha} = \frac{\Delta\rho g r^2}{\sigma\alpha} \tag{5}$$

Figure 2 also shows the modified Bond number for aspect ratios of 0.1 and 0.05. The modified bond number equals unity around 1 to 2 mm for the aspect ratios used, which corresponds to the transition zone observed in Figure 1. Laboratory experiments were used to characterize air-flow patterns as a function of porous media size in light of this modified Bond number.

METHODOLOGY

The experimental apparatus is illustrated in Figure 3. The air was supplied by a compressor and was controlled by a Speedaire filter/regulator. A pre-sparging chamber was used to water saturate the air to minimize water loss from the sparging column. The sparging column consisted of a borosilicate glass tube, approximately 30 centimeters (cm) long and 6.3 cm in outer diameter (5.3 cm inner diameter). The actual length of the packed sample varied from 28.4 to 28.8 cm due to the rubber stoppers used to cap the ends of the column. Air was injected into the sparging column using a cylindrical diffusing stone, 2.1 cm in diameter with a pore size of 60 microns. A 250 milliliter (mL) graduated cylinder was connected to the column through the bottom stopper. It was used as a reservoir to measure the water level in the column and to measure the displaced water volume from the column. The hydrostatic pressure of the water was also controlled by adjusting the height of the reservoir. A capillary barrier was installed in the stopper connection to the reservoir to prevent air migration into the reservoir; this barrier consisted of a short length of 0.42 to 0.50 mm glass beads. Water manometers were used to measure air pressures at the inlet to the diffusing stone and at the top of the sparging column. The air-flow rate through the column was measured with a Gilmont Instruments compact flow meter (model number 12).

Six glass bead sizes were used in the experiments. The sizes were 0.42 to 0.50 mm, 0.71 to 0.80 mm, 1 mm, 1.5 mm, 2 mm, and 3 mm. The 2 and 3 mm bead sizes were purchased from Fisher Scientific, and the remaining bead sizes were purchased from Cataphote, Inc. All glass beads were initially cleaned by the following protocol to remove possible manufacturing residues which might affect the capillary forces: rinse with water, rinse

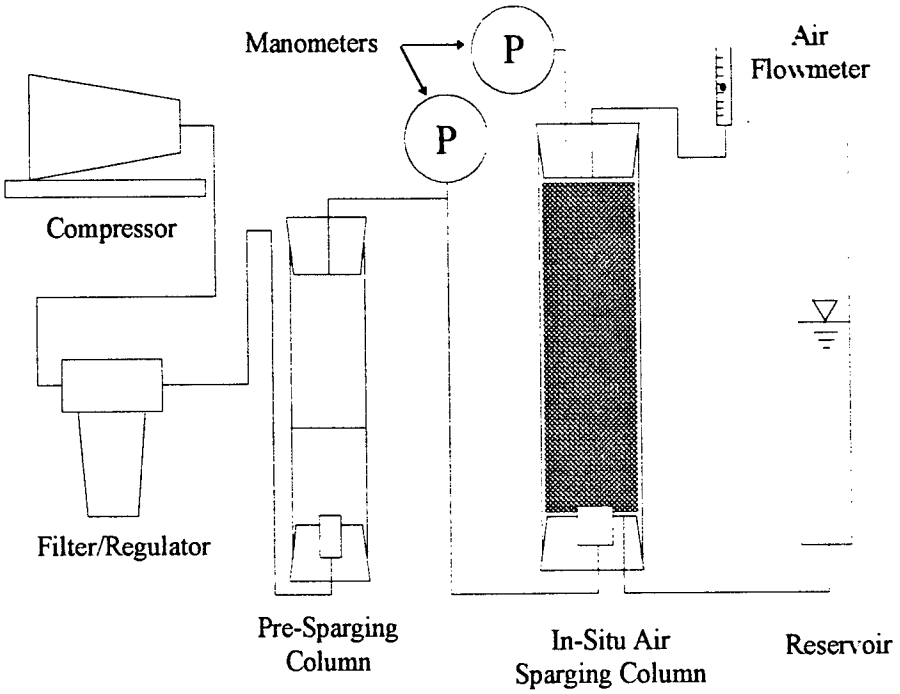

Figure 3 Experimental Apparatus

with hydrochloric acid, rinse with water again, rinse with acetone, allow beads to air dry, rinse with water once more, and finally, heat the beads over night at 105°C. Once cleaned, the beads were packed into the column. The volume of beads to be packed were measured by a volume displacement method. Packing consisted of pouring beads into the column in 2 to 4 cm lifts. Once a lift was poured, a laboratory spatula was used to pierce through the lift and prevent layering effects. A hand held massager was then used to vibrate the column in order to produce a tight pack. Finally, a plunger was used to apply pressure to the lift in an additional effort to produce a tight pack. This procedure was repeated until the entire column was filled. Water was maintained above the top of the beads during packing to avoid trapped air. The total volume of the packed column was calculated by measuring the height of the packed column. The porosity of the packed sample was then calculated using the

volume of the glass beads and the total volume of the packed column.

The range of flow rates were determined by scaling "typical" sparging conditions in the field to the laboratory setup. The scaling was based on assumed field operating conditions of a 10 cubic feet per minute airflow rate, a 20 foot radius of influence, and a 1.5 foot length of screen over which the air exited the injection well. At two boundary areas through which the air flowed, the area immediately around the well and the area at the top of the saturated zone, maximum and minimum air fluxes were estimated, respectively. Using the laboratory sparging column dimensions, the range of flow rates on the laboratory scale were calculated to be between 20 mL per minute (mL/min) and 3,000 mL/min. Due to the experimental apparatus, it was convenient to choose the flow rate as the independent variable, and record all other experimental measurements as a function of the flow rate.

The column was completely saturated after it was packed. Water was then drained from the column until an unsaturated zone developed over approximately one third to one half the column. A reference level was established corresponding to the water table in the column. This reference level was held constant for each experimental run. The initial water volume in the reservoir was recorded. The air was turned on, and slowly increased until a flow rate of approximately 20 mL/min was established. The pressure at the inlet to the diffusing stone, the pressure at the top of the column, the air flow rate, the water level in the reservoir, and the observed flow pattern were then recorded. Descriptions of the patterns were limited to four categories: channel flow, bubble flow, slug flow, and mixed flow. The height of the water level in the reservoir above the reference level was adjusted to equal the pressure reading at the top of the column. This provided control of the water pressure in the column and also prevented excessive desaturation. Several iterations of reservoir adjustment were usually necessary to reached equilibrium conditions. Equilibrium conditions were based on a constant flow rate and an equivalence between the air pressure measured at the top of the column and the height of the water in the reservoir above the reference level. Once equilibrium conditions were reached, the air was slowly turned off. The reservoir was adjusted so the water level was at the same height as the reference mark. The volume of water in the reservoir was then recorded, which was an estimate of the amount of trapped air in the sparging column. The air was turned on again, and the flow rate was increased until the next desired flow was reached. Target flow rates of 80, 200, 500, 1500, and 2000 mL/min were attempted. The same experimental procedures were repeated at each flow rate.

RESULTS AND DISCUSSION

Table 1 summarizes the calculated porosities and the observed flow patterns. The results of pressure and saturation measurements will be presented in later work. The calculated porosities for all glass beads used ranged from 33 to 36 percent. These porosity values fall between a loose cubic packing with a calculated porosity of 47.6%, and a tight rhombohedral packing with a calculated porosity of 26.0% (Bear, 1972, pg. 45). Dullien (1979, pg. 132) reports that close random packing with minimum porosity values of 35.9 to 37.5 have been obtained when packing methods employed vibration.

Visual pattern identification is subjective in nature. In some cases, specific patterns were clearly identified, as in the case of air channels for the smallest porous media size. In other cases, it was difficult to distinguish between trapped air and moving air in air channels, as for the case with the larger bead sizes. Descriptions were limited to one of four choices. Channel flow was used to describe the pattern when areas within the column suddenly desaturated, and remained significantly unsaturated for the duration of the applied pressure. Bubble flow and slug flow were used to describe the patterns characterized by moving bubbles or moving slugs, respectively. The distinction between bubbles/slugs and channels was not always clear. In general, if an area was not significantly resaturated after initial desaturation, then the pattern was labeled channel flow. Mixed flow was used when it appeared that a combination of either bubbles or slugs, and channels were present. All of the observed patterns had a minimal dimension of several grain diameters. For instance, the bubbles observed with the 3 mm porous media where several grain diameters wide.

Flow-pattern observations were made for the two-phase flow as it occurred near the column wall, even for the large porous media. Wall effects prevent tight packing of porous media adjacent to the wall, and produce larger pore spaces. The result is that bubble and slug flow patterns may be produced at the wall, whereas channel flow prevails in the interior of the column. However, for the larger bead sizes, the size of the observed slugs and bubbles, and the ease with which they moved through the media suggest that slug and bubble flow occurred throughout the sparging column.

TABLE 1
EXPERIMENTAL RESULTS

Airflow Rate (mL/min)	Flow Pattern Description	Airflow Rate (mL/min)	Flow Pattern Description
Bead Size : 0.42 to 0.50 mm		**Bead Size : 0.71 to 0.84 mm**	
Calculated Porosity: 36 %		Calculated Porosity: 35 %	
25	Channel Flow	20	Channel Flow
100	Channel Flow	80	Channel Flow
200	Channel Flow	200	Channel Flow
700	Channel Flow	750	Channel Flow
		1475	Channel Flow
		1925	Channel Flow
Bead Size : 1.0 mm		**Bead Size : 1.5 mm**	
Calculated Porosity: 35 %		Calculated Porosity: 34 %	
20	Slug Flow	20	Slug Flow
70	Channel Flow	80	Mixed Pattern
138	Channel Flow	300	Channel Flow
550	Channel Flow	800	Channel Flow
1225	Channel Flow	1450	Channel Flow
1825	Channel Flow	2050	Channel Flow
Bead Size : 2.0 mm		**Bead Size : 3.0 mm**	
Calculated Porosity: 33 %		Calculated Porosity: 35 %	
20	Slug Flow	23	Bubble Flow
90	Slug Flow	75	Bubble Flow
175	Mixed Flow	150	Bubble Flow
450	Mixed Flow	675	Bubble Flow
1150	Channel Flow	1300	Bubble Flow
1625	Channel Flow	2100	Bubble Flow
1850	Channel Flow		
1625	Channel Flow		

Figure 4 presents the observed flow patterns as a function of porous media size. The modified Bond number used to plot the results has an aspect ration of 0.1. As predicted, air channels were dominant for modified Bond numbers less than unity, with a flow transition to slug and bubble flow as the modified Bond number increased above unity. The fact that a transition region was observed over a range of bead sizes from 1 to 2 mm is most likely due to the fact that these porous media sizes have a common distribution of pore spaces, and therefore aspect ratios. The results of these experiments indicate channel flow will occur in porous media less than 2 mm, approximately the size of a medium sand, using the Unified Soil Classification System. The results of this experiment also have implications for ISAS modeling. Darcian-based models have been used to model ISAS processes (Lundegard and Andersen, 1993; Marley et al., 1992b; van Dijke, et al., 1995; Mohtar et al., 1994).

Darcian models are based on the concept of a representative elementary volume (REV). This concept basically assumes that microscopic porous media properties can be described in terms of macroscopic values over some small volume. One such value is the air saturation. Observations during the column experiments question whether an REV concept can be applied to the air saturation. In some instances, high flow rates for example, the air saturation appeared to become sufficiently distributed over the column to apply an REV concept. However, at low flow rates , a large portion of the column remained saturated with water. Care should therefore be used in application of these models to describe all ISAS situations.

CONCLUSIONS

In summary, the air-phase distribution and dynamics during ISAS are complex due to the intricate nature of aquifer material, and the forces controlling multiphase flow in porous media. Multiple air-phase patterns may exist depending on the aquifer characteristics, primarily pore size which is related to soil grain size. A fundamental understanding of these variables is important, however, because of the dependence of mass transfer on the air-phase pattern and distribution. The results of this research provide theoretical support for the conclusion that channel flow will occur in porous media equal to or less than 1 to 2 mm. Other flow patterns, namely bubble and slug flow will occur in media greater than 1 to 2 mm.

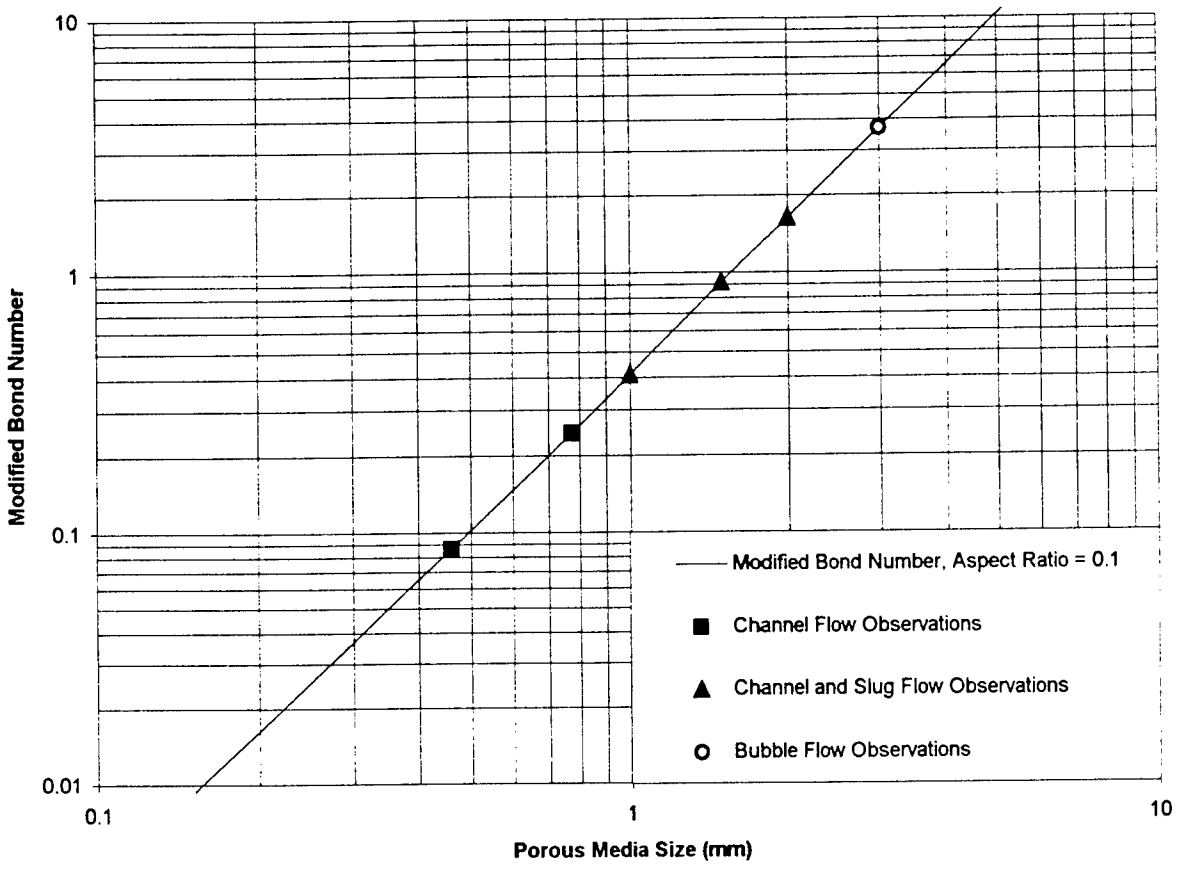
10
1
0.1
0.01
Modified Bond Number
0.1
1
10
Porous Media Size (mm)
Modified Bond Number, Aspect Ratio = 0.1
Channel Flow Observations
Channel and Slug Flow Observations
Bubble Flow Observations

Figure 4

REFERENCES

Acomb, L. J., D. McKay, P. Currier, S. T. Berglund, T. V. Sherhart, and C. V. Benediktsson, Neutron Probe Measurements of Air Saturation Near an Air Sparging Well, in *In Situ Aeration: Air Sparging, Bioventing, and Related Remediation Processes*, edited by Hinchee, R. E., R. N. Miller, and P. C. Johnson, Battelle Press, Columbus, 47-61, 1995.

Ahlfeld, D. P., A. Dahmani, and W. Ji, A Conceptual Model of Field Behavior of Air Sparging and Its Implications for Application, *Ground Water Monitoring and Remediation*, 14(4), 132-139, 1994.

ASTM, *Annual Book of ASTM Standards, Section 4 Construction, Volume 04.08 Soil and Rock; Dimension Stone; Geosynthetics*, ASTM, Pennsylvania, 1993.

Ardito, C. P. and J. F. Billings, Alternative Remediation Strategies: The Subsurface Volatilization and Ventilation System, in *Proceedings of the Conference on Petroleum Hydrocarbons and Organic Chemicals in Ground Water: Prevention, Detection, and Restoration*, National Water Well Association, Dublin Ohio. 281-296, 1990.

Bear, J., *Dynamics of Fluids in Porous Media*, Dover Publications, New York, 1988.

Brooks, M. C., *Groundwater Remediation by In-Situ Air Sparging*, Masters Thesis, Auburn University, Auburn, Al., August 1995.

Brown, R. A. and R. Fraxedas, Air Sparging - Extending Volatilization to Contaminated Aquifers, in *Proceedings of the Symposium on Soil Venting, Houston, Texas, April 29 - May 1*, 249-269, 1991.

Brown, R. A. and F. Jasiulewics, Air Sparging: A New Model for Remediation, *Pollution Engineering*, 24(13), 52-55, 1992.

Brown, R. A., C. Herman, and E. Henry, The Use of Aeration in Environmental Clean- ups, in *Haztech International Pittsburgh Waste Conference, Pittsburgh, Pa., May 14-16*, 2A-1 to 2A-42, 1991.

Chatzis, I., N. R. Morrow, and H. T. Lim, Magnitude and Detailed Structure of Residual Oil Saturation, *Society of Petroleum Engineers Journal*, 23(2), 311-326. 1983.

Conrad, S. H., J. L. Wilson, W. R. Mason, and W. J. Peplinski, Visualization of Residual Organic Liquid Trapped in Aquifers, *Water Resources Research*, 28(2), 467-478, 1992.

Corey, A. T., *Mechanics of Immiscible Fluids in Porous Media*, Water Resources Publications, Colorado, 1990.

Daugherty, R. L., J. B. Franzini, and E. J. Finnemore, *Fluid Mechanics with Engineering Applications*, 8th ed., McGraw-Hill Book Company, New York, 1985.

van Dijke, M. I. J., S. E. A. T. M. van der Zee, and C. J. van Duijn, Multi-phase Flow Modeling of Air Sparging, *Advances in Water Resources*, 18(6), 319-333, 1995.

Dullien, F. A. L., *Porous Media Fluid Transport and Pore Structure*, Academic Press, Inc., San Diego. 1979.

Ji, W., A. Dahmani, D. P. Ahlfeld, J.D. Lin, and E. Hill III, Laboratory Study of Air Sparging: Air Flow Visualization, *Ground Water Monitoring and Remediation, 13 (4), 115-126, 1993.*

Johnson, R. L., P. C. Johnson, D.B. McWhorter, R.E. Hinchee, and I. Goodman, An Overview of In Situ Air Sparging, *Ground Water Monitoring and Remediation*, 13(4), 127-135, 1993.

Juncosa, S. G. T., *Removal of Benzene and TCE form Water and Soil by Air Sparging*, Master's Thesis, University of Massachusetts-Lowell, Lowell, Ma., April 1993.

Kerfoot, W. B., *KVA Analytical Systems Technical Publication #85, Injection Points for Sandy Soil Sparging Systems*, KVA Analytical Systems, Falmouth, Massachusetts, 1992.

Kerfoot, W. B., and D. R. Evans, Zone Control for Spargepoint™ Groundwater Treatment Systems, in *Proceedings of the Seventh National Outdoor Action Conference and Exposition*, pp. 715-722, National Ground Water Association, Dublin, Ohio, 1993.

Leeson, A., R. E. Hinchee, G. L. Headington, and C. M. Vogel, Air Channel Distribution During Air Sparging: A Field Experiment, in *In Situ Aeration: Air Sparging, Bioventing, and Related Remediation Processes*, edited by Hinchee, R. E., R. N. Miller, and P. C. Johnson, Battelle Press, Columbus, 214-222, 1995.

Loden, M. E., *A Technology Assessment of Soil Vapor Extraction and Air Sparging*, U.S. EPA Office of Research and Development, EPA/600/R-92/173, 1992.

Lundegard, P. D., and G. Andersen, Numerical Simulation of Air Sparging Performance, *Proceedings of the Conference on Petroleum Hydrocarbons and Organic Chemicals in Ground Water: Prevention, Detection, and Restoration,* National Ground Water Association, Ohio, 281-296, 1993.

Lundegard, P. D. Actual Versus Apparent Radius of Influence - An Air Sparging Pilot Test in a Sandy Aquifer, *Proceedings of the Petroleum Hydrocarbons and Organic Chemicals in Ground Water: Prevention,*

Detection, and Remediation, National Ground Water Association. Ohio. 1994.

Marley, M. C., Air Sparging in Conjunction with Vapor Extraction for Source Removal at VOC Spill Sites. Presented at the *Fifth National Outdoor Action Conference, Las Vegas, Nevada, May 13-16*, 89-101, 1991.

Marley, M. C., D. J. Hazebrouck, and M. T. Walsh, The Application of In Situ Air Sparging as an Innovative Soils and Ground Water Remediation Technology, *Ground Water Monitoring Review*, 12(2), 137-144, 1992a.

Marley, M. C., F. Li, S. Magee, and D. E. Medina, Application of Models in the Design of Air Sparging Systems, in *Proceedings of HMC Superfund 92, HMCRI 13th Annual Conference and Exhibition, SARA-RCRA-ITSWA-CAA-CWA, Washington, D.C., December 1-3*, 853-857, 1992b.

Middleton, A. C., and D. H. Hiller, In Situ Aeration of Groundwater - A Technology Overview, Presented at *A Conference on Prevention and Treatment of Soil and Groundwater Contamination in the Petroleum Refining and Distribution Industry, Montreal, Quebec. October 16 and 17*, 13.0-13.14, 1990.

Mohtar, R. H., R. B. Wallace, and L. J. Segerlind, Finite Element Simulation of Oil Spill Cleanup Using Air Sparging, *Computational Methods in Water Resources*, 2, 967-974, 1994.

Morrow, N. R., and B. Songkran, Effect of Viscous and Buoyancy Forces on Nonwetting Phase Trapping in Porous Media. In *Proceedings of a Symposium on Subsurface Phenomena in Enhanced Oil Recovery*, Stockholm, Sweden. August 20 - 25, 387 - 410, 1979.

Pankow, J. F., R. L. Johnson, and J. A. Cherry, Air Sparging in Gate Wells in Cutoff Walls and Trenches for Control of Plumes of Volatile Organic Compounds (VOCs), *Ground Water*, 31(4), 654-663, 1993.

Pennel, K. D., G. A. Pope, and L. M. Abriola, Influence of Viscous and Buoyancy Forces on the Mobilization of Residual Tetrachloroethylene During Surfactant Flushing, submitted for publication in *Environmental Science & Technology*, July, 1995.

Roberts, L. A., and D. J. Wilson, Groundwater Cleanup by *in-situ* Sparging. III. Modeling of Dense Nonaqueous Phase Liquid Droplet Removal, *Separation Science and Technology*, 28(5), 1127-1143, 1993.

Sellers, K. L., and R. P. Schreiber, Air Sparging Model for Predicting Groundwater Cleanup Rate, in *Proceedings of the Conference entitled Petroleum Hydrocarbons and Organic Chemicals in Ground Water: Prevention, Detection and Restoration, Eastern Regional Ground Water Issues, November 4-6, 1992, The*

Westin Galleria, Houston, Texas, pp. 365-376, 1992.

Tung, V. X., and V. K. Dhir, A Hydrodynamic Model for Two-Phase Flow Through Porous Media, *International Journal of Multiphase Flow*, 14(1), 47-65, 1988.

Wehrle, K., In Situ Cleaning of CHC Contaminated Sites: Model-Scale Experiments Using Air Injection (In Situ Stripping) Method in Granular Soils. in *Contaminated Soils '90*, edited by Arenak, F., Hinsenveld, M. and van den Brink, W. J. Kluwer Academic Publishers, Netherlands, 1061-1062, 1990.

Wilson, D. J., S. Kayano, R. D. Mutch, and A. N. Clarke, Groundwater Cleanup by *in-situ* Sparging. I. Mathematical Modeling, *Separation Science and Technology*, 27(8&9), 1023-1041, 1992.

Wilson, D. J., Groundwater Cleanup by *in-situ* Sparging. II. Modeling of Dissolved Volatile Organic Compound Removal, *Separation Science and Technology*, 27(13), 1675-1690, 1992.

Wilson, J. L., and S. H. Conrad, Is Physical Displacement of Residual Hydrocarbons a Realistic Possibility in Aquifer Restoration?, *In Proceedings of the NWWA/API Conference on Petroleum Hydrocarbons and Organic Chemicals in Ground Water- Prevention Detection and Restoration*, pp. 274-298, National Water Well Association, Dublin, Ohio, 1984.

Application of a Distribution-Based Assessment of Mission Readiness System for the Evaluation of Personnel Training

David J. Woehr
Associate Professor
Department of Psychology

Texas A&M University
College Station, TX

Final Report for:
Summer Research Extension Program
Armstrong Laboratory

Sponsored by:
Air Force Office of Scientific Research
Bolling AFB, Washington, DC

and

Armstrong Laboratory

December 1996

Application of a Distribution-Based Assessment of Mission Readiness System for the Evaluation of Personnel Training

David J. Woehr, Ph.D.
Associate Professor
Department of Psychology
Texas A&M University

Abstract

The present study summarizes a research project focusing on ways to improve the usefulness of organization level outcome measures of unit readiness/effectiveness. Toward this goal, numerous aircraft maintenance related measures of performance were identified and evaluated. In addition, a measurement approach using unit level outcome measures is presented. The measurement system presented adapts and extends the performance distribution assessment approach proposed by Kane (1986; 1992). It is demonstrated that, while originally used with subjective performance judgments, the system is readily adapted to regularly collected unit level outcomes.

An important characteristic of the measurement system presented is a focus on the range of performance observed. Specifically this approach stipulates that not only is the level of performance important, but the fluctuation or variability in performance must also be considered. In addition, the system incorporates a relativistic scaling of performance information. That is, performance is expressed as a ratio of measured performance to some 'benchmark distribution'. This benchmark distribution may represent established standards, expected, or previously attained levels of performance. This scaling process serves to express actual performance in terms relative to some previously established range of performance.

The representation of performance in distributional form along with relativistic scaling has several important advantages to traditional measurement approaches. First, it allows for a consideration of performance variability as well as average levels of performance. Thus, it allows for an assessment of the consistency of performance and the extent to which negatively valued outcomes are avoided. Second the relativistic scaling process provides measures of the effectiveness of performance on 0-100% scales. This serves to facilitate the comparison and combination of data across diverse performance measures.

The current study presents a demonstration of the proposed measurement system with aircraft maintenance data. Preliminary results indicate that this approach does in fact have the potential to improve the utility of organization level criterion measures.

Application of a Distribution-Based Assessment of Mission Readiness System for the Evaluation of Personnel Training

David J. Woehr, Ph.D.

Introduction

A vital concern for the Air Force is the maintenance of mission capability and readiness. A crucial mechanism for the maintenance of mission readiness is personnel training. There is little, if any, dispute that effective personnel training serves to enhance the effectiveness and capability of the Air Force in general. This fact is reflected in the overwhelming scope of training conducted throughout the Air Force and the tremendous amount of time and resources committed to the training endeavor.

Of tremendous importance to the design, implementation, and revision of training throughout the Air Force, as with any organization, is the ability to evaluate the effectiveness of training interventions. Goldstein (1991) defines training evaluation as: "the systematic collection of descriptive and judgmental information necessary to make effective training decisions related to selection, adoption, value, and modification of various instructional activities." (p. 557) More specifically, the effective evaluation of any training intervention is crucial to informed decision making regarding the intervention. Central to effective training evaluation is the standard or criteria against which the training is evaluated. In addition, the comprehensive evaluation of training interventions mandates the use of multiple criterion measures. The impact of training interventions must be assessed at different levels (e.g., person, work group, organization). Unfortunately, organization level outcome measures are often dismissed as criterion measures due to contamination by extraneous aspects of the work environment. Despite this limitation, the use of these measures is extremely important for demonstrating the utility of training interventions.

Organization Level Criterion Measures

Organization level outcome measures represent global indices of effectiveness. While many commonly used criterion measures focus on the assessment of individual effectiveness, organization level measures often provide more aggregate measures of effectiveness. They typically include results-oriented measures such as quality control indices,

productivity or maintenance indices, promotion rate, salary progression or level, and turnover rates. The value of these measures as criterion measures is somewhat controversial. Two schools of thought can be found in the literature with respect to ways of conceptualizing the criterion construct. One school of thought emphasizes a conceptualization of performance as reflected in overt individual behaviors (e.g., Campbell, et al. 1970; Borman, 1983). This view focuses on the identification of behavioral regularities important to organizational functioning. The other school of thought focuses on outcomes. This view emphasizes the importance of outcomes and results to organizational functioning. Recent theories of the criterion construct, however, have begun to recognize the inextricable relationship between job behaviors and outcomes. Along these lines Binning and Barrett (1989) argue: "... optimal description of the performance domain for a given job requires careful and complete delineation of valued outcomes and the accompanying requisite behaviors" (p. 486).

Problems with Outcome-Based Criterion Measures

The detailed conceptual delineation of the relationship between job performance and outcomes is especially relevant to training evaluation. An important direction for future research is a focus on behavior/outcome linkages and generating empirical support for these linkages. Unfortunately, the operationalization of specific outcome measures generates somewhat of a dilemma for training evaluation. On the one hand, the ultimate value of training lies in its ability to impact outcomes of value to the organization. Outcome measures (e.g., productivity levels, turnover rates, error rates, etc.) at both individual and aggregate levels would appear to be the ultimate criterion of interest for evaluating training interventions. On the other hand, these measures suffer from a number of problems that limit their usefulness as a standard against which to judge the impact of training.

First and foremost among these problems is the fact that these measures are typically contaminated to an undetermined extent by sources of variance over which the individual has no control. Specifically, the measured outcome is to some extent determined by factors other than individual performance. A second problem with outcome measures is that they are not based on a common metric. Outcome measures are often unique to particular units within an organization and thus are difficult to interpret and compare across organizational work groups or divisions. Additionally, the lack of a common metric typically precludes the meaningful aggregation of performance information across organizational units. A third problem is that these measures only provide an indication of outcome as opposed to

the process underlying the outcome. Thus these measures provide little, if any, information about the nature of performance. Finally, the traditional use of outcome measures offers little, if any, means of assessing measurement quality (i.e., how good are the measurements obtained with these measures).

Another major limiting factor with respect to the use of organizational level outcome measures is the lack of conceptual and/or empirical formulations specifying the potential linkages between personnel action and specific outcome measures. For example, if the goal is to evaluate the impact of a particular training program with respect to organizational outcomes, it is important to match the nature and content of the training with specific outcome measures likely to be influenced. If the training program focuses on improving maintenance skills then measures most directly related to maintenance outcomes should be identified and examined. While there may be numerous outcome measures available, little if any information exists pertaining to the performance relevance of these measures.

Thus, although regularly collected and typically readily available, as a criterion against which to judge the impact of various training interventions in organizations, outcome measures have not proven as useful as criteria which are defined in terms of individual behavior. Despite this, however, the use of these measures is extremely important for demonstrating the ultimate utility of training interventions. Consequently, an important goal with respect to training evaluation is the development of ways to improve the utility of organization level criterion measures.

In summary, while organizational level outcome measures are a potentially valuable criterion against which to evaluate training effectiveness, several factors have limited the utility of these measures. These factors include: a) contamination by non-performance related factors; b) lack of a common measurement metric; c) a focus on overall level rather than the performance process; d) lack of any indication of measurement quality; and, e) no conceptual/empirical formulations of the linkage between specific actions and outcomes. Thus, any system that uses outcome measures must address these issues.

Identification of Aircraft Maintenance Related Measures of Performance

One of the primary objectives of the present study was to identify and examine the utility of aircraft maintenance related measures of performance typically collected and used by the Air Force. Measures of performance (MOPs) are qualitative or quantitative measures of system capabilities or characteristics (USAF/TEP, 1994) Toward this end, several sources of data were identified through interviews with supervisory level maintenance personnel. One source of

such data was a combination of CAMS- based maintenance data and unit mission characteristic data. This data is routinely collected and reported by aircraft maintenance units as an index of mission effectiveness. This data takes into consideration both equipment and unit mission and manpower characteristics. Example measures include fully mission capable rate, man hours per flying hours, air and ground abort rates, etc. Table 1 presents specific examples of these measures. A complete listing of the actual measures identified is presented in Appendix A.

Table 1
Sample Maintenance Related Measures of Performance

MEASURE	DEFINITION	FORMULA
Awaiting Maintenance Rate	AWM is a deferred discrepancy that is a repair that cannot be accomplished within 5 days of the original write-up.	# of AWM / # of poss acft X 100
Chargeable Deviations	Number of inspection discrepancies	based on actual count
Fix Rate	# of aircraft that return with inoperable systems & must be returned to MC status within a specified amount of time	# 4/8/12 hour fixes / total # of code 3 breaks
Fully Mission Capable Rate	% of aircraft possessed hrs that were fully mission capable for a unit over a specified period of time	FMC / avg. possessed hours x 100
Man Hour Per Fly Hour	all flying hour categories totaled	man-hours / total flying hours
Repeat Rate	Repeat = the same system malfunctioning on the next flight.	# repeats / local sorties flown x 100

One question with respect to these measures is the degree to which these measures are routinely collected and reported. Quality assurance and summary aircraft performance reports were examined for three different fighter wings. Appendix B indicates which of the MOP's presented in Appendix A are currently reported in the summary reports. Appendix B indicates considereable overlap across the three wings. It is also likely that the measures not currently reported are collected and available for analysis.

Another concern with respect to these measures is that any information derived may be severely limited in that the data might reflect expected levels and/or standards rather than actual performance. If this were the case very little variability in these measures would be expected across units and time frames and their usefulness as criterion measures would be minimal. However, examination of actual data pertaining to these measures indicates that there is in fact sufficient variability to warrant further investigation into the differences across units. Table 2 provides a small sample of a much larger set of actual data collected in the present study for the measures presented in Table 1. This data represents summary information for one fighter wing across 2 fiscal years.

Table 2
Data Sample for Maintenance Related Operational Measures

	FY '94				FY '95			
MEASURE	**MEAN**	**SD**	**MIN**	**MAX**	**MEAN**	**SD**	**MIN**	**MAX**
Awaiting Maintenance Rate	3.57	5.80	1.08	42.85				
Chargeable Deviations	19.70	9.20	3.00	48.00	18.70	18.70	1.00	67.00
Fix Rate	88.35	6.60	73.07	100.00	91.24	6.50	75.00	100.00
Fully Mission Capable Rate	88.46	3.9	78.02	96.87	84.61	6.90	63.32	96.11
Man Hour Per Fly Hour	5.82	3.8	0.30	28.70	5.97	2.40	0.70	21.50

Although a valuable source of information with respect to mission capability, these measures illustrate many of the disadvantages associated with operational measures. For example, the metric of each measure is unique to the characteristic being measured. Thus the data are difficult to combine and summarize across measures. Further, the measures are cumbersome to summarize. That is, while the measures lend themselves to typical overall summations such as mean performance level, such measures of central tendency only provide part of the overall picture. Other

important information including the amount of fluctuation and the percent of time at or above some preset standard is typically not presented in any summary metric.

Despite these limitations, the indices presented in Appendix A have many desirable characteristics with respect to training evaluation. These characteristics include:

1. The measures are regularly and systematically collected.
2. It appears that these indices are both required by and reported to MAJCOM. Thus it is likely that these measures are available Air Force wide.
3. The mission capable/readiness indices reflect both equipment, mission, and manpower characteristics.
4. The indices are easily aggregated from the individual unit level to higher levels of the organization (wing, command, etc.).
5. The indices reflect multiple measures of performance within a specified time span (iterated job function) and thus are readily amenable to the distribution-based measurement system (presented below).

In summary, numerous maintenance related measures of performance were identified. These measures represent organizational level outcomes that provide an indication of system performance. Further, these measures are routinely collected and reported and thus are a potentially valuable source of information for the evaluation maintenance related training programs.

A Distributional Approach to Criterion Measurement

A second objective of the present study was to develop and evaluate a measurement system that increases the utility of regularly collected operational measures of performance. Toward this end a specific measurement system is presented. The measurement approach presented here extends the system for assessing individual performance developed by Kane (1986) to outcome level criteria measurement. It is believed that this approach may offer a partial solution to the problems associated with outcome measures. The original system presented by Kane (1986), labeled Performance Distribution Assessment (PDA), is based on the distributional measurement model postulated by Kane and Lawler (1979). An important characteristic of this model is a focus on the range of performance observed. Specifically, the model stipulates that not only is the level of performance important, but the fluctuation or variance in performance

must also be considered. For example, two individuals may both be appropriately characterized as "average performers"; however, if one is consistently average and the other alternates between very poor and very good, very different pictures emerge with respect to the individuals' performance. Thus performance measurement must assess the range of performance over time. Specifically, performance is defined in terms of the outcomes of job functions that are carried out on multiple occasions within a specified time span (i.e., iterated job functions). It is expected that, due to varying levels of individual ability and motivation as well as varying levels of external constraints, these outcomes will reflect different levels of effectiveness. Performance can subsequently be represented in terms of the frequency at which various outcome levels occurred within a given time span.

Another important characteristic of the PDA approach is that it incorporates a relativistic scaling of performance information. More specifically, performance is expressed as a ratio of actual performance (as reflected in the performance distribution generated) to a maximum feasible performance distribution. This maximum feasible distribution reflects the highest level of performance attainable given the constraints under which the work occurs. This scaling process serves to express performance in terms of a relative range of potential performance. Thus, the method allows for quantifiably excluding from consideration in the evaluation of performance the range of performance that is attributable to circumstances beyond the performer's control.

The representation of performance in distributional form along with relativistic scaling has several important advantages. First, it allows for a consideration of performance variability as well as average levels of performance. Thus it allows for an assessment of the consistency of performance and the extent to which negatively valued outcomes are avoided. In this way more information is provided regarding the idiosyncratic nature of performance. Second, the relativistic scaling process advocated by the PDA process produces measures of the effectiveness of performance on relativized 0-100% scales with common zero and common upper limits of 100%. Thus any given percentage level remains constant in its meaning regardless of the job, division, or even the organizational level in which it occurs. At the same time, the particular outcome measures used to assess performance may be individualized to meet situational demands and organizational constraints. Specifically, if positions have appreciably different content and extraneous-constraint conditions, measures can be scaled to account for these differences.

The PDA approach was originally advocated as method for enhancing individual performance ratings. Specifically, it was formulated to incorporate subjective estimates of individual performance outcome frequencies (i.e., supervisory

ratings of the frequency at which individuals performed at a particular level). However, it's focus on the frequency of particular performance outcomes make it particularly amenable to use with more objective outcome measures. Thus, the application of this methodology to the measurement of organizational outcomes using iterative operational measures appears to be a fruitful avenue for research and may serve to increase the utility of these measures in the training evaluation process.

Table 3
Sample Performance Level Frequencies and Distributional Characteristics for the Man Hour per Fly Hour Measure

Performance Frequencies

Perf. Level	Perf. Range	Utility Weights	Perf. Level Freq.	Perf. Level %	Comparison Level %
1	28.70	-100	0	0	0
2	21.60	-50	1	8	1
3	14.50	0	2	15	10
4	7.40	50	9	69	80
5	.30	100	1	8	9
		Total Obs. =	13		

Distribution Characteristics

	Utility Wt. Scale	Perf. Level Scale
Mean =	38.46	3.77
SD =	34.83	0.70
Skewness =	-1.02	-1.02
Kurtosis =	1.19	1.19
Negative Range Score =	-3.85	
Total Perf. Effectiveness	85.09	

Adaptation of the PDA Approach for Outcome Level Measures

As noted above, the PDA system appears to be well suited for the measurement and scaling of operational criterion measures. For purposes of illustration, Table 3 presents hypothetical evaluation data, presented in PDA format, for the man hour per fly hour MOP. In Table 3 the performance range represents 5 equidistant steps between the highest (best) possible performance outcome (listed as .30 in the Table) and the lowest (worst) performance level (listed as 28.70 in the Table) for the man hour per fly hour measure. These levels represent the lowest and highest (respectively) number of man hours required per fly hour for the wing across the 2 fiscal years. The performance level frequencies are based on an actual count of man hour per fly hour outcomes each month over the course of 1 fiscal year. The utility weights

represent the utility or value to the organization of performance at each of the 5 levels. In the present example, these are hypothetical values. In actuality these weights would be based on SME estimates. The comparison level values represent a "benchmark" distribution. This "benchmark" distribution may represent either an estimated ideal distribution of performance or the actual performance distribution of a comparison unit (i.e., an earlier time frame or another work unit).

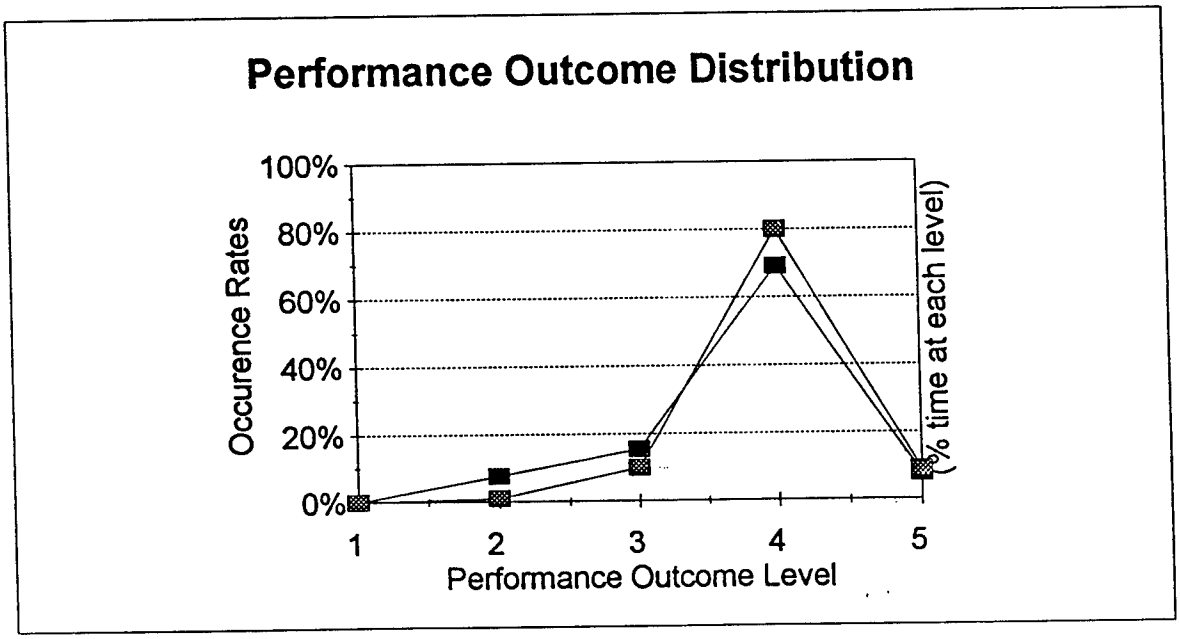

Figure1: Graphical representation of the actual and comparison performance distributions.

Figure 1 shows the relationship between the two performance distributions represented by the actual performance values and the comparison level. Based on this information distributional characteristics for the actual performance values are presented (the "Distributional Characteristics" in Table 3). These characteristics may be expressed in either the utility weight metric or the performance level scale.

An important component of the distributional assessment system presented here is that it provides an overall index of performance that takes into account the level, variability, and utility of performance over time. The total performance effectiveness score (TPE) represents a quantitative index, in a percentage metric, of the proximity of the actual distribution to the comparison distribution. The TPE index is calculated as:

$$TPE = \frac{[\sum_{i=N}^{2} [A_i - (C_i + I_i)]^2 W_i]^{\frac{1}{2}}}{[\sum_{i=N}^{2} [C_i + I_i)^2 W_i]^{\frac{1}{2}}}$$

where:

N = the number of steps or levels in the performance continuum with the Nth level representing the highest level of performance

A_i = the actual occurrence rate observed for the ith level of the performance continuum

I_i = the occurrence rate for the ith level of the comparison performance distribution

C_i = the difference between the sums of the actual and comparison occurrence rates for all levels above the

W_i = the utility weight for the ith level of the performance continuum.

The TPE index specifies one minus the ratio of the observed distance between the actual and comparison distributions and the maximum distance possible. It encompasses all variation present in the actual distribution of performance across all levels of performance. Thus it represents a suitable summary measure of performance. Scores on the index range from 0 to 100 and are comparable across measures and units.

This revised approach to the performance distribution model is labeled here as Distribution-Based Evaluation and Assessment of Mission Readiness (DEAMR). This approach extends the beneficial characteristics of relative distribution based performance assessment to organization level outcome measures. More specifically, characteristics of the DEAMR process include:

1. Performance measurement is relativistic. Outcome measures are scaled relative to maximum possible and minimum acceptable performance levels. Performance distributions are relative to some "benchmark" distribution. Thus, measurement considers the extraneous factors that may influence outcome measures.
2. Performance measurement is based on common metric. All measures are expressed in terms of percentages and thus have minimum and maximum points.
3. Multiple measures of performance are provided; performance is described in terms of mean level, consistency, and negative range avoidance. These multiple measures provide more information about the nature of performance and performance problems.

Another important characteristic of the DEAMR system is that it is easily automated. Relatively little data is required in order to calculate the distributional parameters. This data required includes the highest possible and lowest acceptable performance level, an estimate of the utility weight associated with the lowest acceptable performance level, and the actual frequency of performance outcomes at each of the performance levels. Figure 2 represents the output of a spreadsheet based program specifically designed to provide distributional performance information. The highlighted boxes indicate where data must be input into the program. Performance distribution information is then automatically calculated and displayed both numerically and graphically.

Using DEAMR for Training Evaluation

The mission capability/readiness indices discussed above represent viable potential criterion measures for the evaluation of training effectiveness at the outcome level. Further this data meets the requirements for use with the DEAMR system. Thus it is possible to rescale the data in distributional form. The DEAMR format could then be used to evaluate the effectiveness of specific training interventions.

While the measures identified generally provide a potentially valuable source of information with respect to training evaluation, it is important to consider the further refinement of the data. More specifically, it would be beneficial to

Distribution Characteristics Calculations for:

Unit: "Sample"

Measure: Man Hour Per Fly Hour

Perf. Level	Perf. Range	Utility Weights	Perf. Level Frequency	Perf. Level %	Comp. Level %
1	28.70	-100.00	0.00	0.00	0.00
2	21.60	-50.00	1.00	0.08	0.01
3	14.50	0.00	2.00	0.15	0.10
4	7.40	50.00	9.00	0.69	0.80
5	0.30	100.00	1.00	0.08	0.09
		Total Obs =	13.00	1.00	

Distribution Characteristics	Utility Wt. Scale	*PL Scale*
Mean =	38.46	3.77
SD =	34.83	*0.70*
Skewness =	-1.02	*-1.02*
Kurtosis =	1.19	*1.19*
Negative Range Score =	-3.85	
Total Performance Effectivenes	85.09	%

Step 1 Enter min and max performance levels

Step 2 Enter min. and max utility weights

Step 3 Enter freqs. for each perf. level

Perf level % are calculated

Distributional are

Characteristics calculated

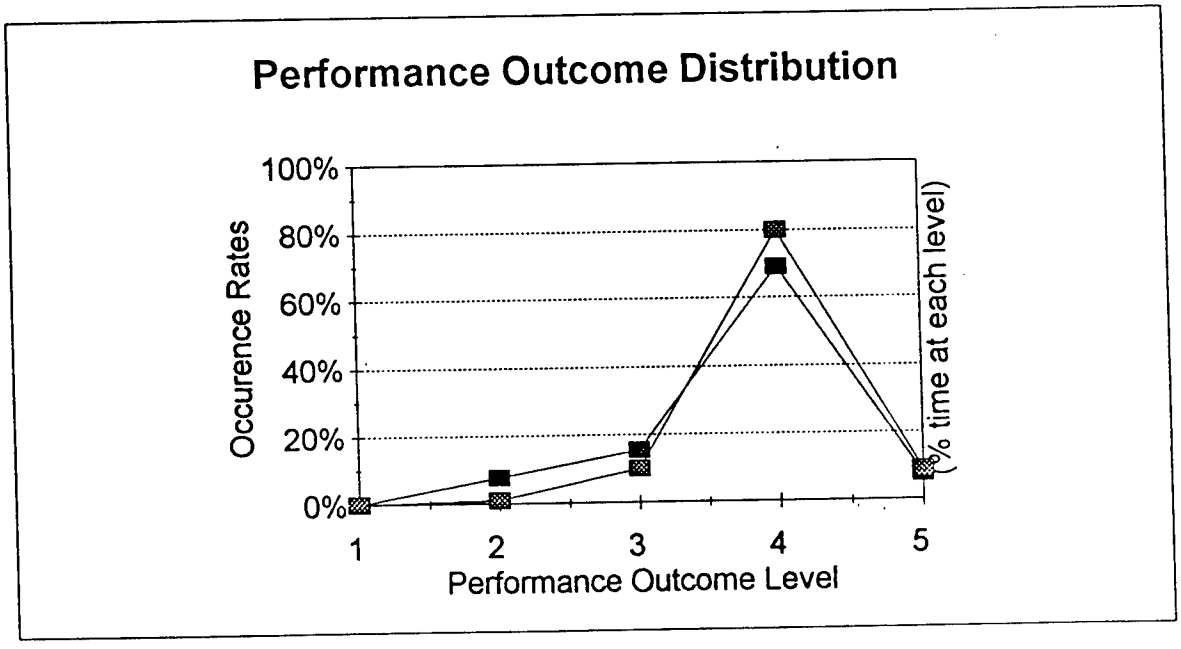

Figure 2: Spreadsheet-based program designed to input MOP data and calculate distributional characteristics

establish a pool of potential indices most relevant to specific training interventions to be evaluated (e.g.,maintenance indices for maintenance technician training). Here it is important to identify and evaluate key measures from the larger pool of potential measures. The focus of this measure evaluation would be to identify indices that are: a) important to unit effectiveness, b) frequently and reliably collected, c) sensitive to individual performance, d) relatively insensitive to system variables, and e) relevant to training intervention. Information about outcome indices may be obtained through either SME workshops or through structured questionnaires. SME's would be used to provide information about each potential measure (e.g., the relative importance of each measure, sensitivity to individual performance) as well as information relevant to the DEAMR process (e.g., item utility weights, optimal possible and minimal acceptable levels, etc.). The listing of measures presented in Appendix B may be modified to provide a preliminary instrument that might be refined and used to identify those measures that are most likely to be affected by better trained personnel. It is only through such systematic examination of the measures available that detailed conceptualizations of the linkages between individual performance and organizational outcome can be established. Ultimately, the effective use of outcome measures for the evaluation of personnel training depends on the delineation of these linkages.

References

Binning, J.F., & Barrett, G.V. (1989). Validity of personnel decisions: A conceptual analysis of the inferential and evidential bases. Journal of Applied Psychology, 74, 478-494.

Campbell, J.P., Dunnette, M.D., Lawler, E.E., & Weick, K.E. (1970). Managerial Behavior, Performance, and Effectiveness. New York: McGraw-Hill.

Goldstein, I.L. (1991). Training in work organizations. In M.D. Dunnette & L.M. Hough (Eds.) Handbook of Industrial and Organizational Psychology, vol. 2, (pp. 507-620). Palo Alto: Consulting Psychologists Press.

Borman, W.C. (1983). Implications of personality theory and research for the rating of work performance in organizations. In F. Landy, S. Zedeck, & J. Cleveland (Eds.) Performance measurement and theory (pp. 127-172). Hillsdale, NJ: Erlbaum.

Kane, J.S. (1986). Performance distribution assessment. In R. Berk (Ed.), Performance Assessment: Methods and Applications, (pp. 237-273). Baltimore, MD: Johns Hopkins University Press.

Kane, J.S., & Kane, K.F. (1992). The analytic framework: The most promising approach for the advancement of performance appraisal. Human Reseource Management Review, 2(1), 37-70.

Kane, J.S., & Lawler, E.E. (1979). Performance appraisal effectiveness: Its assessment and determinants. In B. Staw (Ed.) Research in Organizational Behavior, Vol 1. Greenwich, CT.: JAI Press..

USAF (USAF/TEP). (1994). AFI 99-103, Test and evaluation Process, 25 July 94. Washington, DC.: Author.

Appendix A:

List of Maintenance Related Outcome Measures Identified

MEASURE	DEFINITION	FORMULA
Abort Rate	% of scheduled sorties which must be canceled due to system malfunction	# of air sorties x 100 # of departures or sorties
Air Aborts	Number of air aborts.	
Air Abort Rate		air aborts x 100 (LCL sorties flown + ground abort rates)
Actual Fly Hours		
Actual UTR Rate	Average number of sorties. Deigned to measure how well maintenance community is supporting contracted flying commitment	total sorties flown APA aircraft
Adjusted Scheduling		
Adjusted Sortie Schedule		local sorties scheduled + weather adds + ferry/FCF adds + other adds - weather deletes - sympathy deletes - other deletes
Aircraft Battle Damage Repair Time	self explanatory	sortie generation rate
Aircraft Rearmed Time		sustain forces & operations
Aircraft Refueling	unit's ability to provide air refueling services to users	
Aircraft Regeneration Timing	# of aircraft regeneration within X amount of time	
Aircraft Scheduling Effectiveness Rate	Deals with the flying schedule and deviations to it.	adjusted sortie sched. - chargeable deviation x 100 adj. sortie sched.
Authorized Aircraft	The number of aircraft for the wing as authorized by MAJCOM.	
Availability	the probability that a system is operable & ready to perform its intended mission at any given time	
Aircraft Possessed Hours	total # of aircraft availability over the past 12 months	

MEASURE	DEFINITION	FORMULA
Average Possessed Aircraft	average # of aircraft availability, to include depot NMC time for aircraft possessed by depot above and beyond back-up aircraft inventory (BAI), over the past 12 months	total Acft possessed hrs total days in month x 24
Average Utilization Per Aircraft Per Month	average life units that pass per system during a month	
Awaiting Maintenance		
Awaiting Maintenance Rate		# of AWM X 100 # of poss acft
Awaiting Parts		
Awaiting Parts Rate		# of AWP X 100 # of poss acft
Break Rate	the % of sorties from which an aircraft returns with an inoperable mission-essential system that was previously operable. System malfunction occurring in-flight that renders aircraft not mission capable after landing	# of aircraft breaks x 100 # sorties flown
Cancellation Rate	% of all scheduled sorties or departures that were canceled	# of cancellation x 100 scheduled departures & sorties
Cannibalization Rate	maintenance efforts to compensate for supply problems or for maintenance convenience to launch aircraft on time	
Cannibalizations Per Average Possessed Aircraft	avg # of cannibalization per avg possessed aircraft	total # of cannibalizations avg possessed aircraft
Cannibalizations (removals only) Per Departure Per Sortie	avg # of cannibalization removals per departure or sortie	total # of Cannibalizations # of departures & sorties
Cannibalization Rate		# of Canns X 100 total sorties flwn
Cannot Duplicate Rate		
Chargeable Deviations		
Code 3 Breaks		
Code 3 Break Rate		# code 3 breaks x 100 total sorties flown

MEASURE	DEFINITION	FORMULA
Combat Rate	average # of consecutively scheduled missions flown before aircraft experience critical failures	# of successful sorties flown / (# of scheduled missions - # of ground aborts - # of air aborts)
Deferred Discrepancy Rate (repair which can't be done within 5 days)	A repair which cannot be accomplished within five days of the original write-up.	# of AWM/AWP x 100 / # of possessed aircraft
Delay Discrepancies	total # of non-grounding discrepancies that have been delayed or deferred & will not be worked on within 24 hrs from time discrepancy was found	
Delayed Discrepancy Average	avg number of delayed discrepancies per possessed aircraft	total delayed discrepancies / adjusted avg possessed aircraft
Delay Discrepancy Average, Awaiting Maintenance	avg # of delayed discrepancies per aircraft awaiting maintenance	total discrepancies delayed for maintenance / adjusted avg possessed aircraft
Delayed Discrepancy Average, Awaiting Parts	avg # of delayed discrepancies per aircraft awaiting parts	total discrepancies delayed for parts / adjusted avg possessed aircraft
Deployability	whether the system can be efficiently deployed to the theater of operations within the constraints of the user defined requirements	
Dropped Object Rate	rate of dropped object per 100 sorties. Dropped objects may be a manifestation of material, personnel, or design deficiencies	# of aircraft breaks during measured period x 100 / # of sorties flown during period
Engine Foreign Object Damage Rate	rate of engine FOD's per 1,000 departures	# of FOD incidents / (# of departures & sorties) x (# of engines on aircraft) x 1,000
Essential System Repair Time Per Flight Hour	avg clock time needed to repair mission-essential equipment per operational flight hour	elapsed corrective maintenance + elapsed preventive maintenance / flight hours
Fault Detection Rate		
Fault Isolation Rate		
Fleet Availability	a total # of aircraft availability, to include depot NMC time for aircraft possessed by depot above and beyond back-up aircraft inventory, over the past 12 months	

MEASURE	DEFINITION	FORMULA
Fix Rate	# of aircraft that return with inoperable systems & must be returned to MC status within a specified amount of time	# 4/8/12 hour fixes total # of code 3 breaks
Fully Mission Capable Hours		
Fully Mission Capable Rate	% of aircraft possessed hrs that were fully mission capable for a unit over a specified period of time	FMC x 100 avg. possessed hours
Ground aborts	Number of ground aborts.	
Ground Abort Rate	% of sorties or departures that aborted of the total attempted departures or sorties	ground aborts x 100 LCL sorties flown + ground aborts
Hangar Queen Days		
Hangar Queen Rate		
Hours Flown		
Local Sorties Flown		
Local Sorties Scheduled		
In Flight Emergencies		
In Flights Emergency Rate		
Maintainability	ability of an item to be retained in, or restored to, a specified condition within a given time period when maintenance is performed by personnel having specified skills using prescribed procedures & resources at each prescribed level of maintenance & repair	
Maintenance Completes		
Maintenance Delivery Reliability	% of times aircraft is mission capable at scheduled or actual crew show time & aircraft is capable of flight & will be accepted by aircrew	(total departures or sorties) - (# of aircraft broke at scheduled or actual crew show time) x 100 total departures or sorties
Maintenance Man Hour Per Fly Hour - Corrective	for inherent malfunctions, induced malfunctions, no-defect actions, or total events	
Maintenance Man Hour Per Fly Hour - Improvement	product improvement	

MEASURE	DEFINITION	FORMULA
Maintenance Man Hour Per Fly Hour - Preventive	preventive maintenance	
Maintenance Man Hour Per Fly Hour - Support	direct maintenance man hours required to support a system	
Maintenance Man Hour Per Life Unit	MAJCOMs estimate maintenance man hours per flying hour on their specific needs	
Maintenance Personnel Per Operational Unit	total # of direct maintenance personnel needed for each specified operational unit to perform direct on-equipment maintenance	
Maintenance Plan Rate		total pts earned x 100 total pts scheduled
Maintenance Starts		
Maintenance Turn Time	time required to prepare a returning mission-capable aircraft for another sortie	
Man Hour Per Fly Hour	all flying hour categories totaled	man-hours total flying hours
Man Hour Per Sortie		
Max Schedule Points Earned		
Max Schedule Points Possible		
MDC Man Hours		
Mean Down Time	avg elapsed time between losing mission capable status & restoring the system to MC status	sortie generation rate
Mean Repair Time	avg corrective maintenance time required to return a system or part to operational status	
Mean Time Between Critical Failure	avg time between failure of mission-essential system functions	# of operating hours # or critical failures
Mean Time Between Maintenance Actions	avg flying hours between maintenance events, including scheduled & unscheduled events	sortie generation rate
Million Ton Miles Per Day	aggregate, unconstrained measure of airlift capacity used as a top-level comparative metric	(objective utilization rate) x (blockspeed) x (payload) x productivity factor 1,000,000 nautical miles

MEASURE	DEFINITION	FORMULA
Mission Capable Hours		
Mission Capable Rate	% of aircraft possessed hours that were fully and partially mission capable for a unit over a specified period	PMCM + PMCS + PMCB + FMC APH
Non Mission Capable Both Hours		
Non Mission Capable Hours		
Non Mission Capable Both Rate		NMCB x 100 avg possessed hours
Non Mission Capable Rate		NMCS + NMCM + NMCB avg possessed hrs x 100
Not Operationally Ready - Maintenance	% to total systems not operationally available due to unperformed required maintenance	
Number of Aircraft Necessary to Perform Mission		
Number of Aircraft Successfully Employed	scheduled aircraft arriving at employment base	
Object Utilization Rate	avg # of hours per day the primary aircraft inventory fly, & is measured over two periods: "surge" & "sustained"	surge = the first 45 days of a contingency sustained = time after first 45 days
O&M Days		
O&M Days Not Flown		
Partially Mission Capable-Both Hours		
Partially Mission Capable Hours		
Partially Mission Capable Rate	can perform at least one but not all of its assigned missions	
Partially Mission Capable-Both Rate		partially mission capable both x 100 avg possessed hours
Possessed Availability Rate	a % of aircraft availability over the past 12 months	

MEASURE	DEFINITION	FORMULA
Pproductivity factor	a factor to account for the aircraft returning empty from the theater & positioning legs to onload locations. The productivity factor is constant at 47%	
Payload	based on avg payload observed in the Mobility Readiness Study modeling process using a critical leg distance of 3,200 NM	
Possessed Availability Rate	a % of aircraft availability over the past 12 months	
Pproductivity factor	a factor to account for the aircraft returning empty from the theater & positioning legs to onload locations. The productivity factor is constant at 47%	
Program Hours		
Program Fly hours		
Program Hour UTE Rate		
Program Sorties		
Program UTE rate		
Recurs	The same symtem malfunctioning within 3 flights of the original writeup.	
Recur Rate		# recurs / local sorties flown x 100
Refueling Time		sortie generation rate
Regeneration After Deployment	the deployed unit's ability to attain a combat ready posture for the in-theater commander as soon as possible after arriving at a deployment base	
Reliability	probability that an available system/mission will perform its required function at a specified mission time, in a specified environment, or during a scenario over the duration of a specified mission or over a specified # of sorties	# of missions completed / # of missions attempted

MEASURE	DEFINITION	FORMULA
Repair Turn-Around Time	measured from time item is removed from aircraft until it is repaired & ready for reissue	Air Force standard for repair turn around times for avionics items is 8 days
Repeats	The same system malfunctioning on the next flight.	
Repeat Rate		# repeats x 100 local sorties flown
Retest Okay Rate		
Sorties Flown		
Sorties Scheduled		
Sustainability	system's ability to maintain the necessary level & duration of operations to achieve military objectives. Often measured in # of days	
Total Abort Rate		ground abort rate + air abort rate
Total Aircraft Possession Hours		
Total Non Mission Capable Maintenance Hours		
Total Non Mission Capable Supply Hours		
Total Non Mission Capable Maintenance Rate		NMCM + NMCB x 100 avg possessed hrs
Total Non Mission Capable Supply Rate		NMCS + NMCB x 100 avg possessed hrs
Total Partially Mission Capable Maintenance Hours		
Total Partially Mission Capable Hours		
Total Partially Mission Capable Maintenance Rate		PMCB + PMCM x 100 PAH
Total Partially Mission Capable Supply Rate		PMCB + PMCM x 100 avg possessed hrs

MEASURE	DEFINITION	FORMULA
Utilization Rate	avg life units that pass per system during a specific period, expressed in flight hours or sorties per aircraft per relevant period of time, such as a day or month	avg flight hours # of possessed aircraft or authorized aircraft

Appendix B:

Sample Survey Measure

MEASURE	56th F Wing	31st F Wing	52nd F Wing
Abort Rate		X	X
Air Aborts	X	X	
Air Abort Rate	X		
Actual Fly Hours	X		
Actual UTR Rate	X		
Adjusted Scheduling	XX		
Adjusted Sortie Schedule			
Aircraft Battle Damage Repair Time			
Aircraft Rearmed Time			
Aircraft Refueling			
Aircraft Regeneration Timing			
Aircraft Scheduling Effectiveness Rate	XX	X	X
Authorized Aircraft	X		
Availability			
Aircraft Possessed Hours			
Average Possessed Aircraft	XX		
Average Utilization Per Aircraft Per Month			
Awaiting Maintenance	X		
Awaiting Maintenance Rate		X	
Awaiting Parts	X		
Awaiting Parts Rate		X	
Break Rate	X		X
Cancellation Rate			
Cannibalization Rate	X		X
Cannibalizations Per Average Possessed Aircraft			
Cannibalizations (removals only) Per Departure Per Sortie			

MEASURE	56th F Wing	31st F Wing	52nd F Wing
Cannibalization Rate			
Cannot Duplicate Rate			
Chargeable Deviations	XX		X
Code 3 Breaks	X		
Code 3 Break Rate			
Combat Rate			
Deferred Discrepancy Rate (repair which can't be done within 5 days)			
Delay Discrepancies	X		X
Delayed Discrepancy Average			
Delay Discrepancy Average, Aawaiting Maintenance			
Delayed Discrepancy Average, Awaiting Parts			
Deployability			
Dropped Object Rate			
Engine Foreign Object Damage Rate			
Essential System Repair Time Per Flight Hour			
Fault Detection Rate			
Fault Isolation Rate			
Fleet Availability			
Fix Rate	X	X	X
Fully Mission Capable Hours	XX		
Fully Mission Capable Rate			
Ground aborts	X	X	
Ground Abort Rate			
Hangar Queen Days	X		
Hangar Queen Rate	X		
Hours Flown	X		X

MEASURE	56th F Wing	31st F Wing	52nd F Wing
Local Sorties Flown	X		
Local Sorties Scheduled	X		
In Flight Emergencies	XX	X	
In Flights Emergency Rate	X		
Maintainability			
Maintenance Completes	X		
Maintenance Delivery Reliability			
Maintenance Man Hour Per Fly Hour - Corrective			
Maintenance Man Hour Per Fly Hour - Improvement			
Maintenance Man Hour Per Fly Hour - Preventive			
Maintenance Man Hour Per Fly Hour - Support			
Maintenance Man Hour Per Life Unit			
Maintenance Personnel Per Operational Unit			
Maintenance Plan Rate			
Maintenance Starts	X		
Maintenance Turn Time			
Man Hour Per Fly Hour	X		
Man Hour Per Sortie	X		
Max Schedule Points Earned			
Max Schedule Points Possible			
MDC Man Hours	X		
Mean Down Time			
Mean Repair Time			
Mean Time Between Critical Failure			
Mean Time Between Maintenance Actions			

MEASURE	56th F Wing	31st F Wing	52nd F Wing
Million Ton Miles Per Day			
Mission Capable Hours	XX		
Mission Capable Rate		X	X
Non Mission Capable Both Hours	XX		
Non Mission Capable Hours	X		
Non Mission Capable Both Rate			
Non Mission Capable Rate			
Not Operationally Ready - Maintenance			
Number of Aircraft Necessary to Perform Mission			
Number of Aircraft Successfully Employed			
Object Utilization Rate			
O&M Days	X		
O&M Days Not Flown	X		
Partially Mission Capable-Both Hours	XX		
Partially Mission Capable Hours	X		
Partially Mission Capable Rate			
Partially Mission Capable-Both Rate			
Possessed Availability Rate			
Pproductivity factor			
Payload			
Possessed Availability Rate	XX		
Pproductivity factor			
Program Hours	X		
Program Fly hours	X		
Program Hour UTE Rate	X		
Program Sorties	XX		

MEASURE	56th F Wing	31st F Wing	52nd F Wing
Program UTE rate	XX		
Recurs	XX		
Recur Rate	XX	X	X
Refueling Time			
Regeneration After Deployment			
Reliability			
Repair Turn-Around Time			
Repeats	XX		
Repeat Rate	XX	X	X
Retest Okay Rate			
Sorties Flown	X		X
Sorties Scheduled	X		X
Sustainability			
Total Abort Rate	XX		X
Total Aircraft Possession Hours			
Total Non Mission Capable Maintenance Hours	XX		
Total Non Mission Capable Supply Hours	XX		
Total Non Mission Capable Maintenance Rate		X	X
Total Non Mission Capable Supply Rate		X	X
Total Partially Mission Capable Maintenance Hours	XX		
Total Partially Mission Capable Hours	X		
Total Partially Mission Capable Maintenance Rate			
Total Partially Mission Capable Supply Rate			
Utilization Rate			

ELECTROPHYSIOLOGICAL, BEHAVIORAL, AND SUBJECTIVE INDEXES OF WORKLOAD WHEN PERFORMING MULTIPLE TASKS: MANIPULATIONS OF TASK DIFFICULTY AND TRAINING

Lisa R. Fournier
Assistant Professor
Department of Psychology

Washington State University
Pullman, WA 99163-4820

Final Report for:
Graduate Student Research Program Extension Grant
Armstrong Laboratory

Sponsored by:
Air Force Office of Scientific Research
Bolling Air Force Base, Washington, DC

and

Armstrong Laboratory

February 1997

ELECTROPHYSIOLOGICAL, BEHAVIORAL, AND SUBJECTIVE INDEXES OF WORKLOAD WHEN PERFORMING MULTIPLE TASKS: MANIPULATIONS OF TASK DIFFICULTY AND TRAINING

Lisa R. Fournier
Assistant Professor
Department of Psychology
Washington State University

Abstract

This study examined the effectiveness of using electroencephalogram (EEG) measures such as alpha and theta event-related desynchronization (ERD) and prestimulus ERD power suppression as a measure of mental workload and training in an operator control task. Subjects performed multiple tasks that were similar to those encountered by a pilot inside of an airplane cockpit. These tasks were interactive and included monitoring the path of the airplane (tracking), verbal communications, gauge display changes, and light display changes. Alpha and theta ERD were determined for a communications event that occurred during a single task (communications only) or during multiple tasks (tracking, gauge and light detection) in which workload varied (low, medium, and high). Additional measures, including total percent of alpha and theta power (alpha and theta), heart rate, respiration, eye blinks, behavioral performance, and subjective workload measures were used as converging operations to evaluate the effectiveness of the ERD measures. Results showed that the behavioral, subjective, and peripheral electrophysiological measures were more sensitive to workload than the EEG measures used. In addition, behavioral measures were the best measures of training. Significant ERDs were found for the single task only. In conclusion, alpha and theta ERD do not appear to be an effective index of workload and training in multiple task paradigms due to floor effects encountered in the prestimulus baseline measures. However, prestimulus alpha ERD power and total percent alpha power did discriminate between low and high workload conditions. Data that are consistent with previous research employing single task paradigms are discussed.

ELECTROPHYSIOLOGICAL, BEHAVIORAL, AND SUBJECTIVE INDEXES OF WORKLOAD WHEN PERFORMING MULTIPLE TASKS: MANIPULATIONS OF TASK DIFFICULTY AND TRAINING

Lisa R. Fournier

The main goal of the present study was to examine the feasibility of employing brain electrophysiological measures to monitor changes in mental workload. We were interested in measuring brain event related changes because behavioral and subjective measures are not always reliable indexes of workload (e. g., Yeh & Wickens, 1988). In addition, peripheral psychophysiological measures such as heart rate and respiration do not always allow us to speculate on what type of mental processes are in high demand and at what time points these mental processes are in high demand.

We were specifically interested in the event related amplitude changes or desynchronization (ERD) of the alpha rhythm (Pfurtscheller & Aranibar, 1977; Pfurtscheller & Klimesch, 1989). The usual frequency range for alpha is between 8-12 Hz. In general, alpha rhythm amplitude tends to decrease when a person is alert or engaged in a task, and the amplitude tends to increase when a person is in a relaxed state, with eyes closed. The alpha ERD is a topographically localized decrease in alpha amplitude of short duration (phasic) and has been shown to occur during visual stimulation, auditory stimulation, voluntary movement, and cognitive activity. Figure 1 contains an example of an ERD in the alpha band. Attenuation of the alpha rhythm has been shown to be maximal at the occipital electrode sites for visual-spatial tasks (Pfurtscheller & Aranibar, 1977) and to be maximal at centro-parietal sites when movement is required (Pfurtscheller & Aranibar, 1979). In addition, attenuation of the alpha rhythm has been shown to be maximal over auditory cortex for auditory discrimination tasks (Kaufman, Curtis, Wang, & Williamson, 1991). Furthermore, alpha

ERD amplitude and duration has been shown to vary with task difficulty or cognitive workload. Increases in cognitive workload tends to increase the relative alpha desynchronization amplitude and increase the duration of alpha desynchronization (van Winsum, Sergeant, & Geuze, 1984). Fast event rates (high action demands) within a task has also led to smaller relative desynchronization and shorter ERD than tasks with slow event rates (Geuze & van Winsum, 1987; van Winsum et al., 1984). This latter finding suggests that when events are difficult to predict, alpha desynchronization increases.

Boiten, Sergeant, and Geuze (1992) demonstrated that the size of the ERD depends mainly on the amplitude of the prestimulus alpha power. They also showed the importance of the prestimulus ERD baseline in determining the effort required for a task. They found that subjects given high speed instructions, which required them to put more effort into preparing for the task (increase in attention), caused power to decrease in the prestimulus interval. This suppression was more widespread over the cortex than during accuracy instructions which were presumed to require less effort. A consequence of this heightened activation state was an increase in cortical activation and hence alpha power suppression. In turn, this led to a decrease in ERD amplitude since the power in the prestimulus interval was used as a reference to calculate the ERD. Boiten et al. claim that the reason fast event rates lead to smaller ERDs is due to the decrease in power in the ERD prestimulus baseline. However, it has also been shown that increasing the levels of cognitive load causes the size and duration of the ERD to increase independent of event rate (van Winsum et al., 1984; Boiten et al., 1992). Taken together, these findings suggest that the level of prestimulus alpha power is mainly influenced by the subject's activation state, whereas relative ERD mainly reflects phasic changes in cognitive processing.

Alpha ERD has been successfully used to measure workload in single task paradigms, and these paradigms have typically required the subject to perform simple

tasks such as judging whether a letter occurs within a memory set (Geuze & van Winsum, 1987; van Winsum et al., 1984; Kaufman et al., 1991). We were interested in determining whether the alpha ERD could successfully measure workload while a subject is engaged in multiple tasks. In addition, we were interested in whether the alpha ERD can be used to discriminate performance of novice operators from performance from operators who had received some task training. Moreover, we wanted to determine whether alpha ERD can successfully index workload and learning in real world interactive tasks. If alpha ERD proves to be a successful index of workload, we can use this measure to determine what characteristics in operator displays (e. g., cockpit displays) increase or decrease operator workload.

In the present study, subjects performed multiple tasks that were similar to those encountered by a pilot inside of an airplane cockpit. These tasks were interactive and included monitoring a simulated flight path (tracking), verbal communications, gauge display changes, and light display changes. Each task trial was 3 min in duration. We were mainly interested in measuring the effects of workload (varied by tracking difficulty and event rate of gauge and light changes) on the communication task, which required subjects to classify communications as relevant or irrelevant and carry out instructions given in the relevant messages. We were also interested in how training under the different workload conditions would influence workload demands.

Two different alpha bands 8-10 Hz (alpha 1) and 10-12 Hz (alpha 2) were examined. The alpha 1 ERD has been shown to be more widespread and to represent attentional and motivational processes while the alpha 2 ERD appears more localized and may reflect stimulus-related processing or perhaps semantic encoding (Pfurtscheller et al., 1988; Klimesch et al., 1992; Krause, Lang Laine, Helle, Kuusisto & Porn, 1994; Klimesch, Schimke, Doppelmayr, Ripper, Schwiger & Pfurtscheller, 1996). In addition, the theta band (4-7 Hz) was also examined. Theta power is usually increased during

sleep, and non alert states. It has been shown that increased task demands lead to alpha desychronizations while theta synchronizes (Klimesch, 1996). The prestimulus communication task baselines will also be examined to determine the attentional effort required in the single (communications only) and in the multi-task conditions before the communication event occurs.

In addition to the above psychophysiological measures, we wanted to include other electrophysiological as well as behavioral and subjective measures to provide converging operations to the study of workload and training in a simulated real world task. These other measures included examination of the following based on the entire task trial: 1) total power (fast fourier transform, FFT) of alpha 1, alpha 2, and theta power, 2) peripheral electrophysiological measures of heart beat, eye blinks, and respiration, 3) behavioral measures of reaction time (RT) and accuracy, and 4) subjective ratings of task difficulty.

Method

Subjects.

Four males and six females ages 18 - 26 participated as paid volunteers. All were right-handed and had normal or corrected-to-normal vision (questionnaire). One male subject was excluded from all analysis due to extremely poor task performance leaving a total of 9 subjects.

Electrophysiological Recording.

EKG and Respiration. Heart activity was recorded by Ag/AgCl electrodes placed on the skin above the sternum and fifth intercostal space of the left ribcage. The ground electrode was located above the fifth intercostal space of the right ribcage. Impedences were less than 10 Kohm. Respiration was recorded using a Respitrace system with elastic transducer bands on the chest and abdomen. Respiration amplitude was calculated for each subject prior to data collection. Heart activity and respiration were sampled

continuously at 1000 Hz. Signals were recorded with Grass P511 amplifiers and data were filtered at 10-100 Hz.

Electroencephalogram (EEG) and Electrooculogram (EOG). Neuroscan software, amplifiers, and ElectroCap were used to record EEG over 58 scalp sites (consistent with the international 10/20 system, Jasper, 1958). Each scalp electrode was referenced to linked mastoids. Eye blinks were recorded from electrodes placed above and below the right eye to monitor vertical eye movements and from electrodes placed on the outer canthus of the left and right eye to monitor horizontal eye movements. EOG and EEG signals were recorded with Neuroscan amplifiers (model 5083) with a 60 Hz notch filter. EEG and EOG were sampled continuously at 200 Hz. EEG signals were filtered at 8-12 Hz. EOG signals were filtered at 0.1-30 Hz. Eye-movement artifacts were corrected using Neuroscan's eye-movement correction procedure. (See EEG analysis).

Data were digitally filtered at .1-30 Hz (-6dB gain, =/> -12dB octave slope) and amplified (gain 1000, resolution 084 μV/Bit, range 5 μV) via Synamps (5083) amplifiers, sampled at 200 Hz and stored off-line for analysis. Event markers were input to a separate channel to identify the beginning and end of each trial and the onset of each communications task within a trial.

Seven subjects returned on a separate day and were refitted with the electrode cap for digitization of electrode scalp positions using the Polhemus 3D-Space system. These coordinates were used to establish the weighting factors for the nearest neighboring electrodes when computing reference-free surface Laplacian derivations. Variances between subjects was observed to be extremely low, so for those subjects unable to return, an average value was used to calculate their inter-electrode distances.

Task Apparatus and Stimuli.

Subjects were seated at a table in a sound proof, electrically shielded chamber. A joystick was placed to the right of the subject and a computer mouse and pad was placed to the left of the subject. Subjects controlled the joystick with their right hand and controlled the computer mouse with their left hand. Visual displays were presented on a computer monitor centered 38 inches from the subject. In addition, audio messages (100 Hz) were presented over a speaker (Realistic model 32-2040) centered in front of the computer monitor.

Subjects were presented with visual monitoring tasks, an auditory task, and a tracking task from the Multi-Attribute Task Battery (MATB) developed by J. R. Comstock and R. J. Arnegard (1992). MATB was designed to simulate displays encountered in an airplane cockpit. Figure 2 shows the MATB visual displays for each task and these tasks are described below.

Light Detection Task. Subjects were to detect the offset of a green light and the onset of a red light occurring in the upper left (F5) and upper right (F6) of the system monitoring display, respectively. Normally, the green light appeared in the upper left box and the upper right box was black. The boxes subtended approximately 1.2 deg of visual angle. Subjects indicated that they detected the offset of the green light or the onset of the red light by moving a mouse to the box corresponding to the light fault detected, and then clicking the mouse on this box. This action caused the lights to return to their normal state (either green light on or red light off). The light faults (green off, red on) had a maximum duration of 15 sec.

Gauge Monitoring. Subjects monitored 4 different gauges (2.4 deg visual angle each) and determined whether a yellow pointer fluctuated outside of a specified range. The four gauges (F1, F2, F3, and F4) were located in a horizontal row just below the light boxes. Normally, each yellow pointer independently fluctuated from one unit below to one unit above the center line (see Figure 2). A gauge fault occurred if one of the yellow

pointers fluctuated more than one unit above or below the center line. Subjects indicated the detection of a gauge fault by moving the mouse anywhere on the faulty gauge and clicking the mouse. After clicking the mouse on the faulty gauge, a yellow bar (.12 deg visual angle) appeared at the bottom of the gauge, and the fault was corrected. A gauge fault had a maximum duration of 15 sec.

Tracking. The goal of this task was to keep the airplane symbol, represented by a green circle (.6 deg visual angle), in the center rectangular area (1.8 deg visual angle). (See upper right panel in Figure 2). The disturbance function for tracking consisted of a sum of nonharmonic sine waves. The frequency of the disturbance function varied for low, medium, and high tracking according to the MATB program specifications. Corrective movements of the airplane symbol was controlled by moving the joystick (first order control). When the cross-hatches of the circle and the cross-hatches in the center rectangle were aligned, this represented optimal tracking performance.

Communication. Audio messages were 6 sec in duration and consisted of a 6 digit call sign followed by a command. An example of a message is as follows, "NGT504, NGT504, set first communication to 119.7". The relevant target callsign for each subject was "NGT504". Any other call sign (i. e., "NRK362", "NLS217", "NAL478", "NDL183") was irrelevant (noise) and was to be ignored. The command indicated which channel on the computer screen (lower left in Figure 2) needed to have its frequency adjusted. Four possible channels required adjustments: NAV1, NAV2, COM1, and COM2. These were verbally indicated in the message as "first navigation", "second navigation", "first communication", and "second communication", respectively. A channel was selected by moving the mouse on the channel name (e. g., NAV1) and clicking the mouse. The number to the right of the channel name was the corresponding frequency of that channel. The frequency of the selected channel was changed by clicking the mouse on the arrow icons located to the right of the frequency numbers (see

Figure 2). Selecting the right-most arrow and clicking the mouse caused the frequency to increase (increments of 0.2 units) and clicking the mouse on the left-most arrow caused the frequency to decrease (decrements of 0.2 units). The navigation frequencies ranged from 108.1 to 117.9 and the communication frequencies ranged from 118.1 to 135.9. After the frequency changes were made, the mouse then moved to the "Enter" box (1.2 deg vis angle) located below the channel names. Clicking the mouse on the "Enter" box caused the borders to brighten which indicated that the response was recorded. Text characters (channel name, frequency, and arrows) measured .36 deg visual angle.

Workload ratings. The NASA Task Load index (NASA TLX) developed by Hart and Staveland (1988) was used to obtain a self reported assessment of the subjects workload during the multi-task conditions (see procedure description of conditions). This 10 point multi-dimensional scale. There were a total of six subscales. Subjects rated their exertion from low (1) to high (10) in the following 5 subscales: Mental demand, physical demand, performance, temporal demand, effort, and frustration. Subjects completed the NASA TLX for the 3 levels multi-task conditions (low, med, and high), and each of the task events within each of the multi-task conditions (light detection, gauge monitoring, tracking, and communication). Thus, a total of 5 subscales for each multi-task condition (low, med, and high) was obtained.

Procedure.

Practice. At the beginning of the experiment, subjects practiced controlling the mouse with their left hand. They moved the mouse and clicked on the different task locations within the MATB displays for approximately 9 min.

Experimental Sessions. Each subject was run through four different task conditions: communication only task (single task), multi-task low workload (multi-task low), multi-task medium workload (multi-task med), and multi-task high workload (multi-task high). The trial length for each condition was 3 min.

The single task condition required monitoring of the communication task only. All other tasks (light detection, gauge monitoring, and tracking) were not monitored and maintained a normal state (no fault events or tracking deviations). In all conditions, there were a total of 8 target communication events and 2 noise events. The onset of each event was separated by at least 7 secs.

The multi-task conditions required monitoring of all tasks (communication, light detection, gauge monitoring, and tracking). All of the multi-task conditions contained a total of 10 communication events (8 target, 2 noise). The multi-task conditions varied in the number of fault events (light detection and gauge monitoring), the time interval between fault events and communication events, and tracking difficulty. The multi-task low condition contained 4 light detection events, 4 gauge faults, and a low difficulty disturbance function for tracking. Each event was separated by at least 9 secs. The multi-task med condition contained 12 light detection events, 10 gauge faults, and a medium difficulty disturbance function for tracking. Onset of each event was separated by at least 3 secs. The multi-task high condition contained 16 light detection events, 18 gauge faults, and a high difficulty disturbance function for tracking. Onset of each event was separated by at least 2 secs.

Subjects were instructed to treat tracking as the primary task and the communication as the secondary task. They were told to time share these tasks with the light detection and gauge monitoring tasks. The communication, light detection, and gauge monitoring tasks were to be performed as quickly and accurately as possible. Accuracy (false alarms and misses), RTs, and tracking root mean square (RMS) were recorded. A miss was recorded if subjects did not respond to the communication task, light detection, or gauge fault within 15 sec. A false alarm was recorded if the incorrect communication command, light, or gauge was selected.

Subjects completed six sessions. Session 1 and 6 required both electrophysiological (EEG, EKG, and respiration) and behavioral data collection. In these sessions, subjects completed a total of 24 trials (6 trials of the single task, multi-task low, multi-task med, and multi-task high). In addition, subjects completed the subjective workload rating scales after the last 3 trials which consisted of the multi-task low, med, and high difficulty conditions (randomly ordered). Sessions 2 through 5 were training sessions during which only behavioral data were recorded. In these sessions, subjects completed a total of 30 trials (10 trials in each multi-task condition). The order of task conditions in each session was random with the constraint that no two of the same conditions occurred in sequence. Session 1 and 6 took approximately 3 hours (60 min to hook up electrophysiology apparatus and 90-120 min to perform task). Sessions 2 through 5 took approximately 90-100 minutes. Subjects took a 1-2 min break after each trial and a 10-15 min break midway through each session.

Data Analysis.

Heart Rate/Variability. Heart beats were identified and time intervals between successive R waves were determined and outliers were corrected (Wilson & Oliver, 1990). Inter-beat intervals were processed through a Porges-Bohrer filter (Porges and Byrne, 1992) to determine heart rate variability at filter settings of medium (.06-.14 Hz) and high (.15-.40 Hz) bands.

EEG Analysis. Continuous EEG data were corrected for vertical and horizontal eye-movement artifacts using the NeuroScan correction procedure. The continuous EEG data were then transformed according to the local finite-difference approximation (Hjorth, 1980). All analyses were performed on the artifact corrected Laplacian derivatives of the raw EEG. Equipment failure resulted in the loss site T4L and loss of 2 trials (subject 1, day 1, multi-task low and subject 4, day 2, communications). In 7 other trials from 2 different subjects, data from specific sites were discarded due to excessive noise.

ERDs. The 8 relevant communications task epochs (1 sec pre-stimulus and 5 sec post-stimulus) were identified within each trial. Epochs were digitally bandpass filtered using the Neuroscan frequency analysis. Three different bands were evaluated: alpha 1 (8-10 Hz), alpha 2 (10-12 Hz) and theta (3-7 Hz). The amplitude value for each data point (5 ms resolution) was determined. In addition, an average amplitude value was calculated for 25 consecutive data points in order to decrease variance. These average amplitudes were then squared yielding an absolute power within each band every 125 ms. This provided a total of 48 data points representing an average 6 sec. epoch (1 sec pre-stimulus, 5 sec post-stimulus) for each of the 8 relevant communication events per trial. 3) Individual trial data were log transformed to correct for skewness and the average of the prestimulus period was subtracted from each post-stimulus data point for each trial. An average communication task epoch was then computed for each subject, site, session (1,6), and workload condition (24 epochs per condition per task).

ERD prestimulus baseline. The communication prestimulus baseline (1 sec) was calculated as described above for each task condition (single, and multi-tasks) and session (1, 6).

FFTs. An average Fast Fourier Transform was calculated for each 3 min trial at each electrode site for each subject, session, and workload condition. Each 3 min trial was sorted into 512 ms epochs and averaged within the frequency domain using a Parzens window for smoothing. Results yielded FFTs with a range of 0-128 Hz and a resolution of .39 Hz. The FFTs were then grouped into different bands: theta 4.3-7.8 Hz, alpha 8.3-11.7 Hz, beta1 12.1-15.6 Hz and beta2 16-19.5 Hz. To correct for skewness, data were log transformed and both the absolute and relative powers were compared.

Statistics. All analyses were based on a two-way within subjects analysis of variance (ANOVA) with the factors of condition (single task, multi-task low, multi-task medium, and multi-task high) and session (session 1 and 6). Tukey HSD was used for within condition comparisons at an alpha of .01, unless stated otherwise. ANOVAs were conducted at each electrode site for each bandwidth to evaluate the ERD and FFT data. Results were interpreted as significantly different if five or more nearby electrode sites showed significant differences within a specific bandwidth between conditions (Tukey HSD).

Results and Discussion

A summary of significant results for each of the different measures is provided in Table 1.

Behavioral Data.

Multi-tasks. A composite Z-score was used to evaluate behavioral responses in the multi-task conditions. Behavioral responses were standardized for each task (communication, tracking, light detection, and gauge detection) within each subject by dividing RTs for each task by proportion of correct responses and weighting each task measure by ¼ and summing them together. Composite Z-scores reflecting task performance for the low, medium, and high multi-task workload conditions across session are presented in Figure 3. There was a main effect of condition [$F(1,16)=75.03$, $p < .0001$], a main effect of session [$F(1,8)=225.08$, $p < .0001$], and a significant mutli-task x session interaction [$F(2,16)=14.02$, $p < .01$]. Performance in both session 1 and 6 was worse in the multi-task high, intermediate in the multi-task medium, and best in the multi-task low condition ($p < .05$). In addition, performance was better in session 6 relative to session 1. Furthermore, performance improved more in the high multi-task condition across session relative to the low and medium multi-task conditions ($p < .05$).

Communication. Performance in the communication task was evaluated across the single and multi-task conditions as well as across session. Three different response tasks were required in order to successfully complete the communications task: 1) channel selection, 2) frequency selection, and 3) enter key selection. For simplicity, only the behavioral analysis from the on onset of the message to enter key selection is reported. There was a significant main effect of condition [$F(3,24) = 16.24$, $p < .001$] and a significant main effect of session [$F(1,8) = 56.67$, $p < .001$] on correct RT. In addition, there was a main effect of session on percent errors (miss and false alarms combined) [$F(1,8) = 8.39$, $p < .02$]. As shown in Figure 4, RT was fastest for the single task, and RT became slower for the multi-task conditions as task difficulty increased ($p < .05$). This RT trend was observed in both session 1 and session 6. In addition, for all tasks, RT was faster and miss errors were less frequent in session 6 relative to session 1.

Subjective Ratings.

A composite mean score for ratings on the six workload sub-scales was evaluated for each multi-task condition and session. There was a main effect of condition [$F(2,16) = 13.60$, $p < .001$] only. As shown in Figure 5, subjective workload was greater in the multi-task medium and high conditions relative to the multi-task low condition ($p < .01$).

Peripheral Physiological Data.

Cardiovascular. There was a significant main effect of condition for the heart inter-beat interval [$F(3, 24) = 21.87$, $p < .001$] as well as for the heart rate variability in both the medium (BP) [$F(3, 24) = 13.12$, $p < .001$] and high band [$F(3, 24) = 10.79$, $p < .001$]. As shown in Figure 6, heart rate (beats/min) was higher in all of the multi-task conditions relative to the single task ($p < .001$, respectively]. In addition, heart rate was higher in the multi-task high condition relative to the multi-task low and medium conditions ($p < 05$, respectively); there was no significant difference between multi-task low and medium conditions ($p > .05$). Heart rate variability in both the high and medium

band (see Figures 7 and 8 respectively) was less in the multi-task conditions relative to the single task and variability further decreased as multi-task difficulty increased ($p < .05$ for all comparisons).

Respiration. Although there were no significant effects for respiration amplitude, respiration rate showed a significant effect of condition [$F(3, 24) = 10.24$, $p < .001$]. Figure 9 shows that respiration rate is faster for each of the multi-task conditions relative to the single task condition ($p < .05$, respectively). In addition, respiration rate was faster in the high relative to the low multi-task condition ($p < .05$). However, there was no significant difference in rate between low and medium multi-task or medium and high multi-task conditions.

Blinks. There was a main effect of condition for blink duration [$F(3, 24) = 29.14$, $p < .001$] and amplitude [$F(3, 24) = 9.69$, $p < .001$]. As shown in Figures 10 and 11 respectively, blink duration was shorter and blink amplitude was larger in the multi-tasks relative to the single task ($p < .001$ for duration and $p < .05$ for amplitude). Blink rate showed a significant main effect of condition [$F(3, 24) = 30.75$, $p < .001$] and session [$F(1, 8) = 7.73$, $p < .001$]. Figure 12 shows that blink rate was reduced for the multi-task conditions relative to the single task ($p < .001$, respectively). In addition, blink rate was reduced for both the multi-task medium and high conditions relative to the multi-task low condition ($p < .01$ respectively); there was no significant difference between multi-task medium and high conditions. Furthermore, blink rate was larger in session 2 relative to session 1.

ERD.

The alpha 1, alpha 2, and theta band ERDs were calculated for the communications task in each of the four conditions in each session. There were no significant differences in ERDs for any of the bandwidths across session. However, there was a significant difference in ERDs between the single task and multi-task conditions in

all the bands. Significant communication ERDs across multiple electrode sites were found only in the single task. There were no significant communication ERDs found across multiple electrode sites in the multi-task workload conditions ($p > .05$). Figure 13, 14, and 15 show topographic maps representing the time course for the electrode sites that had significant ERDs in each band (theta, alpha 1, and alpha 2, respectively) for the single task during the 5 sec communication message. Because there was no significant activity during the first 1 sec of the communication message, the topographic maps are shown for the 1 sec after the communication task began (total of 4 sec) and approximately .5 sec after the communication task finished at intervals of approximately .125 sec.

Alpha 1. For alpha 1, significant ERD effects are found as early as 1.38 secs (middle of second call sign) in the left central sites and eventually dominates at the parietal sites. This activity then dissipates and ERD activity occurs again around 4.38 secs (after dial selection instructions, but before frequency setting instructions) mainly in the parietal and occipital sites. Note also the frontal ERD activity at the 4.75-6.0 time points. Alpha 1 ERD differences continue at the parietal and occipital sites throughout the message duration and at least .5 sec after the message.

Alpha 2. For alpha 2, significant effects begin as early as 3.0 secs in the central and left temporal sites (during dial setting instructions, but before frequency setting instructions). By approximately 4.25 secs (after dial setting instructions, but before frequency setting instructions) the number sites indicating significant ERDs is increased, especially at the central, parietal and occipital sites throughout the message duration and .5 sec after the message.

Alpha 1 vs. Alpha 2. Alpha 1 activity appears to be biphasic and more localized in the parietal, occipital sites, and frontal sites. Alpha 2 tends to show early ERD activity at left temporal and central sites, which may reflect auditory processing and motor

activation, respectively. Later on, alpha 2 shows more dominant activity at parietal, occipital, as well as at central sites.

Theta. For theta, significant ERD effects begin as early as 4.38 sec (after dial setting instructions, but before frequency setting instructions) at some parietal and some central sites, and occasionally at the left temporal sites. The number of sites showing significant differences becomes more dominant in the parietal sites throughout the message duration and .5 sec after the message.

The lack of significant ERDs for the multi-task conditions may be due to a floor effect. ERD amplitudes are calculated relative to the prestimulus baseline and if this baseline is reduced due to the demands of the other ongoing tasks, the ERD may show little or no further reduction from the baseline (see also Boiten et al., 1992). In the multi-task baselines, the subject is continuously engaged in tracking and may be engaged in monitoring the gauges and lights. It is known that power decreases, at least for alpha, when subjects are engaged in various tasks. However, during the single task baseline, the subject is not engaged in any task and the baseline EEG power should be higher so that it is possible to show a reduction. Thus, the lack of significant ERDs in the multi-task conditions may be due to a floor effect of power in the prestimulus baseline.

ERD prestimulus baseline.

Consistent with this floor effect idea, Figure 16 shows that there were significant differences in the prestimulus baselines across conditions in the theta, the alpha 1, and alpha 2 bandwidths at several electrode sites. First, the baseline for theta in the multi-task low condition showed decreased power over right central and parietal electrode sites relative to the single task ($p < .05$). Second, the baseline for alpha 1 in all of the multi-task conditions showed decreased power mainly in parietal and some central sites relative to the single task ($p < .05$). Third, the baseline for alpha 2 showed decreased power in all of the multi-task conditions in central, posterior, and occipital sites relative to the single

task ($p < .05$). These findings demonstrate that there was less power for theta, alpha 1 and alpha 2 in the prestimulus baselines for the multi-task conditions relative to the single task. Thus, the lack of ERDs found for these bandwidths are most likely due to floor effects.

Furthermore, alpha 2 showed larger decreases in power in the high workload condition relative to both the low workload condition at right central and parietal sites ($p < .05$). See Figure 17. This finding suggests that there were significant decreases in alpha 2 power as workload increased. Thus, alpha 2 power may be a more sensitive measure of multi-task workload as opposed to measures of alpha and theta ERD.

FFT.

The alpha 1 and 2 bands showed decreases in percent total power at multiple sites for multi-task conditions relative to the single task. Figure 18 shows the significant percent total power changes for the multi-task high condition relative to the single task condition for theta, alpha 1, and alpha 2, respectively. Alpha 1 power decreases at left occipital sites in the multi-task high relative to single task conditions. Alpha 2 power shows decreases in power mainly at left occipital and parietal sites, right central, and at some frontal sites for the multi-task high relative to the single task condition. The theta band showed significant increases in power at multiple sites for the multi-task high condition relative to the single task. Furthermore, there were no significant differences in power across the multi-task conditions in the alpha 1 and theta bands. However, as shown in Figure 19, there was a significant decrease in alpha 2 power for the high workload relative to the low workload condition mainly at right central and parietal sites.

Conclusions

All measures distinguished between the single task and multi-task conditions with the exception of respiration amplitude. However, not all measures were sensitive to the low, medium and high workload conditions. In general, the behavioral, subjective, and

peripheral electrophysiological measures were more sensitive in discriminating among the different workload conditions relative to the EEG measures used (ERD, ERD prestimulus baseline, and FFT). However, the peripheral and subjective measures often did not distinguish either between the low and medium workload conditions or the medium and high workload conditions. Performance (response speed and accuracy) appeared to be the most sensitive measure of workload and training. Cardiovascular measures of heart rate variability (medium and high) also were differentially sensitive to low, medium and high workload. These results were found even though subjectively, subjects viewed task difficulty to be greatest under conditions of high workload but viewed task difficulty to be no different in the low and medium workload conditions. Heart rate results were most consistent with the subjective ratings of workload. A summary of these measures and the other measures are shown in Table 1.

The only significant differences found for the ERD was between the single and multi-task conditions, independent of multi-task workload. The lack of workload sensitivity found for the ERD measures is most likely due to the difficulty in assessing power in each workload condition when several different types of tasks are being carried out. As pointed out by Boiten et al. (1992), ERD measures are dependent on prestimulus power baselines. If the prestimulus baseline power is decreased due to factors of attention and effort, ERDs should be reduced for these conditions. In the present study, the prestimulus baseline power was greatly reduced in all multi-task conditions relative to the single task condition. It is clear that these reductions in prestimulus baseline, at least for alpha 2, were affected by workload. That is, the alpha 2 prestimulus baseline for the communication task was decreased in the multi-task high workload condition relative to the multi-task low workload condition. Thus, consistent with the findings of Boiten et al (1992), we found that task demands influenced the prestimulus baseline. It is unclear, however, whether baseline power was low due to increased effort, increased motor

activity, or increased engagement of attention on other tasks, or some combination of these factors. In the high workload condition, tracking became more difficult which would require more motor activity, and the number of light and gauge detections would also occur at a faster event rates, which would require more display scanning and motor movement as well. If alpha 2 represents stimulus related as opposed to attention processing, it could be that the increased motor activity and increased probability of processing gauge and light detection events underlie decreases in alpha 2 power.

There was also a significant decrease in total percent power (FFT) for alpha 2 in the high workload relative to low workload condition. This indicates that alpha 2 power was reduced throughout the entire high workload trial relative to the low workload trial. Thus, power appears to be a more sensitive measure of workload in continuous, real-world, multi-task environments relative to alpha 2 ERD measures.

Although ERD did not appear to be an effective measure in our workload, multi-task conditions, it was an effective measure in our single task condition. That is, there was a significant decrease in alpha 1, alpha 2, and theta for the communication task when there was no other tasks being carried out (no movement artifact). Similar to Krause et al. (1994), who used a task involving sentence discrimination, we found a biphasic ERD for alpha 1, with the first significant alpha 1 ERD occurring approximately 1.4 sec after the start of the communication message and the second occurring 2 sec later. Alpha 1 ERD has been associated with attention (Pfurtscheller et al., 1988; Klimesch et al., 1992; Krause et al., 1994). Perhaps it is around 1.4 secs that attention to the message is heightened. It is approximately 1.4-2 secs after the message starts in this task that critical task information is given (correct or incorrect callsign). The second phase of the alpha ERD decrease may be due to effortful process of directing the action to be carried out as indicated in the message, especially since there is alpha 1 ERD evident in frontal sites. In sum, this alpha 1 activity appears to be related to attentional factors rather than stimulus

factors because ERD activity was not dominant over central (motor) scalp sites and because ERD activity initially occurred well before responses to the message were executed.

Our findings are generally consistent with the idea that alpha 1 represents attentional effort and alpha 2 reflects stimulus related processing. This is because alpha 1 suppression was shown to be dominant in the peripheral and occipital sites and appeared also at the frontal sites, whereas alpha 2 suppression appeared in the peripheral and occipital sites as well as in the central (motor) sites. This is consistent with the idea that alpha 2 is sensitive to stimulus processing and motor execution of the response associated with the communication message. Alpha 1 did not appear to be as sensitive to motor execution reflected in central sites. In addition, according to the performance RT data, the correct dial was selected in approximately 5.19 sec and the correct frequency was set approximately 7.94 sec and the enter key was selected approximately 9.0 sec after the start of the communication message. Thus, the ERD affects found for both alpha 1 and alpha 2 in the single task do not appear to be completely due to motor artifacts since activity occurred before motor responses were required.

In summary, measures of ERD do not appear to be effective measures in determining workload in continuous, multi-task, real world environments. Motor activity as well as attentional demands under various workload conditions will reduce power in the prestimulus baseline which can lead to floor effects. However, consistent with previous research, the ERD does appear to be an effective measure for workload under single tasks. Similar floor effects may be found with percent total power measurements when examining differences in multiple tasks, although alpha 2 power was an effective index of workload in the present study for low and high workload.

References

Boiten, F., Sergeant, J., & Geuze, R. (1992). Event-related desychronization: the effects of energetic and computational demands. Electroencephalography & Clinical Neurophysiology, 82, 302-309.

Comstock, J. R., & Arnegard, R. J. (1992). The Multi-attribute task battery for human operator workload and strategic behavior research. NASA Technical Memorandum 104174.

Geuze, R., & van Winsum, W. (1987). Event-related desynchronization and P300. Psychophysiology, 24, 272-277.

Hart, S. G., & Staveland, L. E. (1988). Development of NASA-TLX (Task Load Index): Results of empirical and theoretical research. In P. A. Hancock and N. Meshkati (Eds.) Human Mental Workload. Amsterdam: North Holland Press.

Jasper, H. H. (1958). The ten-twenty electrode system of the International Federation. Electroencephalography & Clinical Neurophysiology, 10, 371-375.

Kaufman, L., Curtis, S., Wang, J. Z., Williamson, S. J. (1991). Changes in cortical activity when subjects scan memory for tones. Electroencephalography & Clinical Neurophysiology, 82, 266-284.

Klimesch, W. (1996). Memory processes, brain oscillations and EEG synchronization. International Journal of Psychophysiology, 24, 61-100.

Klimesch, W., Schimke, H., Doppelmayr, M., Ripper, B. Schwaiger, J., Pfurtscheller, G. (1996). Event-related desynchronization (ERD) and the Dm effect: Does alpha desynchronization during encoding predict later recall performance? International Journal of Psychophysiology, 24, 47-60.

Krause, C. M., Lang, H. A., Laine, M. Helle, S. I., Kuusisto, M. J., and Porn, B. (1994). Event-related desynchronization evoked by auditory stimuli. Brain Topography, 7, 107-112.

Pfurtscheller, G. (1977). Graphical display and statistical evaluation of event-related desynchronization (ERD). Electroencephalography and Clinical Neurophysiology, 43, 757-760.

Pfurtscheller, G. (1988). Mapping of event-related desynchronization and type of derivation. Electroencephalography and Clinical Neurophysiology, 70, 190-193.

Pfurtscheller, G., & Aranibar, A. (1977). Event-related cortical desynchronization detected by power measurements of scalp EEG. Electroencephalography & Clinical Neurophysiology, 42, 817-826.

Pfurtscheller, G., & Aranibar, A. (1979). Evaluation of event-related desynchronization (ERD) preceding and following voluntary self-paced movement. Electroencephalography & Clinical Neurophysiology, 46, 138-146.

Pfurtscheller, G., & Klimesch, W. (1989). Cortical activation pattern during reading and semantic classifications studied with dynamic ERD mapping. In: Topographic Brain Mapping of EEG and Evoked Potentials, Maurer K., ed. Berlin: Springer, pp. 303-313.

Pfurtscheller, G., Neuper, C., Mohl, W. (1994). Event-related desynchronization (ERD) during visual processing. International Journal of Psychophysiology, 16, 147-153.

Porges, S. W., & Byrne, E. A. (1992). Research methods for measurement of heart rate and respiration. Biological Psychology, 34, 93-130.

Ritter, W., Simson, R., and Vaughan, H. (1988). Effects of the amount of stimulus information processed on negative event-related potentials. Electroencephalography & Clinical Neurophysiology, 69, 244-258.

Sergeant, J., Geuze, R., & van Winsum, W. (1987). Event-related desychronization and P300. Psychophysiology, 24, p. 272-277.

Wilson, G. W., & Oliver, C. G. (1990). PATS: Psychophysiological Assessment Test System. Proceedings of the Western European Association of Aviation Psychologists, Volume II: Stress and Error in Aviation, pp. 15-25.

van Winsum, W., Sergeant, J. A., & Geuze, R. H. (1984). The functional significance of event related desynchronization of alpha rhythm in attentional and activating tasks. Electroencephalography & Clinical Neurophysiology, 58, 519-524.

Yeh, Y. Y., and Wickens, C. D. (1988). Dissociation of performance and subjective measures of workload. Human Factors, 30, 111- 120.

Table 1.

Summary of significant results for each of the different measures.

Measure	Condition Comparisons: single vs. multi-task	multi-low vs. high	multi-low vs. med	multi-med vs. high	Session	Condition x Session
1) Behavioral						
multi-task	X	n/c	X	X	X	X
communication	X	X	X	X	X	
2) Subjective						
	n/c		X	X		
1) Cardiovascular						
heart beat	X					
HR med. var	X	X	X	X		
HR high var	X	X	X	X		
HR	X	X		X		
4) Respiration						
amplitude						
rate	X	X				
5) Eye Blink						
duration	X					
amplitude	X					
rate	X	X	X		X	
6) ERD						
alpha 1	X					
alpha 2	X					
theta	X					
7) ERD pre-base						
alpha 1	X					
alpha 2	X	X				
theta	X					
8) FFT						
alpha 1	X					
alpha 2	X	X				
theta	X					

X = significant difference $p < .05$
n/c = not calculated

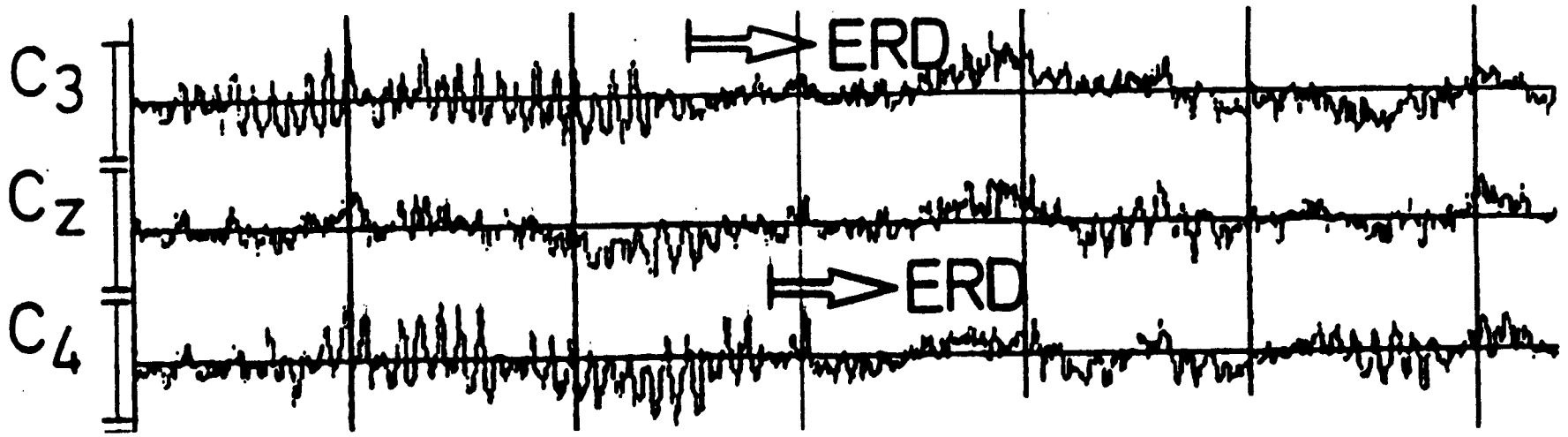

Figure 1. An example of alpha ERD over central scalp sites.

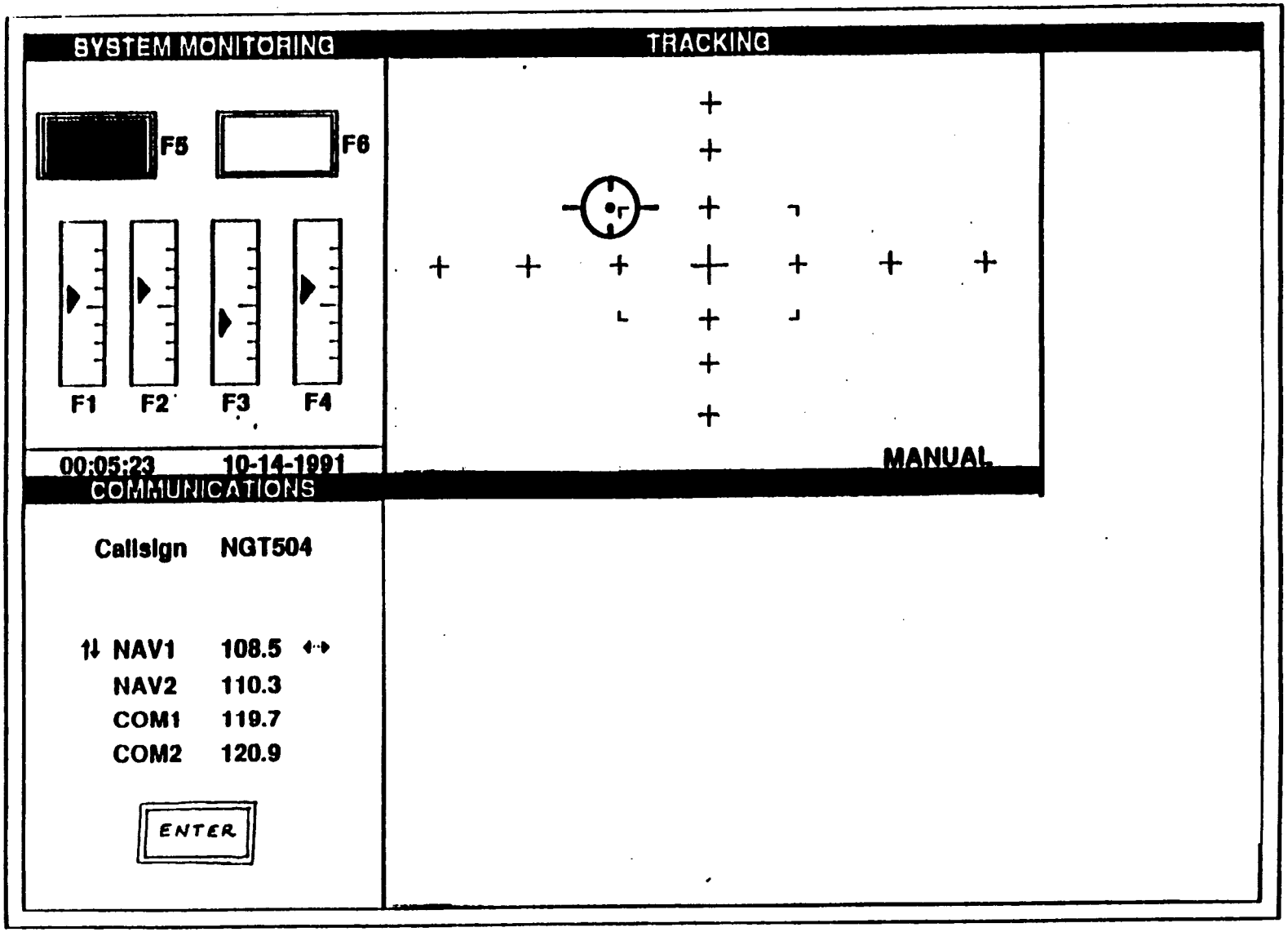

Figure 2. MATB visual display

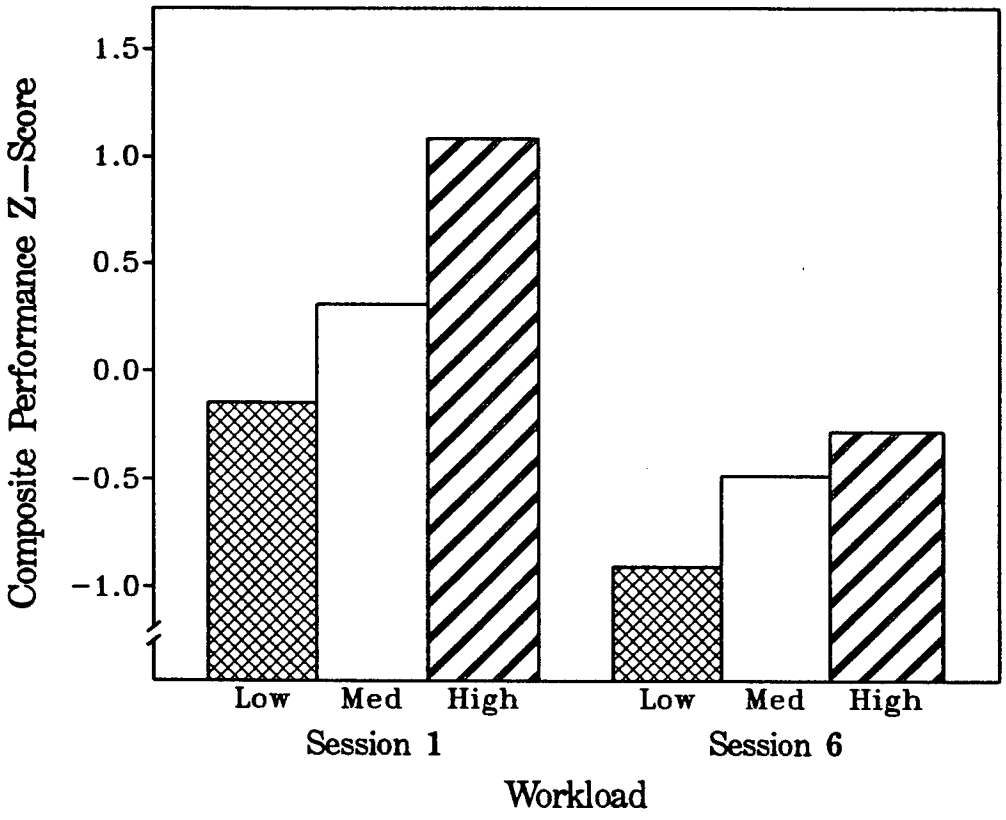
Composite Performance Z-Score
1.5
1.0
0.5
0.0
-0.5
-1.0
Low
Med
High
Low
Med
High
Session 1
Session 6
Workload

Figure 3.

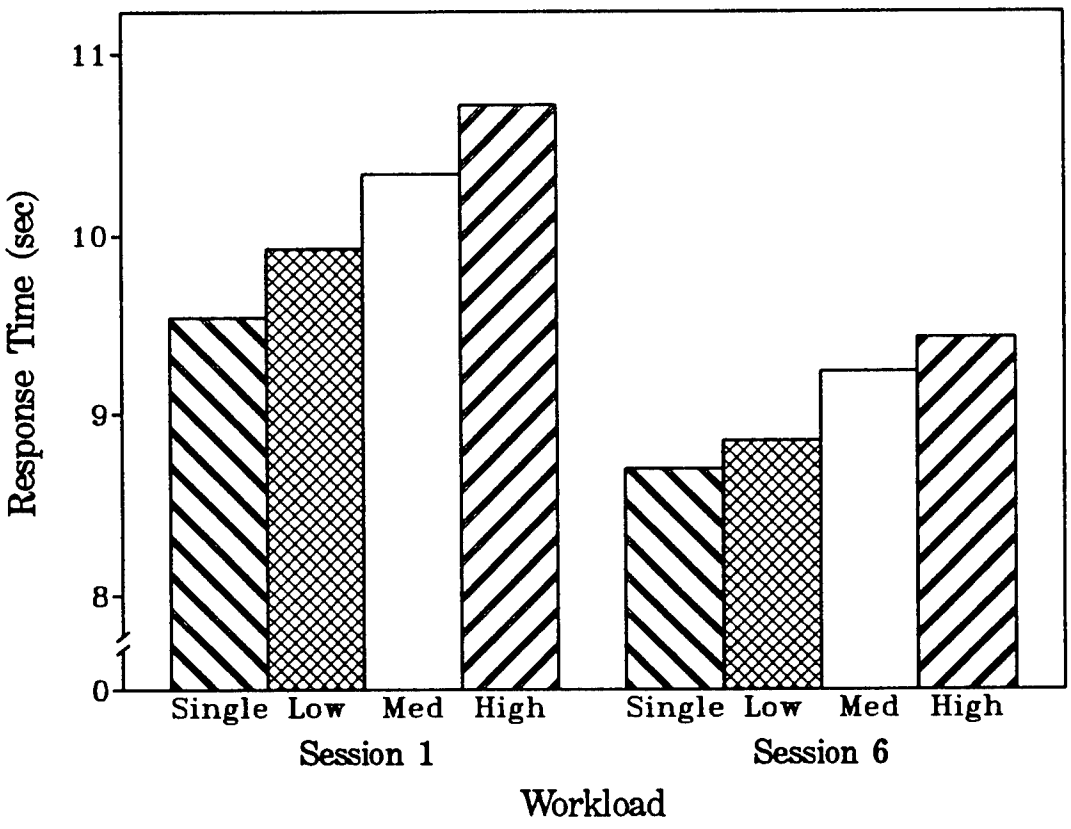
Response Time (sec)
11
10
9
8
0
Single Low Med High
Session 1
Single Low Med High
Session 6
Workload

Figure 4.

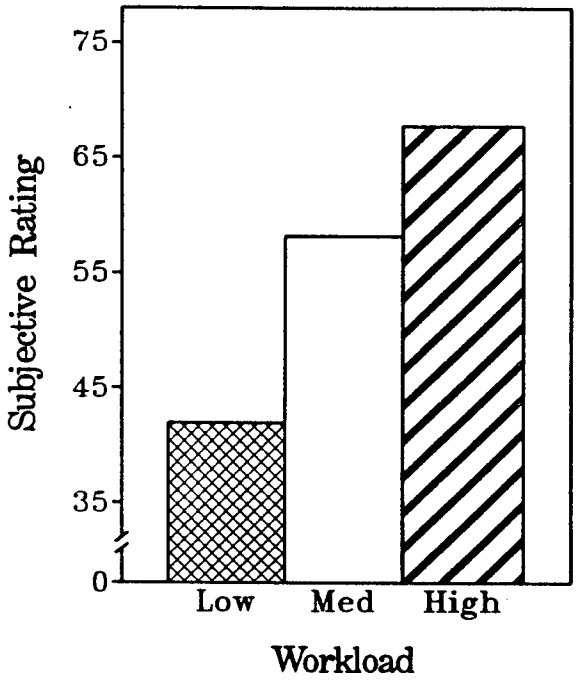

Figure 5.

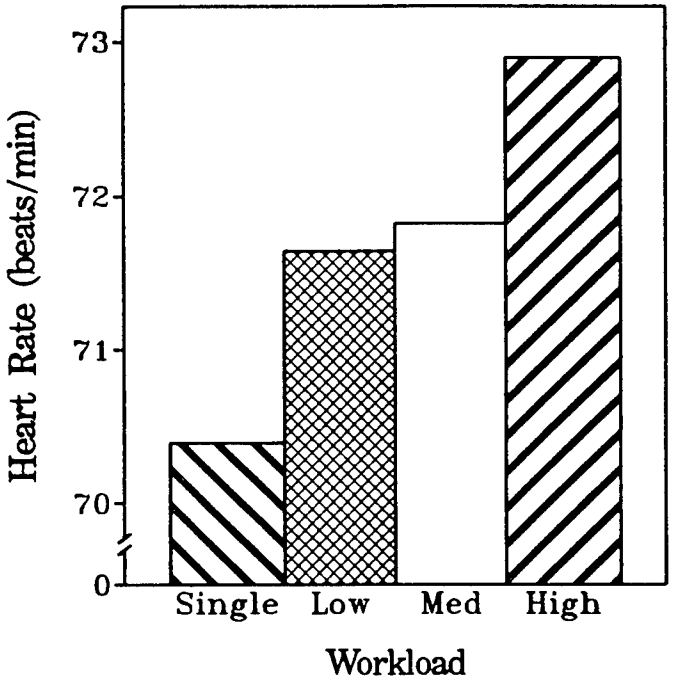
Heart Rate (beats/min)
73
72
71
70
0
Single
Low
Med
High
Workload

Figure 6.

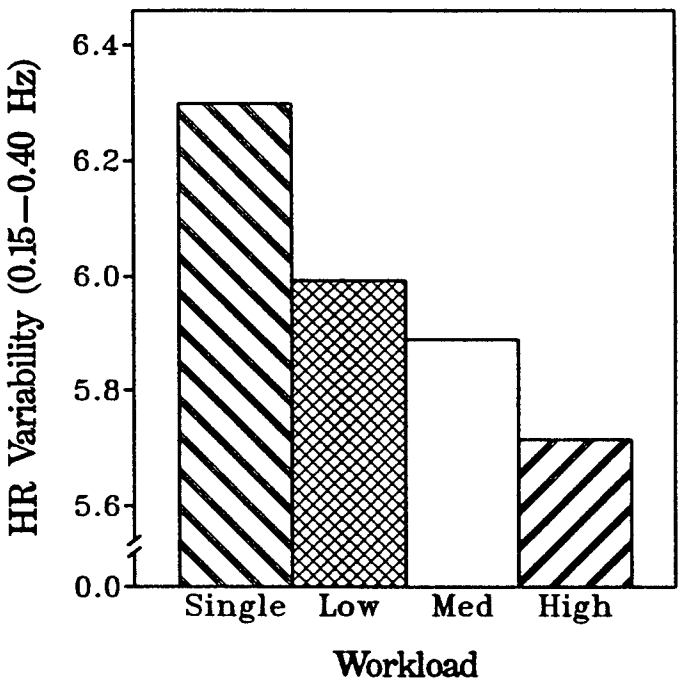
HR Variability (0.15—0.40 Hz)
6.4
6.2
6.0
5.8
5.6
0.0
Single
Low
Med
High
Workload

Figure 7.

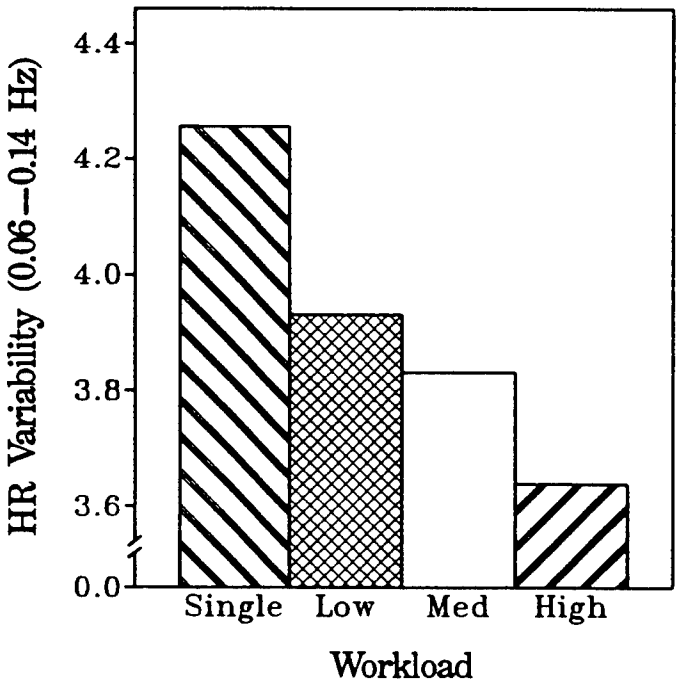
HR Variability (0.06—0.14 Hz)
4.4
4.2
4.0
3.8
3.6
0.0
Single
Low
Med
High
Workload

Figure 8.

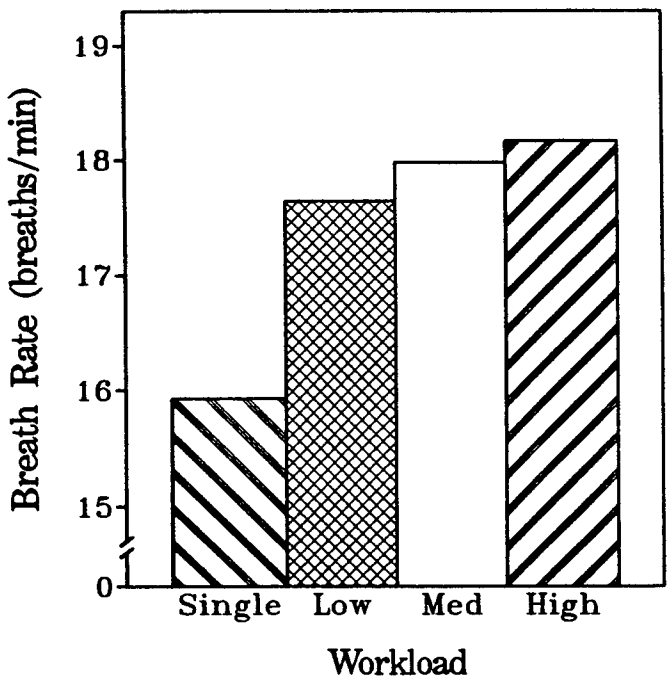
Breath Rate (breaths/min)
19
18
17
16
15
0
Single
Low
Med
High
Workload

Figure 9.

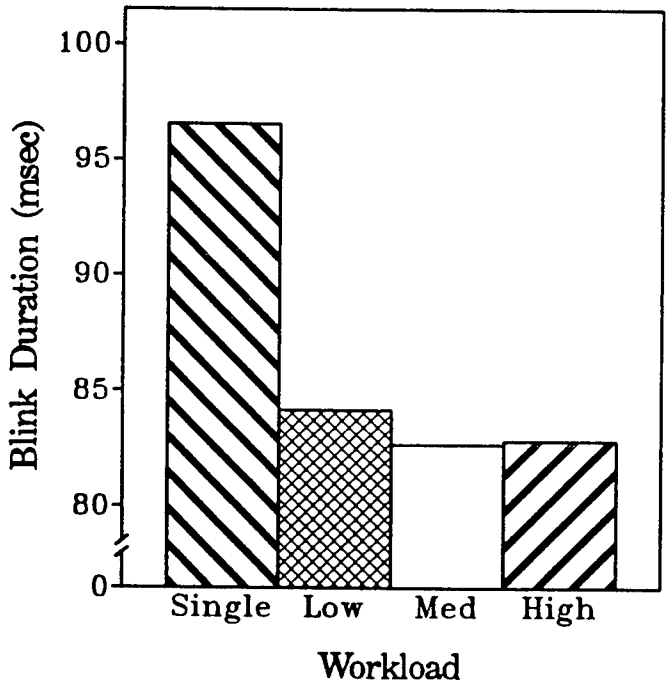
100
95
90
85
80
0
Blink Duration (msec)
Single
Low
Med
High
Workload

Figure 10.

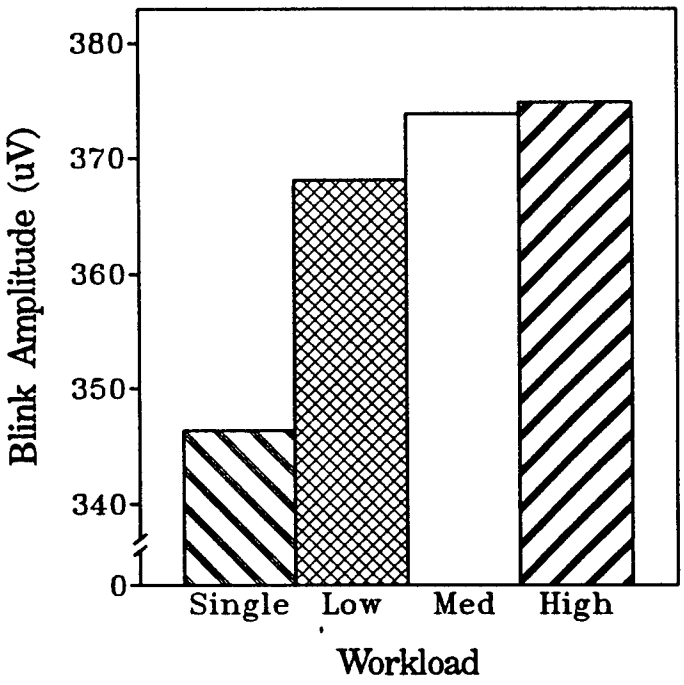
380
370
360
350
340
0
Blink Amplitude (uV)
Single
Low
Med
High
Workload

Figure 11.

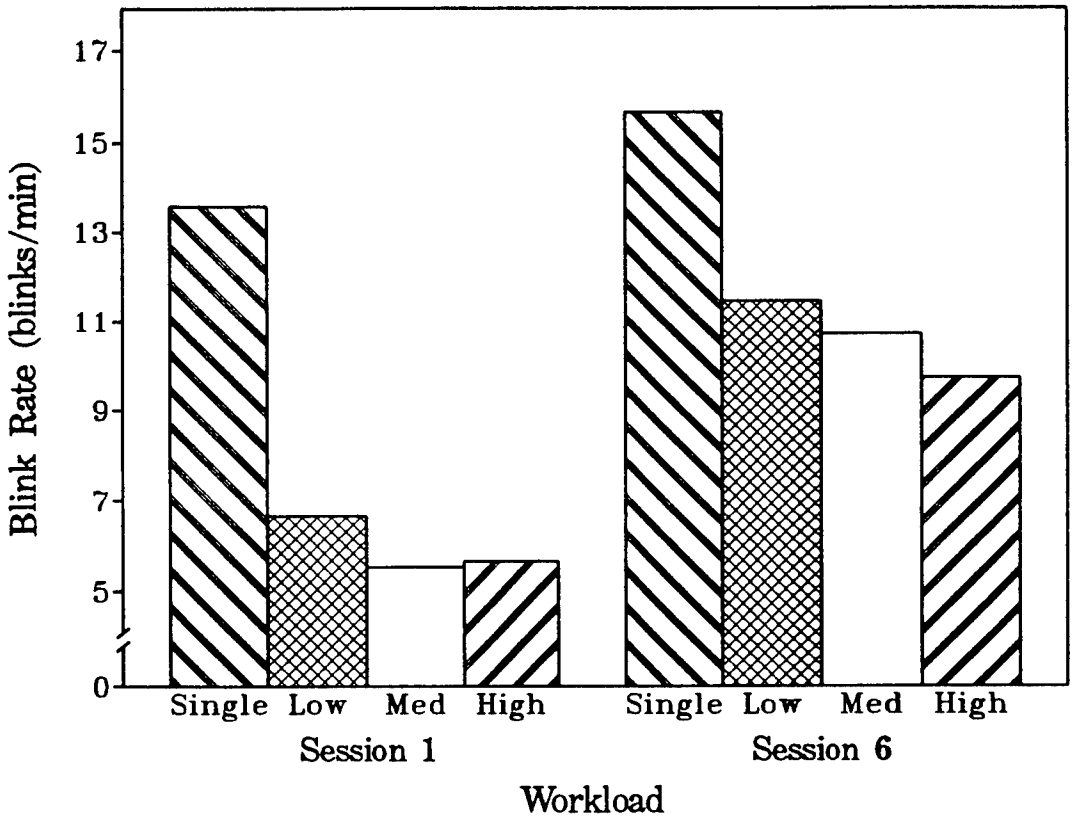
Blink Rate (blinks/min)
17
15
13
11
9
7
5
0
Single
Low
Med
High
Single
Low
Med
High
Session 1
Session 6
Workload

Figure 12.

Alpha1
(8–10 Hz)

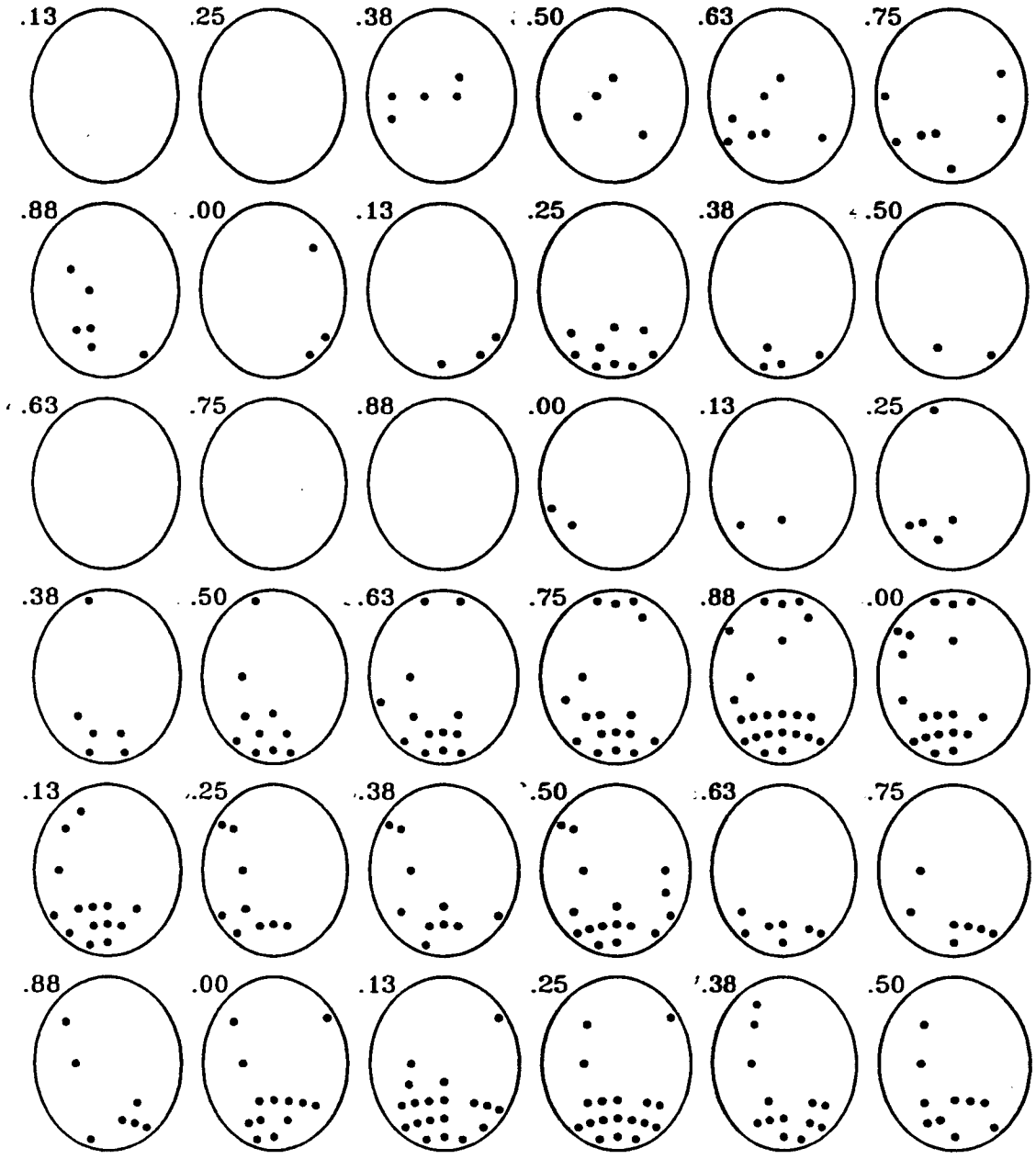

Figure 13. Single task ERD

Alpha2
(10–12 Hz)

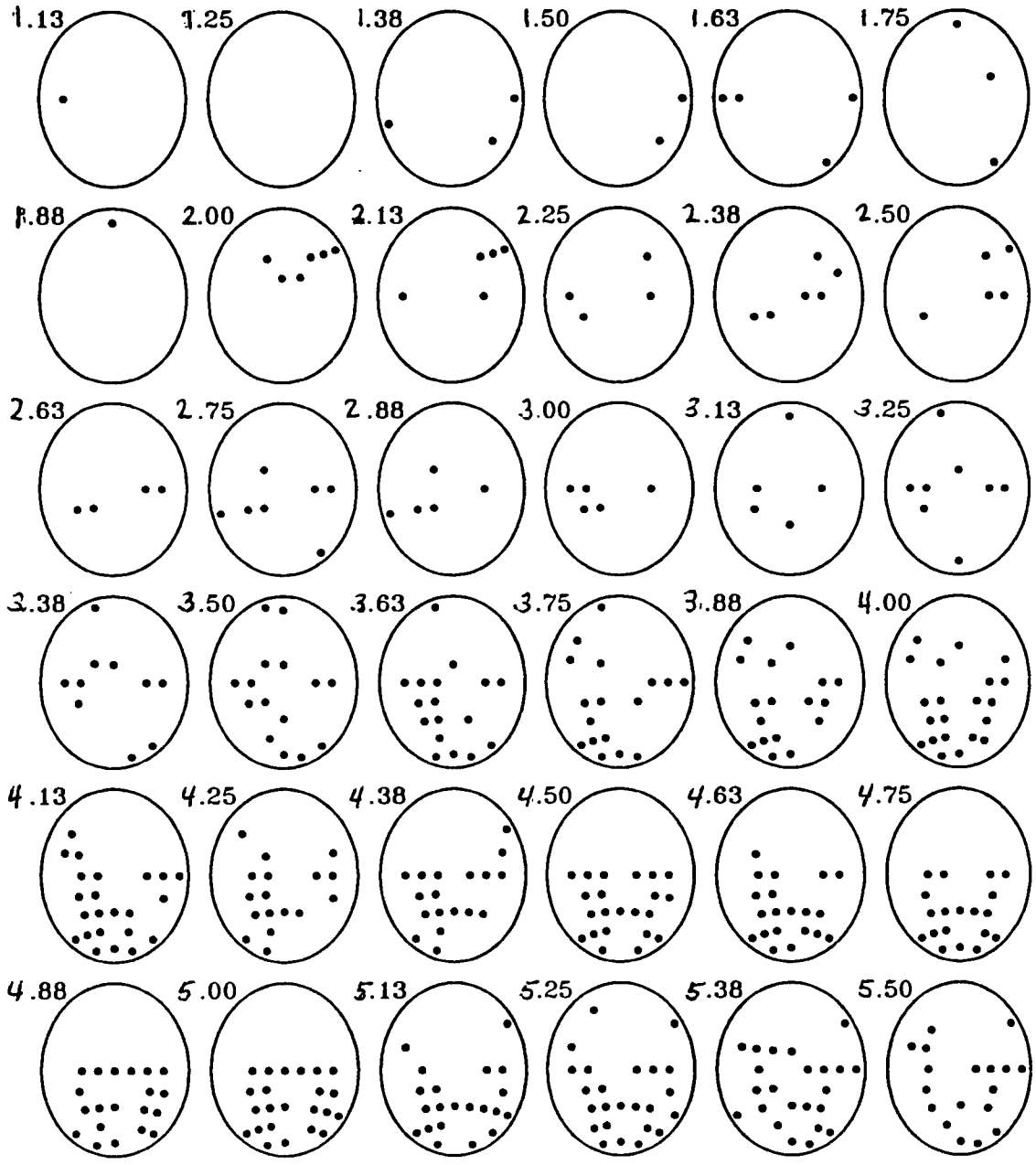

Figure 14. Single task ERD

PROBLEMS ASSOCIATED WITH APPLYING ANTHROPOMETRIC METHODS FOR ERGONOMIC DESIGN

Kristie J. Nemeth
Center for Ergonomic Research

Miami University
Department of Psychology
236D Benton Hall
Oxford, Ohio 45056

Final Report for:
Summer Research Extension Program
Armstrong Laboratory

Sponsored by:
Air Force Office of Scientific Research
Bolling Air Force Base, DC

and

Armstrong Laboratory

December 1996

PROBLEMS ASSOCIATED WITH APPLYING ANTHROPOMETRIC METHODS FOR ERGONOMIC DESIGN

Kristie J. Nemeth

Designers typically have in mind that a new workspace will "fit" the intended population such that all components are reachable and easily usable (Pheasant, 1990). No one would buy a new car if they could not reach both the steering wheel and foot pedals, or if they could not control both the radio and internal temperature while they were driving. The designer needs to have information about the user in order to design for an appropriate match between the workspace and the user's requirements. A variety of tools and guidelines are available to aid designers (e.g., Human Scale, ANSI/HFES 100, MIL-STD 1472D). Unfortunately there are many possible methods for using anthropometric data, and it is not clear which of these methods will allow the designer to accurately meet the goal of accommodating the user. This paper will investigate important aspects of defining the user population, and then methods for using anthropometric data to ensure accurate accommodation.

The first step is to identify the user population (Roebuck, 1995). The type of product would influence who might be interested in its purchase. If an exercise cycle is being designed, then children, the very elderly and pregnant women might not be as interested in the product. The special anthropometric characteristics of these groups would not have to be considered. Both males and females would use this exercise equipment, so our design should take into account their different body types and sizes.

In addition to specifying the user population, the cost of the design must be considered. It may be possible to create an exercise cycle that would accommodate both the extremely small woman and the extremely large man, but this would require considerable component adjustability (e.g., seat height, handle positioning, etc.,). The cost of this adjustability would most likely put the cost of the product beyond the reach of the everyday consumer. It becomes the designers' job to balance adjustability (the percent of the population would could use the product) with the cost of the product. To achieve this balance, it is common practice to try to accommodate 90% of the population (ANSI/HFES 100, MIL-STD 1472D). Although some products/tasks require a higher level of accommodation (e.g., safety measures, doorways, etc.), the process becomes one of diminishing returns in which each additional unit of adjustment yields less benefit in terms of the percentage of satisfied users (Pheasant, 1990).

Each unit of adjustment in the exercise cycle adds to the cost of the product, and the designer has decided that the maximum accommodation for an acceptable product cost is 90%, then it would be important to use an anthropometric method for designing the exercise cycle that most accurately accommodates 90% of the user population. No designer would be pleased to learn that the additional adjustability incorporated into the design would actually accommodate significantly less of the population than desired. There exist many different methods which use body-size data collected in anthropometric surveys to test whether a design will accommodate the user population. The following section outlines several of these methods.

Available Anthropometric Methods

In order to solve any particular design problem, we are attempting to establish those boundary conditions which make an object 'too big,' 'too small,' and so on, with respect to certain design criteria. In the simplest cases we may do this by inspection. This requires us to identify the limiting users - that is, hypothetical individuals, who by virtue of their specific combination of body characteristics, are particularly difficult to accommodate. If the limiting users are accommodated, it necessarily follows that the majority of the population, whose requirements are less demanding, will be accommodated as well. This section describes a variety of methods used to identify limiting users.

The simplest design task is unidimensional. For example, if a doorway is to be designed so that it accommodates 95% of the population, the 95^{th} percentile stature would be the limiting case. If a control is to be located so that 95% of the population can reach it, the 5^{th} percentile reach length would be the limiting case. The 5^{th} and 95^{th} percentile test cases are legitimately used as the limiting cases for unidimensional design tasks.

These same test cases are not so simple to create when the task involves multiple dimensions or task components. Due to the low correlation between body segment sizes, no human has body segments which could be characterized as a single percentile level. It is possible for one individual to have an 86^{th} percentile stature, 3^{rd} percentile upper arm length, 14^{th} percentile lower leg length and 96^{th} percentile neck length. For this reason there are several methods which can be used to create a 5^{th} or 95^{th} "percentile person."

Same-Percentile Value Method

The application of this method involves selecting the same percentile level value for every relevant dimension. A 5th percentile model would have body segments which each correspond to the 5th percentile. For example, both the lower and upper leg lengths would be 5th percentile values. The 95th percentile model would have all 95th percentile dimensions, so the model would have 95th percentile upper and lower leg lengths. Although this method appears to work with a simple biomechanical model, it is impossible to create a human mannequin which has all the same percentile parts. This is due to the fact that percentile distributions are not additive.

If a percentile-mannequin were created using the Same-Percentile Values Method, some segments on the mannequin would accurately be the size of the intended percentile, but many segments would not. For example, the 95th percentile male leg length is 100.8 cm, and the 95th percentile male trunk length is 56.3 cm (Gordon, Bradtmiller, Clauser, Churchill, McConville, Tebbetts, and Walker, 1989). To estimate the 95th percentile male shoulder height we could add leg length to trunk length, for a value of 157.1 cm. The actual value for the 95th percentile male shoulder height is 154.5 cm. Robinette and McConville (1981) demonstrated that a model with 95th percentile lower leg, upper leg, trunk, neck and head lengths would NOT have a 95th percentile stature The two stature values can be off by as much as 10 cm depending on the database used.

Any time two or more dimensions are combined in a model using the Same-Percentile Values Method, the magnitude of the error depends on the percentiles, correlation coefficient and ratio of the standard deviations of the two variables (Kreifeldt & Nah 1995). It is also the case that when adding or subtracting percentiles, the resulting error is generally largest for the most commonly needed percentile values: around the 5th-10th and 80th-95th percentile.

Proportional Method

Another method to create a percentile mannequin is to start with the appropriate stature and estimate the other body segment lengths based on the proportion between the body parts and stature. Pheasant (1986) used a proportional technique originally described by Drillis & Contini (1966) to find these relationships. Using the raw data for the population, the relationship between each body segment and stature was found for every subject. The mean proportion for each body segment is then determined, and can be used to predict the body segment size for a

mannequin of a known stature.

For example, to create a 95th percentile male mannequin, we start with the 95th percentile male stature of 186.8 cm. Using the ANSUR database of Army males (Gordon, Bradtmiller, Clauser, Churchill, McConville, Tebbetts, and Walker, 1989), the leg length is an average of 53% of stature. To predict the leg length of the 95th percentile mannequin, we would apply this proportion to find a leg length of 98.7 cm. As Pheasant (1986) points out, we have not obtained a 95th percentile male thigh length, which is actually 100.8 cm. Instead, we have found the most likely thigh length of a person of 95th percentile stature.

Because these proportions are population-specific, new proportional values should be established for each anthropometric survey. Unfortunately, this is often not well understood and both Drillis & Contini's (1966) and Pheasant's (1986) proportions are used inappropriately. One biomechanical model (Dainoff, Dainoff, Balliett, Bowles, Douglas, & Goernet, 1990) uses link length proportional values to create a percentile-model which predicts the height of a computer keyboard. While this technique may be valid, it is not correct to use the length proportions from Pheasant's (1986) data to predict body segment sizes in the ANSUR survey (Gordon, et al., 1989).

Another concern with this procedure is that simple body-proportion templates assume that all body dimensions, such as lengths, breadths and circumferences, can be accurately represented as given fixed proportions (percentages) of one body dimension, in this case stature. Such a simplistic assumption contradicts the reality that the relationships among body dimensions are neither necessarily linear, nor the same for all persons (Kroemer, 1995).

Consensus Method

Each of the methods described above for creating test case models using percentiles has its associated problems, but is often used because of the limits of an anthropometric survey. For example, if one of the pieces of information collected for each subject in the ANSUR survey was his or her required keyboard height, the model used to predict keyboard height (Dainoff, et al.,1990) would not be necessary. Of course, due to time and financial constraints on data collection, it is not possible to have each subject perform every conceivable task, and assume every conceivable position.

With current advances in computer technology and the availability of the raw data from anthropometric surveys, it is possible to estimate the behavior and posture requirements of each subject in the survey. By returning to the original database we can apply the model for estimating keyboard height to each subject's data. We can then create a new statistical distribution based on the calculated keyboard heights for each individual. From this new distribution, limiting cases can be selected and a design solution can be developed which should more accurately accommodate the population. This method, referred to as the Consensus method, uses every individual in the survey as a test case individual.

In the simple example of keyboard height estimation, one biomechanical model is applied to the data. When the design of the entire workstation is performed, many models are needed to specify all the behaviors required in the workstation (e.g., reaches, clearances, heights, etc.). Using each of these biomechanical models on every individual in the anthropometric survey may become time consuming and overwhelming to the designer. This is especially the case when a 3-D simulation software is used to test ergonomic characteristics of a design by evaluating each test case in the simulated mock-up.

Multivariate Method

To reduce the number of test case individuals while still representing the anthropometric variability found in the population, it is necessary to select a small sample from the database. One such sampling method is the multivariate technique proposed by Zehner, Meindl, and Hudson (1993). Instead of test case models based on percentile models or on every member of the database, the multivariate method is a procedure used to select a small number of test cases which represent the limiting case individuals from true combinations of body sizes.

The first step is to identify the dimensions relevant to the design task. For some tasks this can be as simple as one dimension (e.g., stature is important to doorway heights), while most other tasks (e.g., office workspaces and cockpit design) can involve many dimensions. If only two relevant dimensions were selected, it would be possible to plot the two measurements in a graph simultaneously. Figure 1 shows a distribution of stature on the horizontal axis and weight on the vertical axis. Each individual person is plotted where his or her stature and weight intersect.

Using the mean value for both stature and weight as a starting point, an ellipse can be imposed on the plot which includes any desired percentage of the population. A 90% ellipse would pass near points that are similar to the 5th and 95th percentile person concept (shown as circles in Figure 1). That is, they represent people who are small or large for both values. However, since selecting only the individuals who are both small or large for both stature and weight does not describe all the variability in body size that must be considered in a design, the ellipse would also intersect those points representing an above average height person with below average weight, and a below average height person with above average weight (shown as squares in Figure 1) who are just as likely to occur in the population as any other individual along the perimeter of the circle. The multivariate accommodation method would select at least four points, called representative cases, along the perimeter of the ellipse and use them to describe size variability. The rationale is that several individuals spread along the edge of the ellipse better represent the variety of extreme body types that must be accommodated than does the use of only two points in the distribution (Zehner, et.al., 1993).

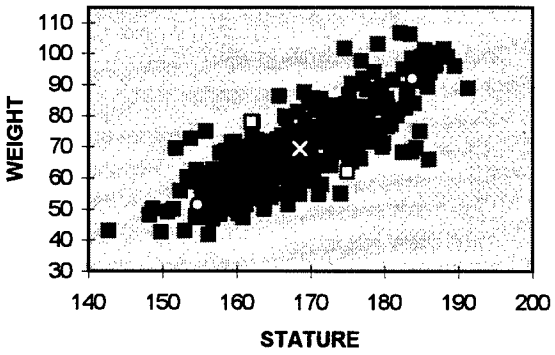

Figure 1. Stature/Weight Bivariate for 1988 ANSUR survey. An accommodation ellipse could be drawn centering on the X, and passing through the circle and square markers.

In most designs, however, more than two variables are needed to ensure the proper accommodation of an individual and his or her equipment. The bivariate approach will be inadequate as soon as a third body size variable such as arm length is considered. The two-dimensional problem described above now becomes a three dimensional one, the ellipse becomes an ellipsoid, and more than four representative cases (points on the surface of the ellipsoid) are necessary to describe the various combinations of these measures. That is, it now becomes necessary to describe tall heavy people with long arms, tall heavy people with short arms, etc.. As each additional measurement is added to the design, an additional dimension or level of complexity is added to the analysis with the accompanying geometrical expansions of the number of representative cases which must be considered in the

design. The problem becomes unworkable very quickly.

A Principal Components Analysis is a statistical approach which helps get around this problem. It reduces the number of measurements needed to describe body size variability by combining a large number of related measures into a smaller set of factors or components based on their correlation or co-variance. For the purpose of constructing accommodation ellipses, each factor can be considered one "measurement."

For most workstation designs, the total number of relevant measures can be reduced to two or three factors (principal components). This means that a bivariate distribution or tri-variate sphere can be used to define population limits and identify the representative cases.

An example which illustrates this method is described by Zehner, Meindl and Hudson (1993). Their example of cockpit accommodation starts with six so-called cockpit dimensions from the 1967 USAF anthropometric survey - Sitting Height, Eye Height Sitting, Shoulder Height Sitting, Thumptip Reach, Buttock-Knee Length, and Popliteal Height Sitting. These dimensions were selected based on typical body size accommodation problems encountered in the cockpit. Such difficulties include the pilot's inability to reach controls (both arm and leg reaches), inadequate clearance for ejection, inability to see the runway over the nose of the plane, inability to assume the very erect posture required for ejection due to inadequate overhead clearance, and finally, a generalized lack of mobility (Zehner, et. al., 1993).

After conducting a Principal Components Analysis on these six body variables, the resulting eigenvalues (variance associated with each component) were examined. According to Zehner's selection criteria, two

Table 1. Summary Statistics and Two-Component Factor Loading Matrix for Selected Dimensions (1967 USAF Survey)

Variable	Component I eigenvectors	Component II eigenvectors
Thmptip-Reach	.694	.518
Buttock-Knee Length	.696	.510
Popliteal Height Sitting	.746	.462
Sitting Height	.886	-.399
Eye Height Sitting	.861	-.410
Shoulder Height Sitting	.809	-.436

Table 2. The derivation of component scores for Subject Number 18139.

	Raw Score	Component I eigenvectors	Linear Combination I	Component II eigenvectors	Linear Combination II
Thumbtip Reach	78.8	0.694	78.8*0.694	0.518	78.8*0.518
Buttock-Knee Length	61.7	0.696	61.7*0.696	0.510	61.7*0.510
Popliteal Height Sitting	41.7	0.746	41.7*0.746	0.462	41.7*0.462
Sitting Height	94.5	0.886	94.5*0.886	-0.399	94.5*-.399
Eye Height Sitting	78.2	0.861	78.2*0.861	-0.410	78.2*-.41
Shoulder Height Sitting	60.3	0.809	60.3*0.809	-0.436	60.3*-.436
			328.6		-4.5

components were considered further. Therefore, a bivariate distribution was appropriate. Table 1 shows the two-component factor loadings for the six dimensions. The data are weighted by these eigenvectors (the weights which define the linear combination for each component) to achieve two component scores for each individual.

Each subject's component scores (see an example derivation in Table 2) are plotted in a bivariate display and a circle is drawn to encompass the central 95% of the population. Eight representative cases are chosen from the perimeter of this circle to represent the anthropometric variability found in the population. Table 3 lists the Z

Table 3. The variable Z scores and percentile values for the Eight Represenative Cases (Zehner, et al., 1993)

Variables	1	2	3	4	5	6	7	8
Thumb Tip Reach	-0.415	-2.313	1.726	-1.726	2.313	2.855	-2.855	0.415
	(34)	(1)	(96)	(4)	(99)	(100)	(0)	(66)
Buttock-Knee Length	-0.437	-2.318	1.700	-1.700	2.318	2.841	-2.841	0.437
	(33)	(1)	(96)	(4)	(99)	(100)	(0)	(67)
Poplitcal Hcight Sitting	-0.669	-2.846	1.539	-1.539	2.846	2.846	-2.846	0.669
	(25)	(1)	(94)	(6)	(99)	(100)	(0)	(75)
Sitting Height	-3.029	-2.952	-1.332	1.332	2.952	1.145	-1.145	3.029
	(0)	(0)	(9)	(91)	(100)	(87)	(13)	(100)
Eye Height Sitting	-2.995	-2.868	-1.368	1.368	2.868	1.061	-1.061	2.995
	(0)	(0)	(9)	(91)	(100)	(86)	(14)	(100)
Shoulder Height Sitting	-2.930	-2.693	-1.451	1.451	2.693	0.878	-0.878	2.930
	(0)	(0)	(7)	(93)	(100)	(81)	(19)	(100)

NOTE: Associated percentile values are located below the Z score values

score values and corresponding percentile values for each dimension of these representative cases. Using a human-model for each of these eight people, Zehner, et. al. (1993) was able to construct design specifications for a cockpit that would more accurately fit 95% of the pilot population.

Anthropometric Method Validation

The purpose of the current project was to determine how accurately the population is accommodated by each of the four model construction methods previously described. To accomplish this, a specific design task which is simple, yet non-trivial was used (described in detail below). The next step involved defining the user population. A model construction method was then used to select the test cases. The biomechanical model (equation defined by the task) was then applied to the test cases' dimensions. The design requirements for each test case were used to create the final design specifications. Lastly, the percent of the population which would be actually accommodated by the design specification was calculated. Each of these steps is further described below.

Example Design Task

The design task used in this project is to develop specifications for a leg-clearance envelope under a table or desk. The three important dimensions include height, width and depth of the non-adjustable space. To determine whether any one individual would be accommodated, the following equations are to be used (the first three are taken from ANSI/HFES 100, 1996 draft):

Height

Definition: the highest point of the thigh in the inclined (forward-tilt) posture.
Relevant dimensions:

$$\text{height} = A + B + \left[(C - D) * \sin\alpha\right]$$

A= popliteal height
B= seated thigh clearance height
C= buttock to knee length
D= abdominal depth
α=5° inclined seatpan

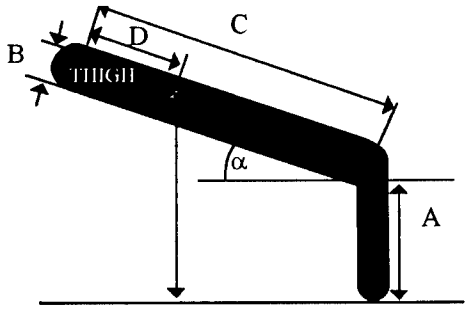

Width

Definition: widest point of hips.
Relevant dimensions:
hip breadth sitting

Depth

Definition: the distance between the front of the belly and the knees in the upright posture.
Relevant dimensions:
C= buttock to knee length
D= abdominal depth

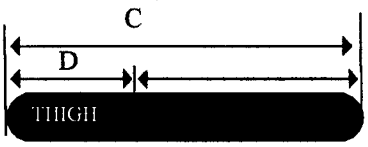

Reach

Definition: the horizontal distance between the front of the belly and the heel, when the lower leg is extended 45°
Relevant dimensions:
A= popliteal height
C= buttock to knee length
D= abdominal depth

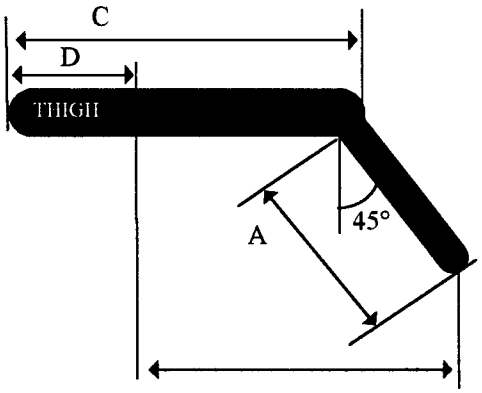

User Population

If *user trials* were conducted, human volunteers would try to perform a variety of tasks in the workspace. Their ability or inability to perform each task would be used to predict the percentage of the actual population that could also perform the tasks. This process is time consuming because all possible tasks must be performed by each individual for each iteration of the design of the workspace. The anthropometric method of limits proves to be a better method to establish final design recommendations with respect to anthropometric and biomechanical criteria. The anthropometric method of limits is a model or analogue of the fitting trial, in which the anthropometric data stand as substitutes for the experimental subjects (Pheasant, 1990). In applying this method, we are attempting to predict, using pencil and paper methods, what the result of a fitting trial would be if we were to perform one.

To represent the user population of office workers, the current project used the anthropometric survey of Army personnel (ANSUR, 1988). For the survey, 2,208 female and 1,774 male soldiers were measured, who were

subsets of soldiers sampled to match the proportions of age categories and racial/ethnic groups found in the active duty army of June 1988. The measured sample is a mix of older and younger subjects: among the men, 30% were aged 31 and over, 25% between 25 and 30, and the others younger. 66% were white, 26% black, 4% Hispanic and the remaining 4% other racial/ethnic groups. Among the women, 22% were aged 31 and over, 32% between 25 and 30, and the others younger. Nearly 52% were white, 42% black, 3% Hispanic, and 4% other racial/ethnic groups.

Soldiers are certainly a subsample of the general population, but they are a biased sample because they are youngish, healthy, and neither extremely small nor big. Thus, their body dimensions may not truly represent the adult civilization population (although it appears that there are no major differences in head, hand, and foot dimensions) (Kroemer, et. al., 1995). The decision to use these data to represent the US adult population is based on the fact that among the US military services, the Army is the largest and anthropometrically least biased sample of the total US adult population (Kroemer, et. al., 1995).

To accommodate both males and females, their distributions must be handled separately. Males and females are not scaled up and down versions of one another. When each of the anthropometric methods is used, test cases will be defined for both male and female populations. The final design specification will be chosen so that all of the test cases are accommodated.

Establishment of Design Specifications

Using each of the four model construction methods, test cases were defined. The design equations were applied to these test cases to determine the size of the clearance envelope each case would require. Fit is defined here numerically with no allowance for space between the legs and the desk. A true design task would include a margin of space for comfort. The final desk design specifications were established by comparing the individual clearance envelopes to create one final envelope that would accommodate all of the test cases. The dimensions from this final envelope define the design specifications.

Calculation of Actual Accommodation

The actual level of accommodation for the recommended design space was calculated by comparing the clearance envelope required by each individual in the ANSUR (1988) anthropometric survey to the recommended

design specifications. For this design task, the true accommodation is calculated in a multi-step process: The first step is to determine the percentage of individuals in the population who can fit under the desk without hitting their thighs on the tabletop. The next step is to establish the percentage of individuals who can fit both legs under the desk. The third step is to find the percentage of individuals who can pull their chairs up to the desk without hitting their knees at the back of the desk. The fourth step is to find the percentage of individuals who can reach their foot to the foot control without extending their lower leg greater than 45° from the vertical. The final step is to calculate the percentage of people who are accommodated by all four desk specifications. The actual accommodation level resulting from each model construction method is defined using this method.

Materials

The ANSUR database is database is available in a set of disks in text format from the Crew System Ergonomics Information Analysis Center (CSERIAC), Wright-Patterson Air Force Base. For this project it has been converted to an Excel spreadsheet format and is stored on a 486 IBM PC. The Principal Components Analysis will be conducted by a program written in C, with the IMSL C Numerical Libraries Toolpak.

Results

The validation procedure was first applied to the Same-Sized Segment Method. The test cases were defined by selecting the 5^{th} and 95^{th} percentile dimensions for both male and female populations. By applying the design equations for height, width, depth, and reach, we can establish the design envelope that each of the four test cases would require. For example, the 5^{th} percentile male test case would need a height of 57.6 cm. If the design specification for height is set to 70.2 cm, then all four of the test cases will be accommodated (see Table 4).

The Same-Size Segment Method assumes that when the limiting cases (test cases) are accommodated, then the middle 90% of the population will also be accommodated. If we calculate the height requirement for each male in the ANSUR database, we find that 97.2% of the male population would be able to fit their legs under a desk of the size we have recommended (see Table 5). When this design specification is compared to the requirements of each female in the ANSUR database, we find that 100% of the females would be able to fit their legs under the desk.

Next, the width clearance required by each of the test cases was calculated. The 5th percentile male needs a width of 32.9 cm. If we set the recommended width to 43.2 cm, then all four test cases will be accommodated. When we look at the requirements of each subject in the population, we find that 99.2% of the male population and 94.8% of the female population would not hit their legs on the sides of the desk.

Next, we calculate the required clearance depth at the knee for each of the test cases. The 5th percentile person needs 36.9 cm. If we set the recommended depth to 37.8 cm, then all four test cases will be accommodated. When we look at the requirements of each subject in the population, we find that 48.3% of the male population and 63% of the female population would be able to pull up to the desk without hitting their knees at the back of the desk.

Finally, the reach dimension is calculated. The 5th percentile person needs 64.8 cm. If the recommended reach is set to 60.7 cm, then all four test cases, and a resulting 95.4% of the male population and 78.3% of the female population will be able to reach the foot control without extended their lower leg greater than 45°.

When we consider the percent of the population who is accommodated by all four dimensions, we find that only 43.1% of the male population, and 39.6% of the female population would fall into this category. Instead of meeting the design criteria of accommodating 90% of the population, 56.9% of the males and 60.4% of the females in the survey would not be able to fit their legs entirely under the desk while reaching the foot control.

This same procedure was conducted on each of the four anthropometric methods described earlier. Tables 4 and 5 show the results these validation tests. Clearly, the Same-Sized Percentile Method and the Proportional Method, fall well short of the design accommodation goal. While the accommodation levels for each desk dimension are accurate for the Consensus Method, the accommodation level drops slightly below the design goal when the total design accommodation is considered. A different problem exists with the Multivariate Method. Each desk dimension results in serious overaccommodation, the resulting total design accommodation is closer to the goal.

Table 4. Test Case Body Dimensions and Resulting Desk Dimensions for Each Accommodation Method.

	Test Case Body Dimensions					Desk Dimensions			
	Ab Dpth	B-K Lgth	Hip Bdth	Pop Ht	Th Clr	Height	Width	Depth	Reach
Same-Sized Percentile Method									
5th Percentile -Males	19.9	56.8	32.9	39.5	14.9	57.6	32.9	36.9	64.8
95th Percentile -Males	29.0	66.8	41.2	47.2	19.0	69.5	41.2	37.8	71.2
5th Percentile -Females	18.5	54.3	34.3	35.2	14.0	52.3	34.3	35.8	60.7
95th Percentile -Females	27.1	63.9	43.2	42.9	18.0	64.1	43.2	36.8	67.1
Proportional Method									
5th Percentile -Males	22.5	57.9	34.5	40.7	15.8	59.6	34.5	35.4	64.2
95th Percentile -Males	25.5	65.6	39.0	46.2	17.9	67.6	39.0	40.1	72.8
5th Percentile -Females	20.8	55.1	36.0	36.4	14.9	54.3	36.0	34.3	60.0
95th Percentile -Females	23.7	62.8	41.0	41.5	17.0	61.9	41.0	39.1	68.4
Consensus Method									
90th Percentile -Males	not applicable					67.5	40.0	42.0	62.3
90th Percentile -Females	not applicable					61.7	42.0	40.6	58.7
Multivariate Method									
Test Case 1 -Males	27.8	67.8	42.6	46.8	16.9	67.2	42.6	40.0	73.1
Test Case 2 -Males	20.6	64.6	33.3	47.2	16.2	67.2	33.3	44.0	77.4
Test Case 3 -Males	19.3	56.9	31.2	38.8	13.9	56.0	31.2	37.6	65.0
Test Case 4 -Males	29.9	59.5	36.8	39.5	18.3	60.4	36.8	29.6	57.5
Test Case 5 -Males	23.8	68.2	38.7	48.6	17.4	69.9	38.7	44.4	78.8
Test Case 6 -Males	18.0	60.2	31.0	43.1	15.2	62.0	31.0	42.2	72.7
Test Case 7 -Males	23.4	55.8	35.1	37.4	16.3	56.5	35.1	32.4	58.8
Test Case 8 -Males	31.2	64.4	40.7	42.8	18.0	63.7	40.7	33.2	63.5
Test Case 1 -Females	29.6	65.4	39.8	40.8	19.0	62.9	39.8	35.8	64.6
Test Case 2 -Females	19.9	62.2	34.8	43.2	14.9	61.8	34.8	42.3	72.8
Test Case 3 -Females	17.9	53.8	33.0	36.1	13.9	53.1	33.0	35.9	61.4
Test Case 4 -Females	26.1	56.0	40.6	34.7	15.5	52.8	40.6	29.9	54.4
Test Case 5 -Females	22.7	64.9	40.8	44.0	16.3	64.0	40.8	42.2	73.3
Test Case 6 -Females	17.3	56.9	32.8	40.3	14.4	58.2	32.8	39.6	68.1
Test Case 7 -Females	20.8	52.7	37.5	34.1	14.8	51.7	37.5	31.9	56.0
Test Case 8 -Females	22.8	61.1	48.9	36.6	17.7	57.6	48.9	38.3	64.2

Table 5. Final Desk Design Specifications for Each Accommodation Method.

	Design Dimensions				
	Height	Width	Depth	Reach	Total
Same-Sized Percentile Method					
	69.5	43.2	37.8	60.7	
Percent of Males Accommodated	97.2%	99.2%	48.3%	95.4%	43.1%
Percent of Females Accommodated	100.0%	94.8%	63.0%	78.3%	39.6%
Proportional Method					
	67.6	41.0	40.1	60.0	
Percent of Males Accommodated	90.2%	94.6%	77.5%	96.9%	67.8%
Percent of Females Accommodated	99.8%	82.4%	86.7%	82.8%	57.7%
Consensus Method					
	67.5	42.0	42.0	58.7	
Percent of Males Accommodated	90.0%	97.4%	89.7%	98.3%	82.0%
Percent of Females Accommodated	99.8%	89.6%	96.0%	90.0%	86.1%
Multivariate Method					
	69.9	48.9	44.4	54.4	
Percent of Males Accommodated	97.8%	100.0%	98.3%	99.8%	96.2%
Percent of Females Accommodated	100.0%	99.9%	99.5%	98.2%	97.4%

Conclusion

After establishing the percent of the population which is accommodated by desk designs developed by each of the four model construction methods, it is possible to make recommendations for a more accurate use of anthropometric data. Due to the theoretical and practical problems with the methodology, it was expected that the Same-Size Percentile method would have the least accurate accommodation, while the proportional method should be better, but still very inaccurate. Considering the low levels of design accommodation found for this task, these methods should not be used in an attempt to accommodate the user population. Due to the high variability within and between individuals' body sizes, the 5^{th} and 95^{th} percentile test cases do not represent limiting cases in the population.

Both the Consensus method and the Multivariate method were expected to produce rather precise accommodation levels. The Consensus method underaccommodates (3.9-8.0%) a similar percent of the population as the Multivariate method overaccommodates (6.2-7.4%). The difference in the design recommendations for each

dimension range between 2.4 cm (height & depth), 4.3 cm (reach), and 6.9 cm (width).

A designer should select between these two anthropometric methods based on how the test cases will be used. Both methods require the use of the raw anthropometric data, but a designer only has to consider 8 test cases for the Multivariate method, while every individual must be considered for the Consensus method. For example, a 3D simulation software may restrict the number of test cases to a minimum. On the other hand, the Multivariate method requires the use and knowledge of sophisticated statistical software (to conduct the Principal Components Analysis), while the Consensus method can be performed with a simple spreadsheet software program. The percentile levels for the design specifications chosen by the Consensus method can be tweaked to ensure accurate total design accommodation (this type of manipulation was not conducted for the current project, but would be a simple procedure).

The selection of an appropriate anthropometric method must consider the task design, and the knowledge, equipment and time available to the designer. Currently there are no simple, accurate solutions.

References

Dainoff, M.J., Dainoff, M.H., Balliett, J., Bowles, W., Douglas, S., and Goernert, P. (1990). Adjustability ranges for VDT workstations. In (Eds., L. Berlinguet and D. Berthelette) Work With Display Units 1989. Elsevier Science Publishers: North-Holland.

Drillis, R., and Contini, R., (1966). *Body Segment Parameters* (Report 1166-03). Office of Vocational Rehabilitation, Department of Health, Education and Welfare. New York: University School of Engineering and Science.

Gordon, C.C., Bradtmiller, B., Clauser, C.E., Churchill, T., McConville, J.T., Tebbetts, I., and Walker, R.A. (1989). 1987-1989 Anthropometric Survey of U.S. Army Personnel: Methods and Summary Statistics. Technical Report NATICK /TR-89-044, U.S. Army Natick Research, Development and Engineering Center, Natick, Massachusetts.

Haselgrave, C.M (1986). Characterizing the Anthropometric Extremes of the Population. *Ergonomics, 22*, 145-154.

Human Factors Society. (1988). American National Standard for Human Factors Engineering of Visual Display Terminal Workstations. Santa Monica, CA: Human Factors Society.

Human Factors Society. (1996, draft). American National Standard for Human Factors Engineering of Visual Display Terminal Workstations. Santa Monica, CA: Human Factors Society.

Kreifeldt, J.G., & Nah, K. (1995). Adding And Subtracting Percentiles - How Bad Can It Be? Proceedings of the Human Factors and Ergonomics Society 39th Annual Meeting. 301-305.

Kroemer, Kroemer, & Kroemer (1995). Ergonomics: How to design for ease and efficiency. New Jersey: Prentice Hall.

Pheasant, S.T. (1986). Bodyspace.

Pheasant, S.T. (1990). Anthropometry and the Design of Workspaces. In (Eds., Wilson & Corlett) Evaluation of

Human Work: A practical ergonomics methodology. Bristol, PA: Taylor & Francis.

Robinette, K.M., and McConville, J.T. (1981). An Alternative to Percentile Models. Society of Automotive Engineers Technical Paper Series, International Congress and Exposition. Detroit, Michigan.

Tatsuoka, M.M., (1988). Multivariate Analysis: Techniques for educational and psychological research. New York: Macmillan Publishing Company.

Zehner, G.F., Meindl, R.S., and Hudson, J.A. (1993). A Multivariate Anthropometric Method for Crew Station Design: Abridged (U). Technical Report AL-TR-1992-0164. Crew Systems Directorate, Human Engineering Division, Armstrong Laboratory, Wright-Patterson Air Force Base, Dayton, Ohio.